

SANDIA REPORT

SAND88-2784 • UC-70

Unlimited Release

Printed December 1988

Yucca Mountain Project

Hydrologic Technical Correspondence in Support of the Site Characterization Plan

Ralph R. Peters

Prepared by
Sandia National Laboratories
Albuquerque, New Mexico 87185 and Livermore, California 94550
for the United States Department of Energy
under Contract DE-AC04-76DP00789

HYDROLOGY DOCUMENT NUMBER 451

"Prepared by Yucca Mountain Project (YMP) participants as part of the Civilian Radioactive Waste Management Program (CRWM). The YMP is managed by the Yucca Mountain Project Office of the U. S. Department of Energy, Nevada Operations Office (DOE/NV). YMP work is sponsored by the Office of Geologic Repositories (OGR) of the DOE Office of Civilian Radioactive Waste Management (OCRWM)."

Issued by Sandia National Laboratories, operated for the United States Department of Energy by Sandia Corporation.

NOTICE: This report was prepared as an account of work sponsored by an agency of the United States Government. Neither the United States Government nor any agency thereof, nor any of their employees, nor any of their contractors, subcontractors, or their employees, makes any warranty, express or implied, or assumes any legal liability or responsibility for the accuracy, completeness, or usefulness of any information, apparatus, product, or process disclosed, or represents that its use would not infringe privately owned rights. Reference herein to any specific commercial product, process, or service by trade name, trademark, manufacturer, or otherwise, does not necessarily constitute or imply its endorsement, recommendation, or favoring by the United States Government, any agency thereof or any of their contractors or subcontractors. The views and opinions expressed herein do not necessarily state or reflect those of the United States Government, any agency thereof or any of their contractors or subcontractors.

Printed in the United States of America
Available from
National Technical Information Service
U.S. Department of Commerce
5285 Port Royal Road
Springfield, VA 22161

NTIS price codes
Printed copy: A10
Microfiche copy: A01

Hydrologic Technical Correspondence in Support
of the Site Characterization Plan

compiled by

Ralph R. Peters
Repository Performance Assessment Division
Sandia National Laboratories
Albuquerque, New Mexico 87185

ABSTRACT

This document is composed of five technical memoranda containing information that has been used in preparing the plan to characterize the site of a prospective high-level radioactive waste repository at Yucca Mountain, Nevada. The Yucca Mountain Project is investigating the feasibility of emplacing high-level waste in unsaturated tuff at this site. The information in this report pertains to (1) how the use of water during construction may affect the surrounding site conditions and consequently affect estimates of the in situ hydrologic parameters and water movement in fractured tuff, (2) calculations concerning the response of a fractured tuff column to changes in vertical flux, (3) changes in groundwater travel-time that may result from water redistribution caused by repository heating, (4) some potential effects of seismicity on water movement and radionuclide transport in the unsaturated zone, and (5) the rate at which a tuff column returns to steady-state conditions after being saturated by a fluctuating water table.

The data contained in this report
was gathered at Quality Assurance Level III

CONTENTS

	<u>Page</u>
Foreword	iv
Introduction	1
Memorandum No. 1 -- NNWSI Hydrologic Analysis No. 8, "Support of Exploratory Shaft Activities"	3
Memorandum No. 2 -- NNWSI Hydrologic Analysis No. 72-19, "Support of Exploratory Shaft Activities"	81
Memorandum No. 3 -- NNWSI Hydrologic Analysis No. 9, "1-D Hydrologic Calculations Concerning Groundwater Travel Time for the Repository as a Result of Water Redistribution Caused by Repository Heating"	131
Memorandum No. 4 -- "The Effect of Seismic and Tectonic Activity on Radionuclide Containment at Yucca Mountain, Nevada"	161
Memorandum No. 5 -- NNWSI Hydrologic Analysis No. 72-26, "A 1-Dimensional Calculation Investigating Water-Table Fluctuation at Yucca Mountain"	183
Appendix A -- Reference Information Base and Site and Engineering Properties Data Base Information	A-1

FOREWORD

This document contains five separate technical memoranda supporting information in the statutory draft of the site characterization plan for the Yucca Mountain Project. The Project is studying the feasibility of emplacing high-level waste in the unsaturated zone at Yucca Mountain, Nevada. The memoranda have been collected in this report as a convenient way to provide, in a form that may be referenced, previously unpublished information cited in the site characterization plan.

Ralph R. Peters
Repository Performance Assessment Division
Sandia National Laboratories

October 1988

INTRODUCTION

The Yucca Mountain Project currently is investigating the feasibility of disposing of high-level waste in the unsaturated zone of Yucca Mountain in southern Nevada. A large number of analyses are needed in support of the development of a plan to characterize the Yucca Mountain site.

Many of these analyses must deal with the unsaturated rock at the site because the proposed emplacement zone is 150-550 m above the water table. To design tests needed to characterize the unsaturated zone and to evaluate the potential effects of site-characterization activities on postclosure system performance, the effect of construction activities and testing activities on the unsaturated zone must be estimated. Some of the characterization tests and construction activities may have only a transient effect on the unsaturated zone; others may affect the site for a long time (thousands of years). Estimates of the response that may be expected from the characterization tests are necessary to determine whether the tests will provide the necessary information in a reasonable time. To define the disturbed zone, the movement of water resulting from heat produced by high-level waste must be addressed. Finally, phenomena such as tectonic activity or fluctuation of the water table may affect the unsaturated zone and thus affect the release rate of radionuclides to the accessible environment.

This report collects five memoranda which report preliminary calculations that contribute to these analyses. The one-dimensional computer code TOSPAC* has been used for all of the calculations. The memoranda have been reproduced exactly as they were written. Changes in the accepted values of hydrologic properties and boundary conditions may have occurred since some of them were written; however, these changes are not included because they are not judged to change significantly the primarily qualitative, preliminary results presented in the memoranda.

The first two memoranda address the effect of drilling fluids on the unsaturated zone. In the reported simulations, water under high pressure (2 bars) is injected for as long as 100 min into a matrix material (no fractures) with properties currently thought to be representative of the welded-tuff unit in the emplacement horizon. The simulations indicate that the extent of water penetration into the matrix is small (<5 cm). These two memoranda differ in the description of the matrix characteristic curves used in the calculations.

The first two memoranda also investigate the response of a column of fractured tuff to changes in applied flux at the upper boundary. An

Dudley, A. L., R. R. Peters, J. H. Gauthier, M. L. Wilson, M. S. Tierney, and E. A. Klavetter, "Total System Performance Assessment Code (TOSPAC), Volume 1: Physical and Mathematical Bases," SAND85-0002, prepared by Spectra Research Institute and Sandia National Laboratories, Albuquerque, NM, December 1988.

experiment of this sort might be useful to validate mathematical models of flow in fractured tuffs in the unsaturated zone. The simulations indicate that the time required to change from one steady-state condition with a 0.1-mm/yr vertical flux to another steady-state condition with a 0.5-mm/yr vertical flux is 500-10,000 yr, depending on the hydrologic properties of the tuff matrix.

The third memorandum investigates the effect of pushing water away from the repository by heating; it attempts to determine whether this process may be used to define a "disturbed-zone boundary." In this simulation, a vertical column initially exists in a steady-state condition with a vertical flux of 0.1 mm/yr. Water is injected into the rock mass below the repository at a rate of 11 mm/yr for 90 yr, roughly simulating the water movement induced by heat from the emplaced waste. Then at either 90 or 1090 yr later (times that bracket current estimates of when water will resume its original downward movement through the repository), the vertical flux is reset to the initial condition. Particles are injected into the flow field at many points and times, and their travel times to the water table are calculated. The travel times of particles injected into the upper 90 m of the column during the high-flux period are affected by the increase and, consequently, are reduced from 400,000 to 300,000 yr.

The fourth memorandum discusses the effect of seismic and tectonic activity on the hydrologic conditions in the unsaturated zone. One concern is the possibility that seismic activity may dam an arroyo lying over a fault zone and make it possible for a large storm to produce a pond that injects a large amount of water into the unsaturated zone. In this memorandum, the water-ponding scenario is simulated by injecting a 10-m-tall column of water into a fault zone. The results of the simulation indicate that the water flux at the proposed repository level may double about 10,000 yr after the water is injected.

The fifth memorandum investigates the time required for the unsaturated zone to return to its initial steady-state condition after the water table has risen temporarily. In the simulation, the water table is elevated either to the land surface (550 m above the current water table) or to a point 100 m above the repository (340 m above the current water table), and the rock mass is allowed to relax to the steady-state condition corresponding to a vertical flux of 0.1 mm/yr. The results of the simulations indicate that more than 10,000 yr are required before the system reaches conditions near steady state.

MEMORANDUM NO. 1

**NNWSI HYDROLOGIC ANALYSIS NO. 8
SUPPORT OF EXPLORATORY SHAFT ACTIVITIES**

Sandia National Laboratories

Albuquerque, New Mexico 87185

date: April 14, 1986

to: R. R. Peters, 6312

from: R. R. Peters, 6312
J. H. Gauthier, 6312

R. R. Peters
J. H. Gauthier

subject: NNWSI Hydrologic Analysis No. 8 - Support of Exploratory Shaft Activities

We have completed two different analyses that may provide guidance to personnel currently involved in defining experiments for the Exploratory Shaft. These analyses were defined in a memo to J. H. Gauthier and R. R. Peters and dated January 30, 1986. These analyses were formally assigned as NNWSI Hydrologic Analysis No. 8. A report is attached to this memo that defines the calculations performed and discusses the results of the calculations.

RRR:JHG:6312:mjh:1507r
Attachment

Copy to:

6310 T. O. Hunter
6312 F. W. Bingham
6312 A. L. Dudley
6312 J. H. Gauthier
6312 N. K. Prindle
6312 H. S. Tierney
6313 T. E. Blejwas
6313 E. A. Klavetter
6313 R. M. Zimmerman
6315 S. Sinnock
6315 Y. T. Lin
6310 10/12144/SNL/QII
6310 72/12144/8/QII
6310 NNWSICF

HYDROLOGIC CALCULATIONS CONCERNING ACTIVITIES IN THE EXPLORATORY SHAFT

Introduction

The activities associated with the construction of the Exploratory Shaft and related facilities could affect in situ conditions. In particular, the use of water in drilling and mining activities may significantly affect the surroundings and thus affect estimates of the in situ hydrologic parameters. The values of the estimated hydrologic parameters and estimates of their accuracy may affect performance assessment activities.

Experiments being planned in the Exploratory Shaft facilities may significantly aid in understanding flow mechanisms in unsaturated, fractured tuff. The results of these experiments may also be used to validate computer codes. Performance assessments of the Yucca Mountain site will likely require both a conceptual model of flow and validated computer codes.

This report discusses both issues, and defines and discusses the results of analyses that may aid in decisions regarding future activities.

I) Effect of Construction Activities on In Situ Activities

The construction of the Exploratory Shaft and the underground facilities, and preparations for various experiments in the underground facilities will require considerable drilling and coring. Drilling may be used in construction of drifts. Coring is used to obtain samples, obtain access to the rock mass for measurements, etc. A debate is currently going on concerning whether holes should be drilled or cored using standard techniques (water is used as the working fluid) or whether the holes should be drilled or cored dry (air is used as the working fluid). Both techniques will, to some extent, affect the surrounding rock mass. Air-drilling and air-coring will dry the surrounding rock to some extent. Water-drilling and water-coring may force water into the surrounding fractures and matrix blocks. At this time, the use of water is thought to have a larger affect on the surroundings due to the possibility of significant penetration of water into the matrix blocks. The manner in which these holes are drilled or cored may affect the hydrologic parameters of the surroundings and thus, the accuracy of estimates of in situ conditions in this area. The level of accuracy of the estimates of in situ conditions will likely affect performance assessments of the Yucca Mountain site.

The first analysis set discussed in this report (titled "Application of High Pressure Water to a Matrix Block") investigates the depth of penetration of water into the densely welded matrix material. The results of these calculations provide information that may be useful in deciding what circumstances may allow standard techniques and what circumstances require the use of air as the drilling fluid. Some preliminary conclusions are presented in the section "General Discussion and Conclusions."

APPLICATION OF HIGH PRESSURE WATER TO A MATRIX BLOCK

Definition of Analysis

The first set of analyses investigated the response of a matrix block to water drilling-fluid under high pressure. The matrix block geometry and boundary conditions are shown in Figure 1. The stratigraphy is that found at drill hole USW G-4 (Ortiz et al., 1985). The block extends from a position roughly in the center of unit TSw2 to the water table.

The lower boundary condition is a pressure-head condition set by the water table. There are two different initial conditions defined in Table 1. The first is a no flow condition that results in a saturation at the top of the column of about 65% for the material properties used in this calculation. The second initial condition is defined by having a steady flow of 0.1 mm/yr throughout the column that results in a saturation at the top of the column of about 88%. The upper boundary condition is variable with three different cases defined in Table 1. All three cases apply 20 meters of pressure head (about 30 psig) to the rock matrix at the top of the column. The cases differ as to the length of time that high pressure water is applied (1, 10, and 100 minutes). After the end of the time that the high pressure water is applied, the upper boundary condition is reset to the initial condition (either 0.0 or 0.1 mm/yr flux). Water is not allowed to flow up and out of the column after the end of the time the high-pressure water is applied. The total number of calculations is six (3 different times for application of pressure-head at the upper surface times 2 initial conditions).

Table 1 Calculational Cases for Investigating the Results of Applying High Pressure Water to a Matrix Block.

Case	Initial Condition (flux - mm/yr)	Time the High-Pressure Water is Applied (min.)
1	0.0	1.0
2	0.0	10.0
3	0.0	100.0
4	0.1	1.0
5	0.1	10.0
6	0.1	100.0

The properties of the two units (TSw2 and CHnz) are listed in Table 2. The paper by Klavetter and Peters (in preparation) contains a discussion of the terms and nomenclature used in this table and is the source of the data listed in Table 2. Because we are interested in the response of the matrix to high pressure water, the fractures were eliminated from this problem set by setting their porosity equal to zero.

The mathematical model for water movement at Yucca Mountain used in this analysis was the composite porosity model as described in Klavetter and Peters (in preparation). The computer code used for this analysis was TOSPAC (Dudley et al., in preparation) which incorporates the hydrologic model described in the previous reference.

Table 2 Tuff Properties for Problem Set I

	<u>Unit TSw2-3</u>	<u>Unit CHnz</u>
<u>Matrix Properties</u>		
Porosity (n_m)	0.11	0.28
Hydraulic Conductivity ($K_{m,b}$) (m/s)*	1.9×10^{-11}	2.0×10^{-11}
Sat. Curve Parameter - S_r	0.080	0.110
Sat. Curve Parameter - α (1/m)	0.00567	0.00308
Sat. Curve Parameter - β	1.798	1.602
<u>Fracture Properties</u>		
Porosity (n_f)†	0.0×10^{-5}	0.0×10^{-5}
Rock Mass Coefficient of Consolidation ($\alpha'_{bulk} - 1/m$)	5.8×10^{-7}	$26. \times 10^{-7}$
Compressibility of Water (β'_w) is $9.8 \times 10^{-7}/m$		

* 1.0 mm/yr is equal to 3.2×10^{-11} m/s

† The fracture porosity (n_f) is set to zero for the first problem set.

Calculation Results and Discussion

The calculational mesh used to perform the calculations is shown in Figure 2. The cell size ranged from the order of meters in the middle of the column to 1 millimeter at the top of the mesh where the pressure-head boundary condition was applied. The mesh also was made fairly fine at the interface between units TSw2 and CHnz and at the lower boundary. This calculational mesh was used for all the calculations reported on in this document.

The results for the calculational cases investigating the penetration of water into a matrix block are presented in the order listed in Table 1. The figures for each calculational case are presented in the following order:

- A) Pressure head versus distance (top 10 cm of the column) at about 10 different times,
- B) Saturation versus distance at about 10 different times,
- C) Water flux versus distance at about 10 different times,

- D) Pressure head versus time at 3 locations near the top of the column (0.2 cm, 1.0 cm and 10 cm)
- E) Saturation versus time at 3 locations near the top of the column
- F) Water flux versus time at 3 locations near the top of the column

The results of Case 1 (No flow initial condition - 20 m pressure head applied for 1 minute) are seen in Figures 3-8. Figure 3 shows that the pressure pulse penetrates the matrix block about 3 cm. Figure 4 shows that matrix block saturation is increased by 5 percentage points or more to a depth of about 0.5 cm. The change in saturation at a depth of 10 cm is negligible. According to Figure 5 the water flux is very high at the top surface of the block at the beginning of the simulation (10^{-6} m/s \approx 30,000 mm/yr) but quickly drops toward zero (\approx 1 mm/yr at 1 wk) after the upper boundary condition is reset to zero flux. Figures 6-8 indicate that there is little change in hydrologic parameters except very near the top surface of the matrix block. For example, according to Figure 7 the saturation at 1

cm depth rises 3 percentage points about one-half day after the pressure-pulse is applied and then slowly goes back toward the initial condition over the following month. At a time of 10^7 seconds (approximately 4 months) the average saturation for the top 10 cm of the block has increased about 0.3 of a percentage point.

The results of Case 2 (No flow initial condition - 20 m pressure head applied for 10 minutes) are seen in Figures 9-14. As one would expect, the water penetrates further into the matrix block than for the previous case, but the affect is not ten times as large. For example, in this case the saturation has increased by 5 percentage points or more to a depth of 1.5 cm while in the previous case this point reached a depth of 0.5 cm. Figure 13 indicates the average water saturation to a depth of 10 cm at 4 months has increased about 1 percentage point while for the previous case the increase in average saturation was about 0.3 percentage point.

The initial water injection rate seen in Figure 11 is about the same as that seen in Figure 5. However, it falls off rapidly during the period when the 20 m pressure-head boundary condition is applied at the top of the column. Thirty seconds after the pressure-head boundary condition is applied the water flux is 10^{-6} m/s while at 10 minutes it is 2×10^{-7} m/s. This "choking" of flow is the reason that Case 2, which has the 20 m pressure-head boundary condition ten times longer than Case 1, does not inject ten times as much water as Case 1.

The results of Case 3 (No flow initial condition - 20 m pressure head applied for 100 minutes) are seen in Figures 15-20. Again we see an increase in water penetration when these figures are compared to the previous set. Because the water injection rate decreases with time (10^{-6} m/s at 30 seconds and 10^{-7} m/s at 100 minutes) this case injects less than 10 times as much water as case 2. According to Figure 16, the saturation has increased by 5 percentage points down to depth of about 5 cm (Case 1: 0.5 cm, Case 2: 1.5 cm) and there is a 3 percentage point increase in saturation down to 10 cm depth at 4 months (case 1: 0.3 point, Case 2: 1.0 point). The matrix at a depth of 0.01 m is nearly saturated at 3×10^3

seconds (1 hour) but desaturates fairly quickly after the upper boundary condition is reset to a no flow condition.

The results of Case 4 (0.1 mm/yr initial condition - 20 m pressure head applied for 1 minute) are seen in Figures 21-26. Comparison of the "no flow" case (Case 1) with these results shows that there is much less penetration in this case. For example, at a depth of 0.5 cm the saturation changed from .88 to .91 for case 4 while for case 1 it changed from .65 to .70. The reason that there is less penetration apparent is the initial saturation for Case 4 is larger (88%) than that for Case 1 (65%). Therefore, the Case 4 matrix has a higher hydraulic conductivity (about ten times larger) than that for Case 1. This higher conductivity allows water to move much more freely at depth in Case 4 (compare Figures 8 and 26 at times greater than 100 seconds), so the change in saturation for Case 4 is less than that for Case 1. The increase in water saturation at 0.1 meter depth is negligible.

The results of Case 5 (0.1 mm/yr initial condition - 20 m pressure head applied for 10 minutes) are seen in Figures 27-32. The trends seen in previous cases are reproduced here. The water injection rate resulting from the 20 m pressure-head boundary condition decreases from about 5×10^{-7} m/s at 30 seconds to about 1×10^{-7} m/s at 10 minutes. The saturation in the matrix has increased from that seen in Case 4, but by the time approximately 1 month has passed the matrix has returned to its initial state of saturation. Inspection of the flux curves for the time period of 3 hr through 1 month for Cases 2 and 5 (Figures 11 and 29) reveals that the water injected into the matrix in Case 5 is able to move more quickly than the water in Case 2, allowing the matrix to quickly return to its initial state. This case is the first to cause the matrix to become saturated to a depth of 0.01 meters.

The results of Case 6 (0.1 mm/yr initial condition - 20 m pressure head applied for 100 minutes) are seen in Figures 33-39. In this case the matrix is saturated to a depth of about 2 cm at the end of 100 minutes. However, the high conductivity of the matrix allows water to drain from the matrix and it returns to within 1 percentage point of its initial state in about

one month (see Figures 34 and 37). The matrix is essentially back to the initial condition within 1 year.

The results of these calculations indicate that the application of high-pressure water to matrix material, like that found in the repository zone, will not cause water penetration to large depths (<5 cm). They also show the water quickly redistributes so that the increase in matrix saturation is small in the region near where the water was injected (<3 percentage points rise in saturation at 1 month).

General Discussion and Conclusions

It has been a general concern that the application of drilling water to the fractured tuff may cause the in-situ conditions to change significantly. One bound may be evaluated by assuming that the water is injected into the fractures and then over a long period of time it moves into the matrix. The change in matrix saturation depends on the relative volumes of the matrix and the fractures because the water is first stored in the fractures and then moves into the matrix.

$$\Delta S_m = n_f / n_m \quad (1)$$

Values of the parameter n_f are probably in the range of 10^{-5} to 10^{-3} (Sinnock et al., 1984; Peters et al., 1984) while the parameter range for n_m in TSw2 is from 0.05 to 0.15. The maximum change in matrix saturation then is of the order of $10^{-3}/0.05 = 0.02$ or less. Thus, it appears that pervasive flooding of the fractures will not significantly affect the matrix saturation.

The matrix may take up water during the time that high pressure water is being injected into the rock mass, forming pockets of high saturation around the regions where drilling occurred. The upper bound on this change in matrix saturation was calculated by assuming that the high-pressure water is applied to the matrix throughout the drilling process. (In the actual case, some portions of the rock mass will see water under lower pressures than the pump pressure and for periods of time shorter than the actual drilling takes place.) The results of this sort of bounding calculation have been discussed in the previous section. The conclusion reached was that no significant change in saturation will be noticeable after the passage of a month or so.

Thus, it appears that drilling with water will not significantly affect the state of saturation of the rock. This statement assumes that relatively low-pressure water (<30 psig) is applied to the rock for relatively short periods of time (<100 minutes). It also implicitly assumes that there is an attempt to limit the amount of water used underground. For example, it is obvious that allowing a pond of water to stand for many weeks must affect the local state of saturation. These results and conclusions are subject to the limitations of the models used and the data available, especially the conductivity curves for the matrix.

II) Experiments Investigating the Movement of Water in a Fractured, Unsaturated Tuff

Experiments in the Exploratory Shaft are being planned to investigate the flow of water in an unsaturated, fractured tuff. The results of these experiments directly affect the conceptual model of water flow in unsaturated, fractured tuff, and may be used to validate computer codes. Performance assessments of the Yucca Mountain site require good understanding of the manner in which water flows in Yucca Mountain and validated computer codes to do the calculations required for licensing.

The second analysis set (titled "Response of a Tuff Column to Changes in Flux") discussed simulates an experiment that investigates the response of a column of rock to increases in flux where the flow of water at the final steady-state condition is primarily in the matrix. The purpose of these calculations is to look at the response of the fractured tuff to changes in flux and to estimate the time it takes for the upper meter or so of the rock column to move from one steady-state condition to another. Performance assessment planning may be affected by gaining understanding of the data that may be available from this sort of experiment and whether the results can be used for developing conceptual models and for computer model validation.

RESPONSE OF A TUFF COLUMN TO CHANGES IN FLUX

Definition of Analysis

The second analysis set investigated the response of a fractured tuff column to changes in flux. The fractured tuff column and boundary conditions are shown in Figure 39. The stratigraphy is that found at drill hole USW G-4 (Ortiz et al., 1985). The block extends from a position roughly in the center of unit TSw2 to the water table.

The lower boundary condition is a pressure-head condition set by the water table. There are two different initial conditions defined in Table 3. The first is a no flow condition that results in a saturation at the top of the column of about 65% for the material properties used in this calculation. The second initial condition is defined by having a steady flow of 0.1 mm/yr throughout the column. This results in a saturation at the top of the column of about 88%. The upper boundary condition is changed at the beginning of the calculation to a constant flow rate of 0.5 mm/year.

Table 3 Calculational Cases for Investigating the Response of a Tuff Column to Changes in Flux

Case	Initial Condition (flux - mm/yr)
1	0.0
2	0.1

The mathematical model for water movement at Yucca Mountain used in this analysis was the composite porosity model as described in Klavetter and Peters (in preparation). The computer code used in this analysis was TOSPAC (Dudley et al., in preparation) which incorporates the hydrologic model described in the previous reference.

The properties of the two units (TSw2 and CHnz) are listed in Table 4. The paper by Klavetter and Peters (in preparation) contains a discussion of the terms and nomenclature used in this table. Because we are interested in the response of the fractured tuff to changes in flux the fracture porosity used is that listed in Table 4; the fracture porosity was not set to zero as it was in the previous analysis.

Table 4 Tuff Properties for Problem Set II

	<u>Unit TSw2-3</u>	<u>Unit CHoz</u>
<u>Matrix Properties</u>		
Porosity (n_m)	0.11	0.28
Hydraulic Conductivity ($K_{m,b}$) (m/s)*	1.9×10^{-11}	2.0×10^{-11}
Sat. Curve Parameter - S_r	0.080	0.110
Sat. Curve Parameter - α (1/m)	0.00567	0.00308
Sat. Curve Parameter - β	1.798	1.602
<u>Fracture Properties</u>		
Porosity (n_f) [†]	$18. \times 10^{-5}$	4.6×10^{-5}
Compressibility ($\delta n_f / \delta \sigma'$) (1/m)	$12. \times 10^{-8}$	2.8×10^{-8}
Hydraulic Conductivity ($K_{f,b}$) (m/s)	3.1×10^{-9}	9.2×10^{-9}
Fracture Saturation Coefficients are $S_r = 0.0395$, $\alpha = 1.285/m$, $\beta = 4.23$		
Rock Mass		
Coefficient of Consolidation ($\alpha'_{bulk} - 1/m$)	5.8×10^{-7}	$26. \times 10^{-7}$
Compressibility of Water (β'_w) is $9.8 \times 10^{-7}/m$		
* 1.0 mm/yr is equal to $3.2 \times 10^{-11} m/s$		

Results and Discussion

The results for the calculational cases investigating response of a tuff column to changes in flux are presented in the order listed in Table 3. The figures for both calculational cases are presented in the following order:

- A) Pressure head versus distance (from the top of the column to the water table) at 15 different times,
- B) Saturation versus distance at 15 different times,
- C) Water flux versus distance at 15 different times,

- D) Pressure head versus distance (top 3 meters of the column) at 15 different times,
- E) Saturation versus distance (top 3 meters of the column) at 15 different times,
- F) Water flux versus distance (top 3 meters of the column) at 15 different times,

- G) Pressure head versus time at 3 locations near the top of the column (1.0 cm, 10. cm and 100 cm)
- H) Saturation versus time at 3 locations near the top of the column
- I) Water flux versus time at 3 locations near the top of the column

The first set of figures (Fig. 40-48) show the results of increasing the flux from 0.0 mm/year to 0.5 mm/year. Figures 40-42 show the pressure head, saturation, and flux profiles for the entire column for the entire simulation. The first pressure-head profile that is labeled in these figures is the one at 100 years; the profiles at earlier times are very near the initial condition and are difficult to separate on these figures. Figure 42 shows that flux at the top of the column very quickly (≈ 100 years) reaches the steady-state value of 0.5 mm/year. However, Figures 40 and 41 indicate that the steady-state pressure head and saturation at the top of the column is not reached until about 10,000 years after the flux was changed at the top of the column. These figures indicate that it takes approximately 500 years for the top of the column to reach pressure head and saturation values halfway between the initial condition and the final,

steady-state condition. Figures 40 and 41 show that, in this matrix-dominated flow regime, the whole column reaches steady state at about the same time. Figure 41 indicates that the water input to the column spreads very rapidly due to the large pressure-head gradients (see Figure 40). Therefore, the pressure-head and saturation at the top of the column cannot reach steady state until the rest of the column reaches steady state. In a field experiment, the flow would be three dimensional not one dimensional as it was in these calculations. This implies that it may not be possible to do this experiment at all because a large portion of the mountain would have to have water injected into it before the experimental region would reach steady state.

Figures 43-45 show pressure-head, saturation, and flux profile plots for the top three meters of the mountain. Figures 43 and 44 show the pressure head and saturation profiles rising in a uniform manner to the steady-state condition at 10,000 years. Figure 45 shows the flux profile that is very steep at early times (0 - \approx 10 years) and then flattens out at the final condition in later years (>200 years).

Figures 46-48 show the pressure head, saturation, and flux versus time at three different depths (1 cm, 10 cm and 100 cm). Figures 46 and 47 indicate that the pressure head and saturation at three different depths are approximately the same throughout the simulation and that the steady-state condition is reached at all three depths at approximately the same time (10,000 years). Figure 48 shows the time when the flux reaches its steady-state value is a function of depth. At about 100 years the flux is nearly at its steady-state value at all three depths.

Figures 49-57 show the results of a simulation where the flux was increased from 0.1 mm/year to 0.5 mm/year. The initial saturation in the column has increased considerably (compare Figures 41 and 50) with the initial saturation at the top of the column being about 65% for the previous case and about 88% for this case. However, the results seen in these figures are qualitatively the same as those for the previous case. It takes a few years (\approx 100 years) for the flux at the top of the column to reach steady state (see Figure 57) but it takes a very long time for the pressure

head and saturation to respond to the change in flux. In both cases, it takes about 500 years for the pressure head and saturation at the top of the column to reach values halfway between the initial condition and the steady-state condition (compare Figures 40 and 49, and Figures 41 and 50). In both cases, it takes about 10,000 years to reach steady state. The pressure-head gradient, which spreads the incoming water, is less in this case than in the previous case but the matrix conductivity has increased by about a factor of ten over that of the previous case, allowing the water to be spread out in about the same manner as in the previous case.

General Discussion

The results of simulations of both cases show the same result. The hydrologic parameters that are measurable (pressure-head and saturation) respond very slowly to changes in flux if the flow of water is primarily in the matrix. Over-driving the system by increasing the flux (e.g., 5.0 mm/yr instead of 0.5 mm/year) will cause pervasive flow of water in the fractures to be initiated (this is not desirable because the purpose of a part of the experiment will be to investigate hydrologic phenomena for the situation where the water flow is primarily in the matrix). It appears that it may not be possible to perform a field-scale experiment to investigate the matrix-dominated flow of water in a fractured, porous medium. Lab-scale experiments using highly conductive matrix materials may be the only possibility for investigating matrix-dominated flow of water in a fractured, porous medium. These results and conclusions are subject to the limitations of the models used and the data available, especially the conductivity curves for the matrix. However, major changes in the data would probably be required in order to significantly affect the qualitative results.

References

Dudley, A. L., R. R. Peters, M. S. Tierney, E. A. Klavetter, J. H. Gauthier, and M. Wilson. In preparation. "Total Systems Performance Assessment Code (TOSPAC) Volume 1: Physical and Mathematical Bases," SAND85-0002, Sandia National Laboratories, Albuquerque, NM.

Klavetter, E. A., and R. R. Peters. In preparation "Estimation of Hydrologic Properties for an Unsaturated, Fractured Rock Mass," SAND84-2642, Sandia National Laboratories, Albuquerque, NM.

Ortiz, T. S., R. L. Williams, F. B. Nimick, B. C. Whittet, and D. L. South. 1985. "A Three-Dimensional Model of Reference Thermal/Mechanical and Hydrological Stratigraphy at Yucca Mountain, Southern Nevada," SAND84-1076, Sandia National Laboratories, Albuquerque, NM.

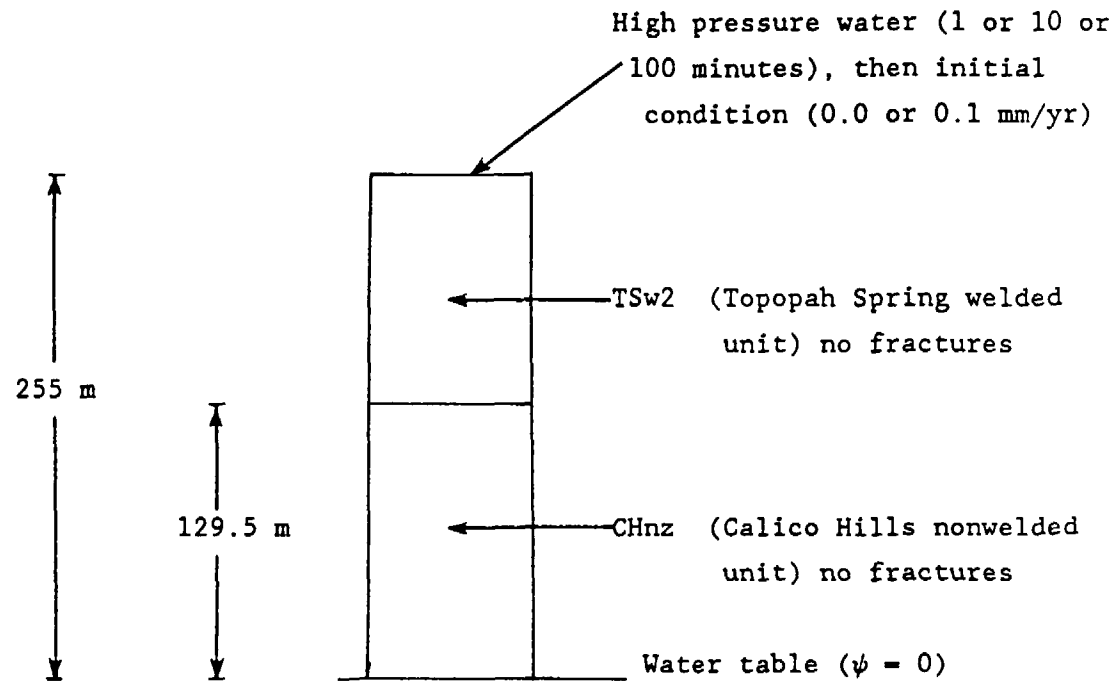


Figure 1 Geometry and Boundary Conditions for the Problem Set
"Application of High Pressure Water to a Matrix Block"

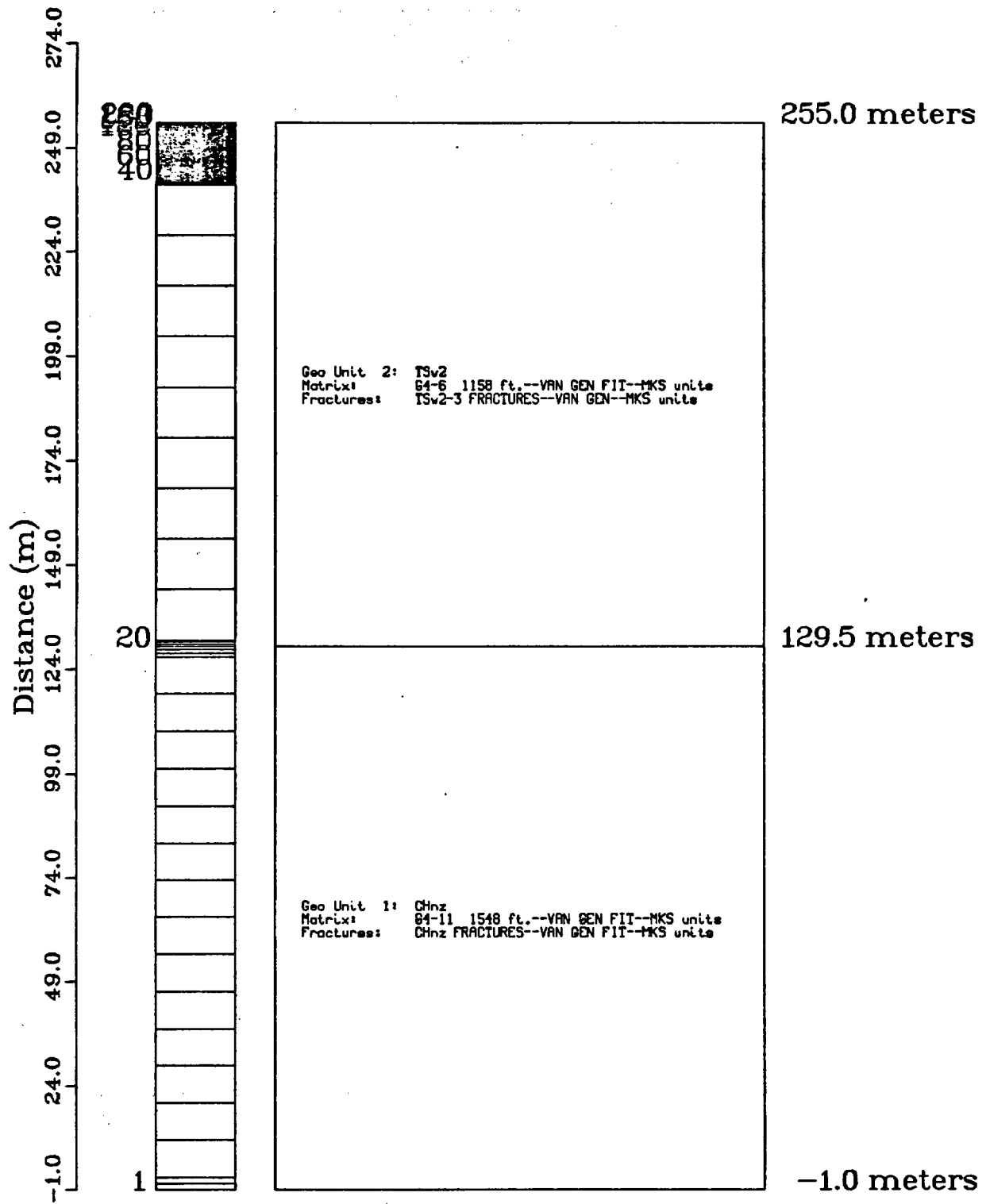


Figure 2. Computational mesh

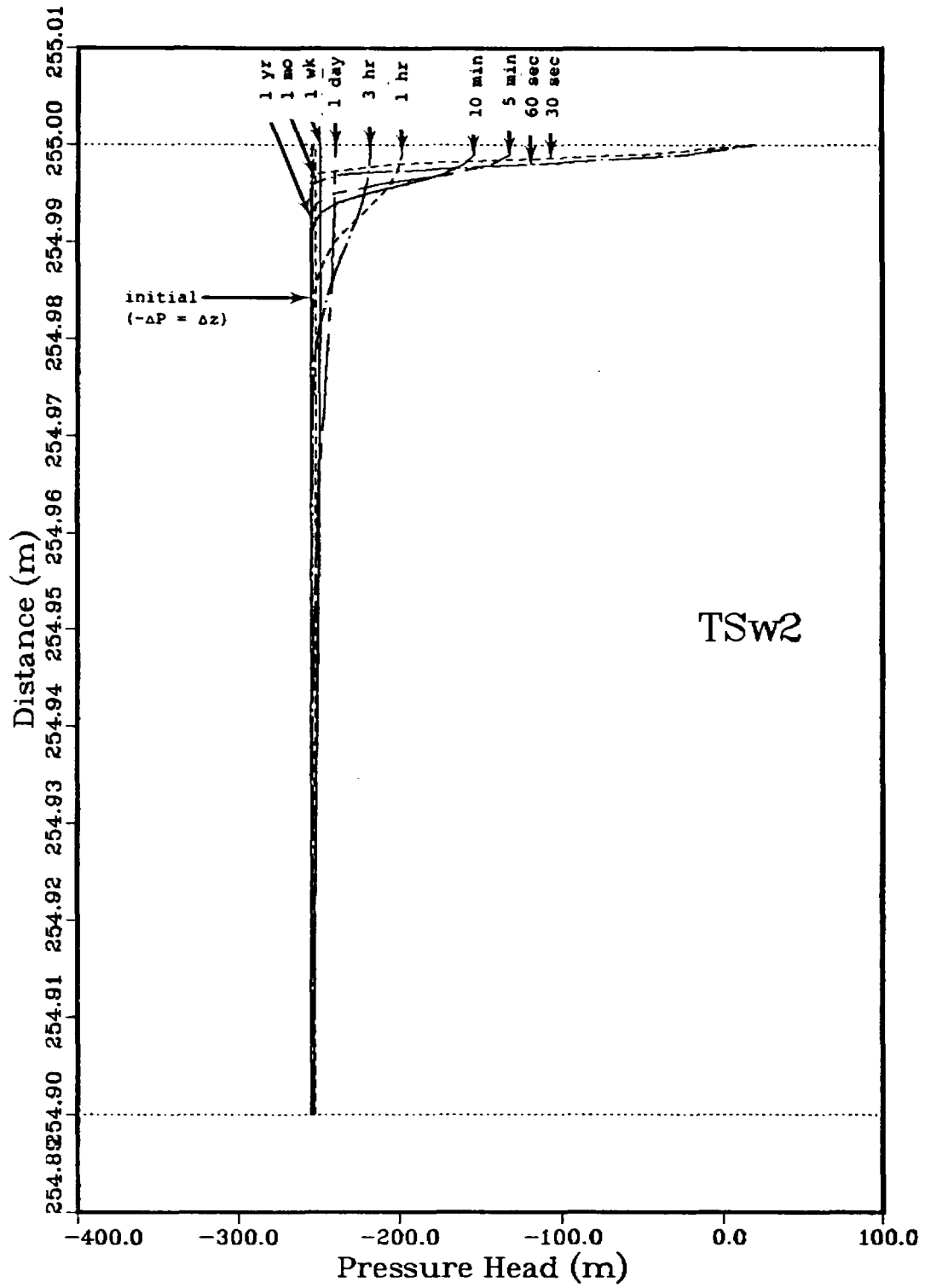


Figure 3. Matrix-block water penetration
 Initial condition - no flow
 20 m pressure head for 1 minute

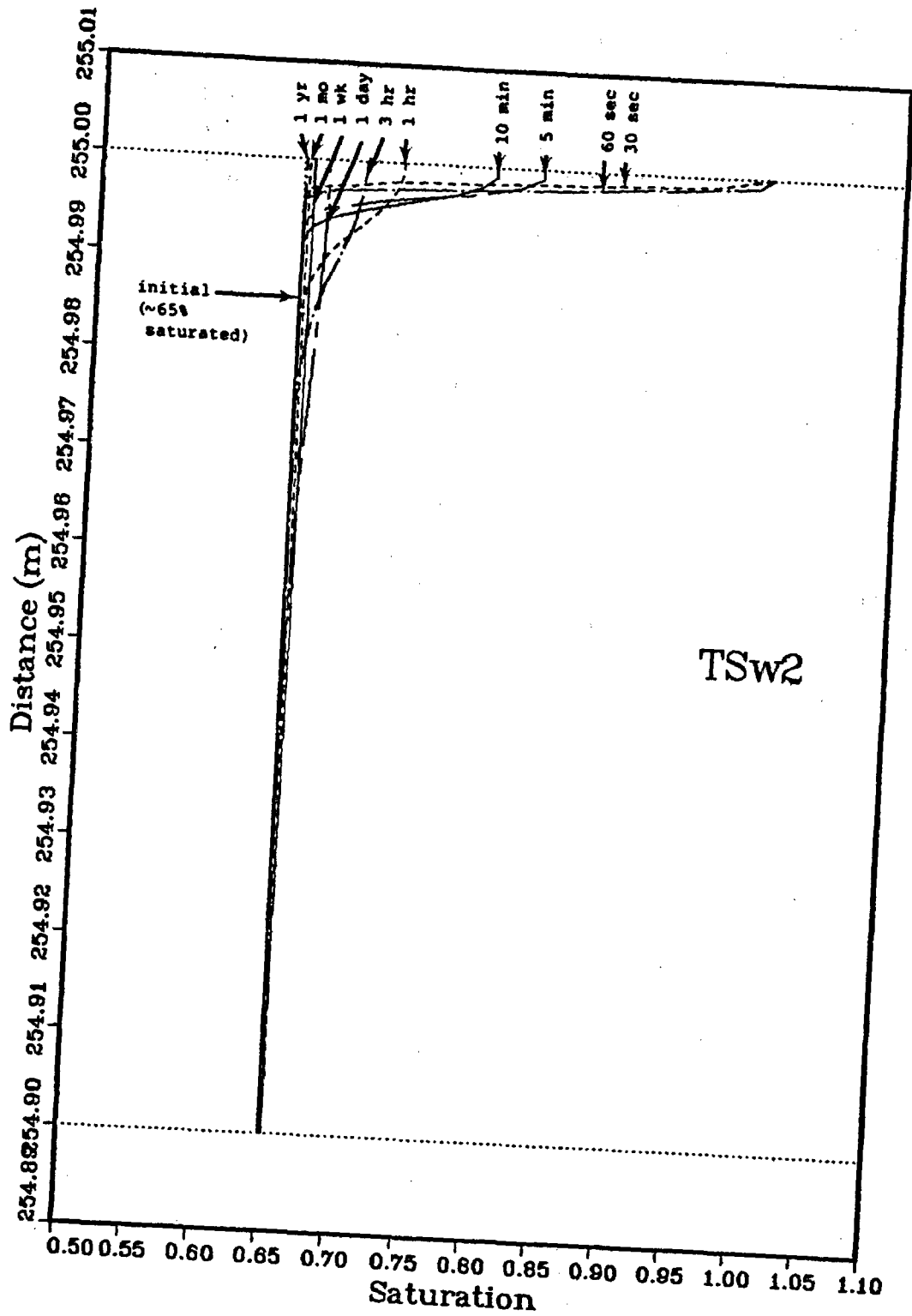


Figure 4. Matrix-block water penetration
 Initial condition - no flow
 20 m pressure head for 1 minute

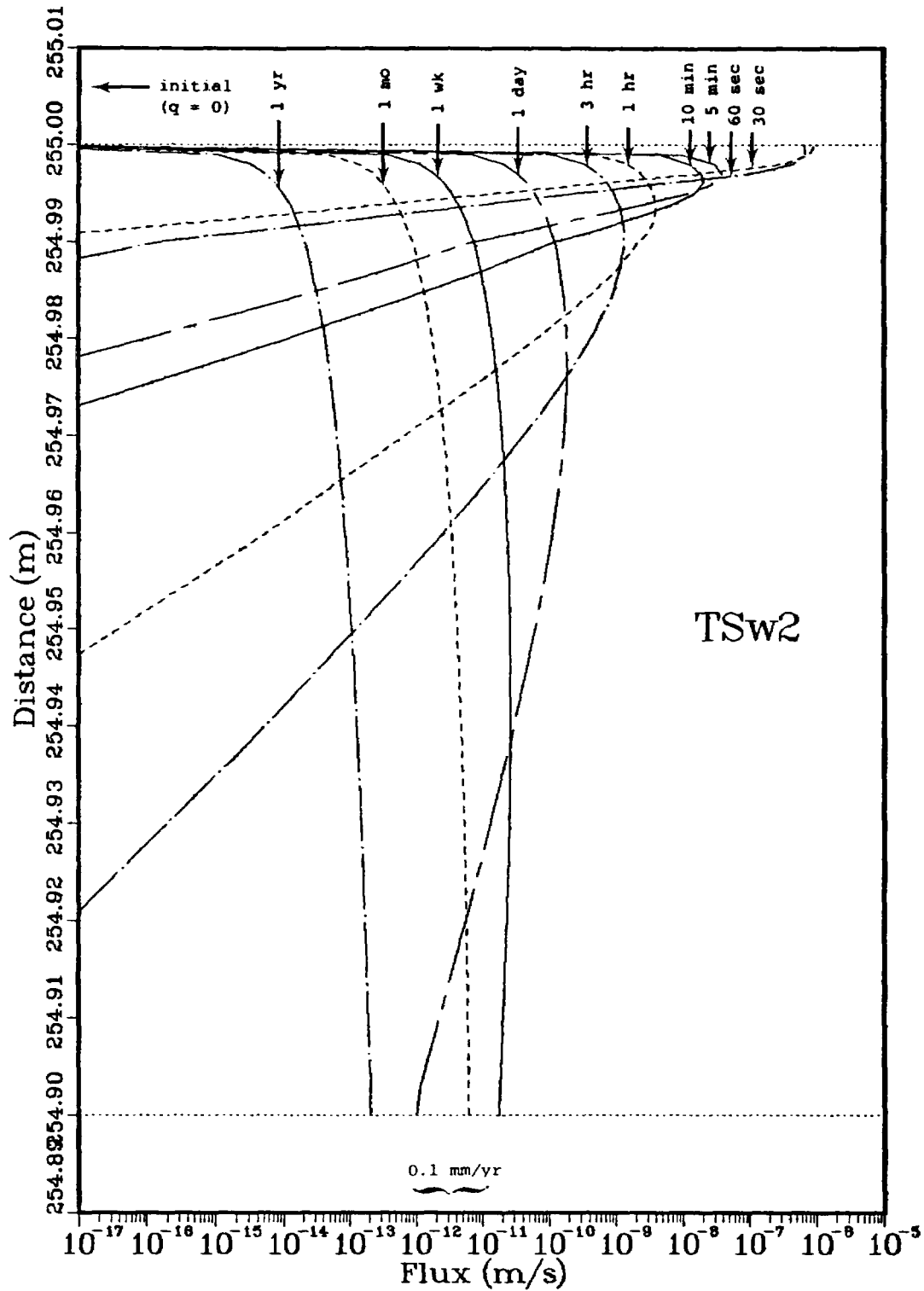


Figure 5. Matrix-block water penetration
 Initial condition - no flow
 20 m pressure head for 1 minute

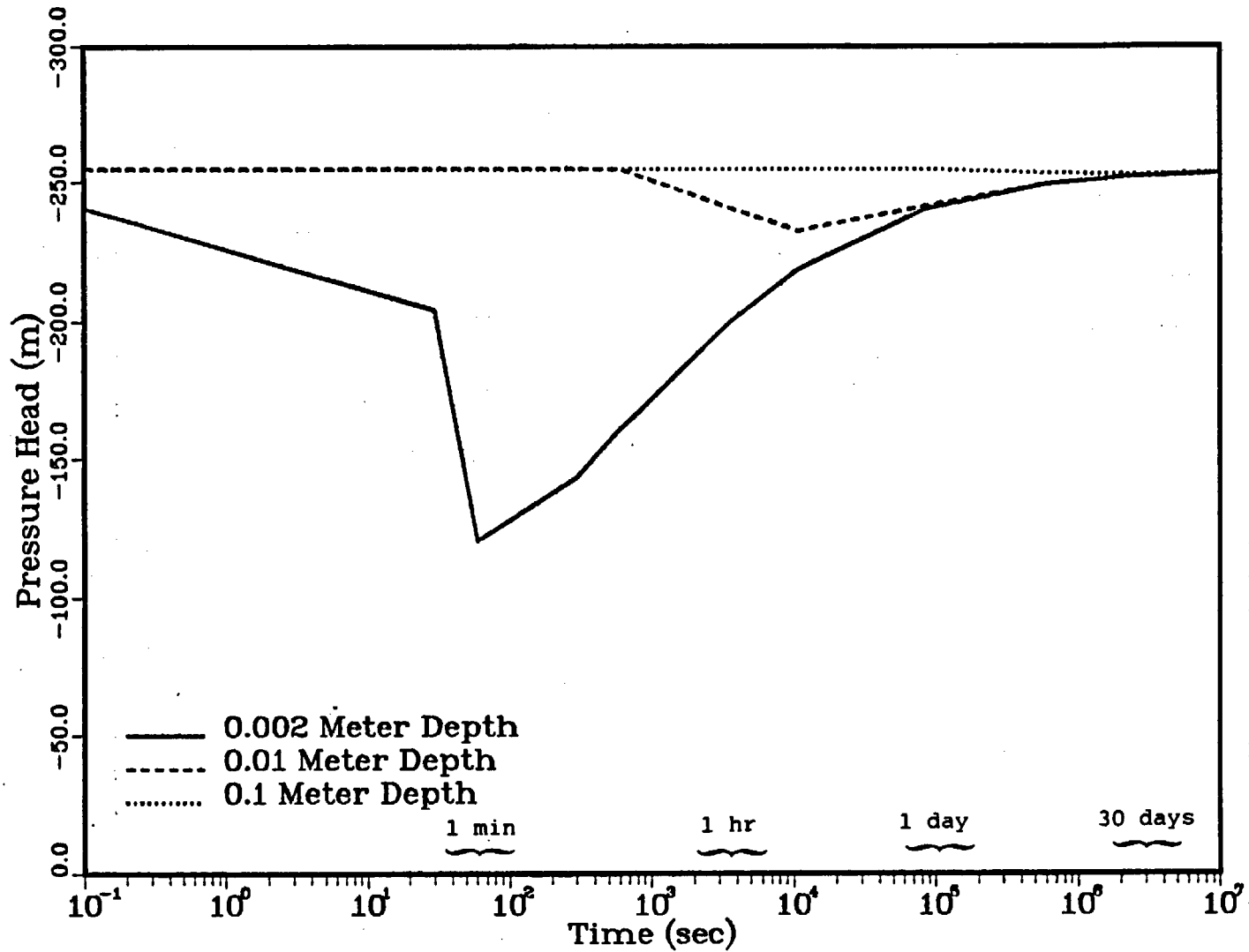


Figure 6. Matrix-block water penetration
 Initial condition - no flow
 20 m pressure head for 1 minute

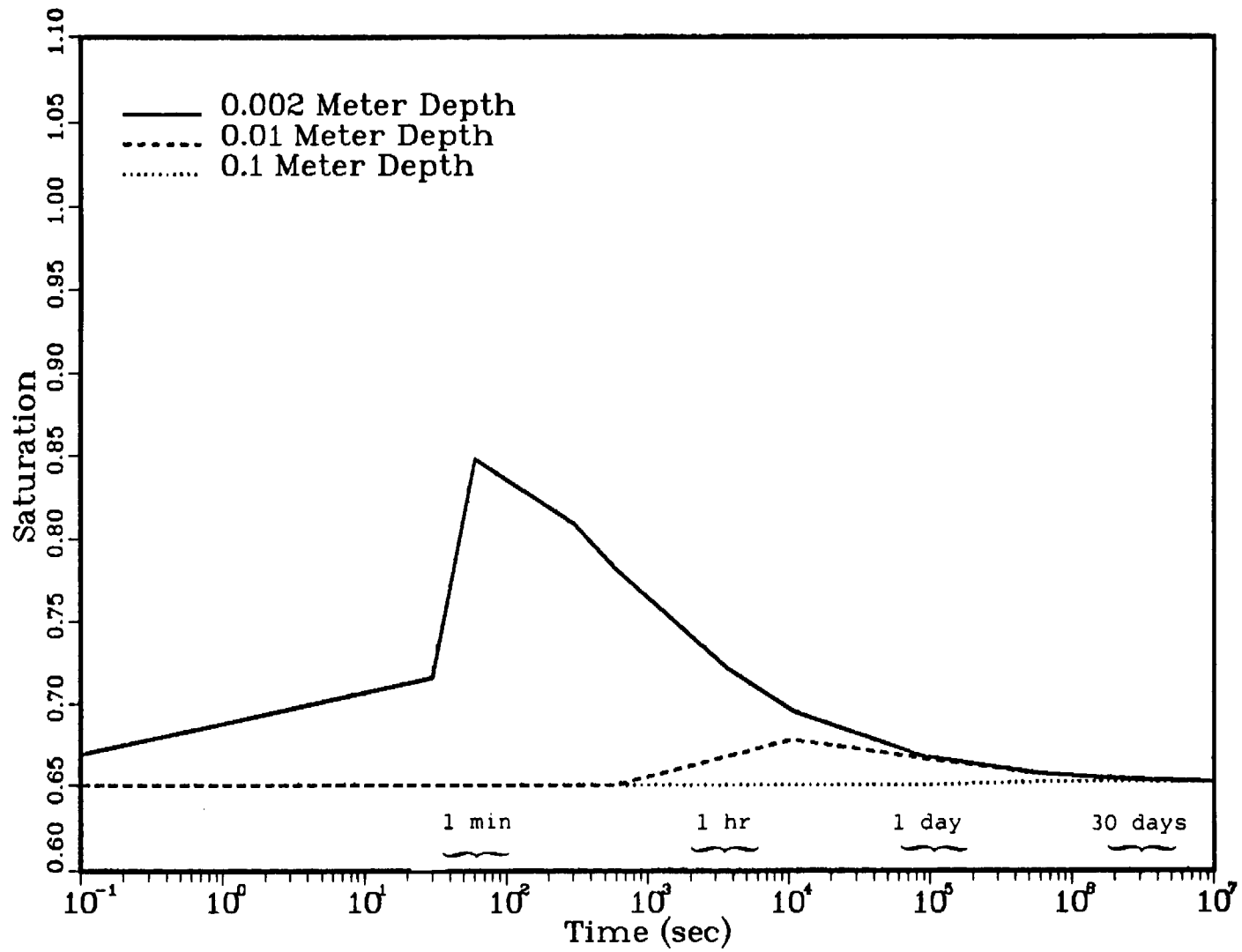


Figure 7. Matrix-block water penetration
Initial condition - no flow
20 m pressure head for 1 minute

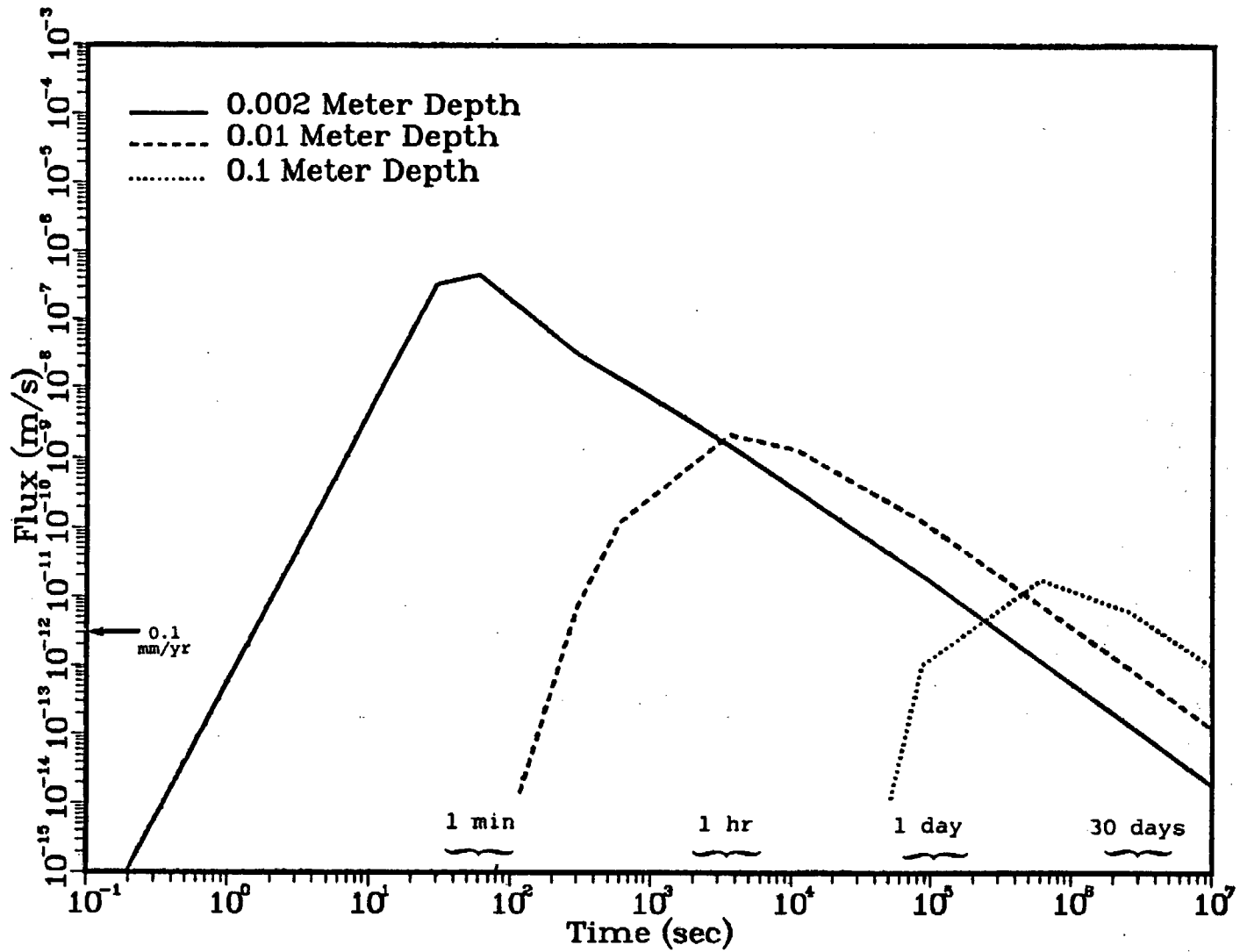


Figure 8. Matrix-block water penetration
 Initial condition - no flow
 20 m pressure head for 1 minute

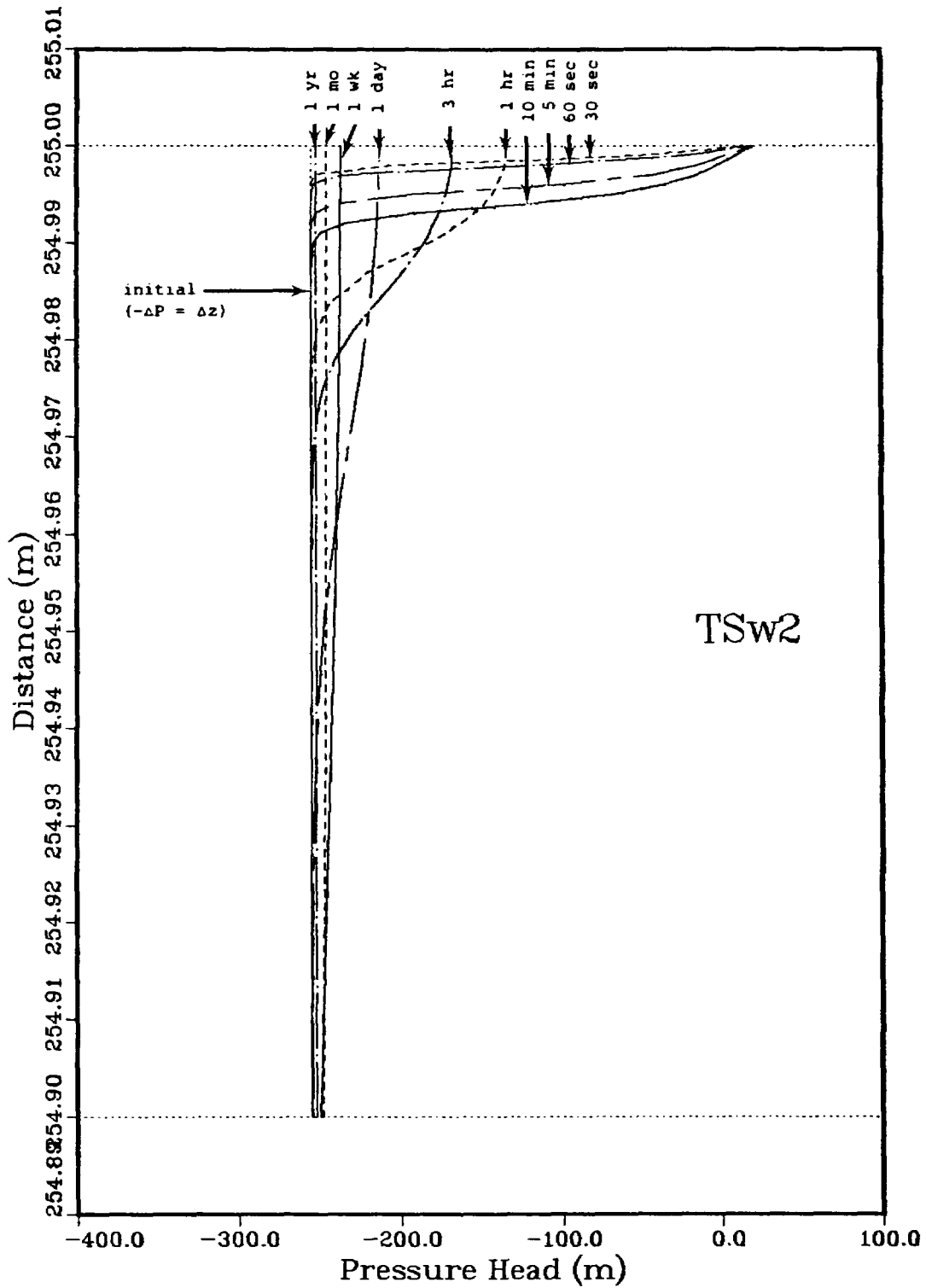


Figure 9. Matrix-block water penetration
 Initial condition - no flow
 20 m pressure head for 10 minutes

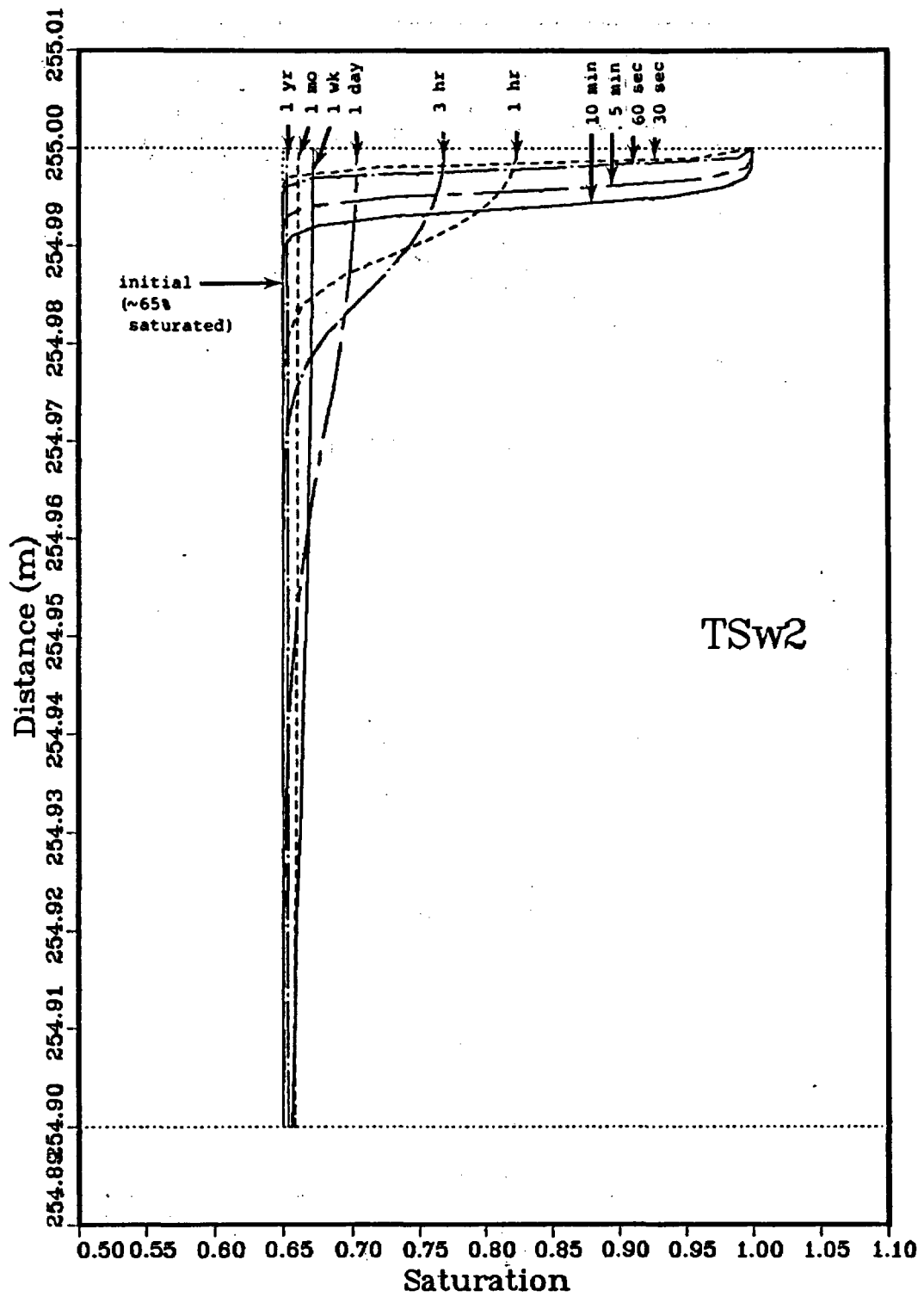


Figure 10. Matrix-block water penetration
 Initial condition - no flow
 20 m pressure head for 10 minutes

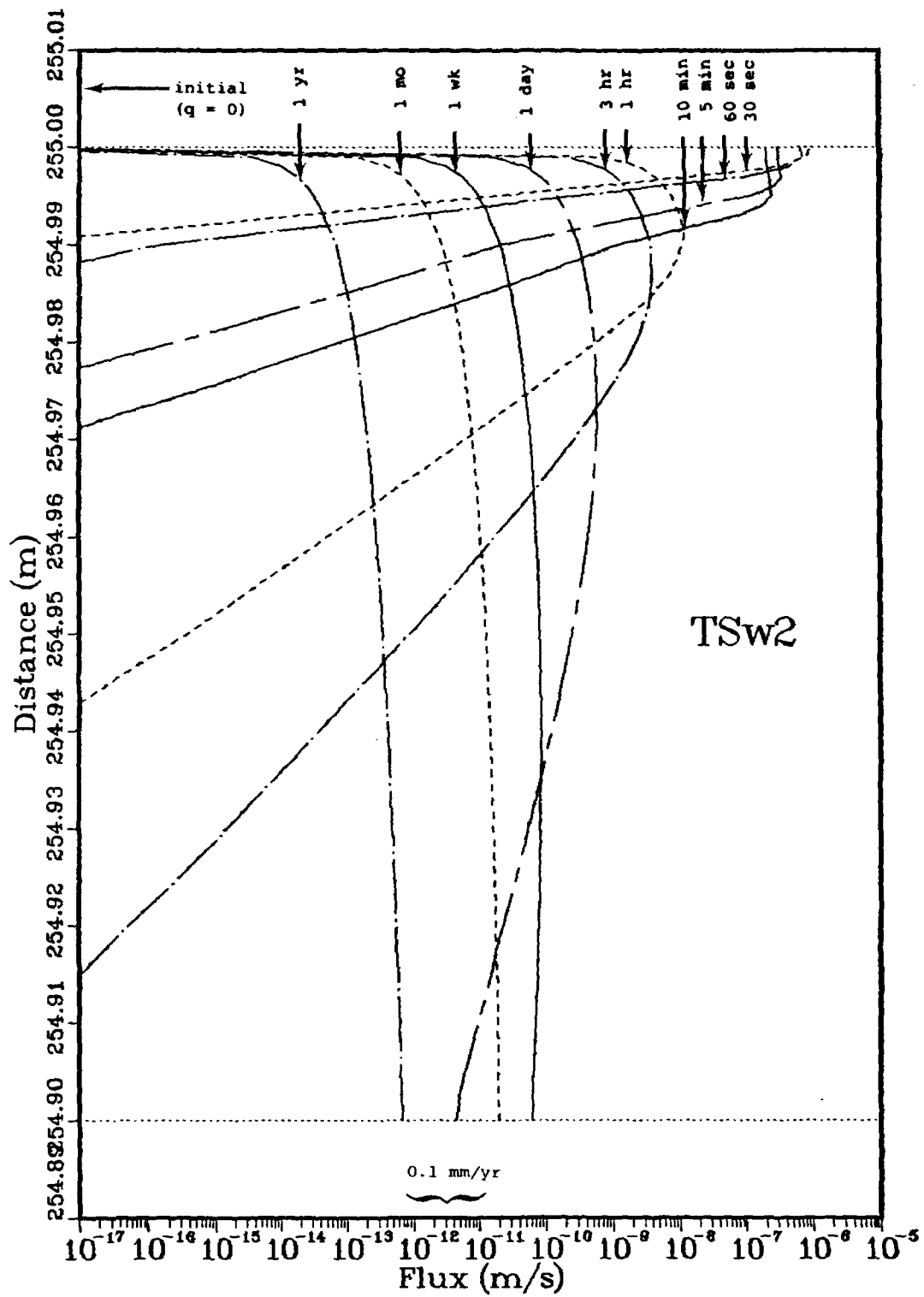


Figure 11. Matrix-block water penetration
 Initial condition - no flow
 20 m pressure head for 10 minutes

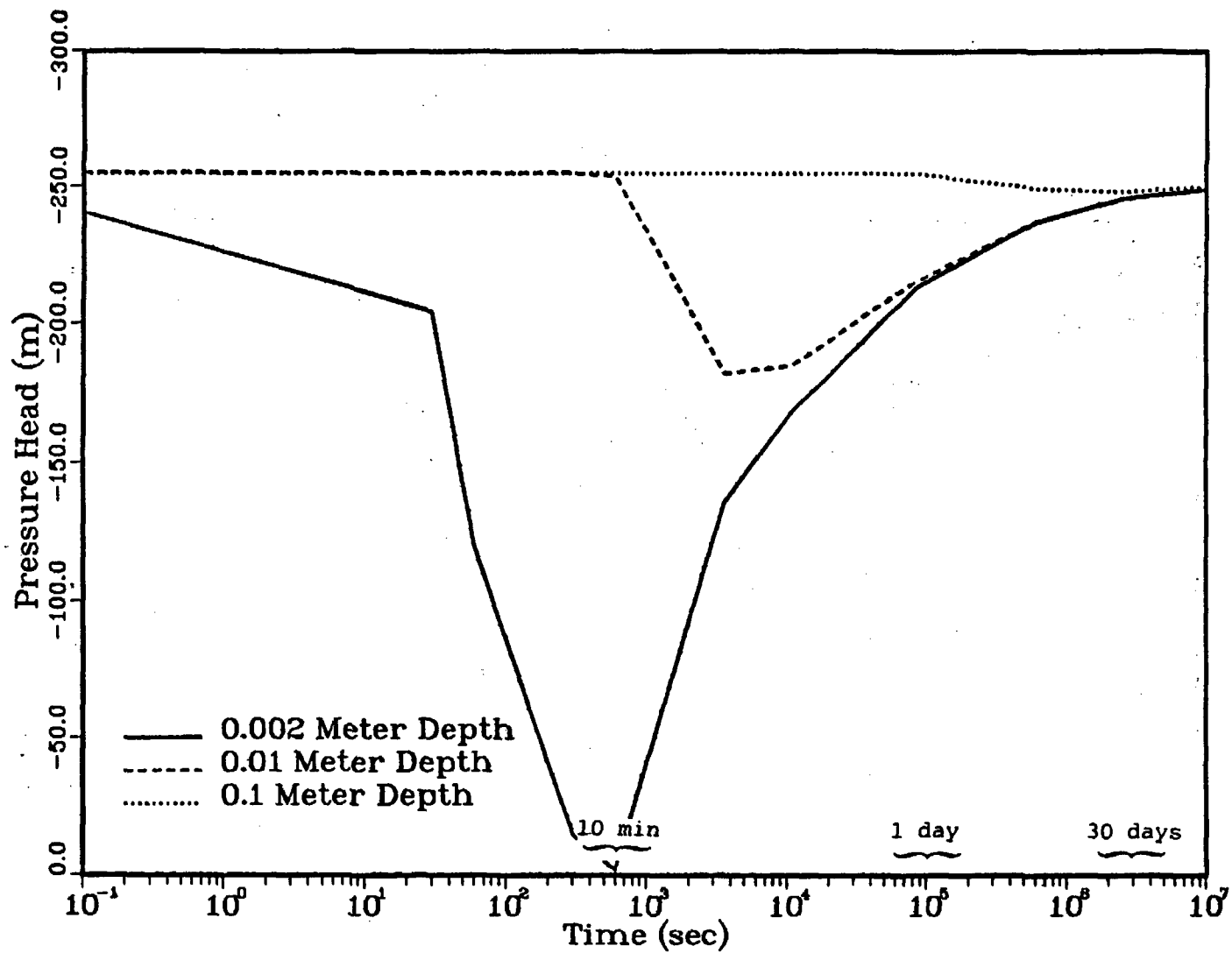


Figure 12. Matrix-block water penetration
Initial condition - no flow
20 m pressure head for 10 minutes

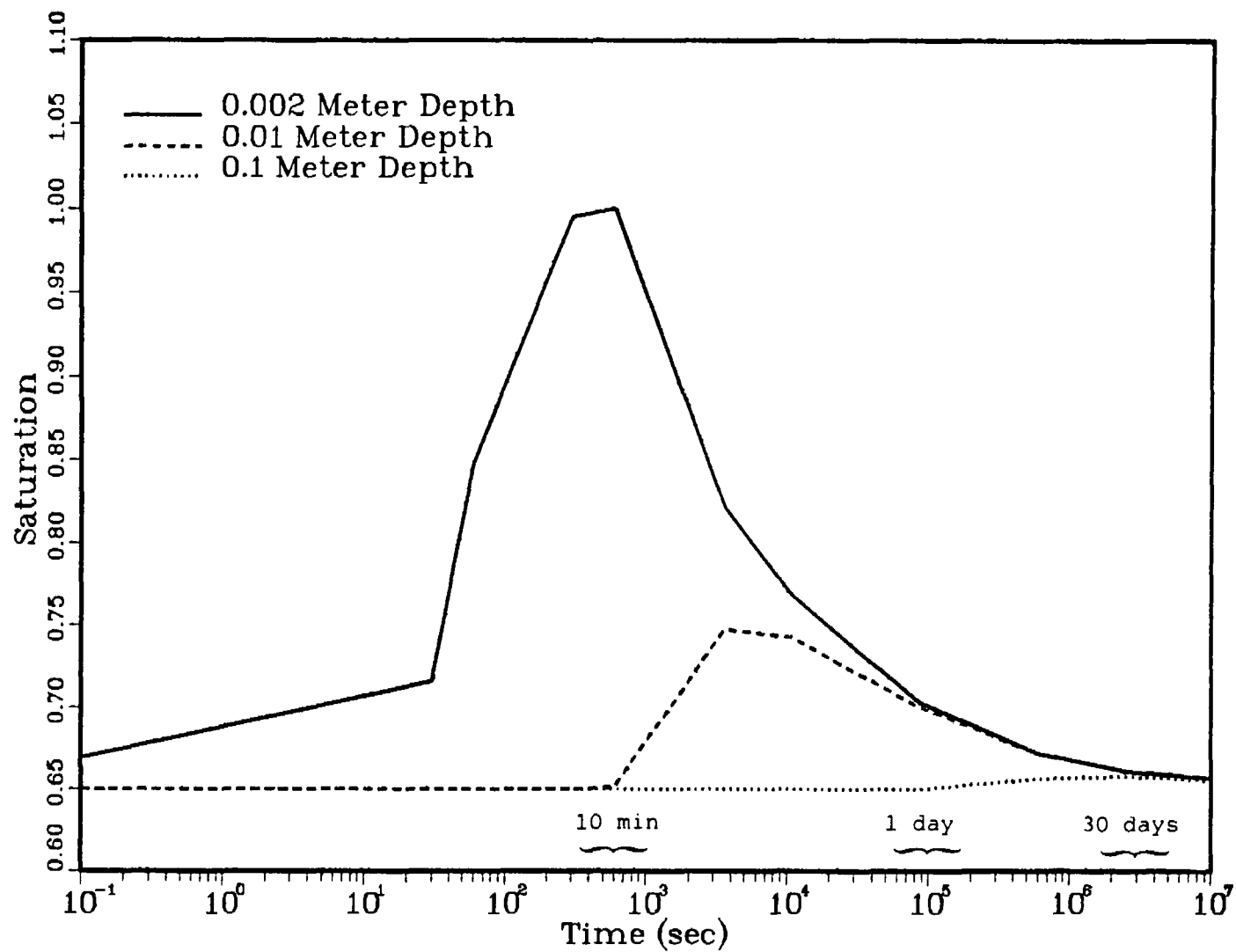


Figure 13. Matrix-block water penetration
 Initial condition - no flow
 20 m pressure head for 10 minutes

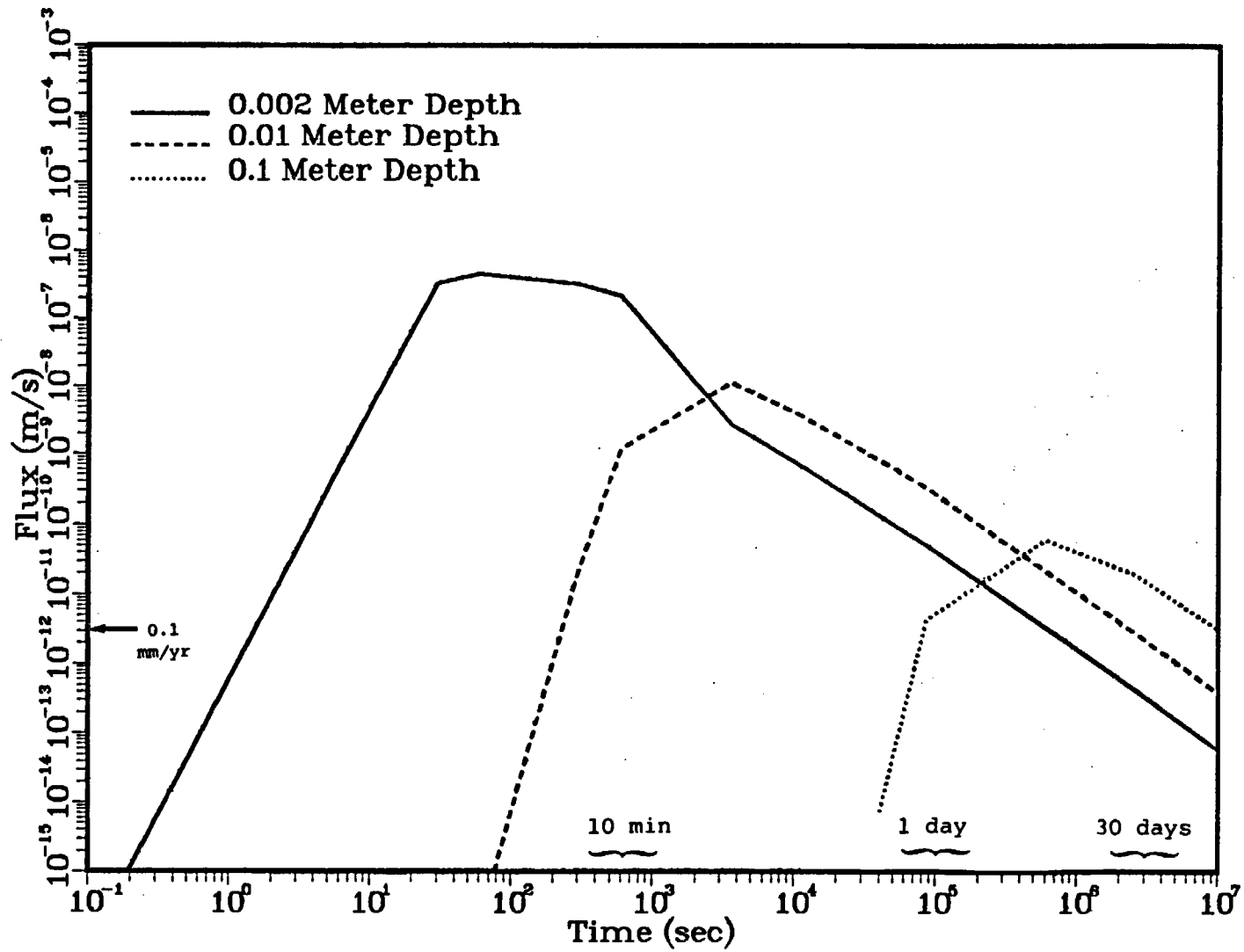


Figure 14. Matrix-block water penetration
 Initial condition - no flow
 20 m pressure head for 10 minutes

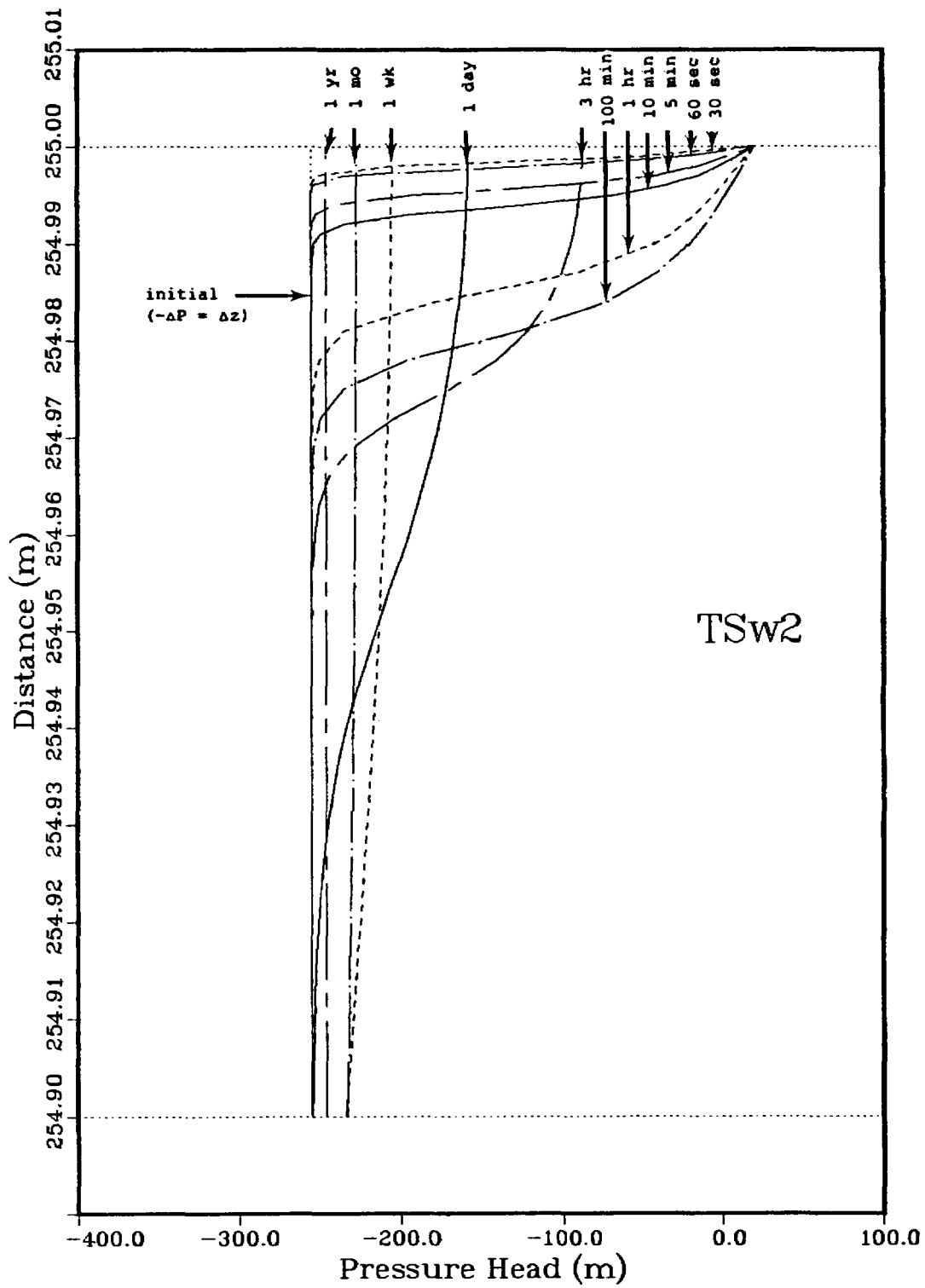


Figure 15. Matrix-block water penetration
 Initial condition - no flow
 20 m pressure head for 100 minutes

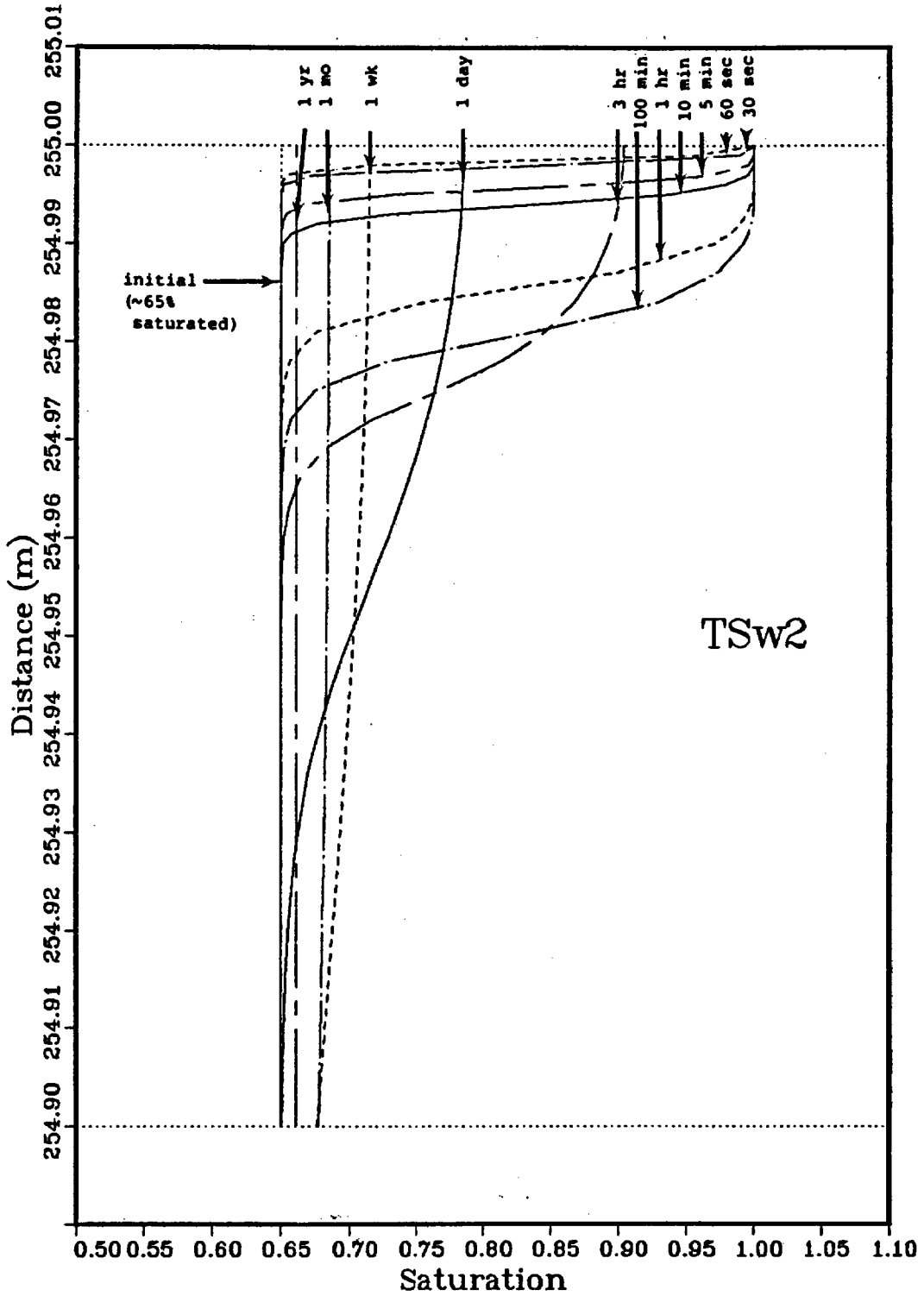


Figure 16. Matrix-block water penetration
 Initial condition - no flow
 20 m pressure head for 100 minutes

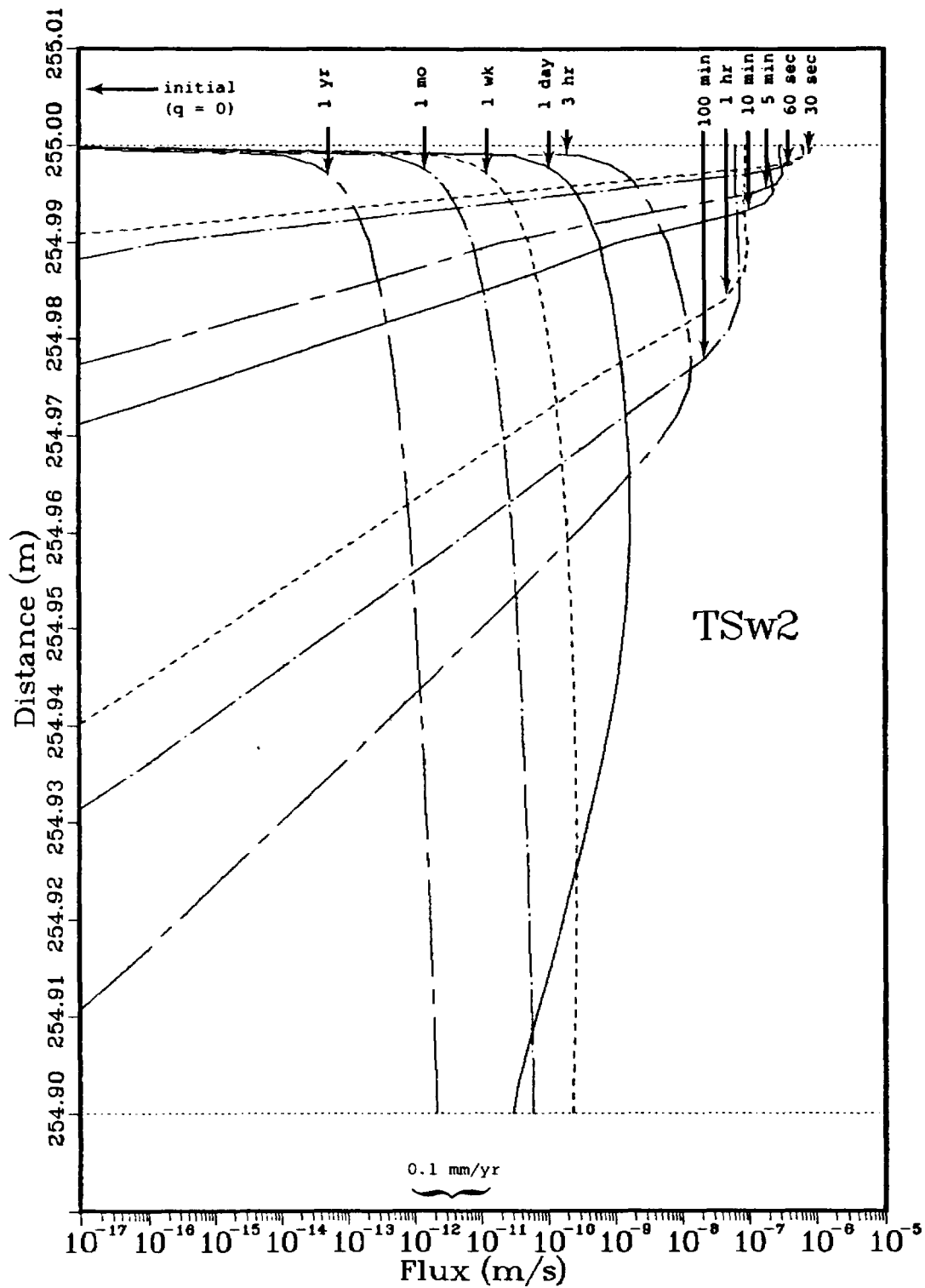


Figure 17. Matrix-block water penetration
 Initial condition - no flow
 20 m pressure head for 100 minutes

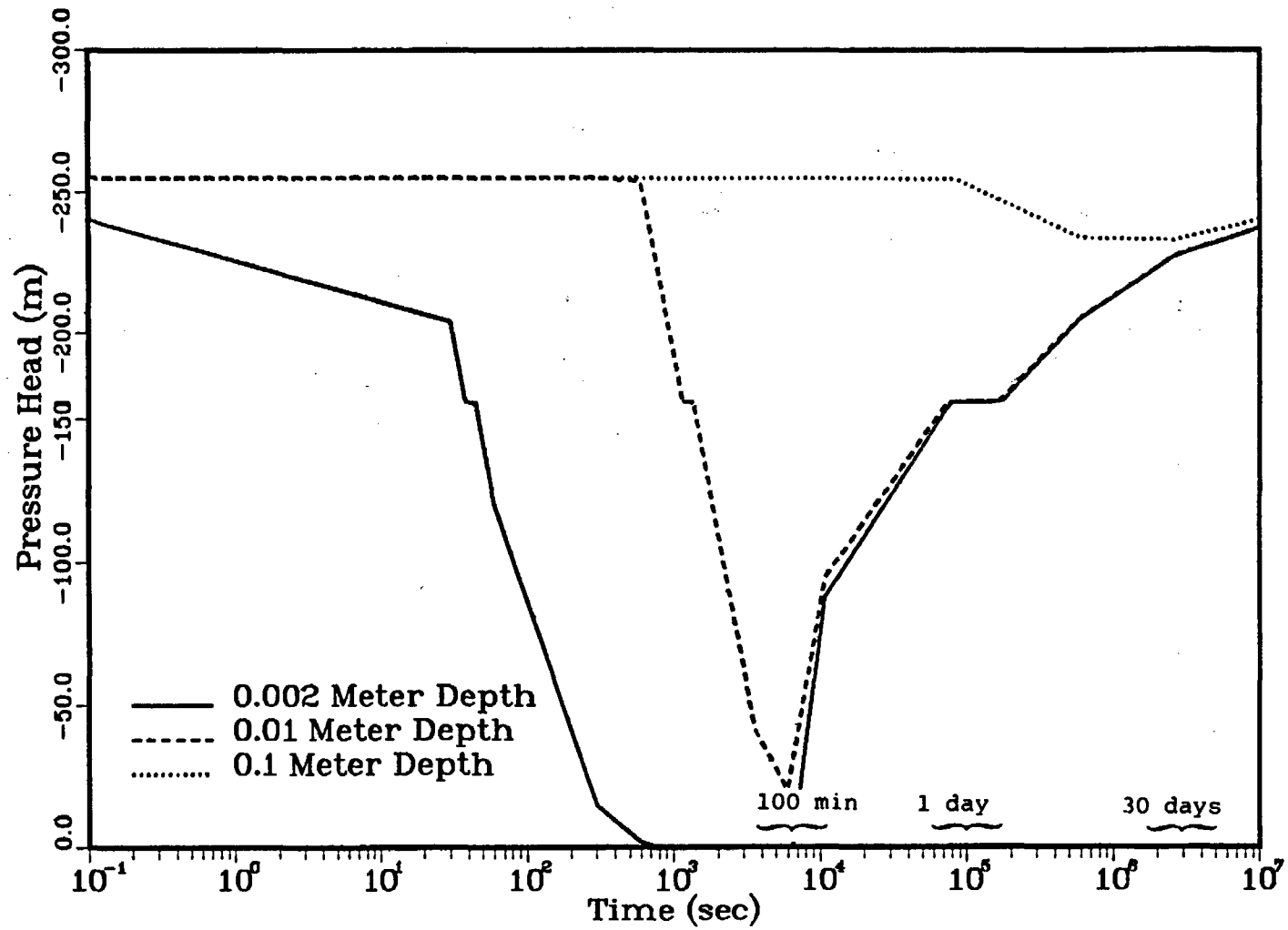


Figure 18. Matrix-block water penetration
 Initial condition - no flow
 20 m pressure head for 100 minutes

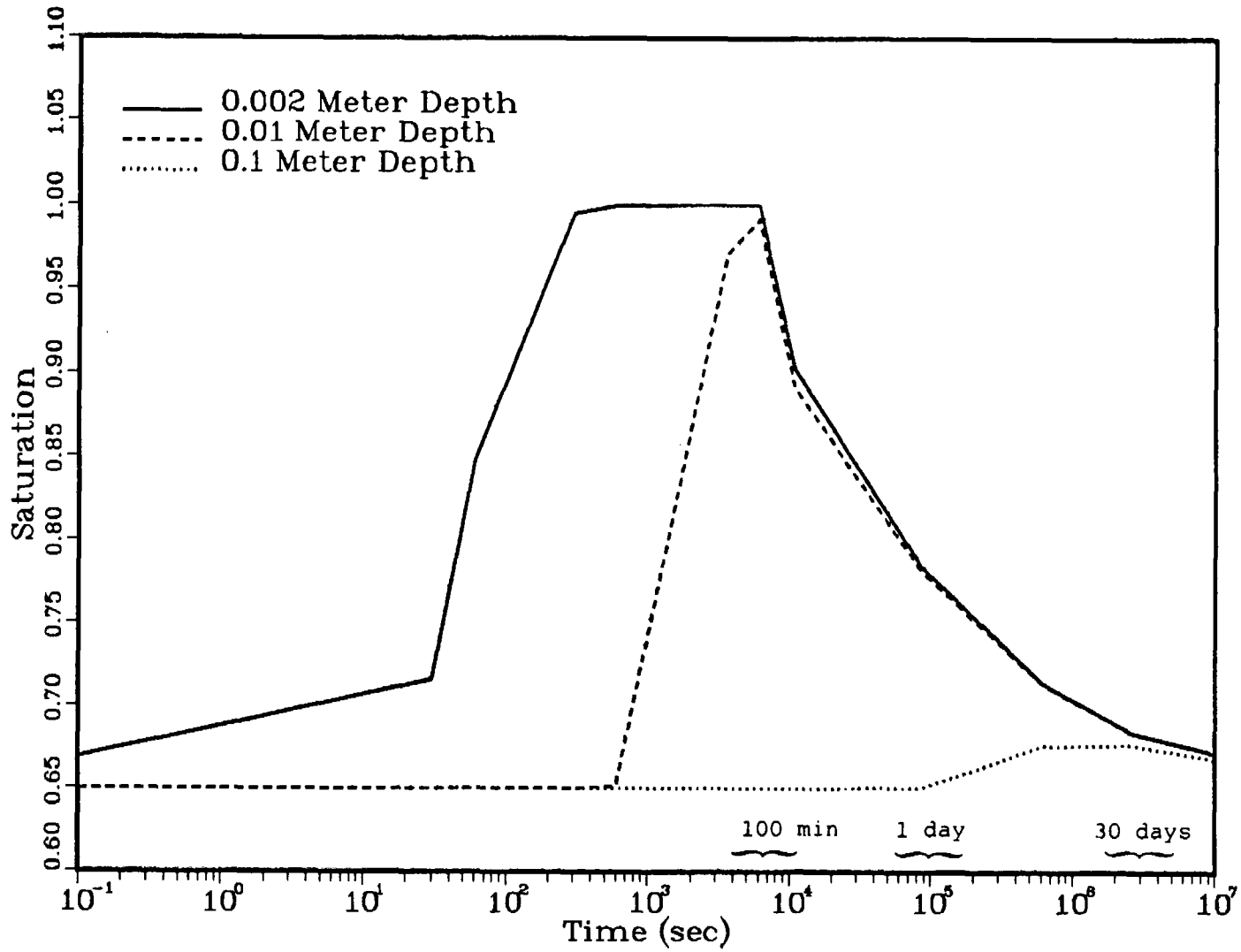


Figure 19. Matrix block water penetration
Initial condition - no flow
20 m pressure head for 100 minutes

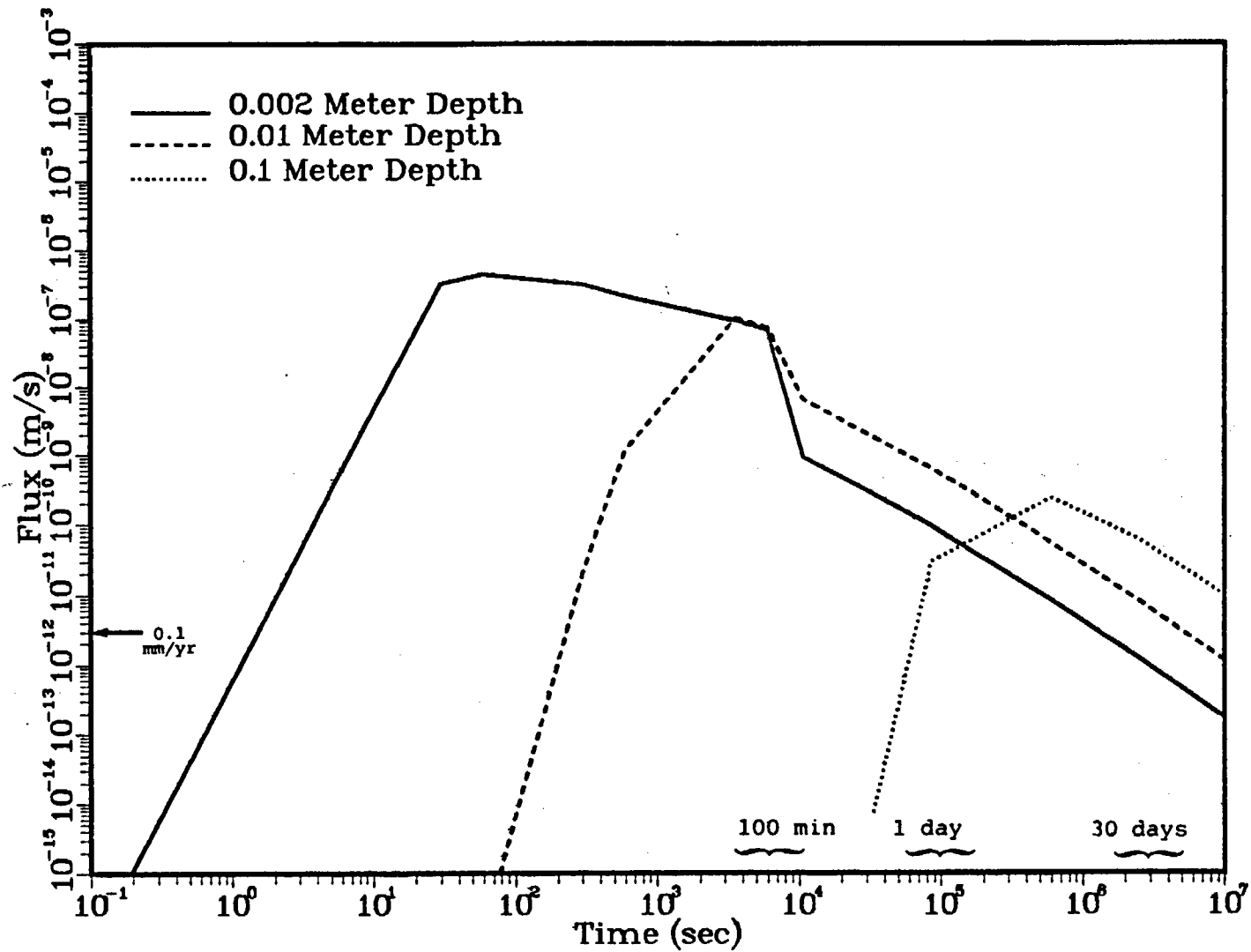


Figure 20. Matrix-block water penetration
 Initial condition - no flow
 20 m pressure head for 100 minutes

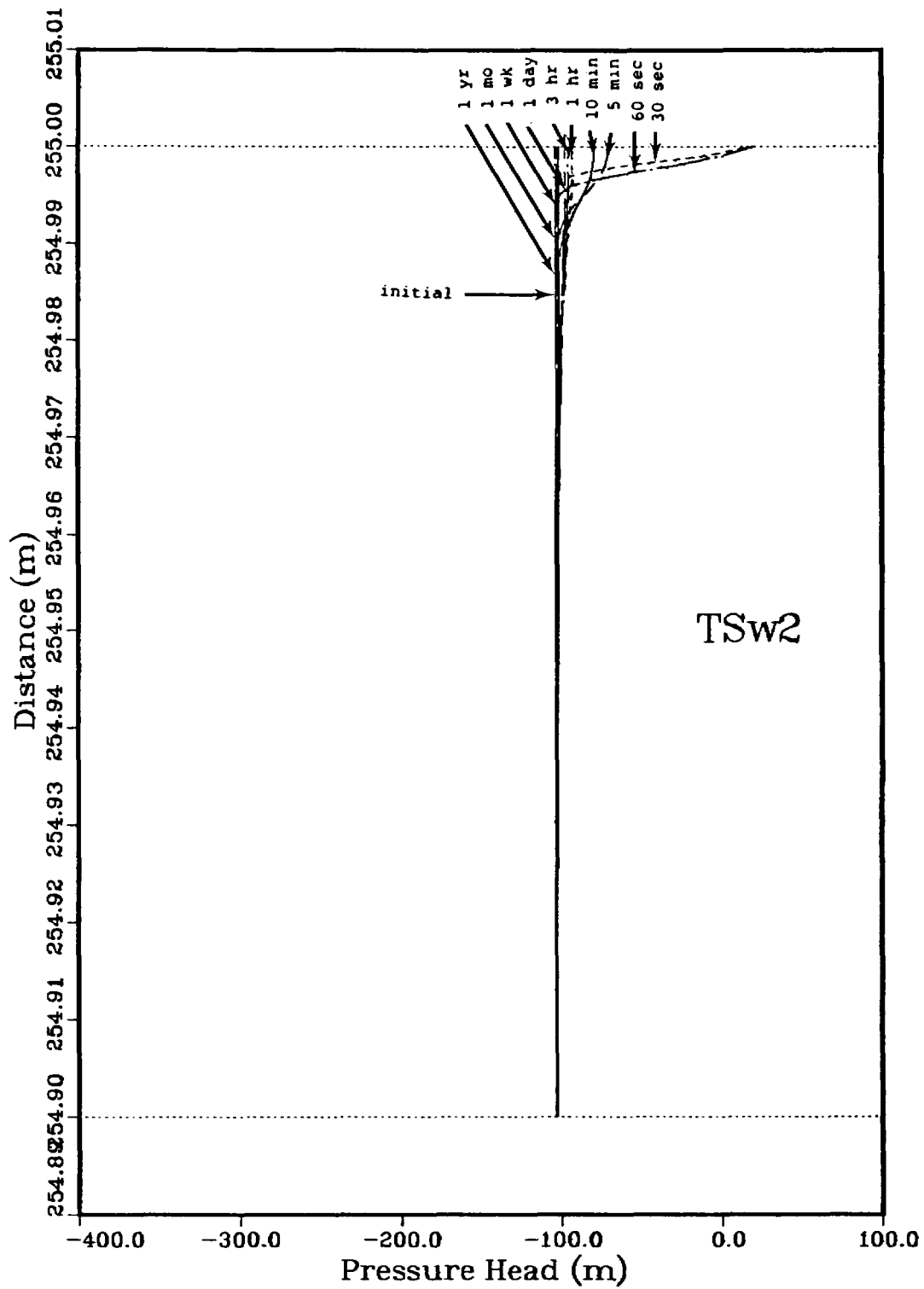


Figure 21. Matrix-block water penetration
 Initial condition - 0.1 mm/yr flow
 20 m pressure head for 1 minute

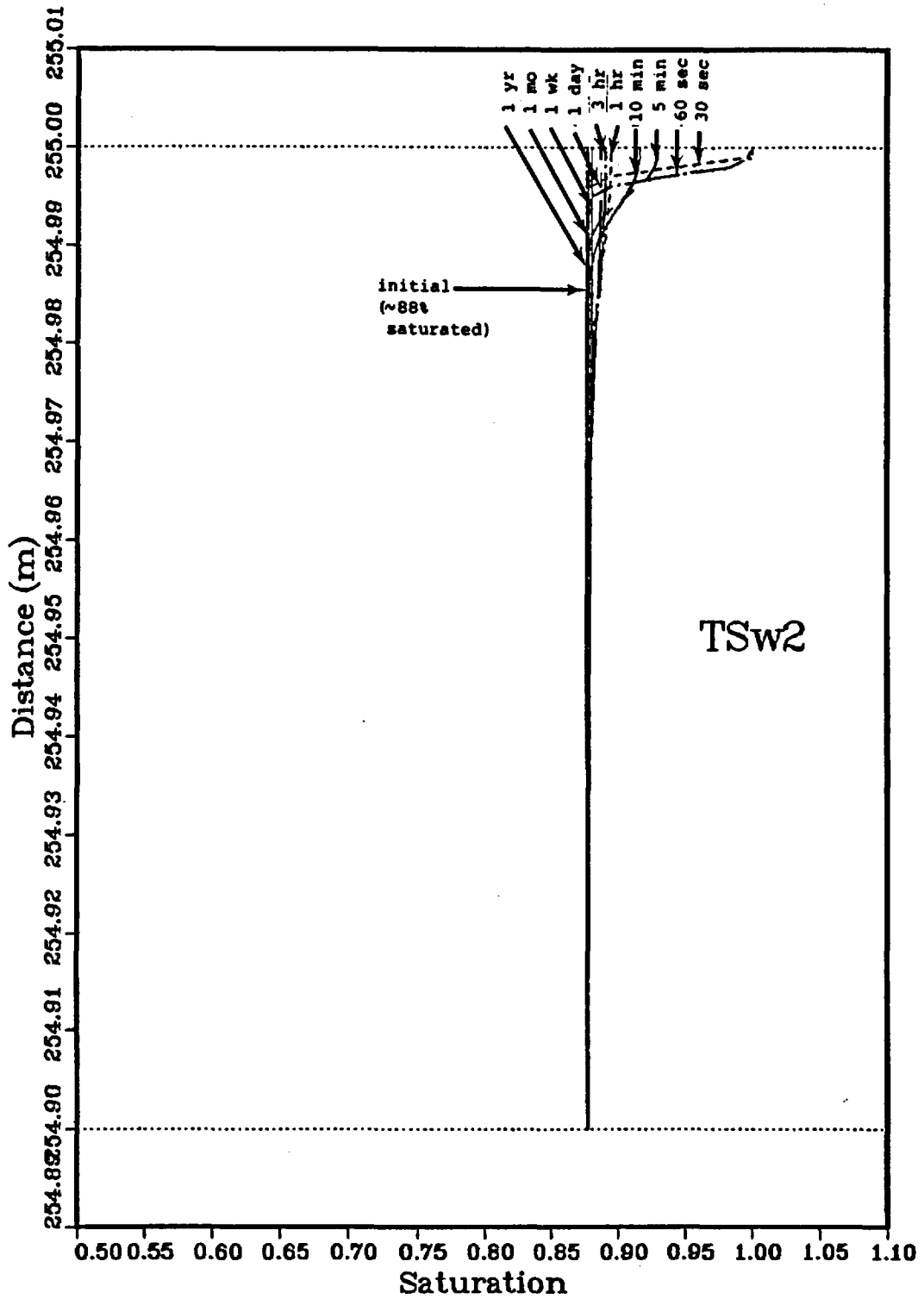


Figure 22. Matrix-block water penetration
 Initial condition - 0.1 mm/yr flow
 20 m pressure head for 1 minute

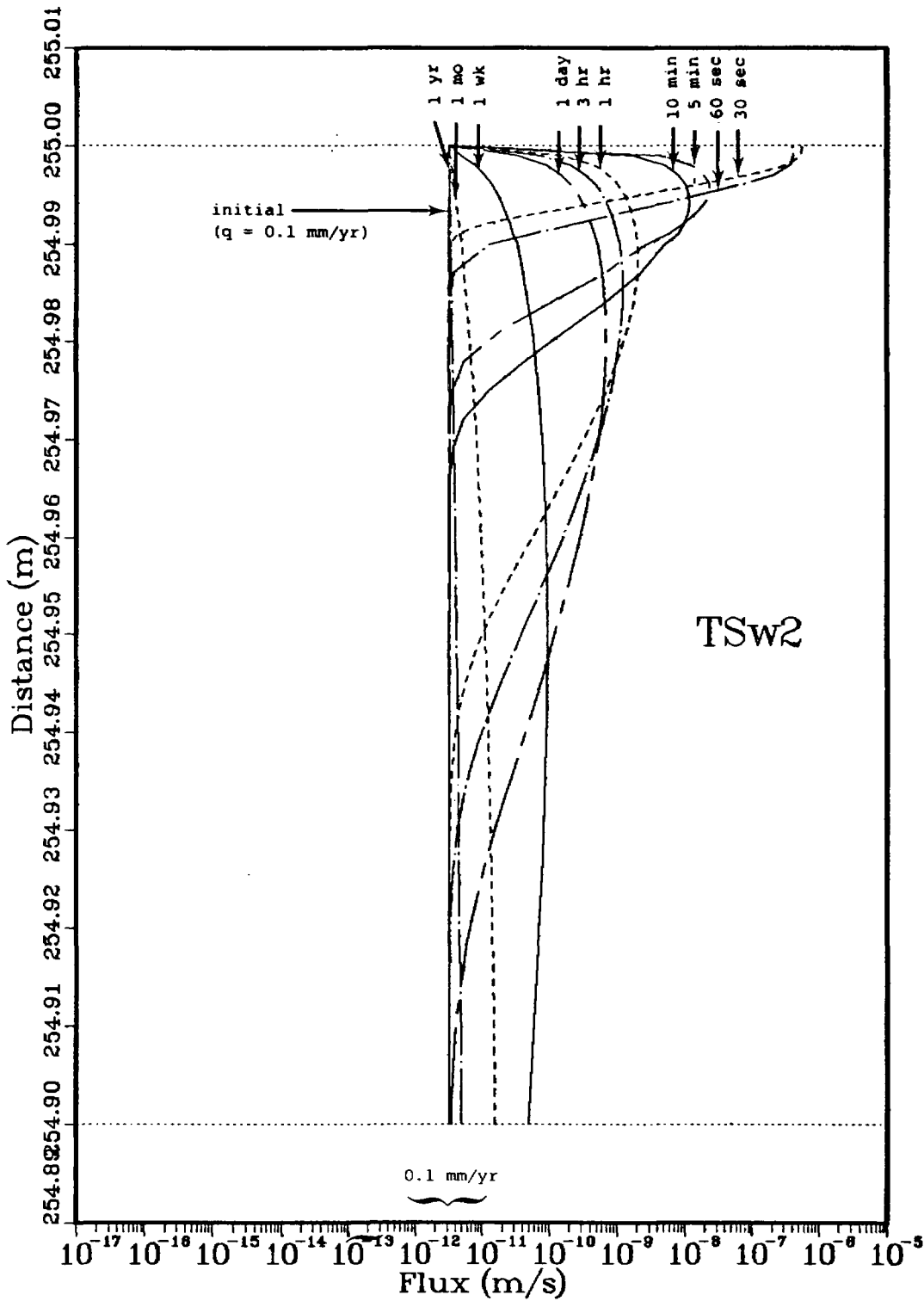
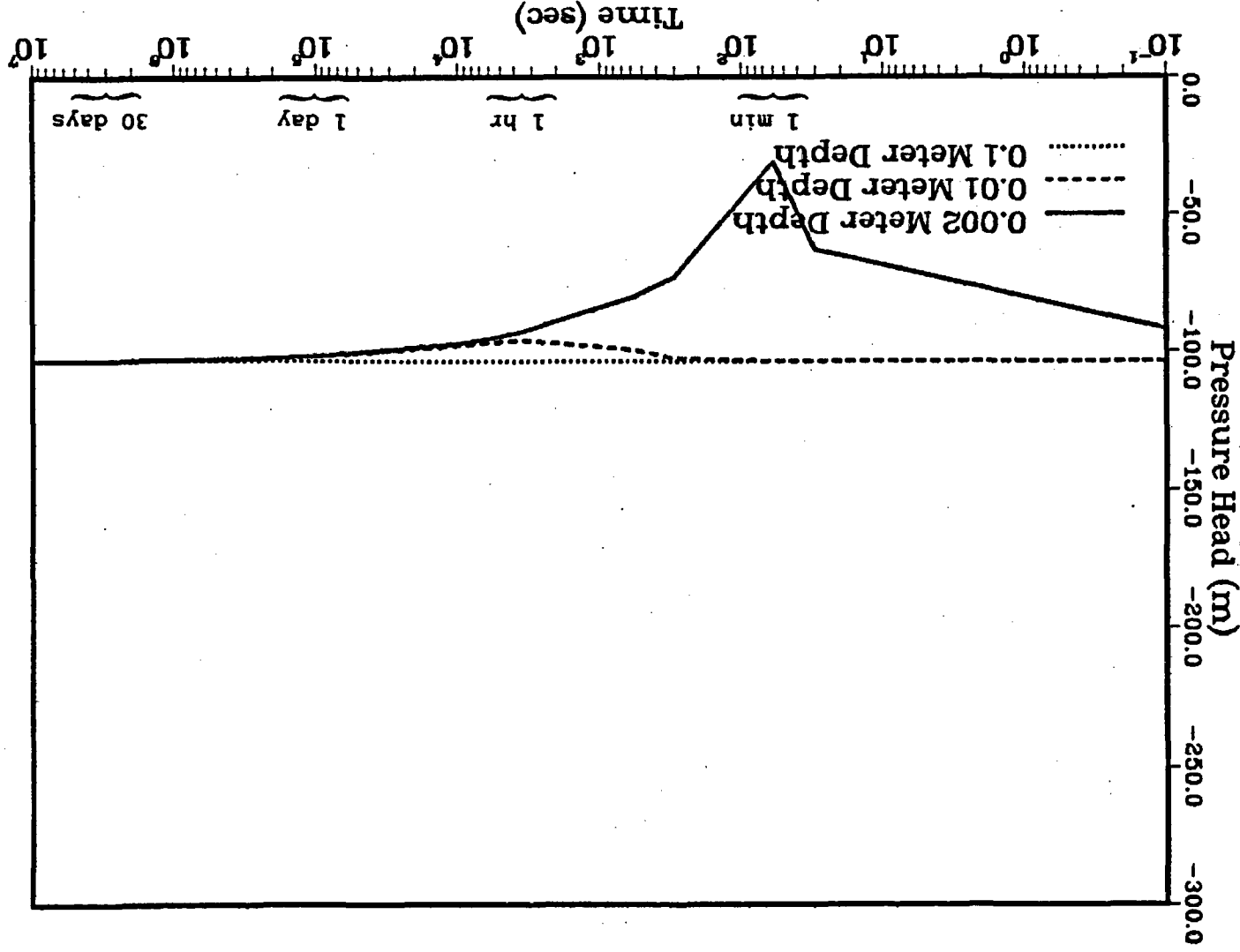


Figure 23. Matrix-block water penetration
 Initial condition - 0.1 mm/yr flow
 20 m pressure head for 1 minute



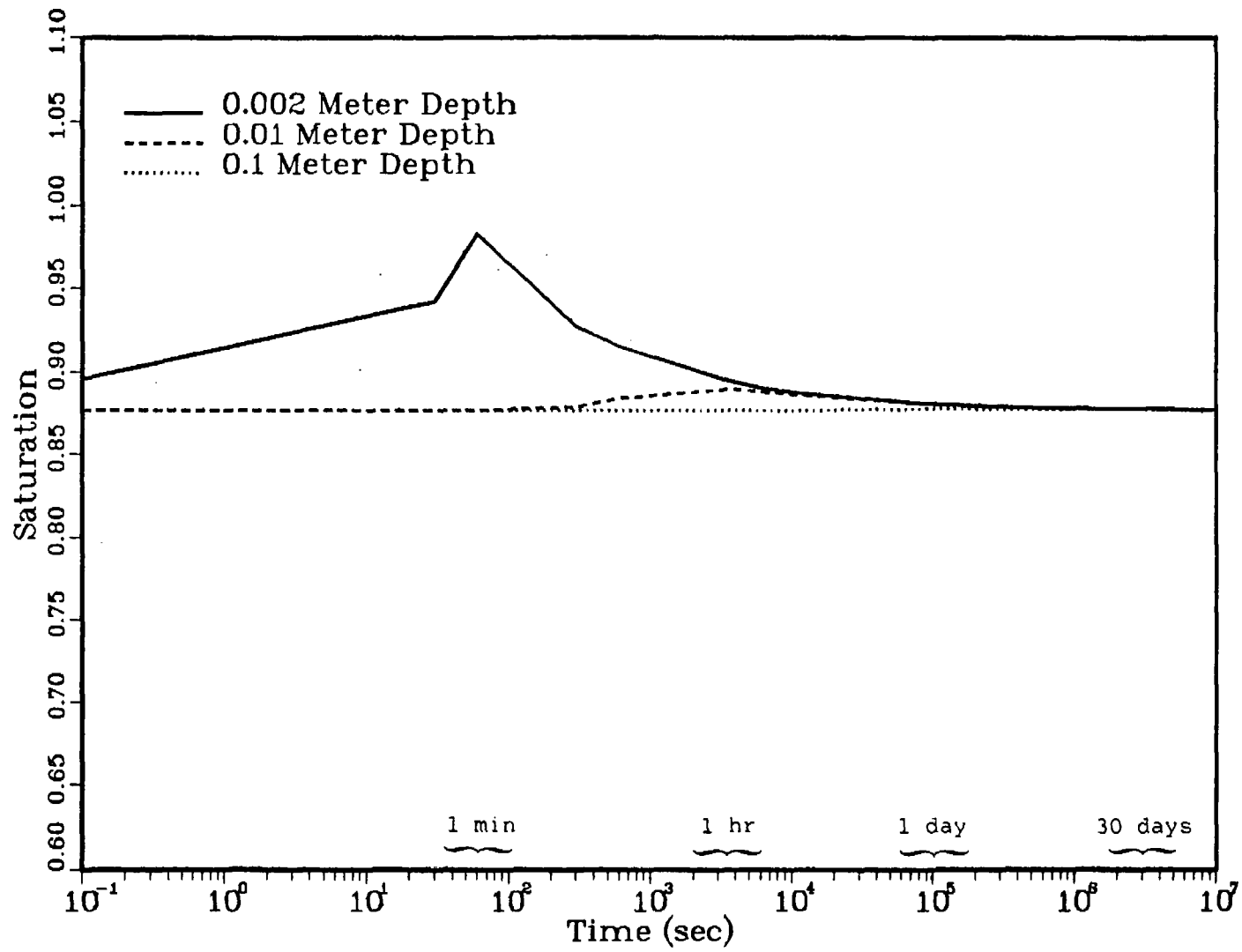


Figure 25. Matrix-block water penetration
Initial condition - 0.1 mm/yr flow
20 m pressure head for 1 minute

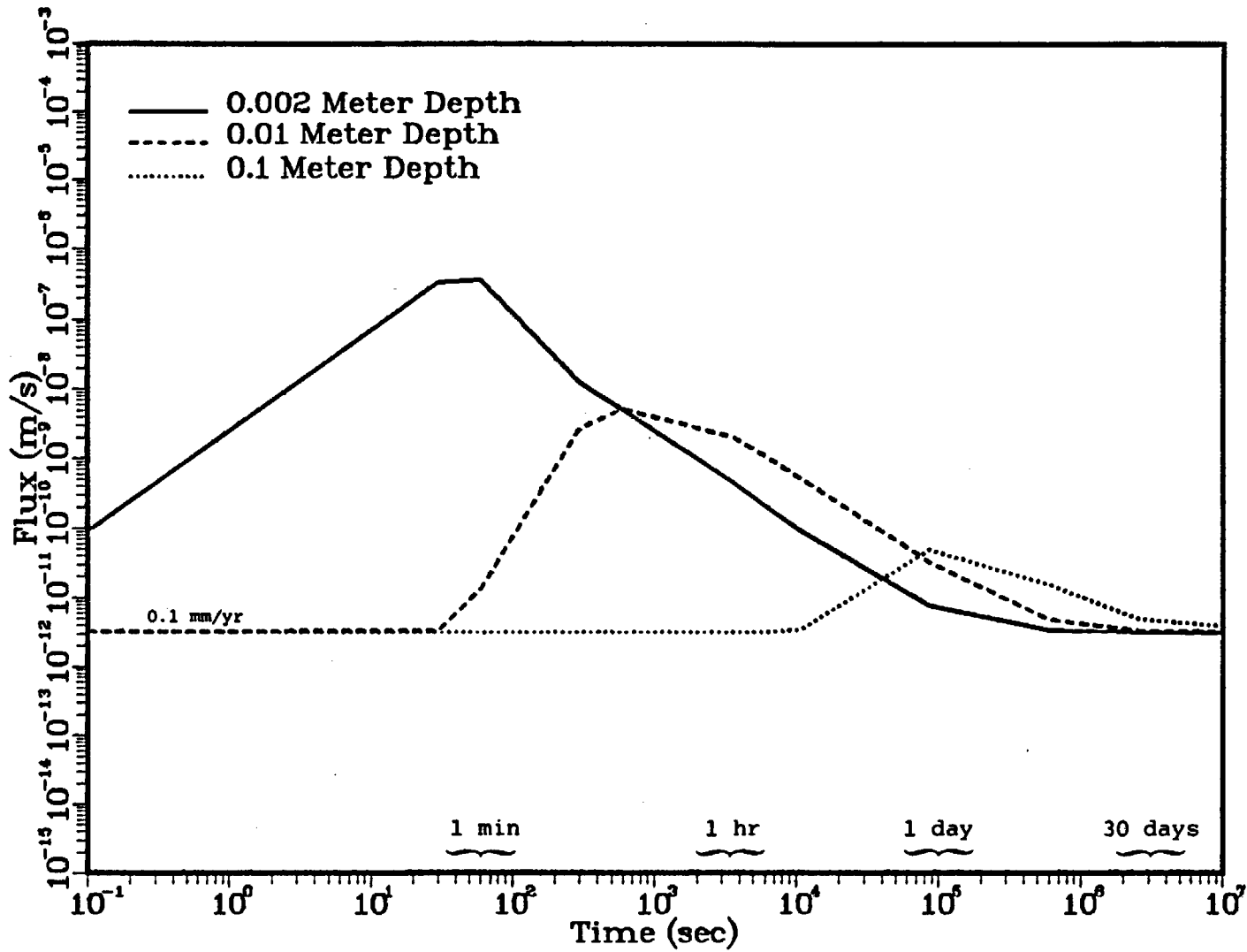


Figure 26. Matrix-block water penetration
 Initial condition - 0.1 mm/yr flow
 20 m pressure head for 1 minute

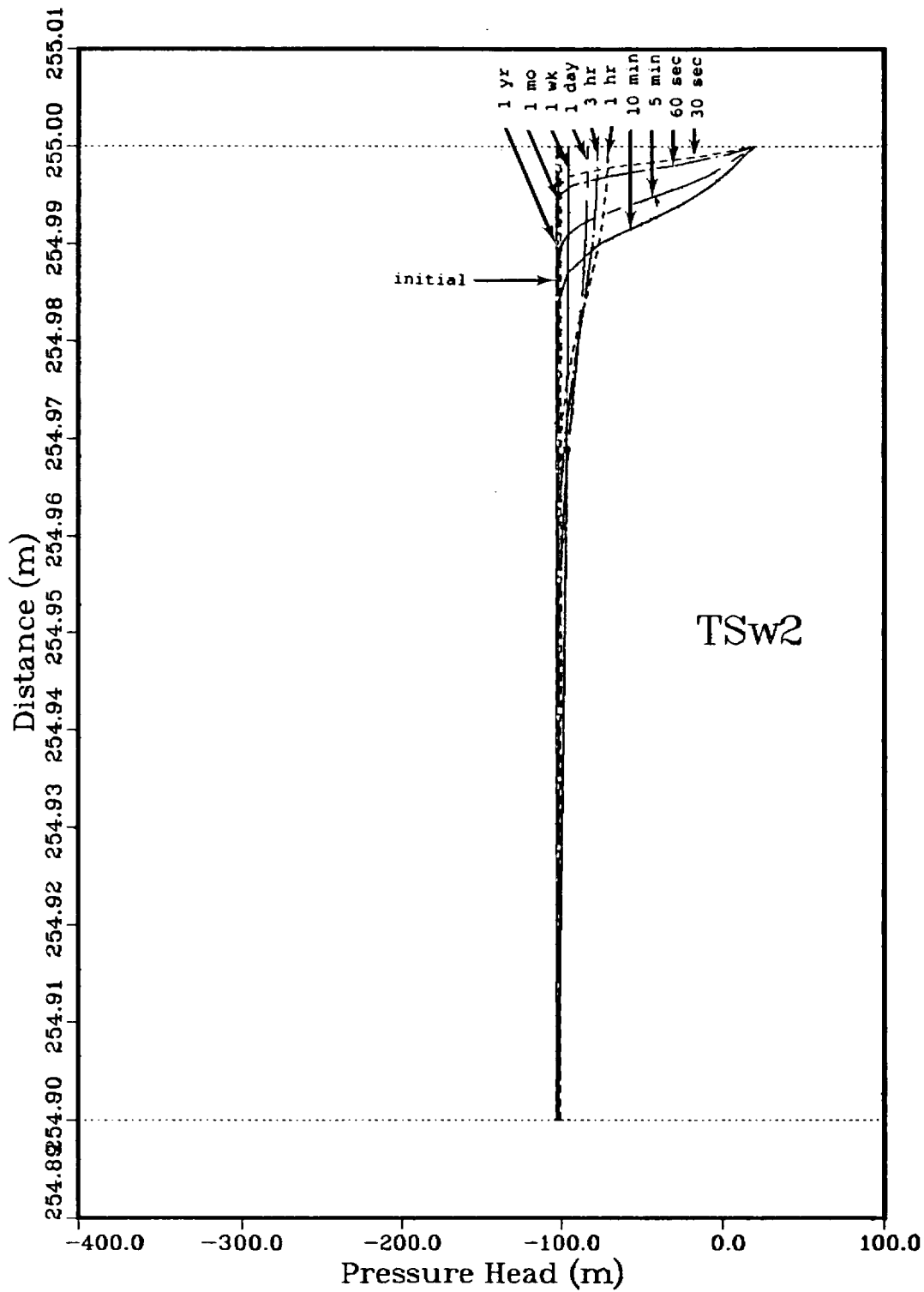


Figure 27. Matrix-block water penetration
 Initial condition - 0.1 mm/yr flow
 20 m pressure head for 10 minutes

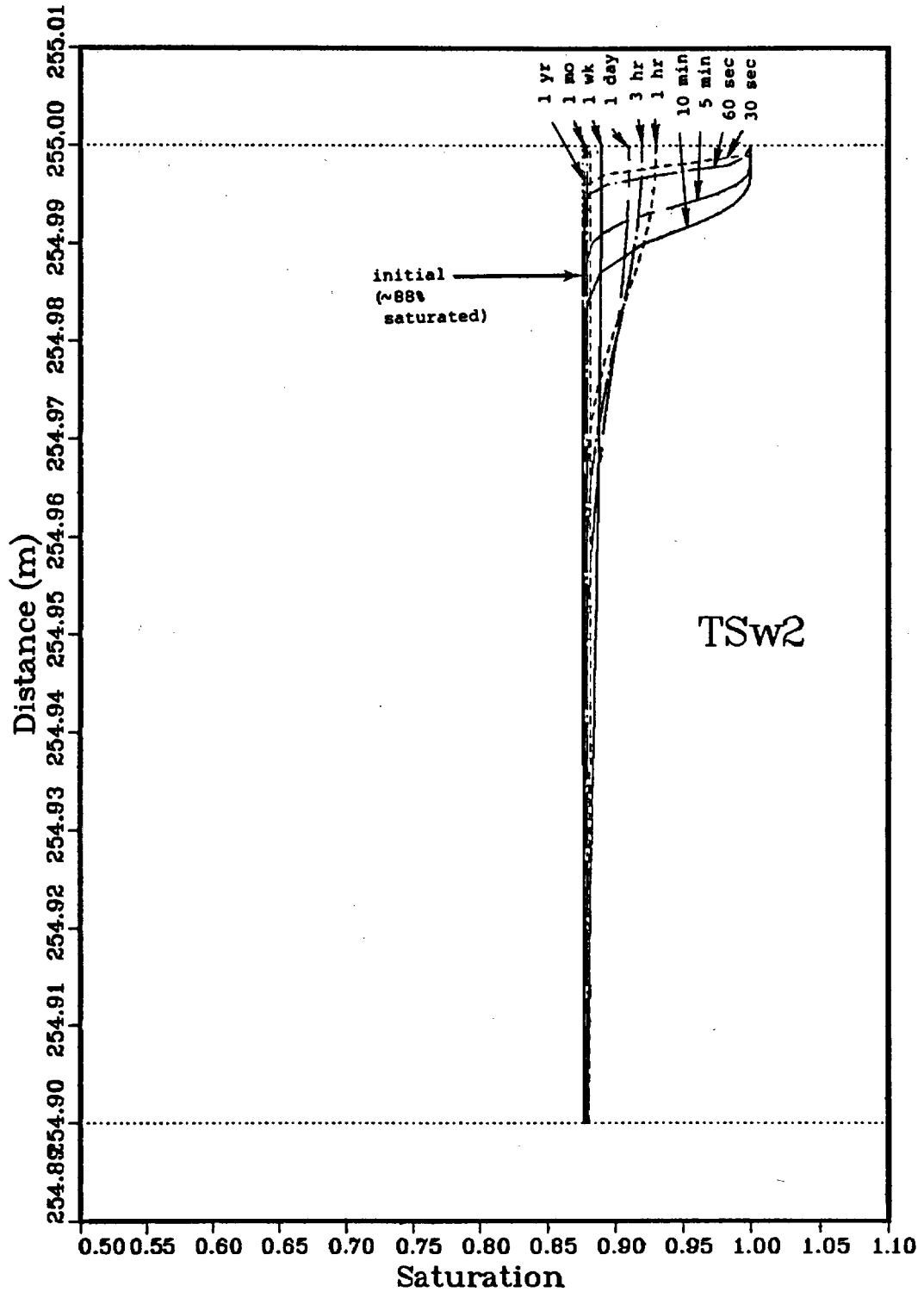


Figure 28. Matrix-block water penetration
 Initial condition - 0.1 mm/yr flow
 20 m pressure head for 10 minutes

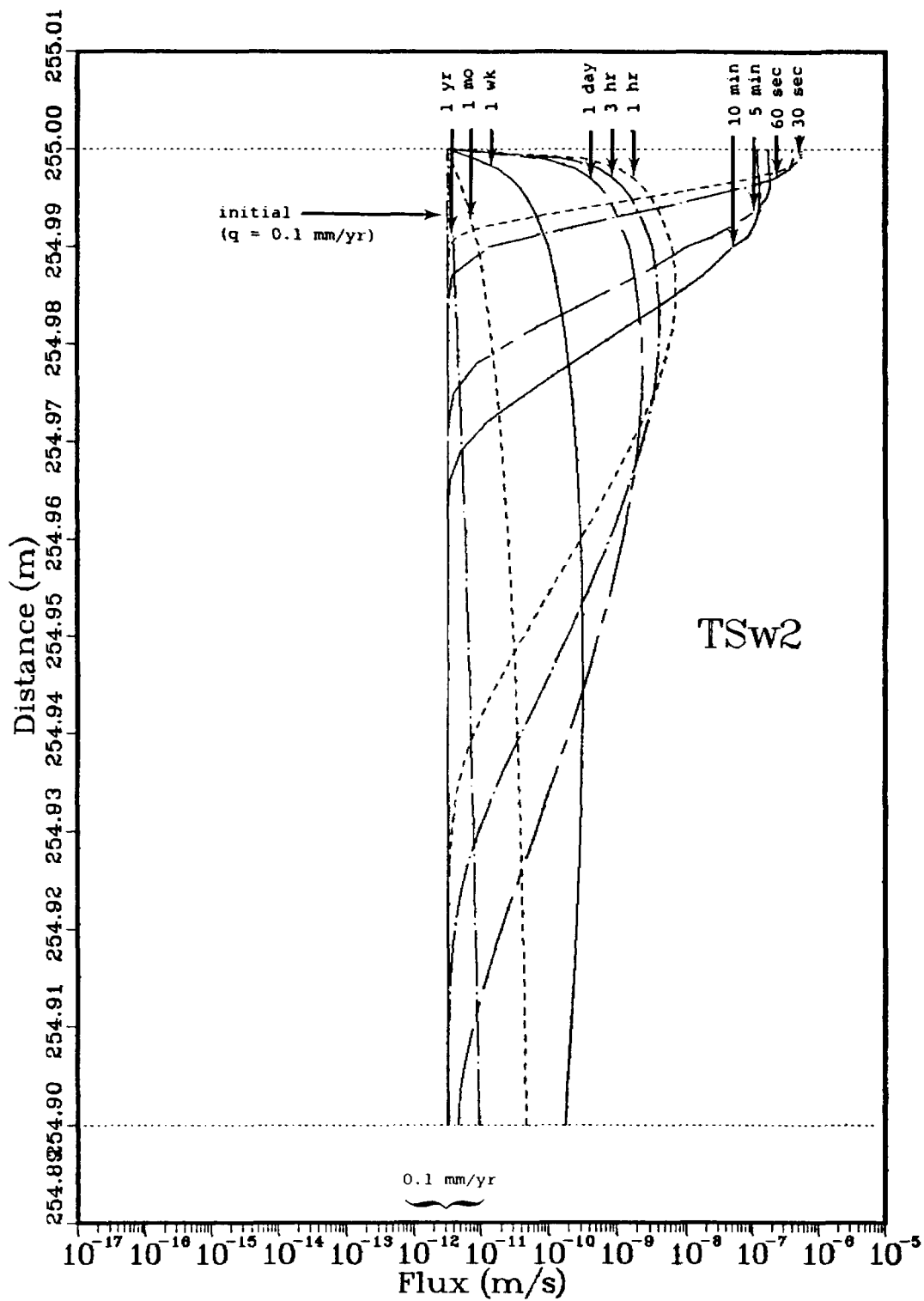


Figure 29. Matrix-block water penetration
 Initial condition - 0.1 mm/yr flow
 20 m pressure head for 10 minutes

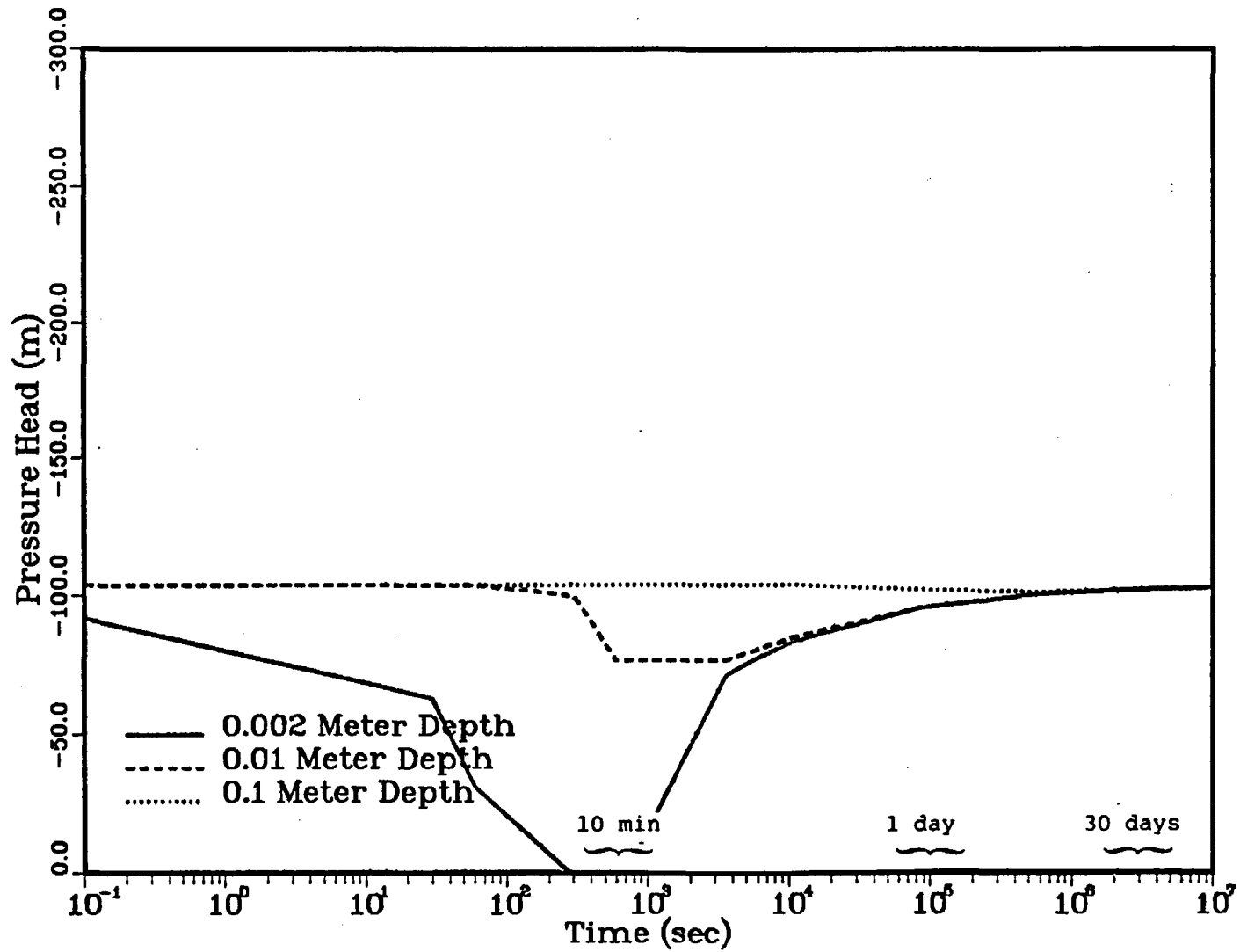


Figure 30. Matrix-block water penetration
Initial condition - 0.1 mm/yr flow
20 m pressure head for 10 minutes

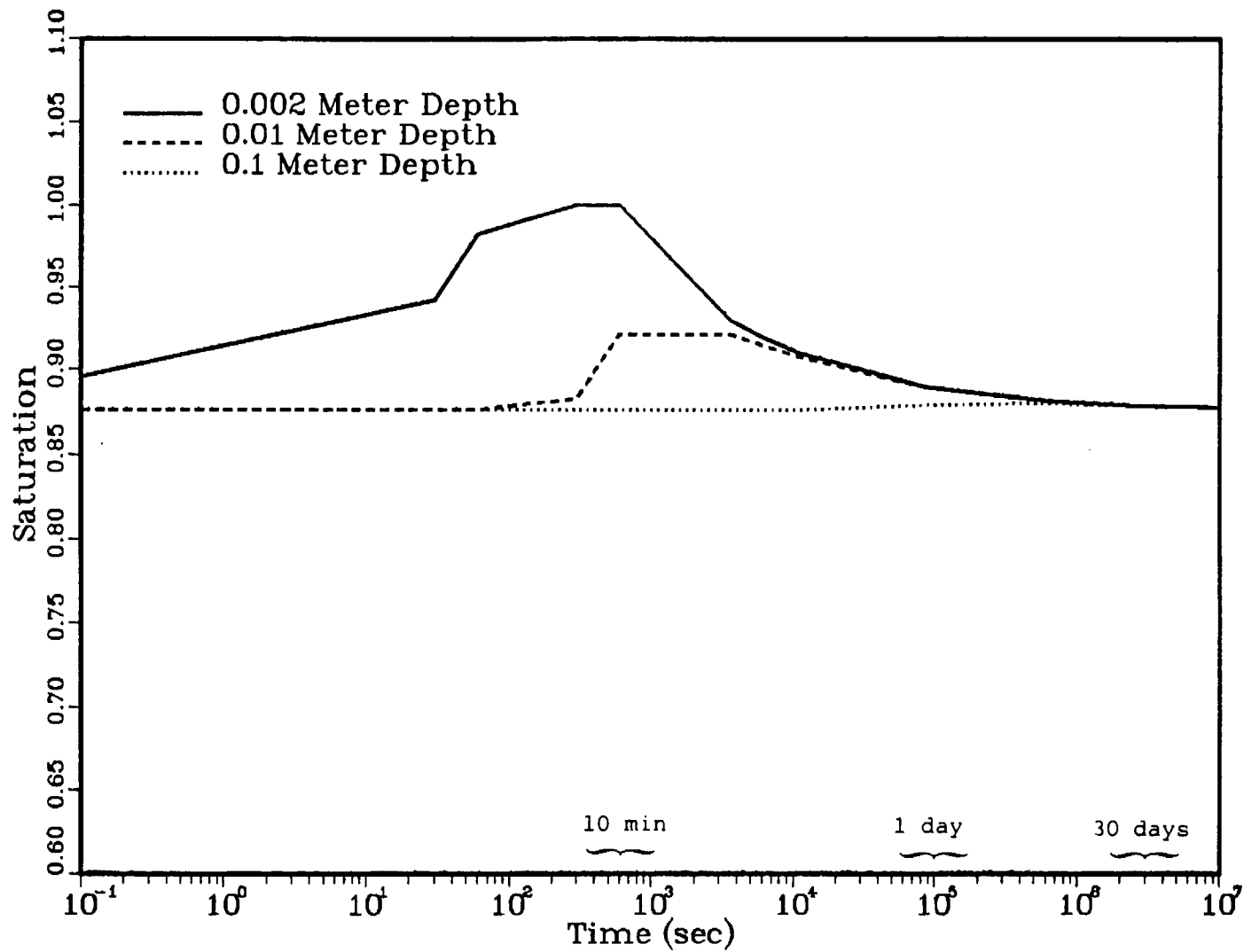


Figure 31. Matrix-block water penetration
Initial condition - 0.1 mm/yr flow
20 m pressure head for 10 minutes

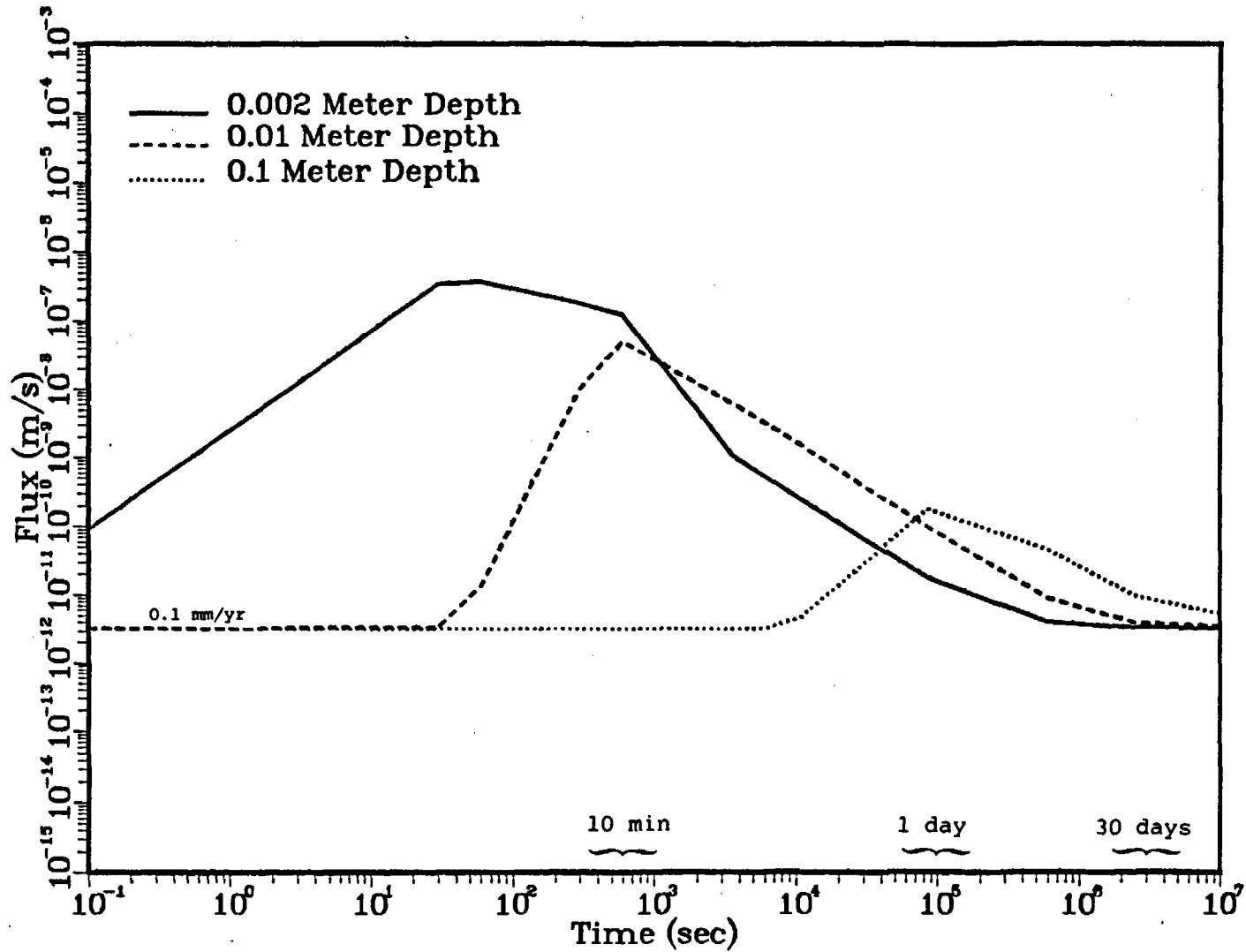


Figure 32. Matrix-block water penetration
 Initial condition - 0.1 mm/yr flow
 20 m pressure head for 10 minutes

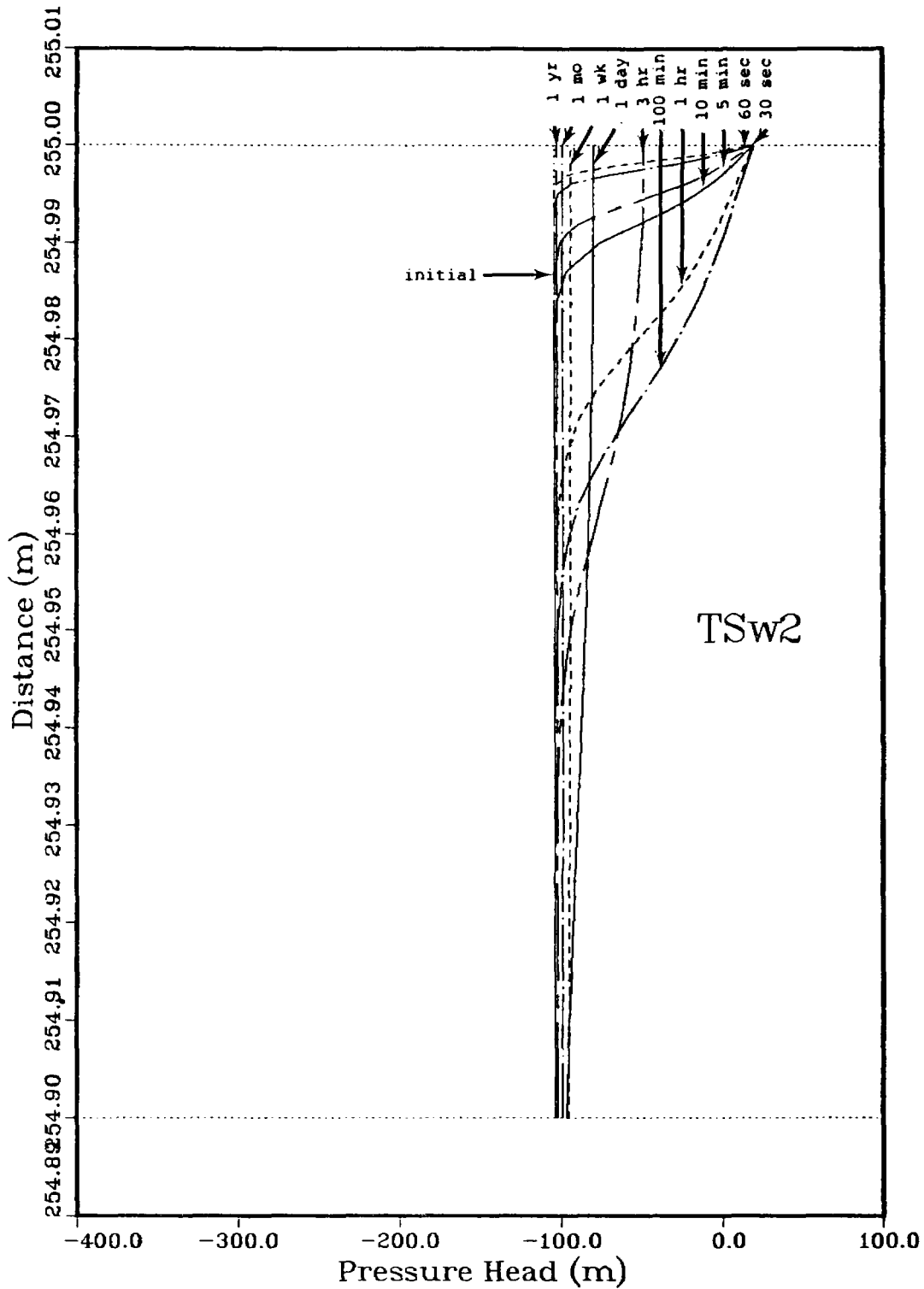


Figure 33. Matrix-block water penetration
 Initial condition - 0.1 mm/yr flow
 20 m pressure head for 100 minutes

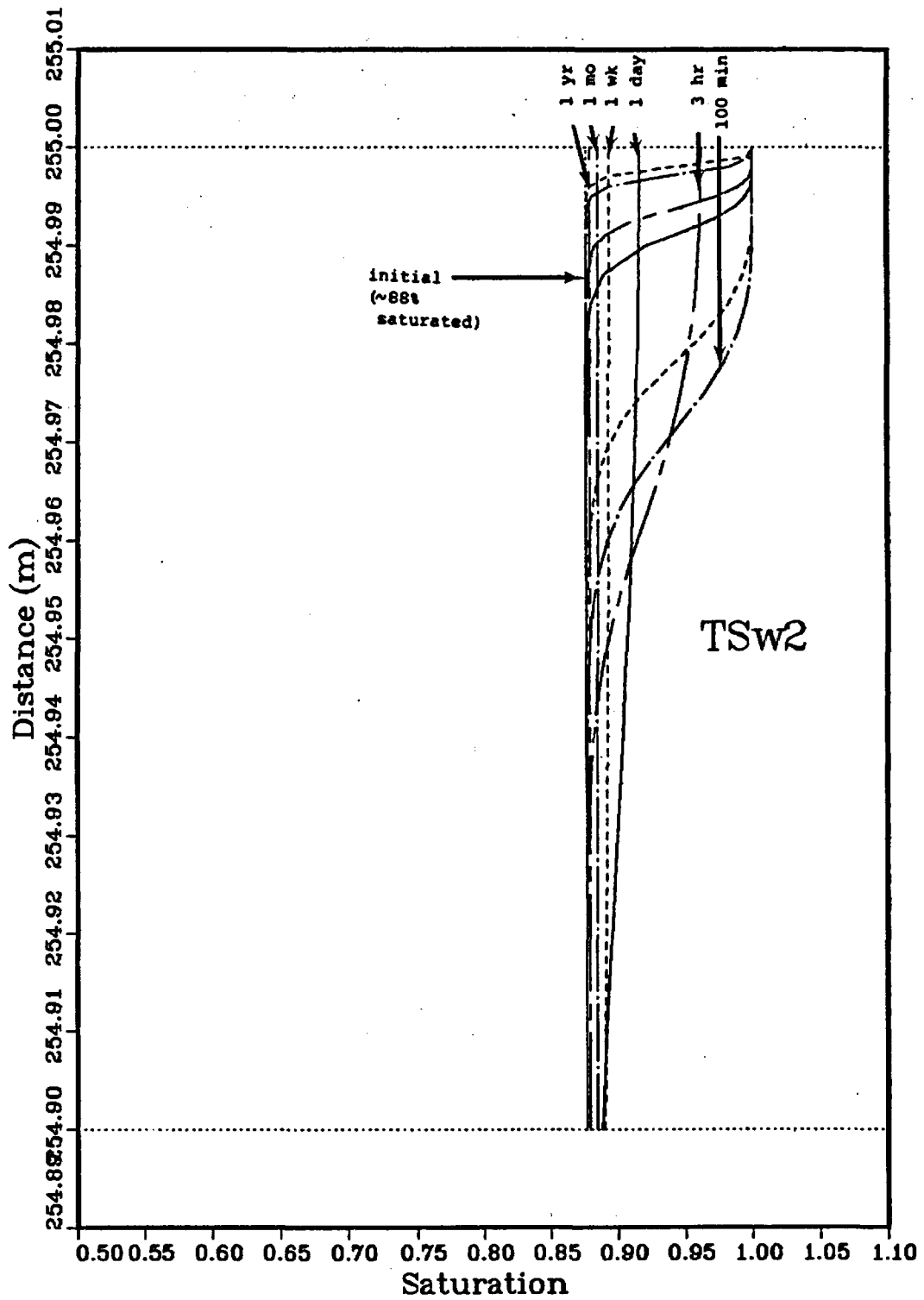


Figure 34. Matrix-block water penetration
 Initial condition - 0.1 mm/yr flow
 20 m pressure head for 100 minutes

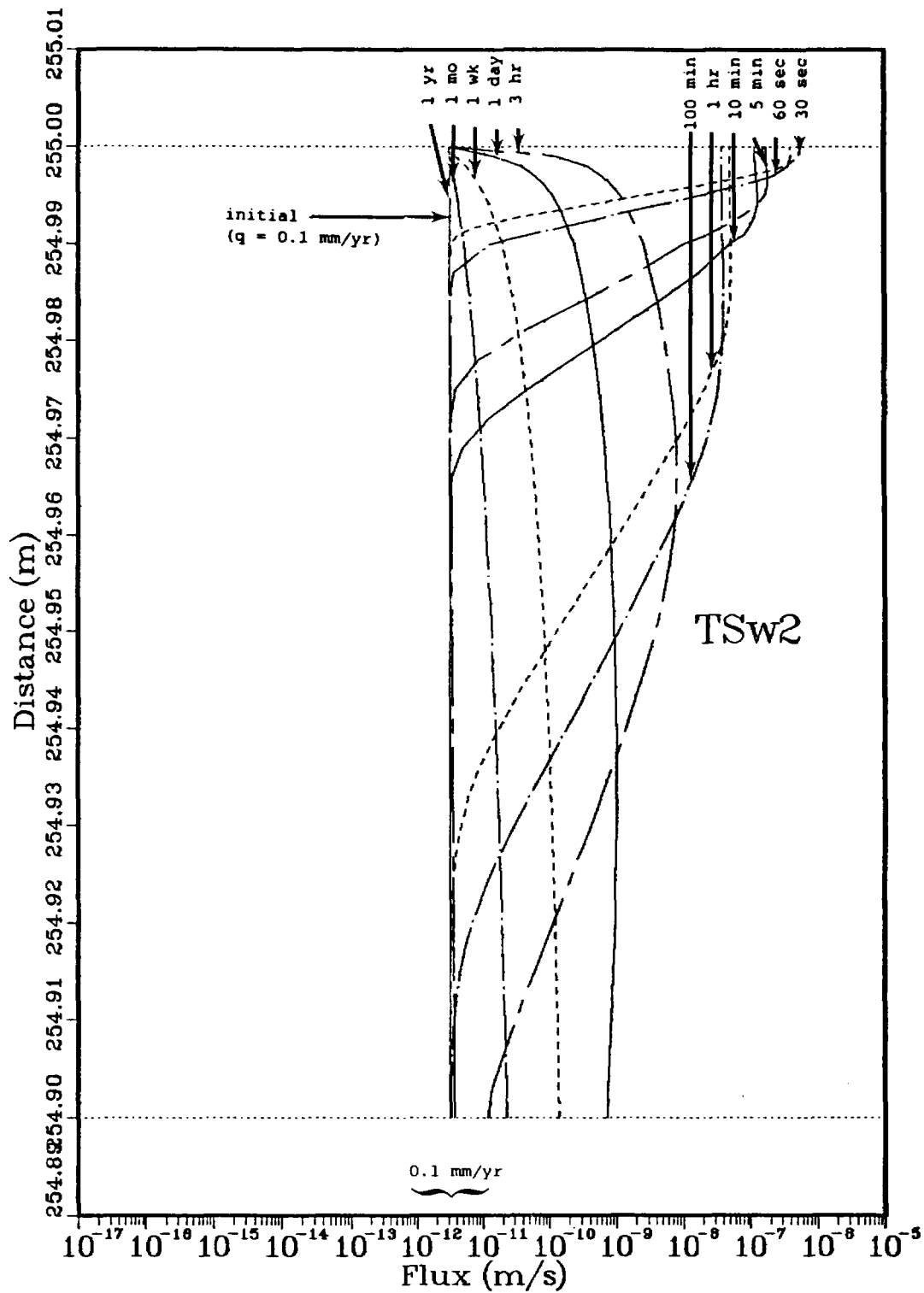


Figure 35. Matrix-block water penetration
 Initial condition - 0.1 mm/yr flow
 20 m pressure head for 100 minutes

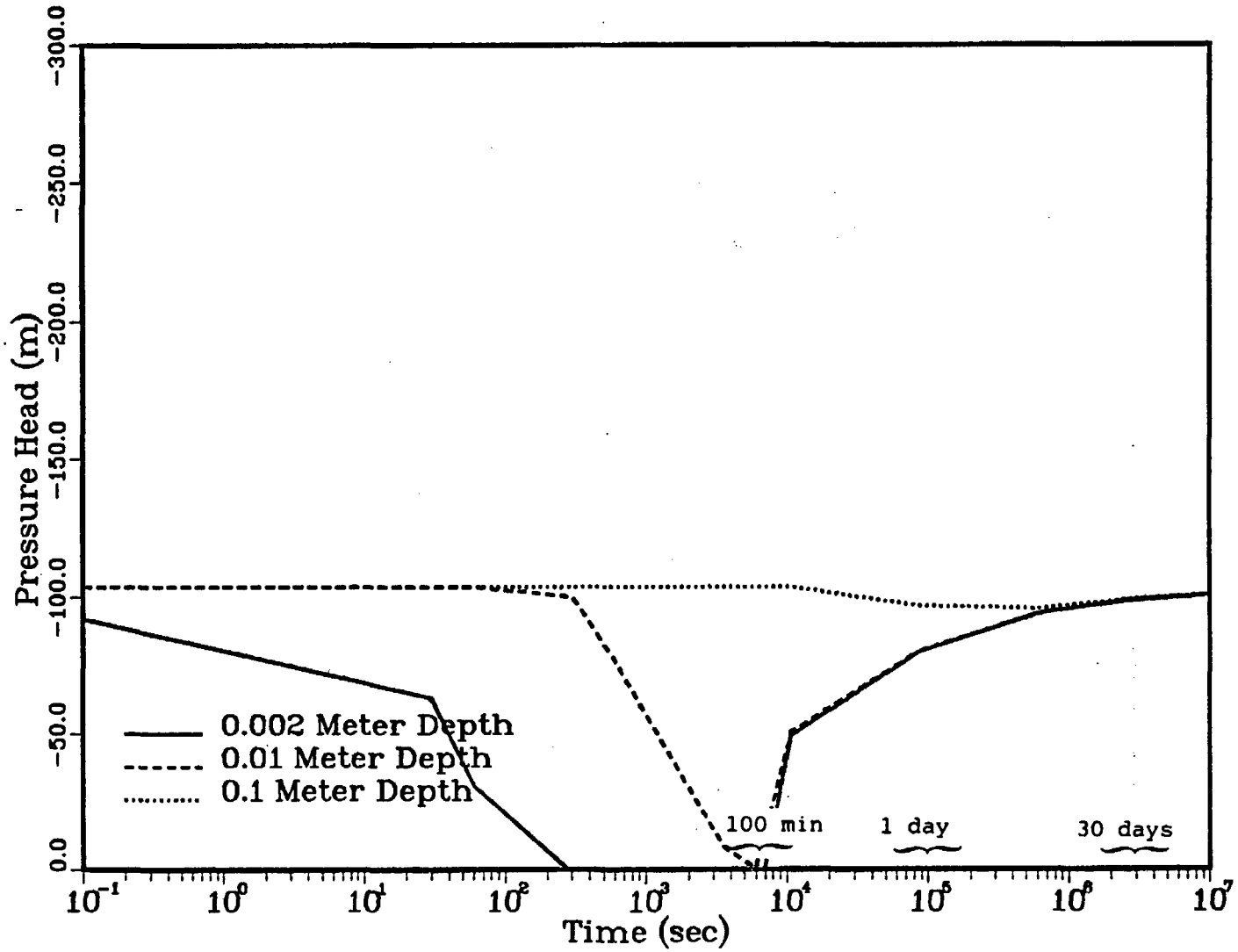


Figure 36. Matrix-block water penetration
Initial condition - 0.1 mm/yr flow
20 m pressure head for 100 minutes

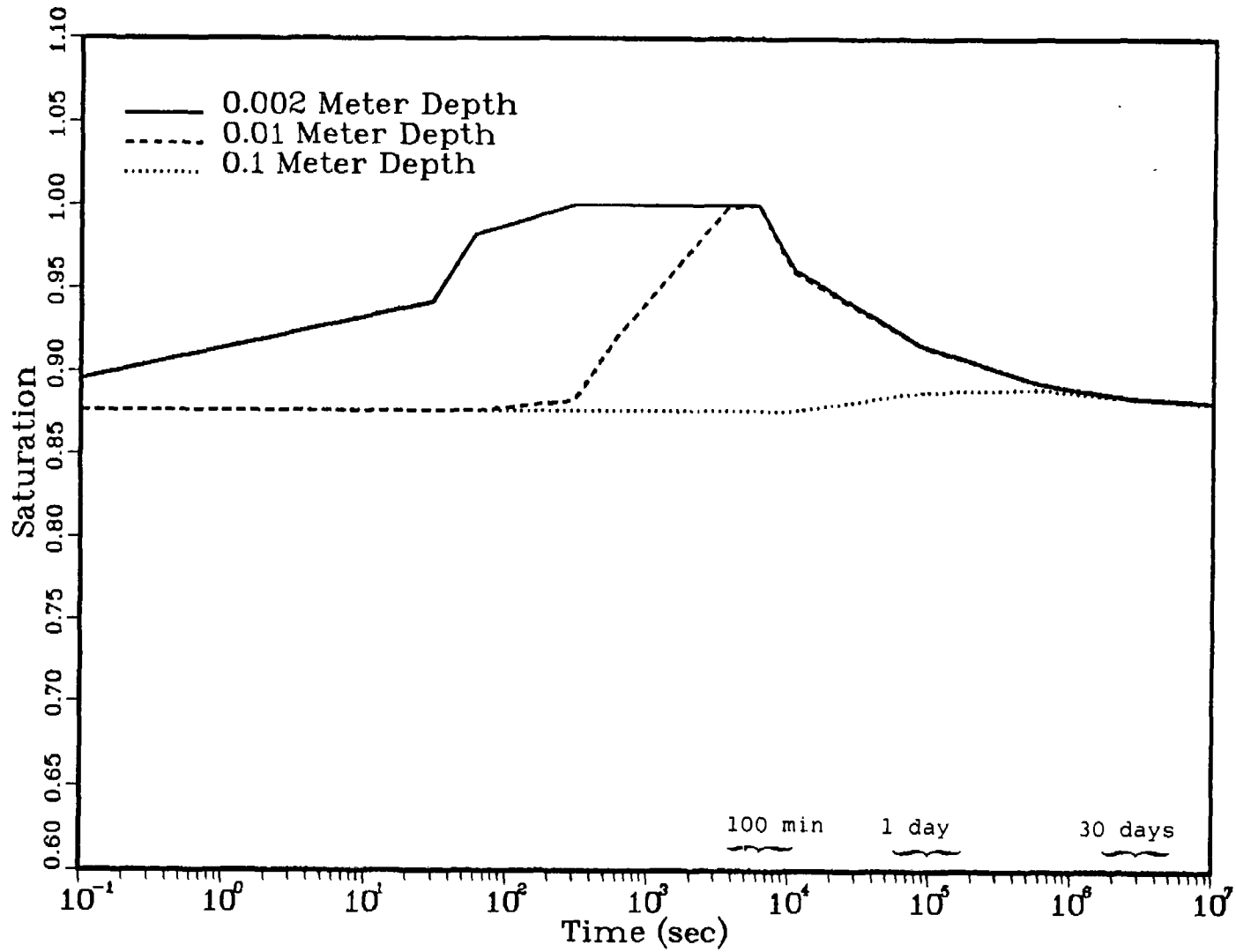


Figure 37. Matrix-block water penetration
Initial condition - 0.1 mm/yr flow
20 m pressure head for 100 minutes

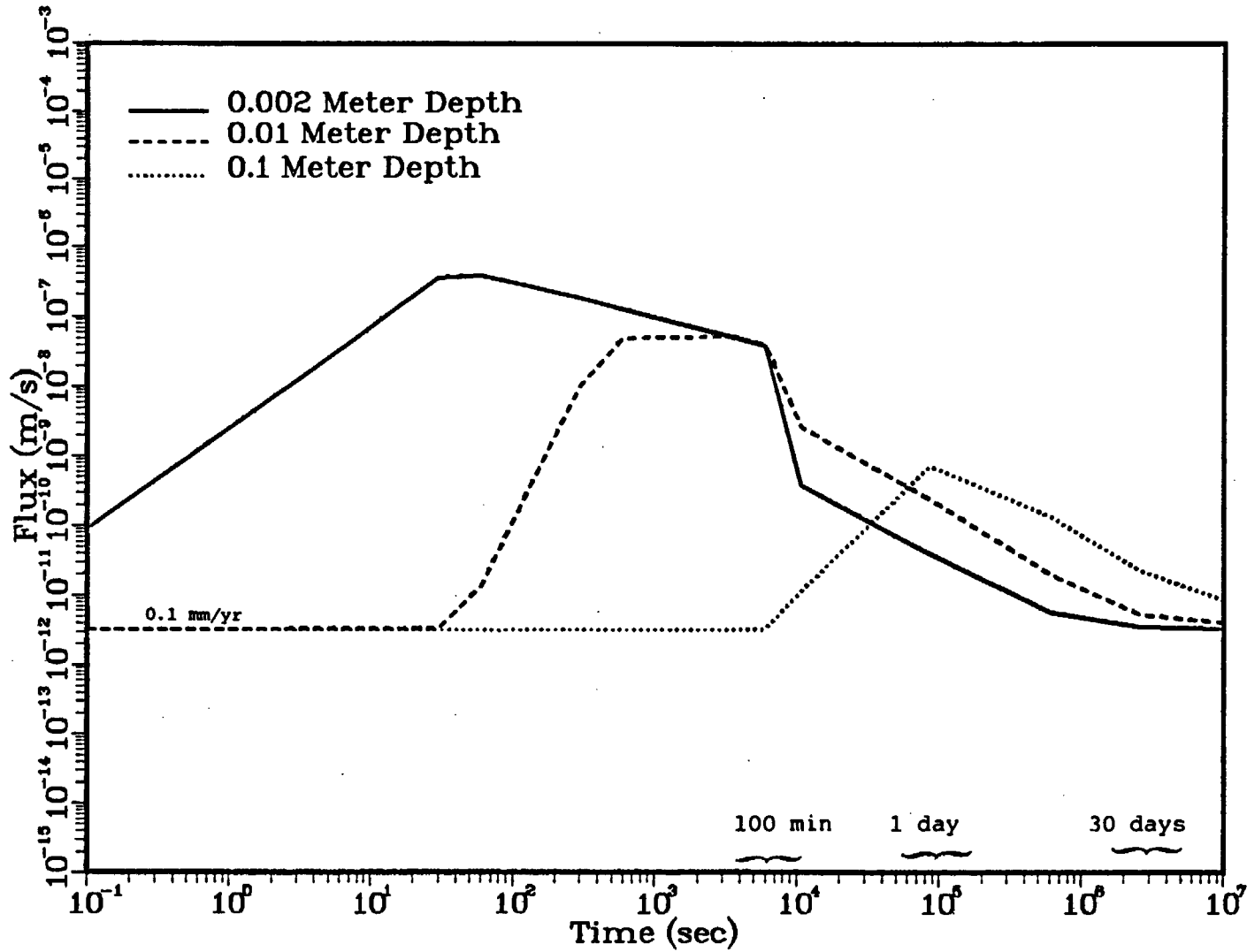


Figure 38. Matrix-block water penetration
 Initial condition - 0.1 mm/yr flow
 20 m pressure head for 100 minutes

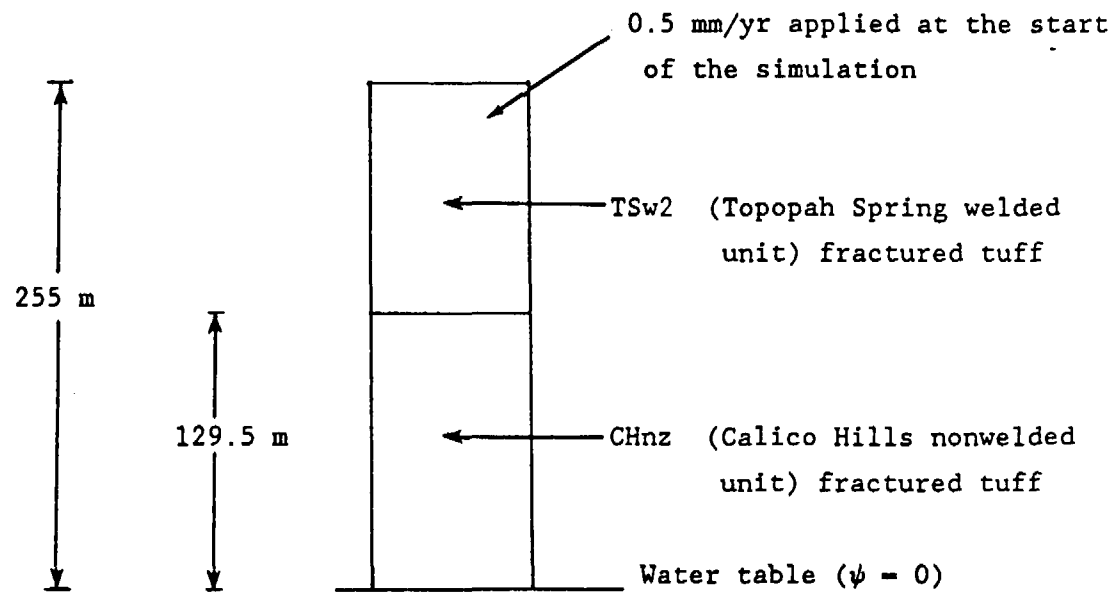


Figure 39 Geometry and Boundary Conditions for the Problem Set
"Response of a Tuff Column to Changes in Flux"

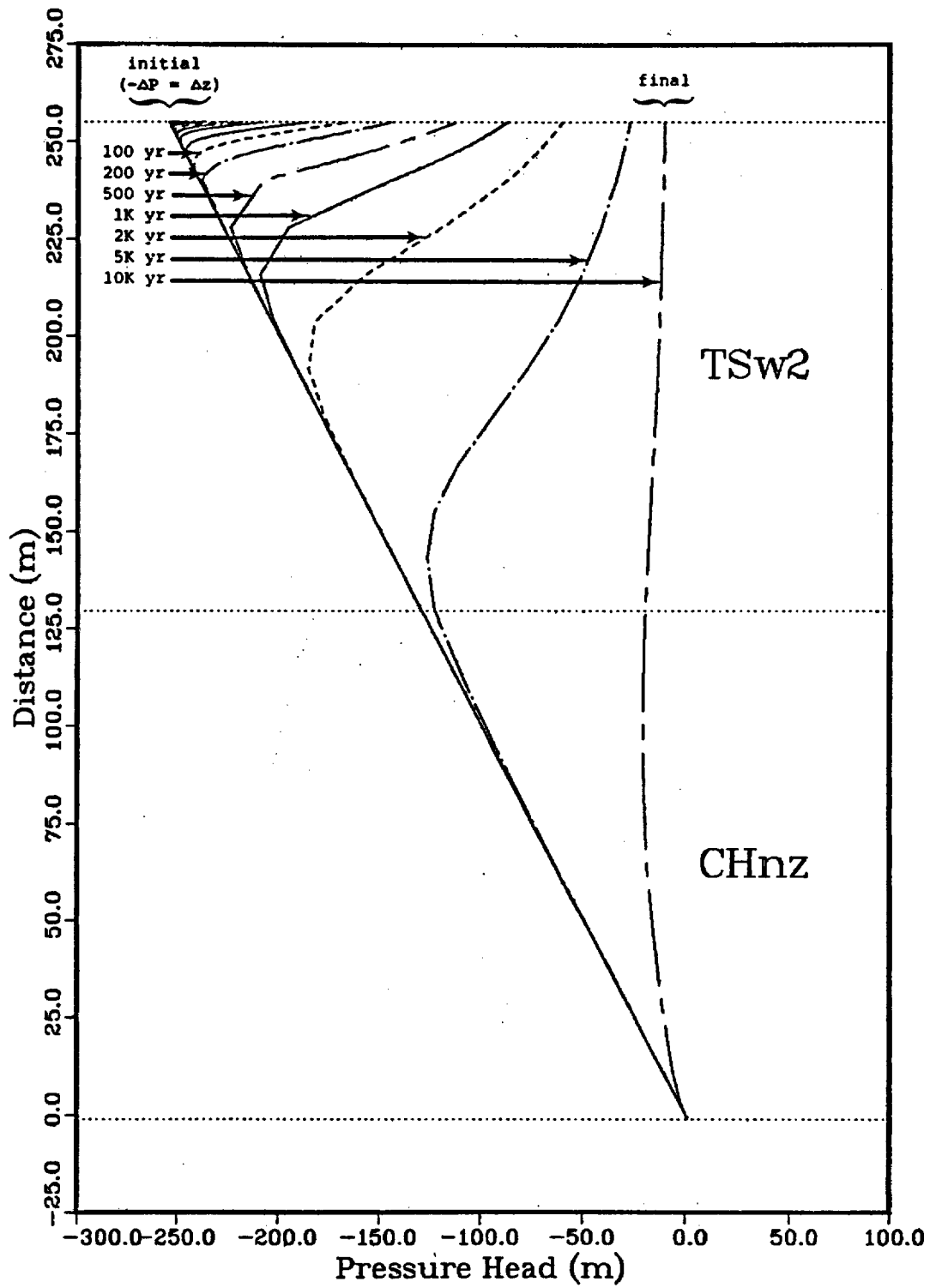


Figure 40. Water flux changed from 0.0 mm/yr to 0.5 mm/yr

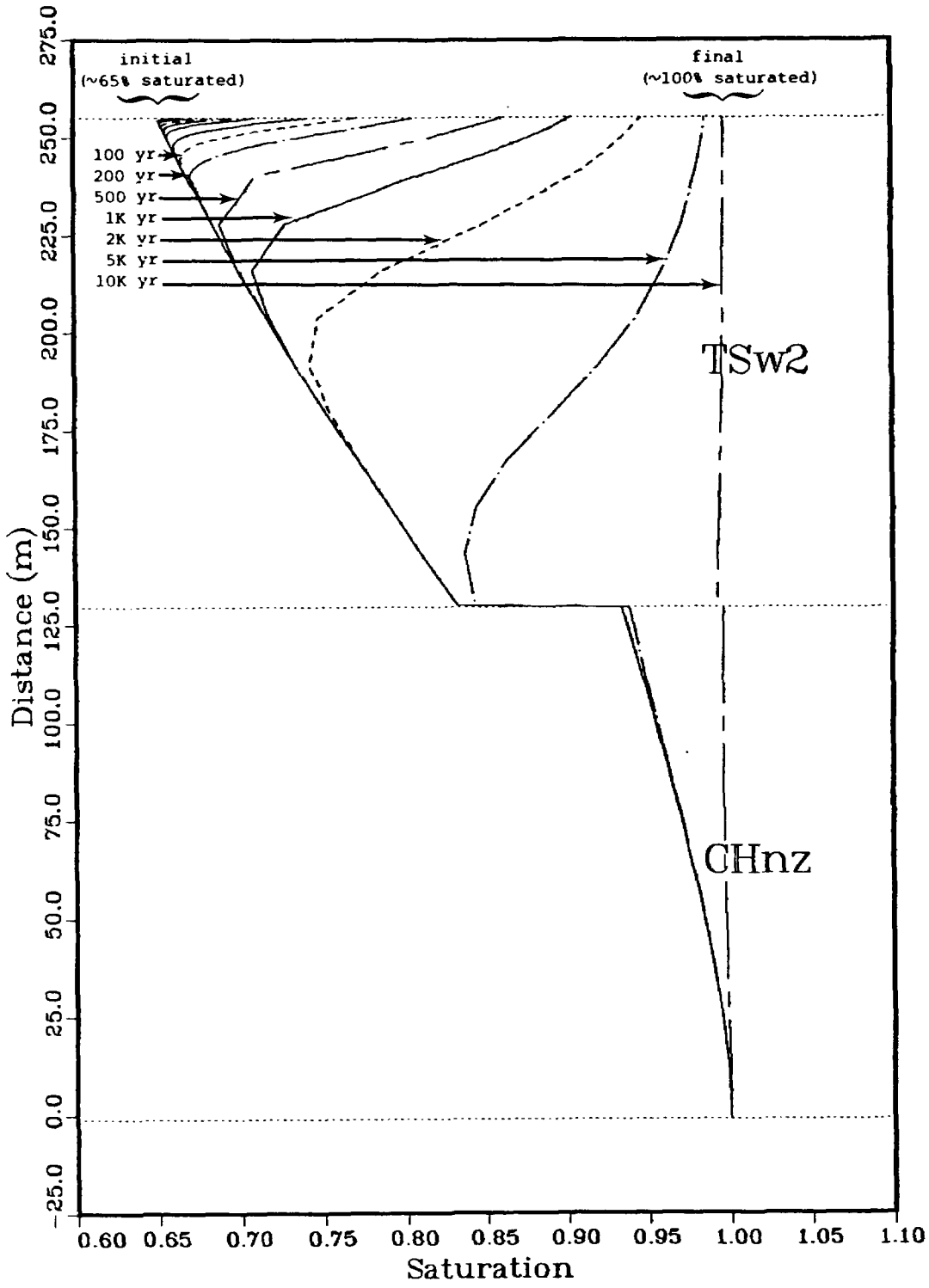


Figure 41. Water flux changed from 0.0 mm/yr to 0.5 mm/yr

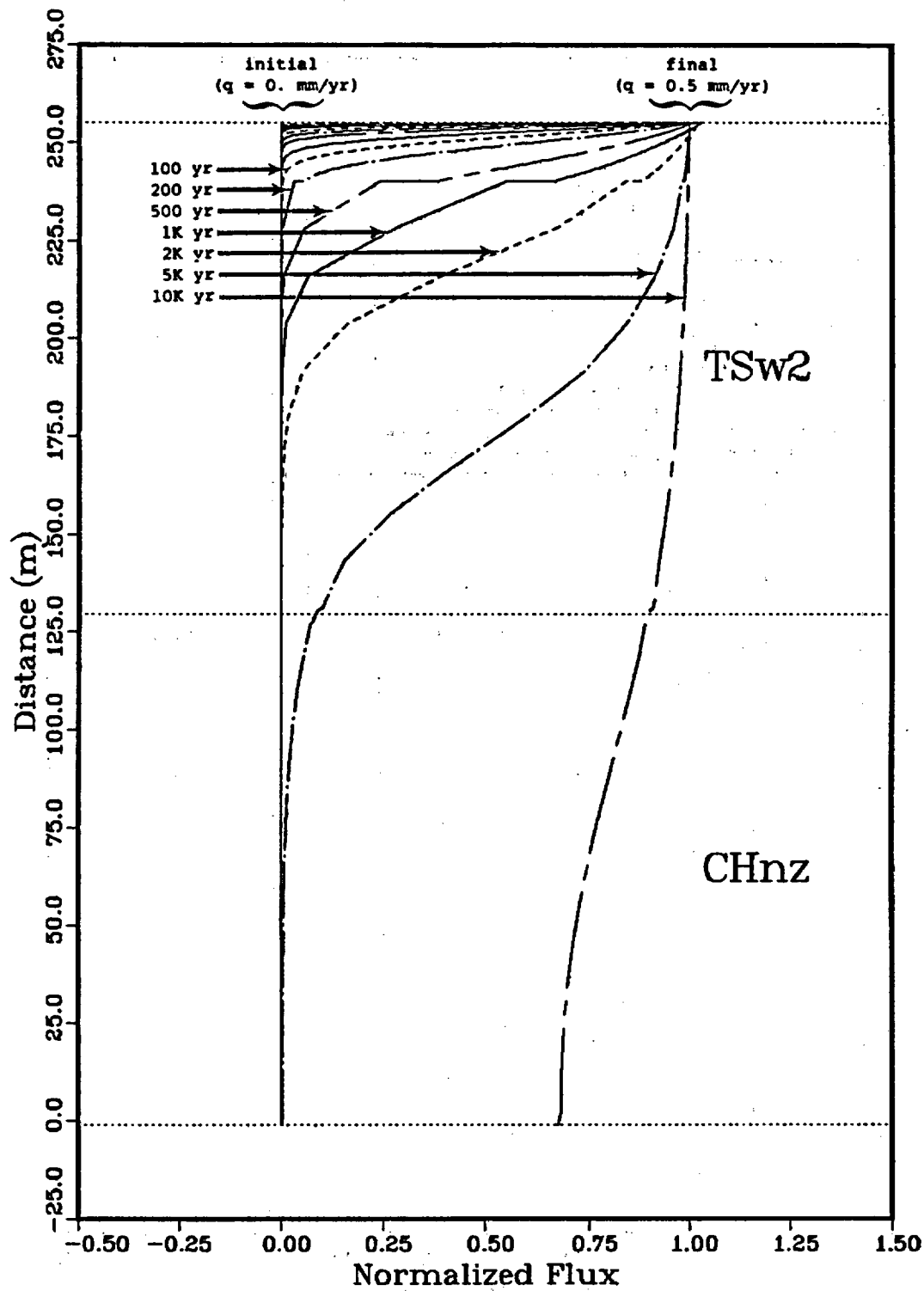


Figure 42. Water flux changed from 0.0 mm/yr to 0.5 mm/yr

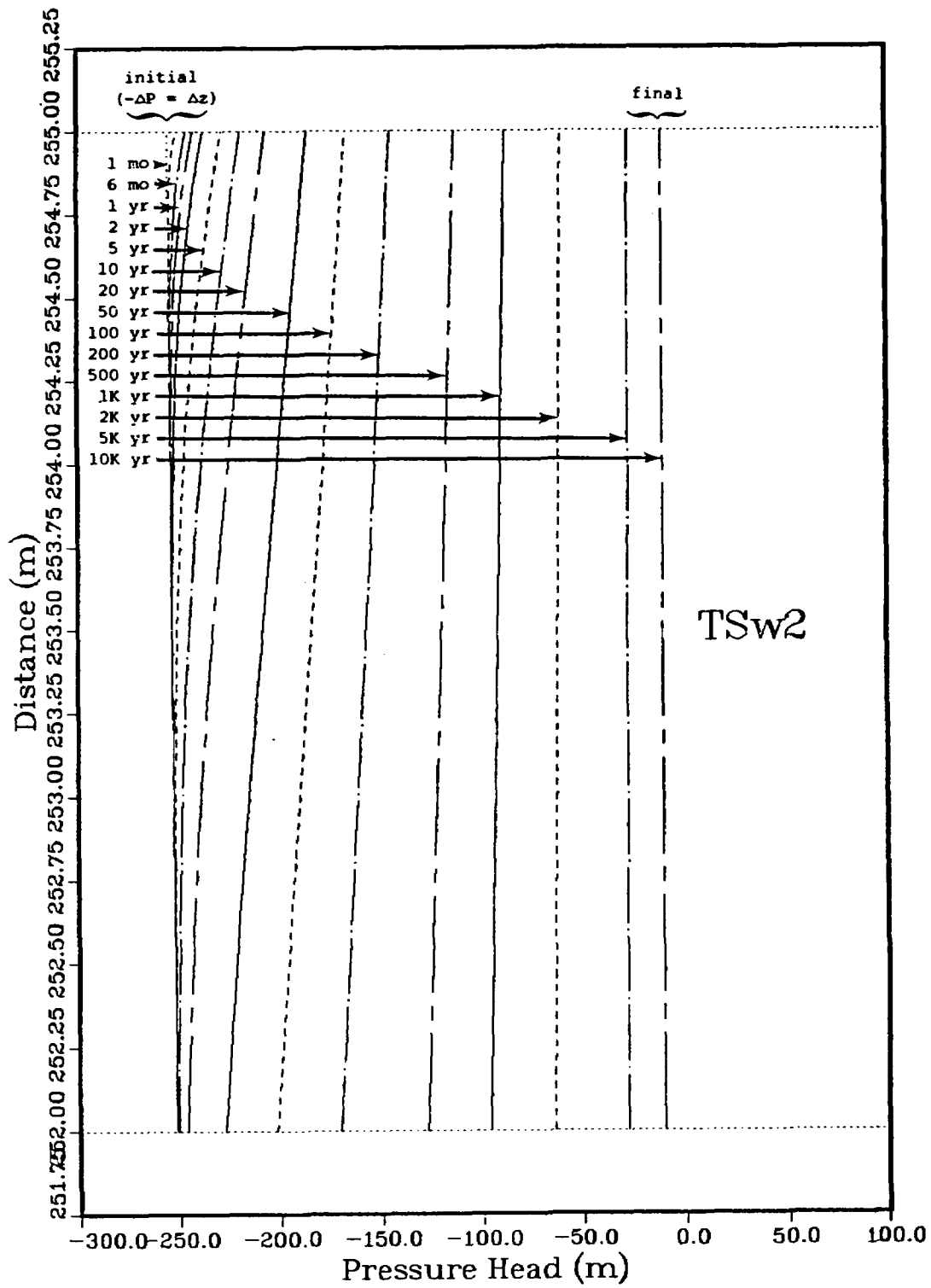


Figure 43. Water flux changed from 0.0 mm/yr to 0.5 mm/yr

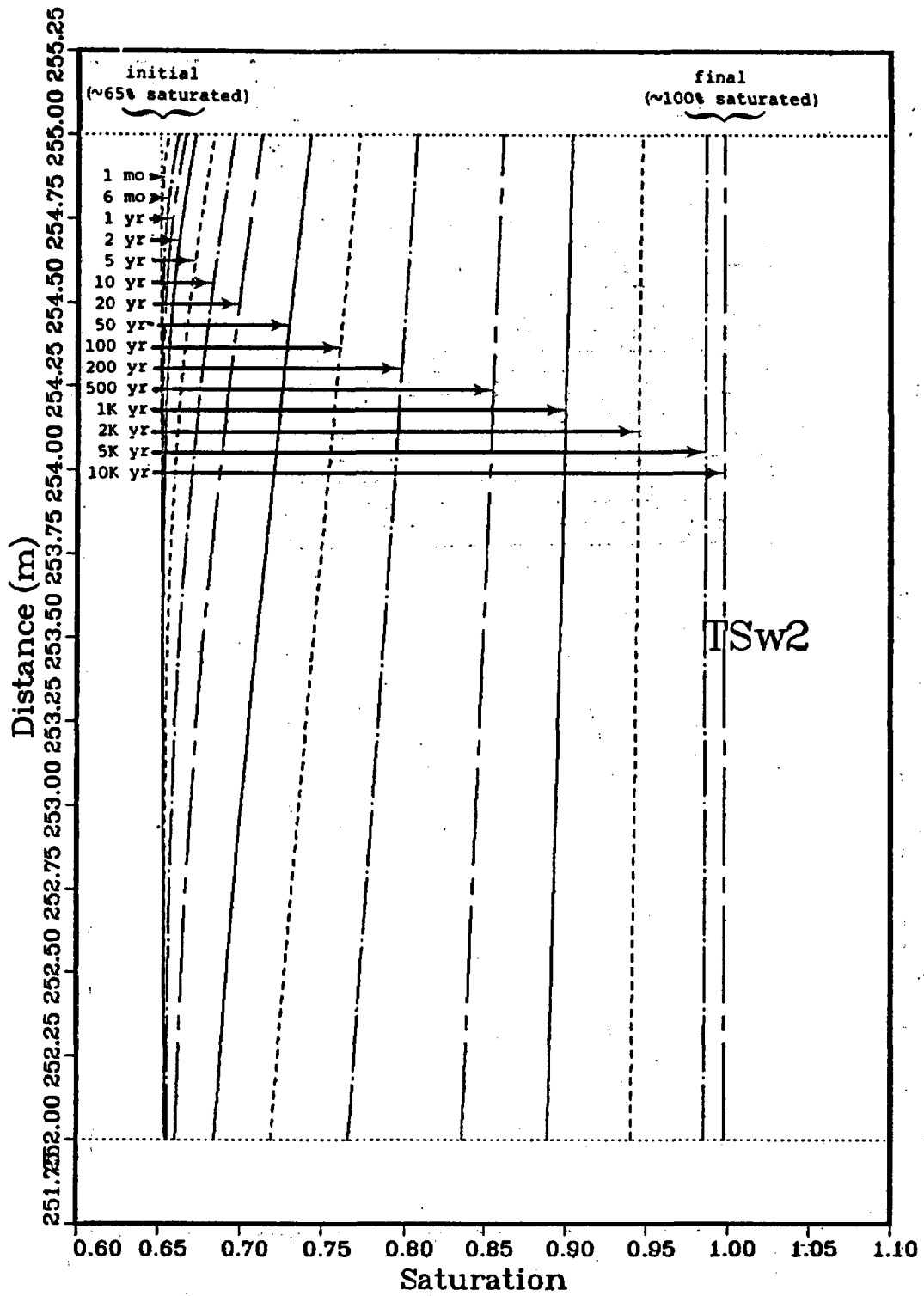


Figure 44. Water flux changed from 0.0 mm/yr to 0.5 mm/yr

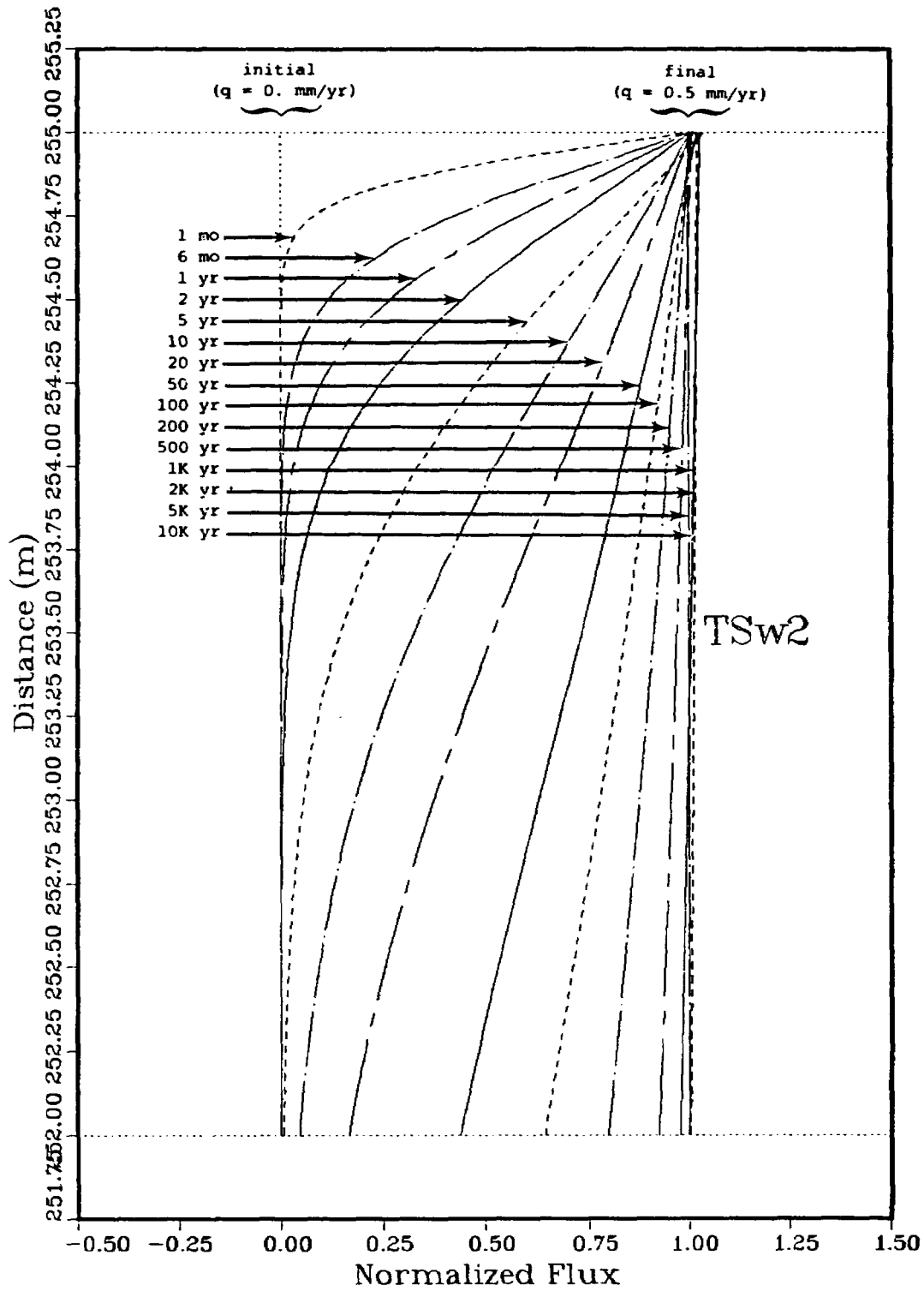


Figure 45. Water flux changed from 0.0 mm/yr to 0.5 mm/yr

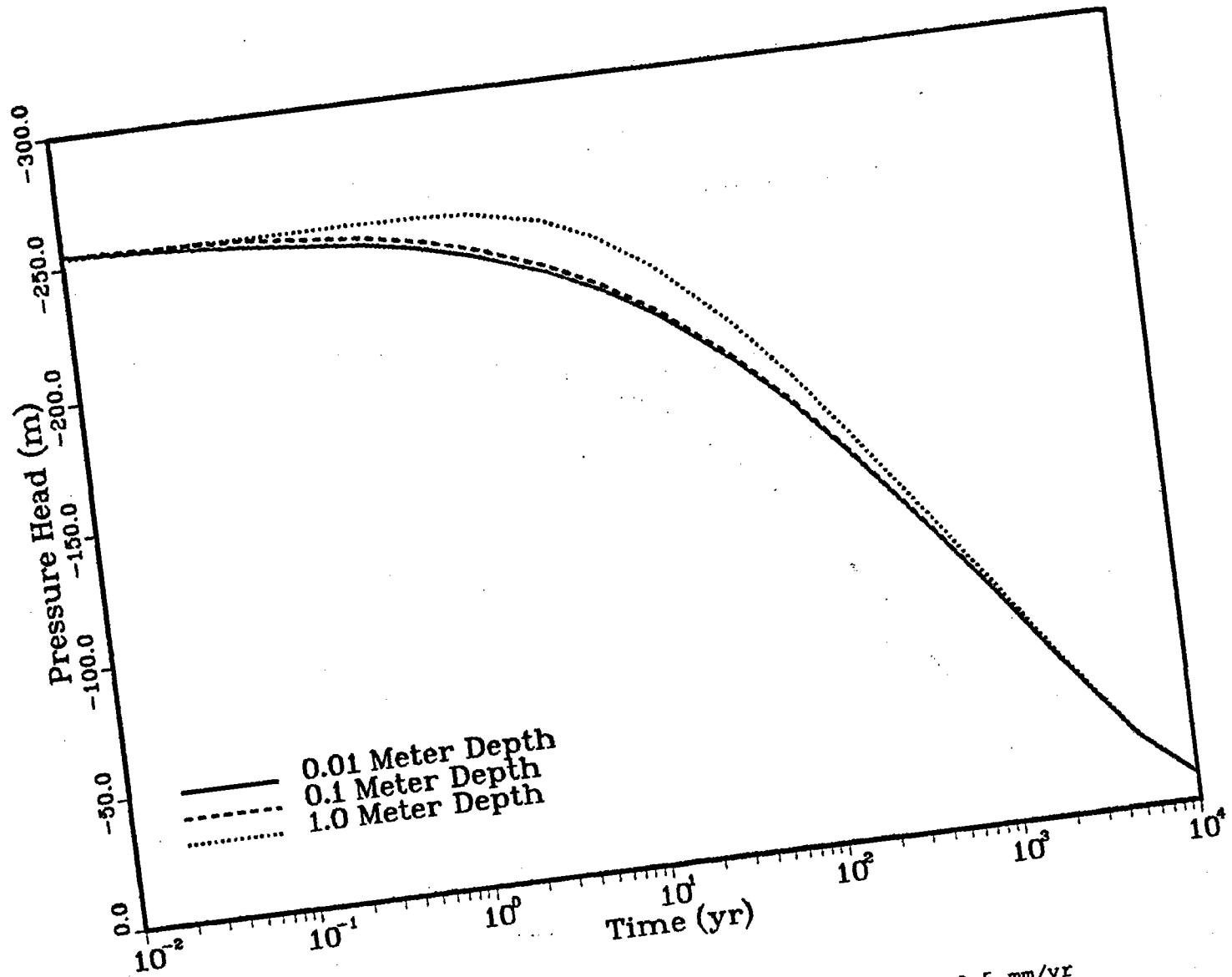


Figure 46. Water flux changed from 0.0 mm/yr to 0.5 mm/yr

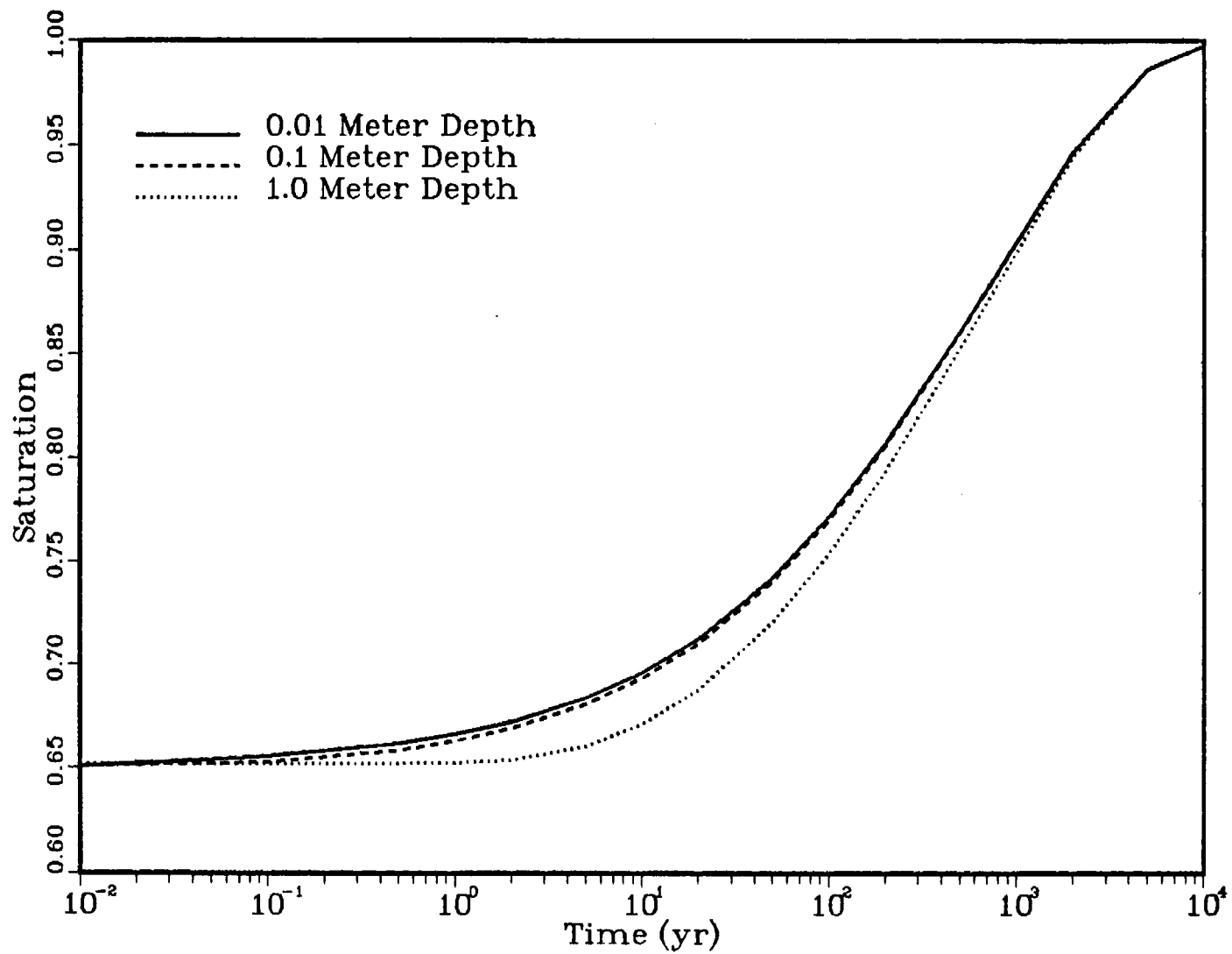


Figure 47. Water flux changed from 0.0 mm/yr to 0.5 mm/yr

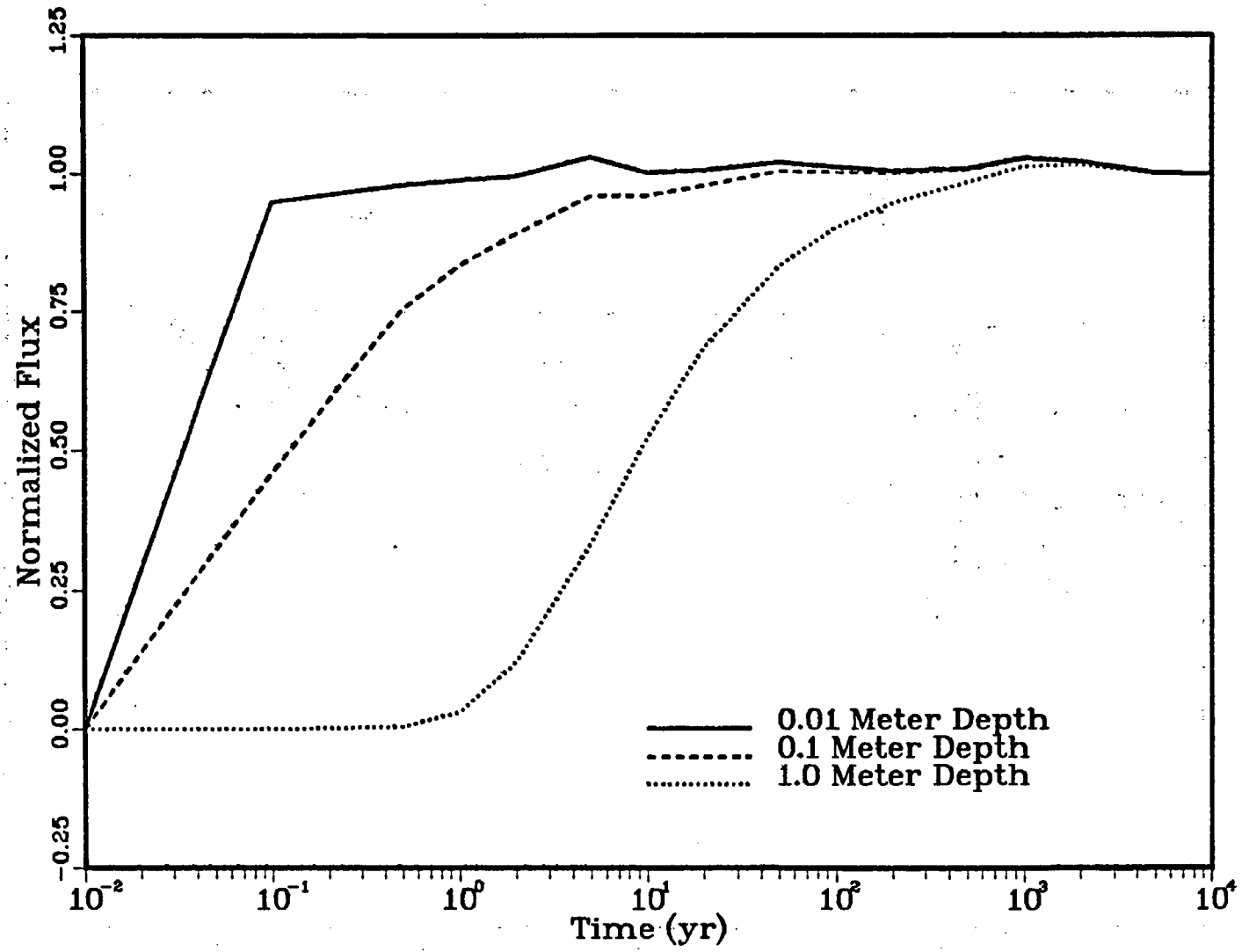


Figure 48. Water flux changed from 0.0 mm/yr to 0.5 mm/yr

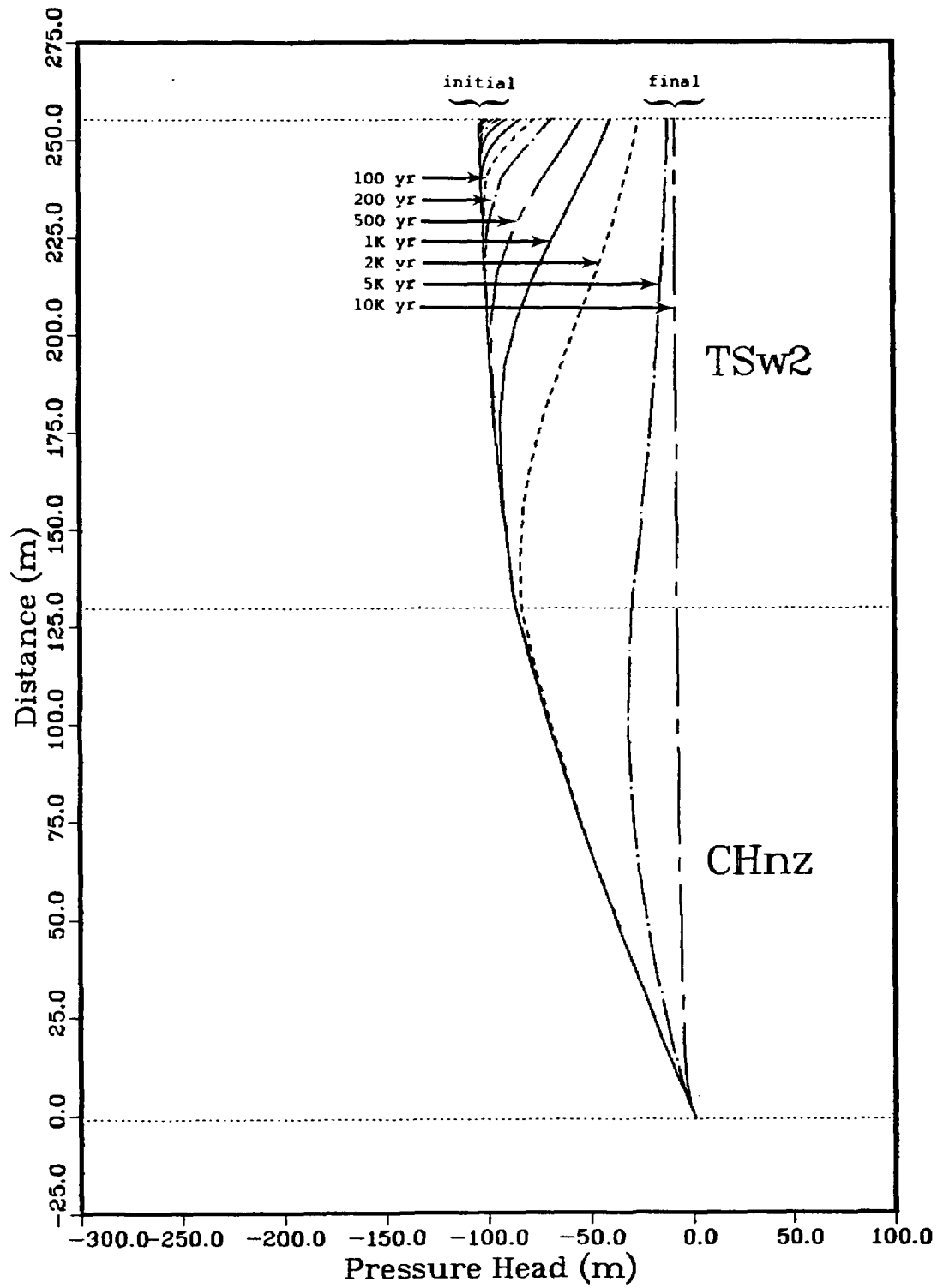


Figure 49. Water flux changed from 0.1 mm/yr to 0.5 mm/yr

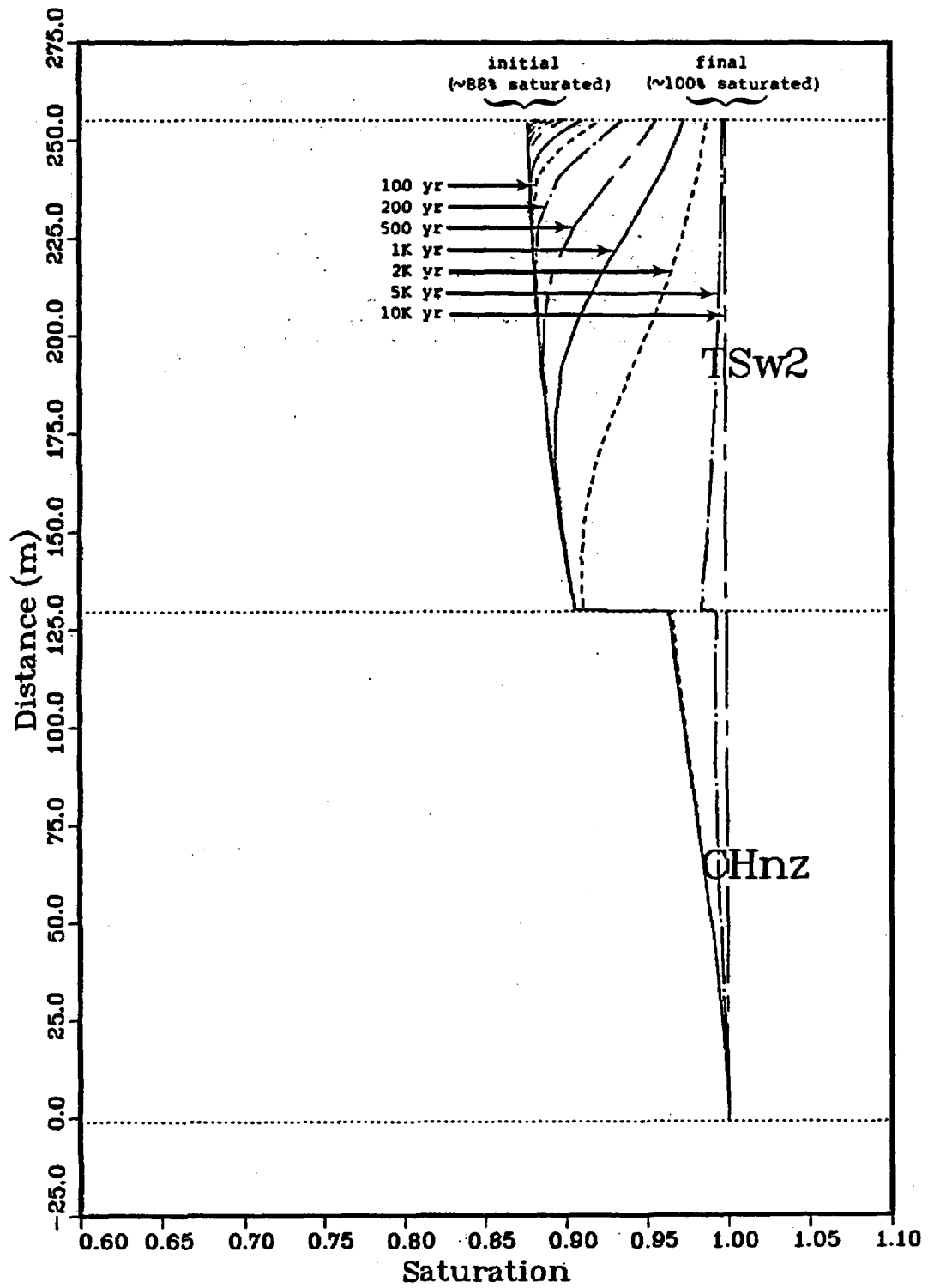


Figure 50. Water flux changed from 0.1 mm/yr to 0.5 mm/yr

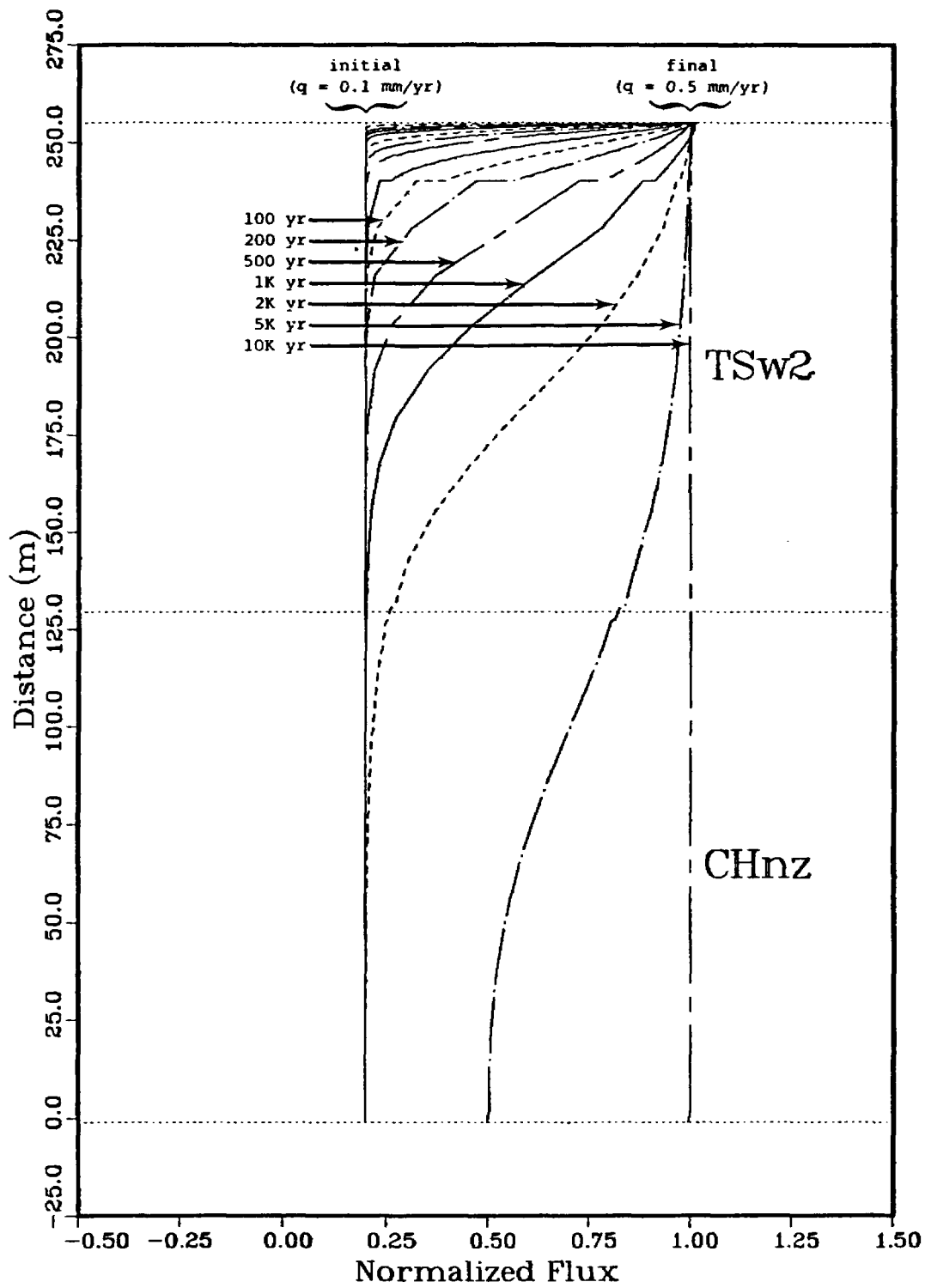


Figure 51. Water flux changed from 0.1 mm/yr to 0.5 mm/yr

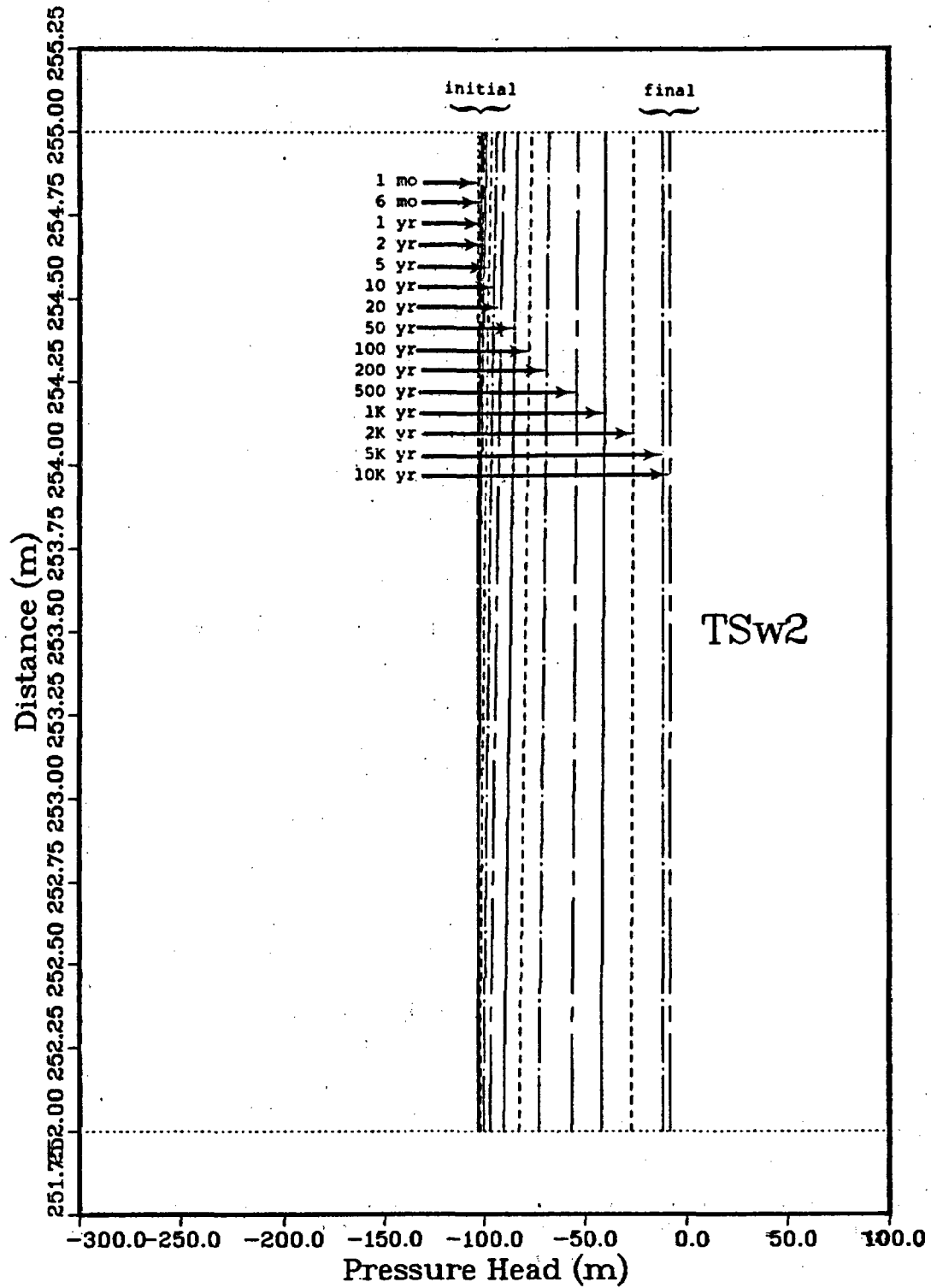


Figure 52. Water flux changed from 0.1 mm/yr to 0.5 mm/yr

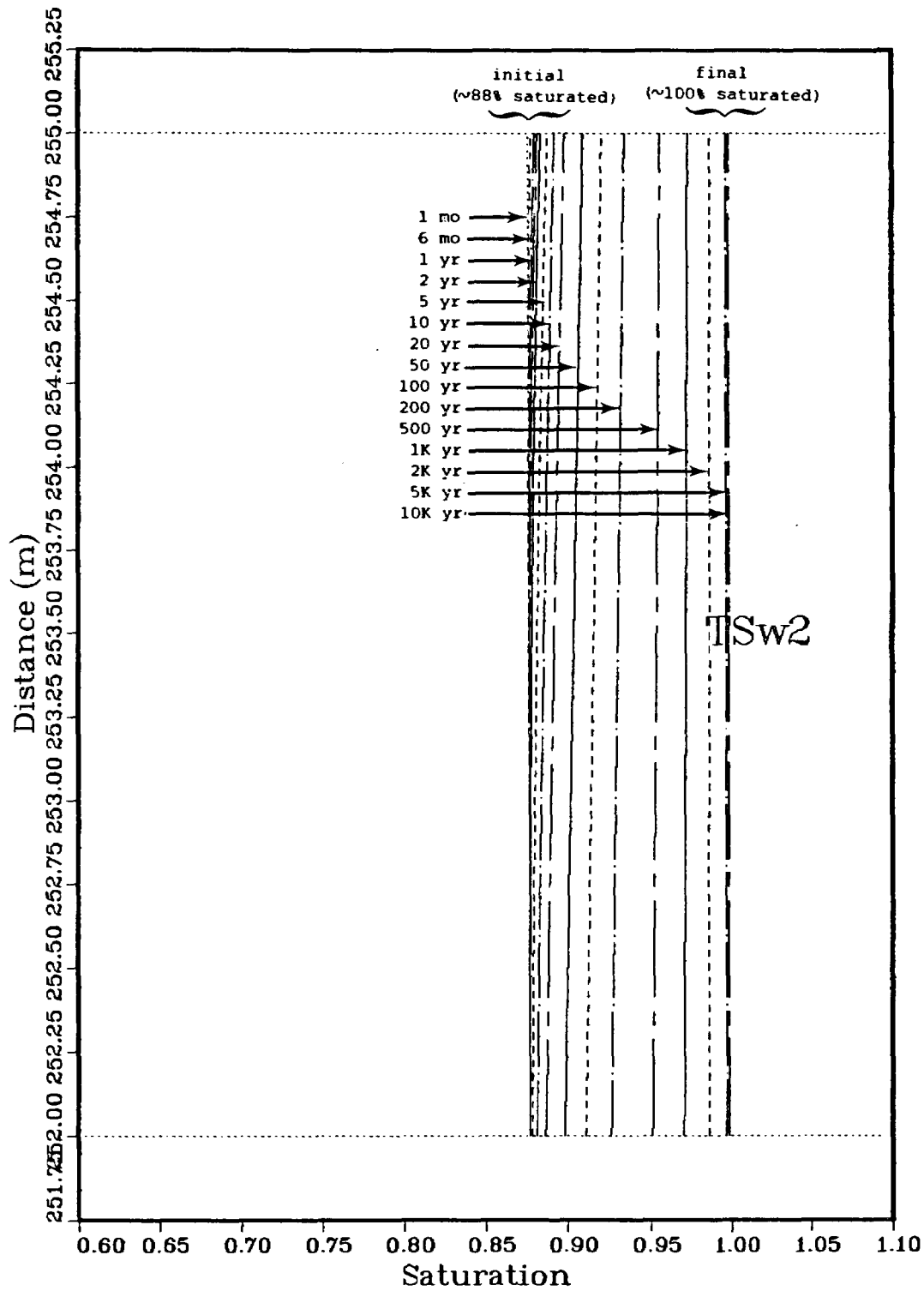


Figure 53. Water flux changed from 0.1 mm/yr to 0.5 mm/yr

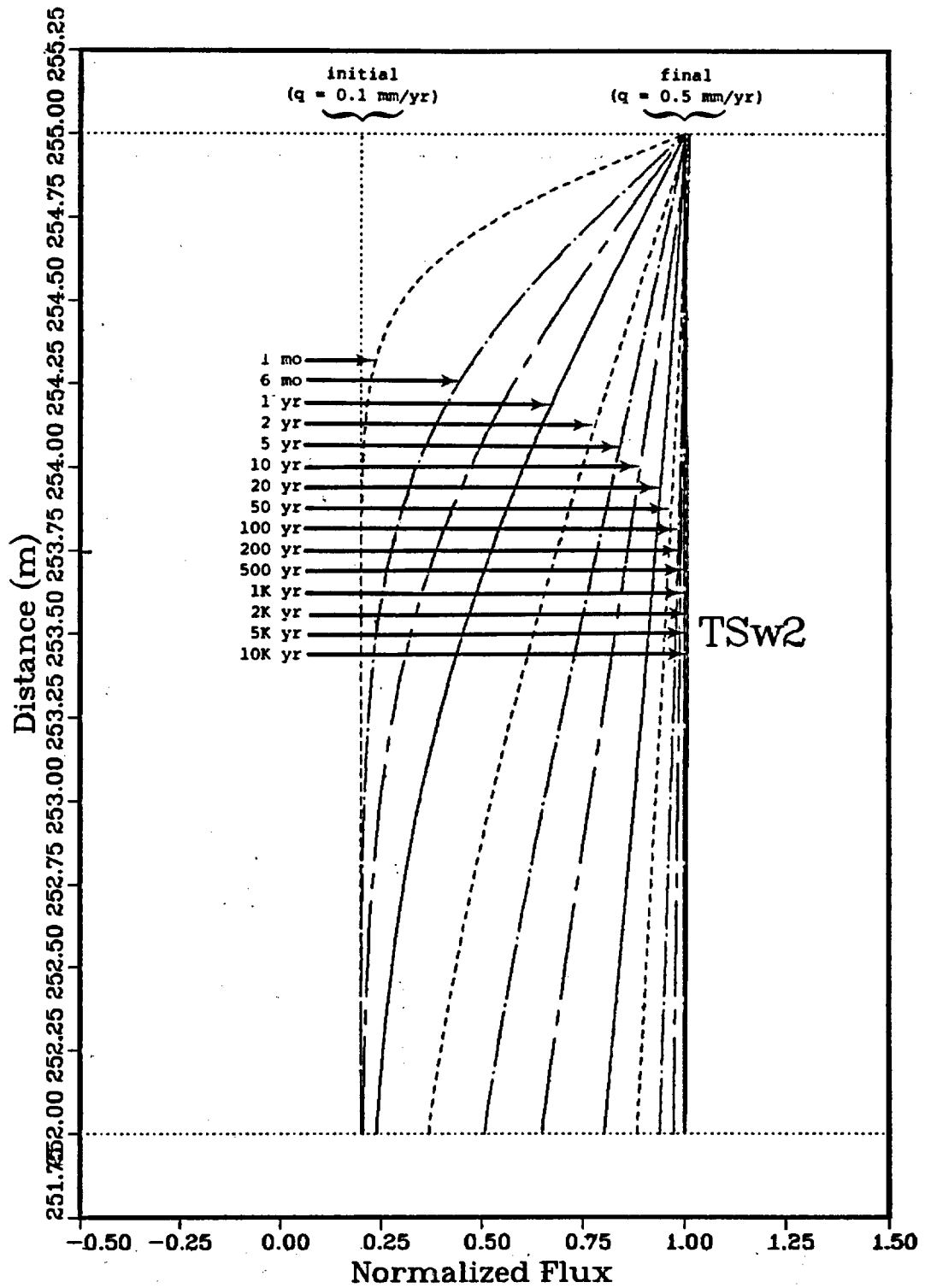


Figure 54. Water flux changed from 0.1 mm/yr to 0.5 mm/yr

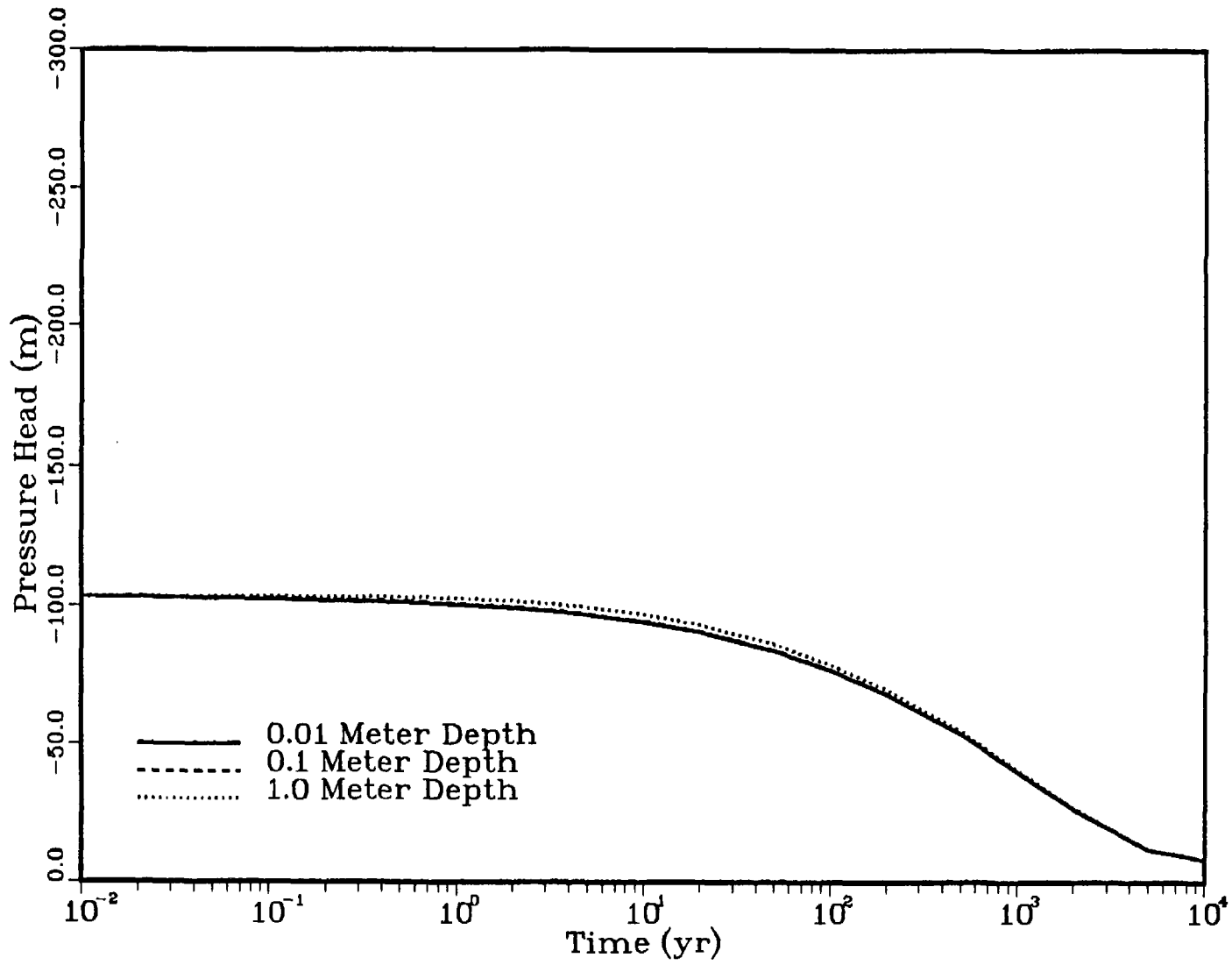


Figure 55. Water flux changed from 0.1 mm/yr to 0.5 mm/yr

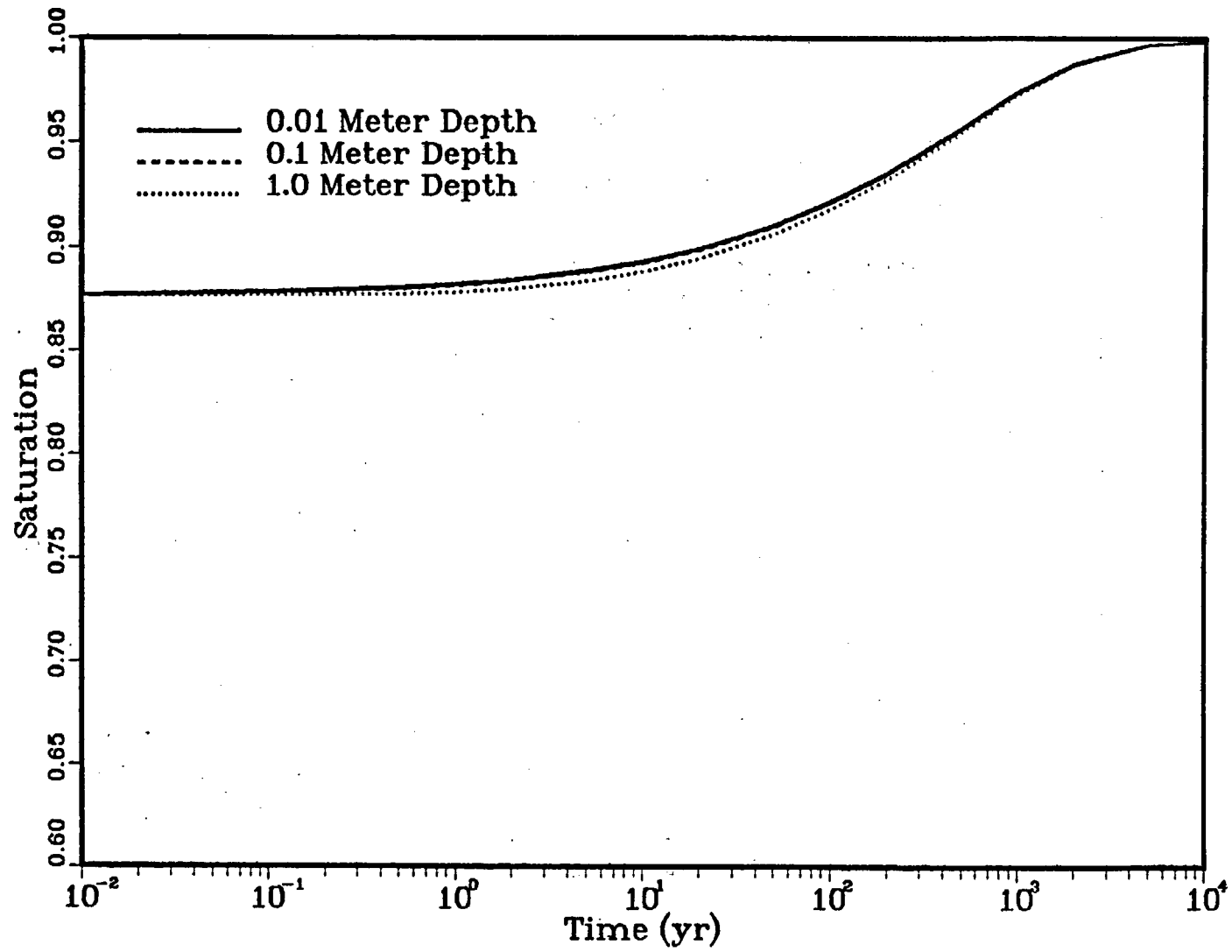


Figure 56. Water flux changed from 0.1 mm/yr to 0.5 mm/yr

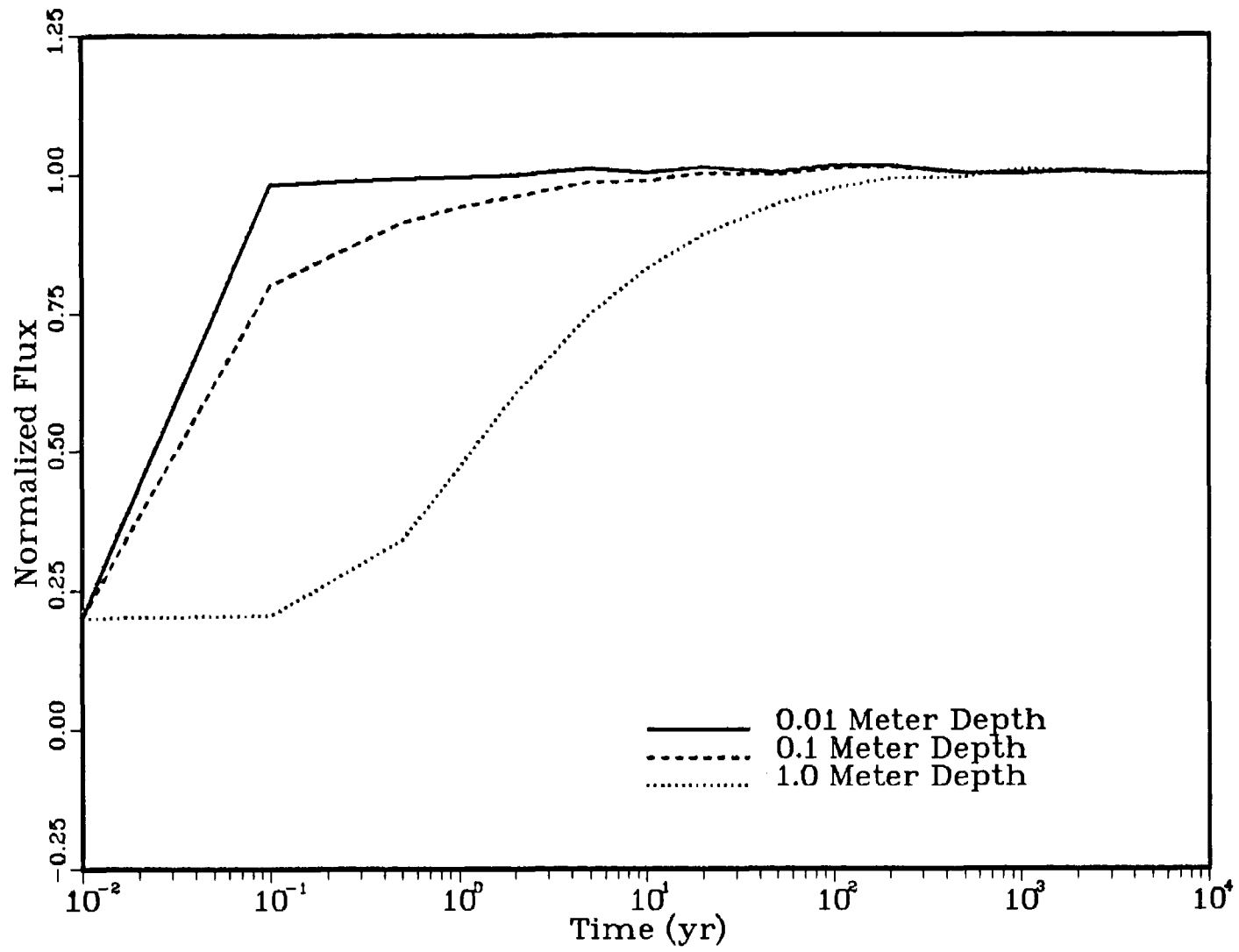


Figure 57. Water flux changed from 0.1 mm/yr to 0.5 mm/yr

MEMORANDUM NO. 2

NNWSI HYDROLOGIC ANALYSIS NO. 72-19
SUPPORT OF EXPLORATORY SHAFT ACTIVITIES

date: June 30, 1987

to: Ralph R. Peters, 6312

from: Ralph R. Peters, 6312
J. H. Gauthier, 6312

R Peters
JH Gauthier

subject: NNWSI PDM 72-19 - Support of Exploratory Shaft Activities

We have completed two different analyses that may provide guidance to personnel currently involved in defining experiments for the Exploratory Shaft. These analyses were defined in a memo to J. H. Gauthier and R. R. Peters from R. R. Peters and dated March 23, 1987. These analyses were formally assigned in NNWSI Problem Definition Memo 72-19. A report is attached to this memo that defines the calculations performed and discusses the results of the calculations. These calculations are nearly identical to a subset of the calculations assigned as NNWSI Hydrologic Analysis No. 8 (results reported in a memo to R. Peters from R. Peters and J. H. Gauthier, dated April 14, 1986); the difference between the two being the matrix saturation curves used in the calculations. A major portion of this report discusses the differences in hydrologic response that result from shifting from the saturations curves used in Hydrologic Analysis No. 8 to those used in Hydrologic Analysis 72-19. A major result of this analysis is the quantitative indication that major changes in the matrix saturation curve (well within those currently proposed by NNWSI participants) can significantly influence the phenomenology of flow and calculational estimates of water flow in unsaturated tuff.

Copy to:

6310 T. O. Hunter
6312 F. W. Bingham
6312 A. L. Dudley
6312 J. H. Gauthier
6312 R. R. Peters
6312 M. S. Tierney
6312 M. L. Green

6313 T. E. Blejwas
6313 E. A. Klavetter
6313 R. M. Zimmerman
6315 S. Sinnock
6310 10-12144-SNL/QIII
6310 72-12144-19/QIII
6310 NNWSI CF

HYDROLOGIC CALCULATIONS CONCERNING ACTIVITIES IN THE EXPLORATORY SHAFT

Introduction

The activities associated with the construction of the Exploratory Shaft and related facilities could affect in situ conditions. In particular, the use of water in drilling and mining activities may significantly affect the surroundings and thus affect estimates of the in situ hydrologic parameters. The values of the estimated hydrologic parameters and estimates of their accuracy may affect performance assessment activities.

Experiments being planned in the Exploratory Shaft facilities may significantly aid in understanding flow mechanisms in unsaturated, fractured tuff. The results of these experiments may also be used to validate computer codes. Performance assessments of the Yucca Mountain site will likely require both a conceptual model of flow and validated computer codes.

This report discusses both issues, and defines and discusses the results of analyses that may aid in decisions regarding future activities. Calculations done for Hydrologic Analysis No. 8 (HA 8 -- results reported in a memo to R. Peters from R. Peters and J. H. Gauthier, dated April 14, 1986) addressed these issues using information which included matrix saturation curves based on thermocouple-psychrometer test data. The calculational set discussed in this report (Hydrologic Analysis 72-19 -- HA 72-19) is a subset of the calculations discussed in the April 1986 memo with the difference between the two calculation sets being the matrix saturation curves; the curves used in the current calculations are based on mercury intrusion data and are shifted much closer to zero (e.g., the pressure head at a matrix saturation of 50% for the Topopah Spring welded unit in the April 1986 memo was about -420 m, for the current calculations it is -16 m). A major emphasis of this report is to discuss the differences between the two calculational sets and to determine whether the conclusions reached in the April 1986 memo are still valid.

EFFECT OF CONSTRUCTION ACTIVITIES ON IN SITU ACTIVITIES

The construction of the Exploratory Shaft and the underground facilities, and preparations for various experiments in the underground facilities will require considerable drilling and coring. Drilling may be used in the construction of drifts. Coring is used to obtain samples, obtain access to the rock mass for measurements, etc. A debate is currently going on concerning whether holes should be drilled or cored using standard techniques (water is used as the working fluid) or whether the holes should be drilled or cored dry (air is used as the working fluid). Both techniques will, to some extent, affect the surrounding rock mass. Air-drilling and air-coring will dry the surrounding rock to some extent. Water-drilling and water-coring may force water into the surrounding fractures and matrix blocks. If most of the water used in drilling and coring is forced into the fractures then the change in matrix saturation will be very small at any location (see discussion below in "General Discussion" section). If there is significant penetration of water into the matrix blocks there may be significant, localized changes in the matrix saturation. Thus, the manner in which these holes are drilled or cored may affect the hydrologic parameters of the surroundings and thus, the accuracy of estimates of in situ conditions in this area. The level of accuracy of the estimates of in situ conditions will likely affect performance assessments of the Yucca Mountain site.

The first analysis set discussed in this report (titled "Application of High Pressure Water to a Matrix Block") investigates the depth of penetration of water into the densely welded matrix material. The results of these calculations provide information that may be useful in deciding what circumstances may allow standard techniques and what circumstances require the use of air as the drilling fluid. Some preliminary conclusions are presented in the section "General Discussion."

Application of High Pressure Water to a Matrix Block

Definition of Analysis

The first analysis investigated the response of a matrix block (no fractures) to water drilling-fluid under high pressure. The matrix block geometry and boundary conditions are indicated in Figure 1. The stratigraphy is that found at drill hole USW G-4 (Ortiz et al., 1985). For the purposes of this calculation the rock-mass properties of the entire column are those of TSw2. In the paper by Rulon et al. (1986), the saturation properties of the unit below the repository (CHnz) were estimated from linear interpolation of a set of data points. It would be difficult to use this data, so the saturation curve for unit TSw2 is used instead. The results in the region of interest (this region is 120 m above the interface with unit CHnz) should be affected very little by the saturation curve used for CHnz. The block extends from a position roughly in the center of unit TSw2 to the water table.

The lower boundary condition was a pressure-head condition set by the water table. The initial condition and the upper boundary condition were set to the conditions that were found to give the largest penetration of water into the matrix in HA 8. The initial condition was defined by having a steady flow of 0.1 mm/yr throughout the column. This resulted in a saturation at the top of the column of about 80%. The boundary condition applied a pressure head of 20 m (about 30 psig) to the rock matrix at the top of the column for 100 minutes. After the end of the time that the high pressure water was applied, the upper boundary condition was reset to the initial condition (0.1 mm/yr flux). Water was not allowed to flow up and out of the column after the end of the time the high-pressure water was applied.

The mathematical model for water movement at Yucca Mountain used in this analysis was the composite porosity model as described in Klavetter and Peters (1986). The computer code used in this analysis was TOSPAC (Dudley et al., In preparation) which incorporates the hydrologic model described in the previous reference.

The properties of the rock column are listed in Table 1. The paper by Klavetter and Peters (1986) contains a discussion of the terms and nomenclature used in this table and is a source of the data listed in Table 1 with one exception. The matrix saturation curve used for the rock column is that reported by Rulon et al. (1986). The matrix saturation-curve values used in HA 8 are included in Table 1 for comparison purposes. These two matrix saturation curves are plotted in Figure 2. The fracture saturation curve plotted in Figure 2 is relevant to the next analysis set ("Response of a Tuff Column to Changes in Flux"); it is not relevant to these discussions.

The NNWSI Reference Information Base (RIB) contains information concerning only two of the parameters in Table 1; the matrix saturated hydraulic conductivity and matrix porosity. However, the values in the RIB are very close to those listed in Table 1.

$$\text{RIB values: } n_m = .1062, K_{m,b} = 2.3 \times 10^{-11} \text{ m/s}$$

The values in Table 1 are identical (with the one noted exception) to those in HA 8 so the results of this analysis can be compared with those of the previous analysis.

Because we are interested in the response of the matrix to high pressure water, the fractures were eliminated from this analysis by setting their area equal to zero.

Table 1
Fractured-Tuff Properties for Both Analysis Sets

<u>Matrix Properties</u>	<u>Unit TSw2</u> ¹	
Porosity (n_m)	0.11	
Hydraulic Conductivity ($K_{m,b}$) (m/s) ²	1.9×10^{-11}	
Sat. Curve Parameter - S_r	0.318^3	0.080^4
Sat. Curve Parameter - α (1/m)	0.112^3	0.00567^4
Sat. Curve Parameter - β	3.040^3	1.798^4

¹ The properties of unit Chnz were set equal to those of unit TSw2 - see the text for further discussion.

² 1.0 mm/yr is equal to 3.2×10^{-11} m/s

³ These values obtained from Rulon et al. (1986).

⁴ These values, taken from HA 8, are included for comparison purposes.

Table 1 (continued)
Fractured-Tuff Properties for Both Analysis Sets

<u>Fracture Properties</u>	<u>Unit TSw2</u> ¹
Porosity (n_f) ²	18. x 10 ⁻⁵
Compressibility ($\partial n_f / \partial s'$) (1/m)	12. x 10 ⁻⁸
Hydraulic Conductivity ($K_{f,b}$) (m/s)	3.1 x 10 ⁻⁹

Fracture Saturation Coefficients are $S_r = 0.0395$, $\alpha = 1.285/m$, $\beta = 4.23$

Rock-Mass Coefficient of Consolidation ($\alpha'_{bulk} - 1/m$)	5.8 x 10 ⁻⁷
--	------------------------

Compressibility of Water (β'_w) is 9.8 x 10⁻⁷/m

¹ The properties of unit Chnz were set equal to those of unit TSw2 - see the text for further discussion. Note: The fracture properties used in HA 72-19 and HA 8 are identical.

² The fracture porosity (n_f) is set to zero for the first analysis.

Calculation Results

The calculational mesh used to perform the calculations is shown in Figure 3. It is identical to the one used in HA 8. The cell size ranged from the order of meters in the middle of the column to 1 millimeter at the top of the mesh where the pressure-head boundary condition was applied. For HA 8, the mesh also was made fairly fine at the interface between units TSw2 and CHnz (which have the same material properties for calculations discussed in this report) and at the lower boundary.

The calculational case discussed in this report corresponds to the calculational case in HA 8 that showed the greatest penetration of water into the matrix block. This report contains figures from HA 8 (April 1986 report) for comparison purposes. The figures for this calculational case are presented in the following order:

- Figure 4. Pressure head versus distance (top 10 cm of the column) at 11 different times,
- Figure 5. Saturation versus distance at 11 different times,
- Figure 6. Water flux versus distance at 11 different times,
- Figure 7. Pressure head versus time at 3 locations at the top of the column (0.2 cm, 1.0 cm and 10 cm)
- Figure 8. Saturation versus time at 3 locations at the top of the column
- Figure 9. Water flux versus time at 3 locations at the top of the column

The pressure head profiles (Figure 4) show the affect of the much different saturation curves. The initial pressure head in the rock matrix is much closer to zero for HA 72-19 than for HA 8. The initial pressure head in most of the rock column for these two analyses is the pressure head where the rock conductivity equals the flux. This condition is satisfied at a pressure head of -8 m for HA 72-19 and -100 m for HA 8.

In the current calculation, the saturation profiles (Figure 5) show that water penetrates about 1 cm at the end of 100 minutes. This distance is about one-half that seen for HA 8. This also indicates that about one-half as much water is injected into the matrix in HA 72-19 as in HA 8. The major reason for the difference in penetration distance and amount of water injected into the matrix is the tremendous difference in initial pressure heads in the the rock matrix (see Figure 4). In HA 8, water at 20 m pressure head was being pushed into rock that had an initial pressure head of -100 m. In the current analysis, water at 20 m pressure head is being pushed into rock that has an initial pressure head of -8 m. In the current calculation, the saturation profile returns to the initial condition more slowly. However, in both cases the profile is within a few percent of the initial condition 1 month after the pulse of water was injected into the matrix block.

The flux profiles (Figure 6) also show that less water is injected into the rock than in HA 8. For example, at 1 day the HA 8 flux is about 8×10^{-10} m/s over a distance of about 10 cm while the HA 72-19 flux is 2×10^{-10} m/s over a distance of about 3 cm. A smaller amount of water is injected in HA 72-19 because of the lower pressure-head gradients.

Figures 7, 8, and 9 show time-history plots of the pressure head, saturation, and flux at various locations near the surface of the block. The HA 8 results and those of the current calculation are slightly different. However, after a a few months both calculations show that hydrologic conditions have nearly returned to the initial state. For example, the matrix saturation in both cases is within one percent of the initial state 30 days after the water injection.

The following statement is taken from the April 1986 report (page 10); it appears to be a valid summation of the results seen for the current calculations.

"The results of these calculations indicate that the application of high-pressure water to matrix material, like that found in the repository zone, will not cause water penetration to large depths (<5 cm). They also show the water quickly redistributes so that the increase in matrix saturation is small in the region near where the water was injected (<3 percentage points rise in saturation at 1 month)."

General Discussion

It has been a general concern that the application of drilling water to the fractured tuff may cause the in-situ conditions to change significantly. The results of water injection into the fractured tuff may be bounded by two calculations. In the first bounding calculation, it is assumed that water first moves through the fractures (with minor amounts being absorbed into the matrix) and then, over a long period of time, the water in the fractures equilibrates with that in the matrix with most of the water in the fractures moving into the partially saturated matrix. The second bounding calculation assumes that the injected water moves into the matrix forming a wet region near the injection point. The actual situation is intermediate between these two extremes.

In the first scenario, the change in matrix saturation depends on the relative volumes of the matrix and the fractures because the water is first stored in the fractures and then moves into the matrix.

$$\Delta S_m = n_f / n_m \quad (1)$$

Values of the parameter n_f are probably in the range of 10^{-5} to 10^{-3} (Sinnock et al., 1984; Peters et al., 1984) while the parameter range for n_m in TSw2 is from 0.05 to 0.15. The maximum change in matrix saturation then is of the order of $10^{-3}/0.05 = 0.02$ or less. Thus, it appears that pervasive flooding of the fractures will not significantly affect the matrix saturation.

The matrix may take up water during the time that high pressure water is being injected into the rock mass, forming pockets of high saturation around the regions where drilling occurred. The upper bound on this change in matrix saturation was calculated (in HA 8 and in HA 72-19) by assuming that the high-pressure water is applied to the matrix throughout the drilling process. (In the actual case, some portions of the rock mass will see water under lower pressures than the pump pressure and for periods of time shorter than the actual drilling takes place.) The conclusion reached in the previous section was that no significant change in saturation will be noticeable after the passage of a month or so.

Thus, it appears that drilling with water will not significantly affect the state of saturation of the rock. This statement assumes that relatively low-pressure water (<30 psig) is applied to the rock for relatively short periods of time (<100 minutes). It also implicitly assumes that there is an attempt to limit the amount of water used underground. For example, it is obvious that allowing a pond of water to stand for many weeks must affect the local state of saturation. These results and conclusions are subject to the limitations of the models used and the data available, especially the saturation and conductivity curves for the matrix. However, comparison of the calculational results in this report (using a saturation curve based on mercury-intrusion data) and those in HA 8 (using a saturation curve based on thermocouple-psychrometer data) show that the conclusion "drilling with water will not significantly affect the state of saturation of the rock" is not affected greatly by the choice of saturation and conductivity curves.

**EXPERIMENTS INVESTIGATING THE MOVEMENT OF WATER
IN A FRACTURED, UNSATURATED TUFF**

Experiments in the Exploratory Shaft are being planned to investigate the flow of water in an unsaturated, fractured tuff. The results of these experiments directly affect the conceptual model of water flow in unsaturated, fractured tuff, and may be used to validate computer codes. Performance assessments of the Yucca Mountain site require good understanding of the manner in which water flows in Yucca Mountain and validated computer codes to do the calculations required for licensing.

The second analysis set (titled "Response of a Tuff Column to Changes in Flux") discussed simulates an experiment that investigates the response of a column of rock to increases in flux where the flow of water at the final steady-state condition is primarily in the matrix. The purpose of these calculations is to look at the response of the fractured tuff to changes in flux and to estimate the time it takes for the upper meter or so of the rock column to move from one steady-state condition to another. Performance assessment planning may be affected by gaining understanding of the data that may be available from this sort of experiment and whether the results can be used for developing conceptual models and for computer model validation.

Response of a Tuff Column to Changes in Flux

Definition of Analysis

The second analysis set investigates the response of a fractured tuff column to changes in flux. The fractured tuff column and boundary conditions are shown in Figure 10. The stratigraphy is that found at drill hole USW G-4 (Ortiz et al., 1985). For the purposes of this calculation the rock-mass properties of the entire column are those of TSw2. In the paper by Rulon, the saturation properties of the unit below the repository (CHnz) were estimated from linear interpolation of a set of data points. It would be difficult to use this data, so the saturation curve for unit TSw2 is used instead. The results in the region of interest (120 m above the interface with unit CHnz) should be affected very little by the saturation curve used for CHnz. The column extends from a position roughly in the center of unit TSw2 to the water table.

The lower boundary condition is a pressure-head condition set by the water table. There are two different initial conditions defined for this analysis set. The first is a no flow condition that results in a saturation at the top of the column of about 30% for the material properties used in this calculation. The second initial condition is defined by having a steady flow of 0.1 mm/yr throughout the column. This results in a saturation at the top of the column of about 80%. The upper boundary condition is changed at the beginning of the calculation to a constant flow rate of 0.5 mm/yr.

The mathematical model for water movement at Yucca Mountain used in this analysis was the composite porosity model as described in Klavetter and Peters (1986). The computer code used in this analysis was TOSPAC (Dudley et al., In preparation) which incorporates the hydrologic model described in the previous reference.

The properties of the rock mass are listed in Table 1. The paper by Klavetter and Peters (1986) contains a discussion of the terms and nomenclature used in this table and is a source of the data listed in Table 1 with one exception. The matrix saturation curve used for the rock column is that reported by Rulon et al. (1986). The matrix saturation curve values used in HA 8 are included in Table 1 for comparison purposes. These two matrix saturation curves and the fracture saturation curve are plotted in Figure 2. Because we are interested in the response of the fractured tuff to changes in flux the fracture porosity used is that listed in Table 1; the fracture porosity was not set to zero as it was in the previous problem.

Calculation Results

The results for the calculational cases investigating the response of a tuff column to changes in flux are presented in the order discussed above. The figures for both calculational cases are presented in the following order:

- A) Pressure head versus distance (from the top of the column to the water table) at 14 different times,
- B) Saturation versus distance at 14 different times,
- C) Water flux versus distance at 14 different times,
- D) Pressure head versus distance (top 3 m of the column) at 14 different times,
- E) Saturation versus distance (top 3 m of the column) at 14 different times,
- F) Water flux versus distance (top 3 m of the column) at 14 different times,
- G) Pressure head versus time at 3 locations at the top of the column (1.0 cm, 10. cm and 100 cm)
- H) Saturation versus time at 3 locations at the top of the column
- I) Water flux versus time at 3 locations at the top of the column

The results for HA 8 are also plotted on these figures for comparison. (The HA 72-19 set and the HA 8 set used different matrix saturation curves - see Figure 2.) Because Unit TSw2 properties were used all the way to the water table in HA 72-19 and Unit Chnz properties were used for lower part of the column in HA 8, the results at later times when the flux wave is in the lower portion of the column, strictly speaking, are not comparable.

The first set of figures (Fig. 11-19) show the results of increasing the flux from 0.0 mm/yr to 0.5 mm/yr. Figures 11-13 show the pressure head, saturation, and flux profiles for the entire column for the entire simulation. The results of HA 72-19 and those of HA 8 are fundamentally different in character. Profiles of the hydrologic parameters show that for HA 72-19 a "shock wave" forms while for HA 8 there is a gentle increase in the hydrologic parameter (e.g., see the saturation profiles in Figure 12 or the pressure-head profiles in Figure 14). The reason for the difference is the difference in matrix saturation curves. The saturation curve used in HA 72-19 when compared to that in HA 8 (see Figure 2) drops very quickly to the residual saturation and so is able to "isolate" the flux wave from the surroundings more effectively. A more complete discussion of the factors controlling the width of the transition zone from the initial flux to the final flux (about 25 m for HA 72-19 analyses and more than a 100 m for HA 8 analyses) may be found in Dudley, et al. (In preparation). The flux profile is difficult to accurately calculate in the region near the shock wave and there is a tendency for overshooting the actual value (see the 10,000 year profile for HA 72-19 in Figure 13). This overshoot problem can be solved by using a finer mesh and smaller time steps (see Dudley, et al., In preparation), but the solutions presented in this memo are thought to be accurate enough to investigate the phenomena. The fundamental difference in the manner in which the water flows (a "shock wave" versus "diffusive" flow) causes the specific differences discussed below.

The first pressure-head profile that is labeled in the HA 72-19 portion of Figure 11 is the one at 500 years; the profiles at earlier times have not penetrated far enough down the column to be resolved. Figure 13 shows that flux at the top of the column very quickly (≈ 100 years) reaches the steady-state flux value of 0.5 mm/yr. However, Figures 11 and 12 indicate that the steady-state pressure head and saturation at the top of the column is not reached until about 500 years (10,000 years for HA 8) after the flux was changed at the top of the column. Figure 15 indicates that it takes approximately 20 years (500 years for HA 8) for the top of the column to reach saturation values halfway between the initial condition and the final, steady-state condition. Figures 11 and 12 show that, in this matrix-dominated flow regime, for HA 72-19 the upper portions of the column reached steady state long before the lower portions reach steady-state conditions. This is in direct contrast to the results seen in HA 8 where the whole column reaches steady state at about the same time.

It must be noted that in a field experiment, the water flow will be three dimensional not one dimensional as it was in these calculations. This implies that it may not be possible to do this experiment at all because a large volume of rock must have water injected into it before the experimental region will reach steady state.

Figures 14-16 show pressure-head, saturation, and flux profile plots for the top three meters of the mountain. Figure 14 shows the pressure-head profile for the HA 72-19 calculations moving as a "shock wave" down through the column, while the pressure-head profiles for HA 8 show a slow, uniform rise. Figure 15 shows the HA 72-19 saturation rising in a uniform manner even though the pressure head shows an abrupt change; this behavior results from the extremely nonlinear relationship between the pressure head and the saturation. Figure 16 shows the HA 72-19 flux profiles are very steep at early times (< 1 year) and then flatten out at the final condition in later years. The results of HA 8 show a much more gentle increase in the flux. "Steady-state" flux in the top 0.5 m is reached at about 200 years for both HA 72-19 and HA 8 analyses. One should note that when the flux reaches "steady state" in some interval (e.g., for HA 8 the top 0.5 meter of the 200 year flux profile is very near the final, steady-state value of 0.5 mm/yr)

the saturation and pressure heads may be far from their steady-state values (for HA 8 the saturation has moved to a value midway between the initial value and the final value).

Figures 17-19 show the pressure head, saturation, and flux versus time at three different depths (1 cm, 10 cm and 100 cm). Figures 17 and 18 indicate that the pressure head and saturation at three different depths are considerably different in the HA 72-19 calculations while in HA 8 they are approximately the same throughout the simulation. The HA 72-19 steady-state saturation is reached at different times at the three depths with steady state at 10 cm depth being reached at about 500 years. In HA 8, the steady-state saturation is reached at all three depths at approximately the same time (10,000 years). Figure 19 shows the time when the flux reaches its steady-state value is a function of depth. At about 100 years the flux is nearly at its steady-state value at all three depths for both sets of analyses.

Figures 20-28 show the results of a simulation where the flux was increased from 0.1 mm/yr to 0.5 mm/yr. The initial saturation in the column has increased considerably (compare Figures 12 and 21) with the HA 72-19 initial saturation at the top of the column being about 30% for the previous case and about 80% for this case. However, the results seen in these figures are qualitatively the same as those for the previous case. It takes ≈ 100 years for the flux at the top of the column to reach steady state for both HA 72-19 and HA 8 (see Figure 28). The HA 72-19 pressure head and saturation at the top of the column reach "steady state" in about 500 years (see Figures 26 and 27). In contrast, it takes a very long time for the HA 8 pressure head and saturation to respond to the change in flux.

General Discussion

The hydrologic parameters that are measurable (pressure-head and saturation) respond fairly quickly (≈ 500 years) for HA 72-19 while for HA 8 they respond very slowly ($\approx 10,000$ years) to changes in flux if the flow of water is primarily in the matrix. Thus, the results of simulations of both cases point to the same conclusion: the response time is long compared to a reasonable time period for an experiment.

Over-driving the system by increasing the flux (e.g., 5.0 mm/yr instead of 0.5 mm/yr) will cause pervasive flow of water in the fractures to be initiated (this is not desirable because the purpose of a part of the experiment would be to investigate hydrologic phenomena for the situation where the water flow is primarily in the matrix). It appears that it may not be possible to perform a field-scale experiment to investigate the matrix-dominated flow of water in a fractured, porous medium. Lab-scale experiments using highly conductive matrix materials may be the only possibility for investigating matrix-dominated flow of water in a fractured, porous medium. These results and conclusions are subject to the limitations of the models used and the data available.

A major result of both HA 8 and HA 72-19 is the quantitative indication that major changes in the matrix saturation curve (well within those currently proposed by NNWSI participants) can significantly influence the phenomenology of flow and calculational estimates of water flow in unsaturated tuff. It would appear that this matter needs to be investigated and resolved. (See Klavetter and Peters (1987) for further information concerning this topic.)

REFERENCES

Dudley, A. L., R. R. Peters, M. S. Tierney, E. A. Klavetter, J. H. Gauthier, and M. Wilson. In preparation. "Total Systems Performance Assessment Code (TOSPAC) Volume 1: Physical and Mathematical Bases," SAND85-0002, Sandia National Laboratories, Albuquerque, NM.

Klavetter, E. A., and R. R. Peters. 1986. "Estimation of Hydrologic Properties for an Unsaturated, Fractured Rock Mass," SAND84-2642, Sandia National Laboratories, Albuquerque, NM.

Klavetter, E. A., and R. R. Peters. 1987. "An Evaluation of the Use of Mercury Porosimetry in Calculating Hydrologic Properties of Tuffs From Yucca Mountain, Nevada" SAND86-0286, Sandia National Laboratories, Albuquerque, NM.

Ortiz, T. S., R. L. Williams, F. B. Nimick, B. C. Whittet, and D. L. South. 1985. "A Three-Dimensional Model of Reference Thermal/Mechanical and Hydrological Stratigraphy at Yucca Mountain, Southern Nevada," SAND84-1076, Sandia National Laboratories, Albuquerque, NM.

Peters, R. R., E. A. Klavetter, I. J. Hall, S. C. Blair, P. R. Heller, and G. W. Gee. 1984. "Fracture and Matrix Hydrologic Characteristics of Tuffaceous Materials from Yucca Mountain, Nye County, Nevada," SAND84-1471, Sandia National Laboratories, Albuquerque, NM.

Rulon, J., G. S. Bodvarsson, and P. Montazer. 1986. "Preliminary Numerical Simulations of Groundwater Flow in the Unsaturated Zone, Yucca Mountain, Nevada," LBL-20553, Lawrence Berkeley Laboratory, Berkeley, CA.

Sinnock, S., Y. T. Lin, and J. P. Brannen. 1984. "Preliminary Bounds on the Expected Postclosure Performance of the Yucca Mountain Repository Site, Southern Nevada," SAND84-1492, Sandia National Laboratories, Albuquerque, NM.

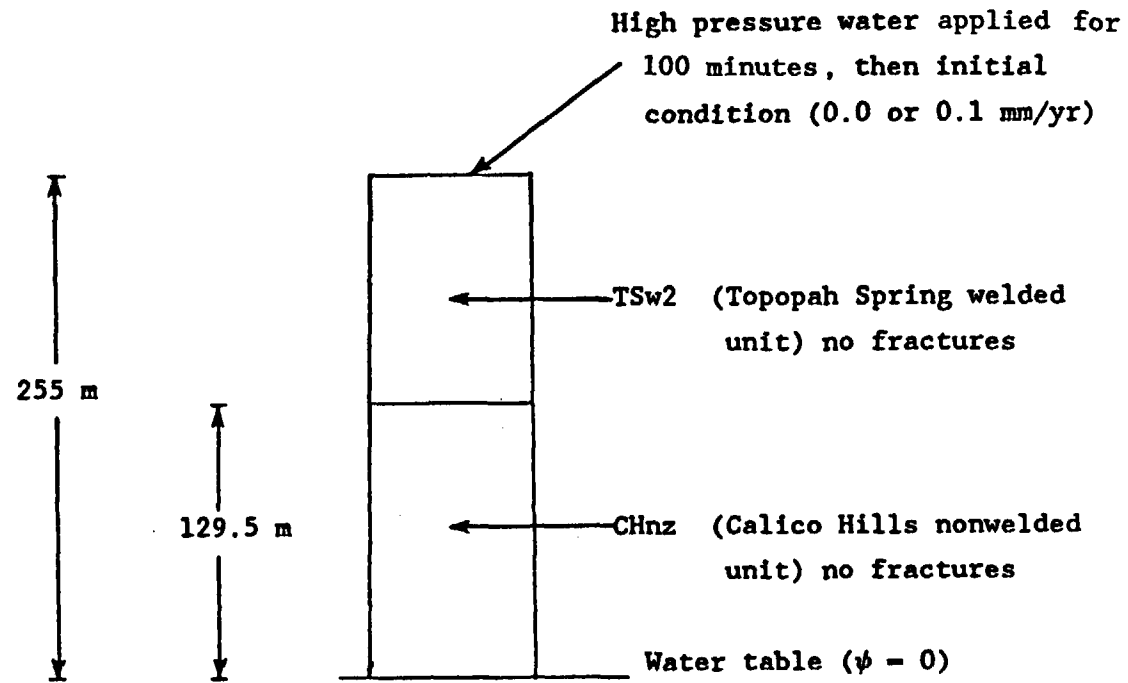


Fig. 1. Matrix column geometry and boundary conditions for the high pressure water application problem; Analysis 72-19 used material properties for TSw2 throughout the column.

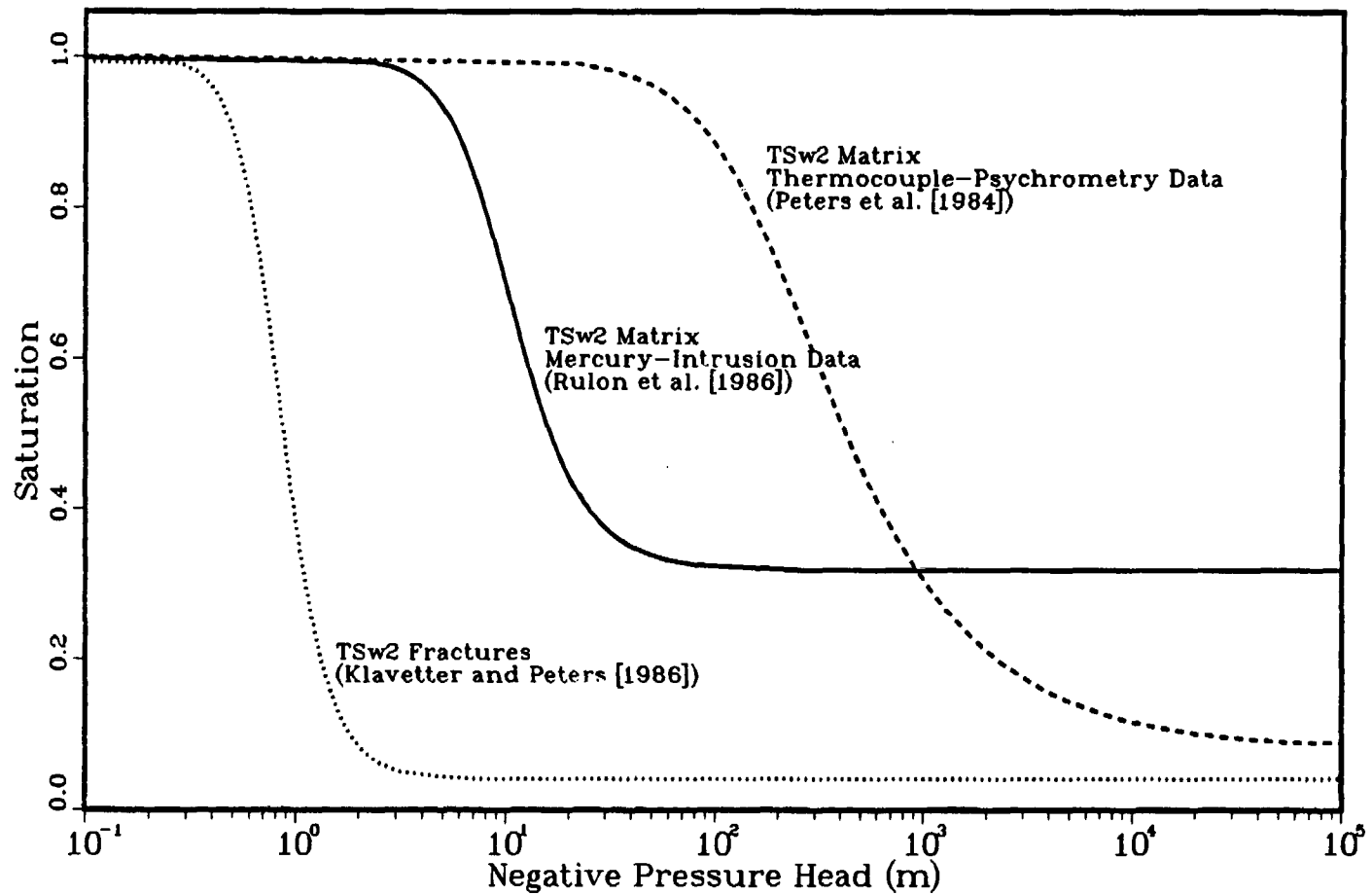


Fig. 2. Saturation curves for TSw2: Analysis 8 used the matrix curve reported by Peters et al. [1984]; Analysis 72-19 used the matrix curve reported by Rulon et al. [1986]; the fracture curve is used by both Analysis 8 and Analysis 72-19, however only in the flux-change experiment problem.

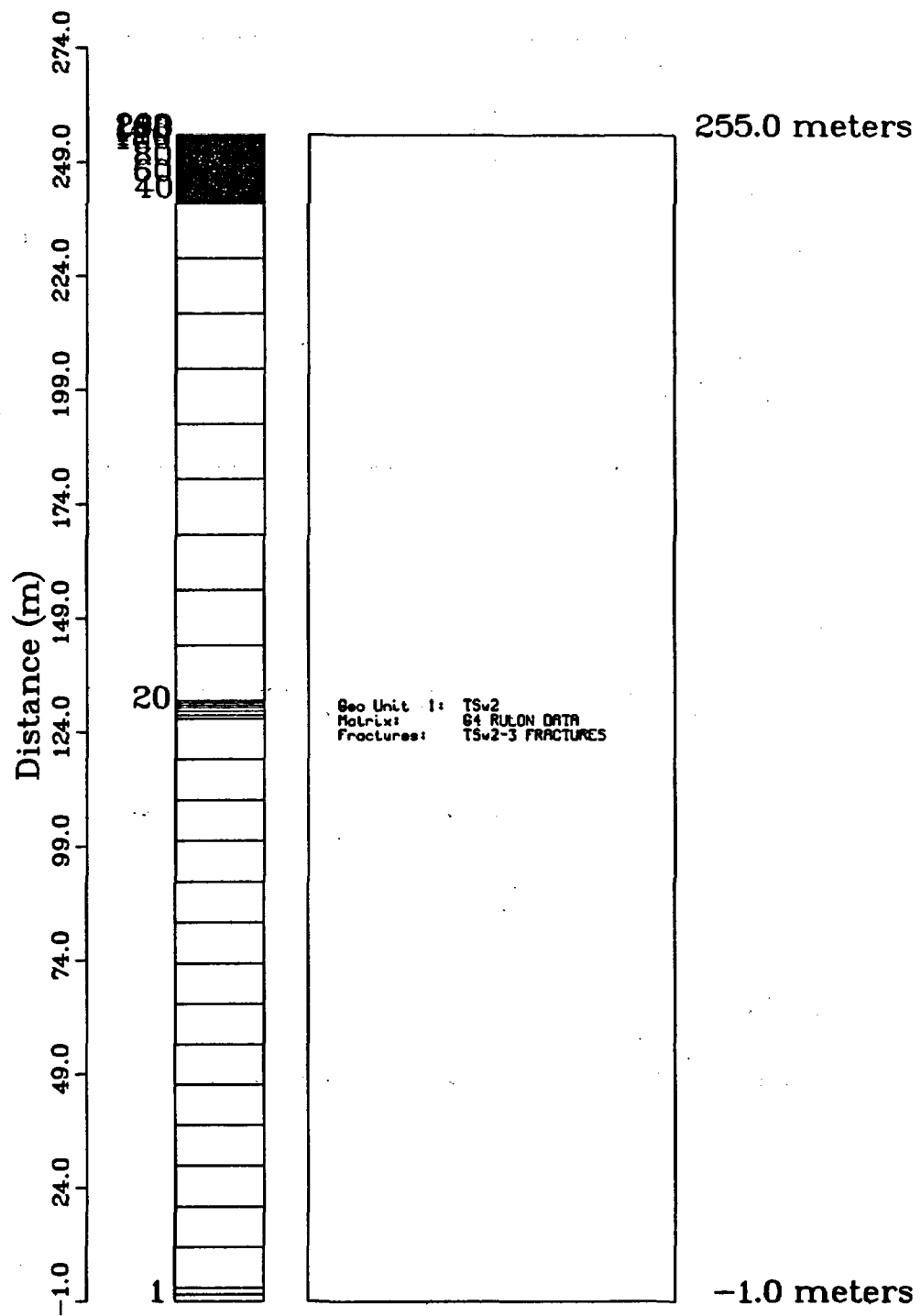


Fig. 3. Computational mesh used in Analysis 72-19 for both the high pressure water application problem and the flux-change experiment problem.

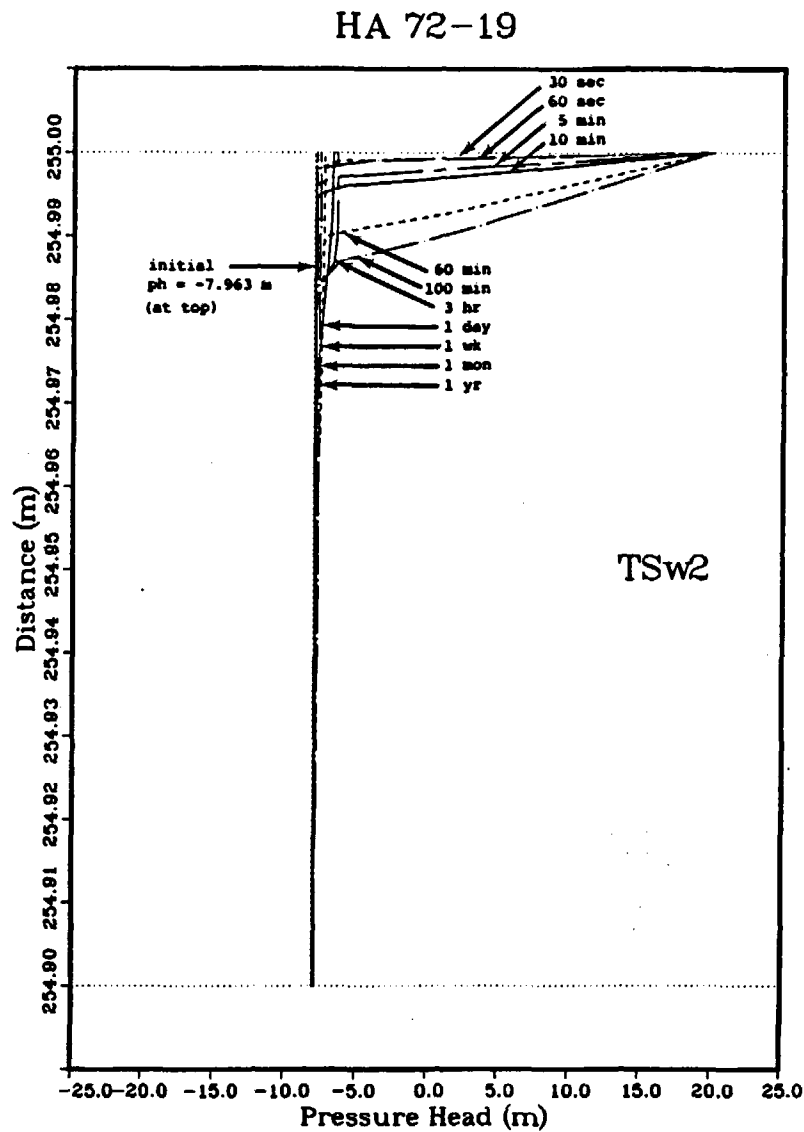
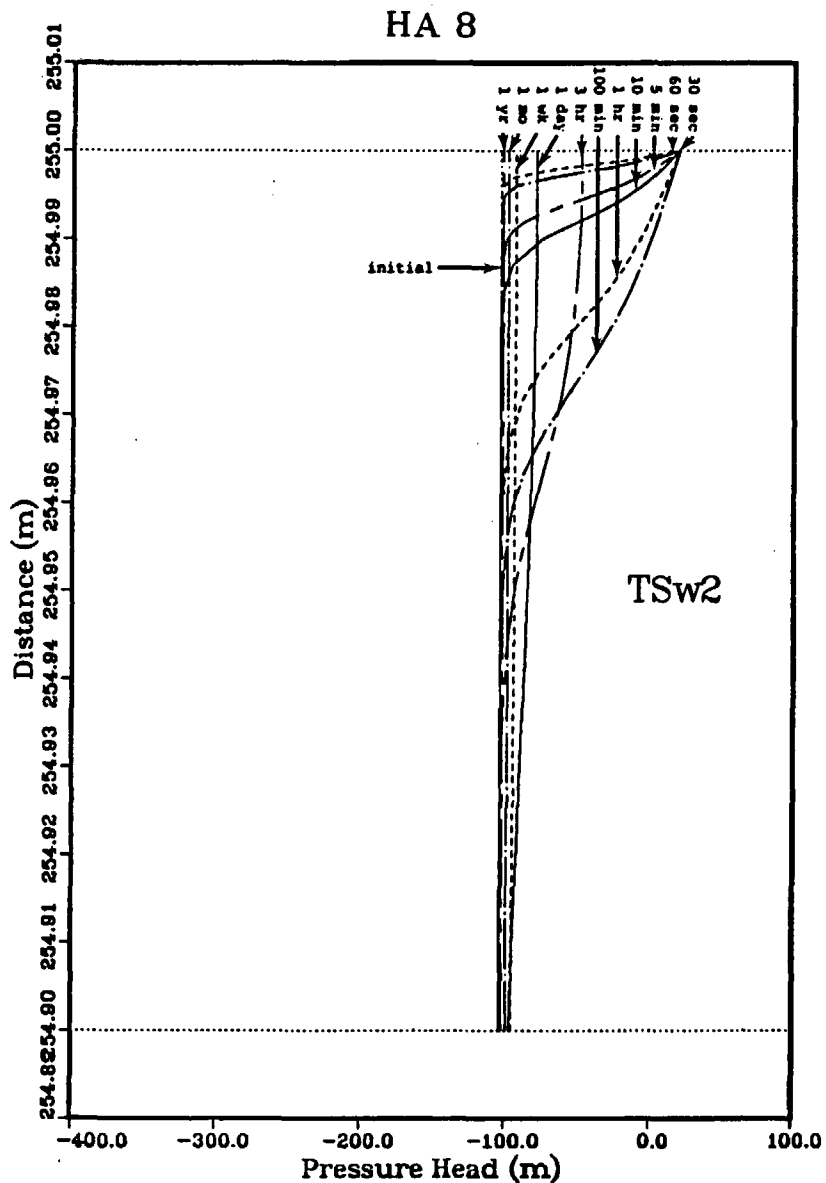


Fig. 4. Pressure head versus distance (top 10 cm of the column) at specific times for the high pressure water application problem: results of Analysis 8 are on the left; results of Analysis 72-19 are on the right.

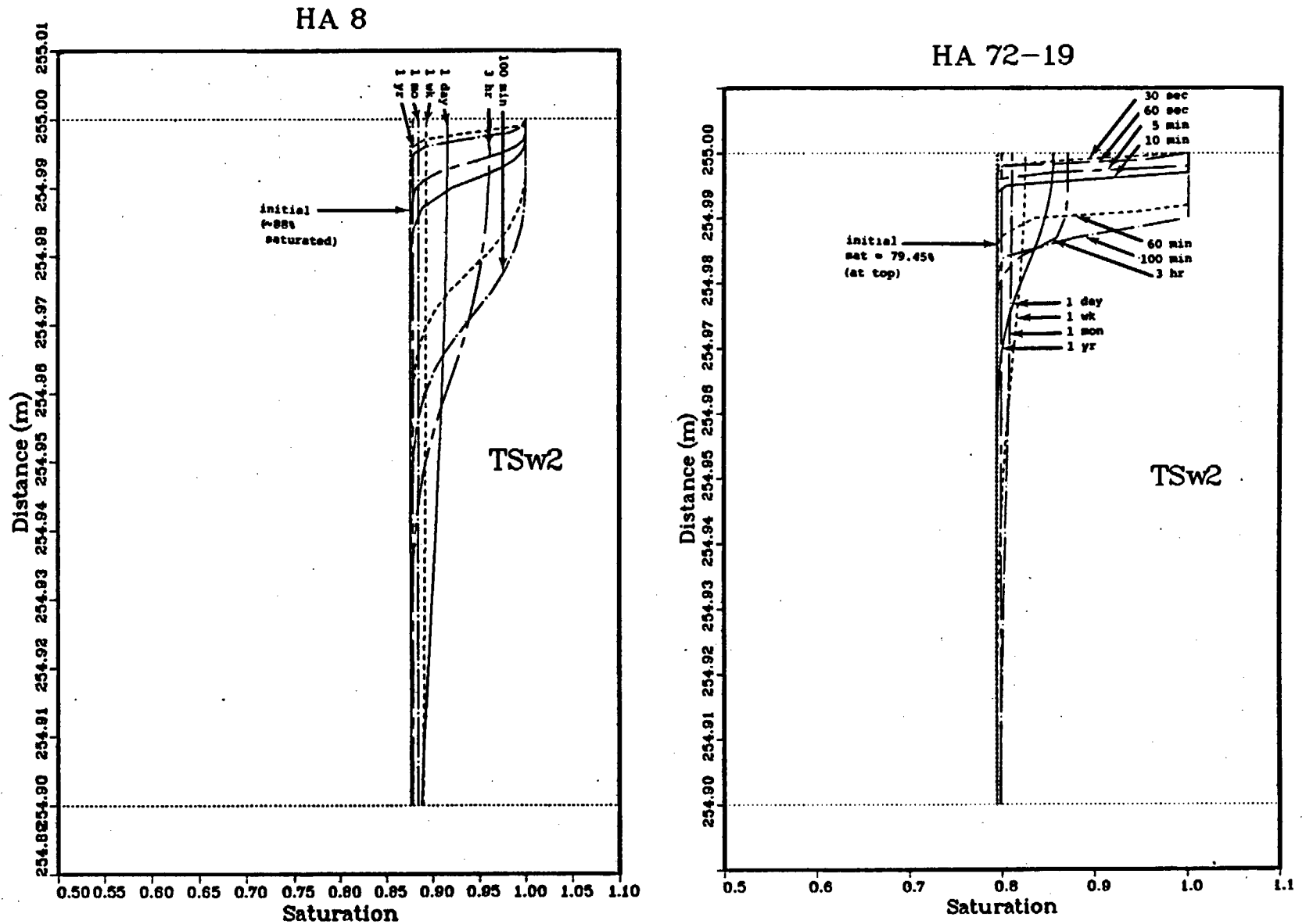


Fig. 5. Saturation versus distance (top 10 cm of the column) at specific times for the high pressure water application problem: results of Analysis 8 are on the left; results of Analysis 72-19 are on the right.

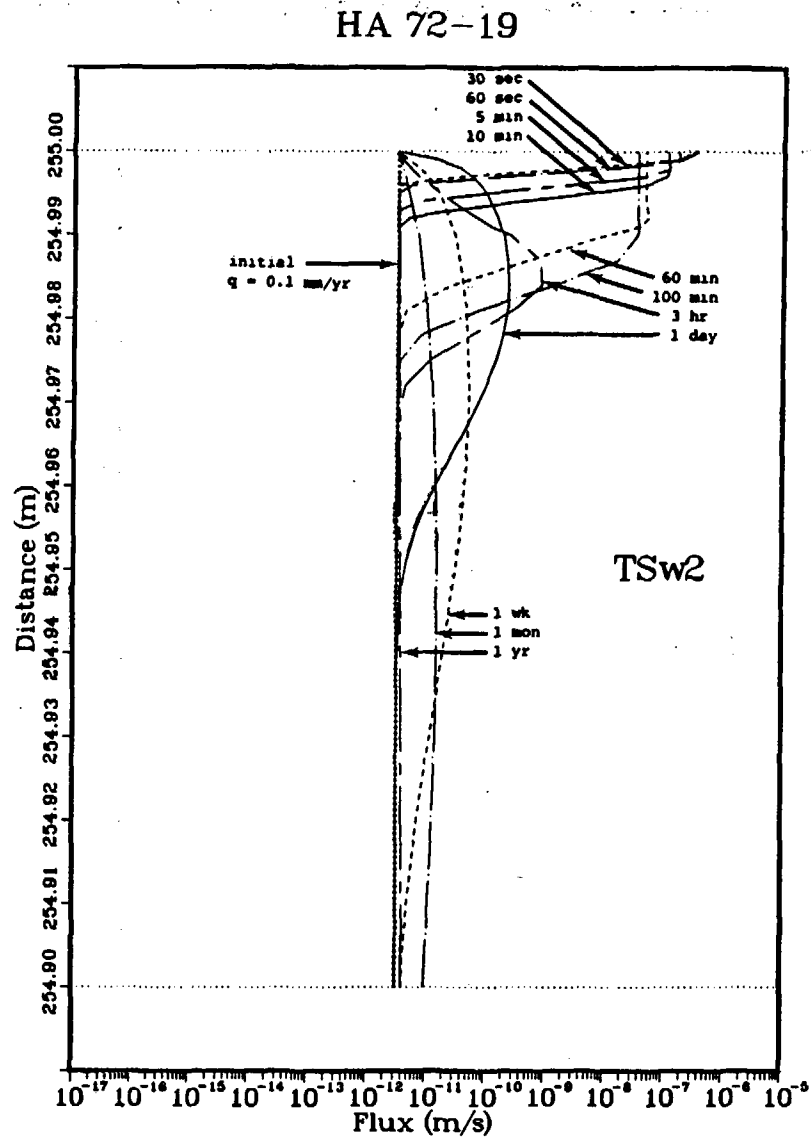
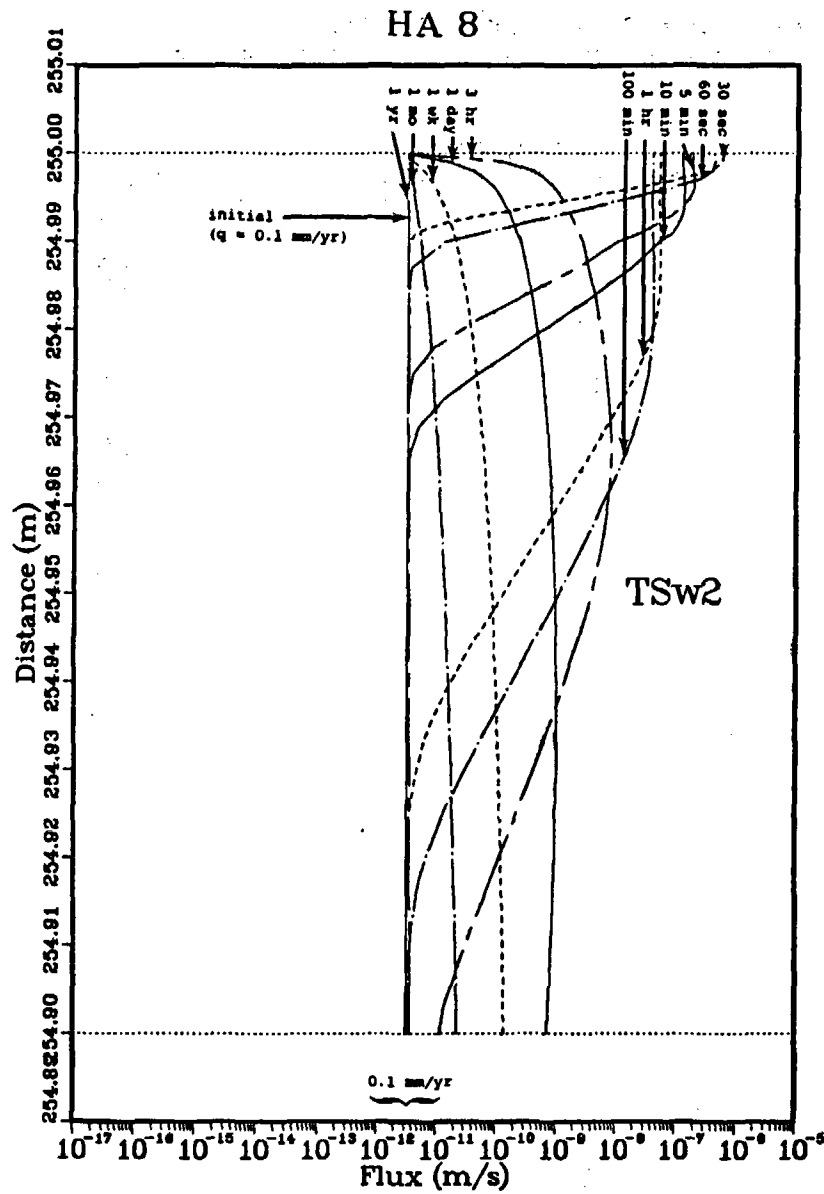


Fig. 6. Water flux versus distance (top 10 cm of the column) at specific times for the high pressure water application problem: results of Analysis 8 are on the left; results of Analysis 72-19 are on the right.

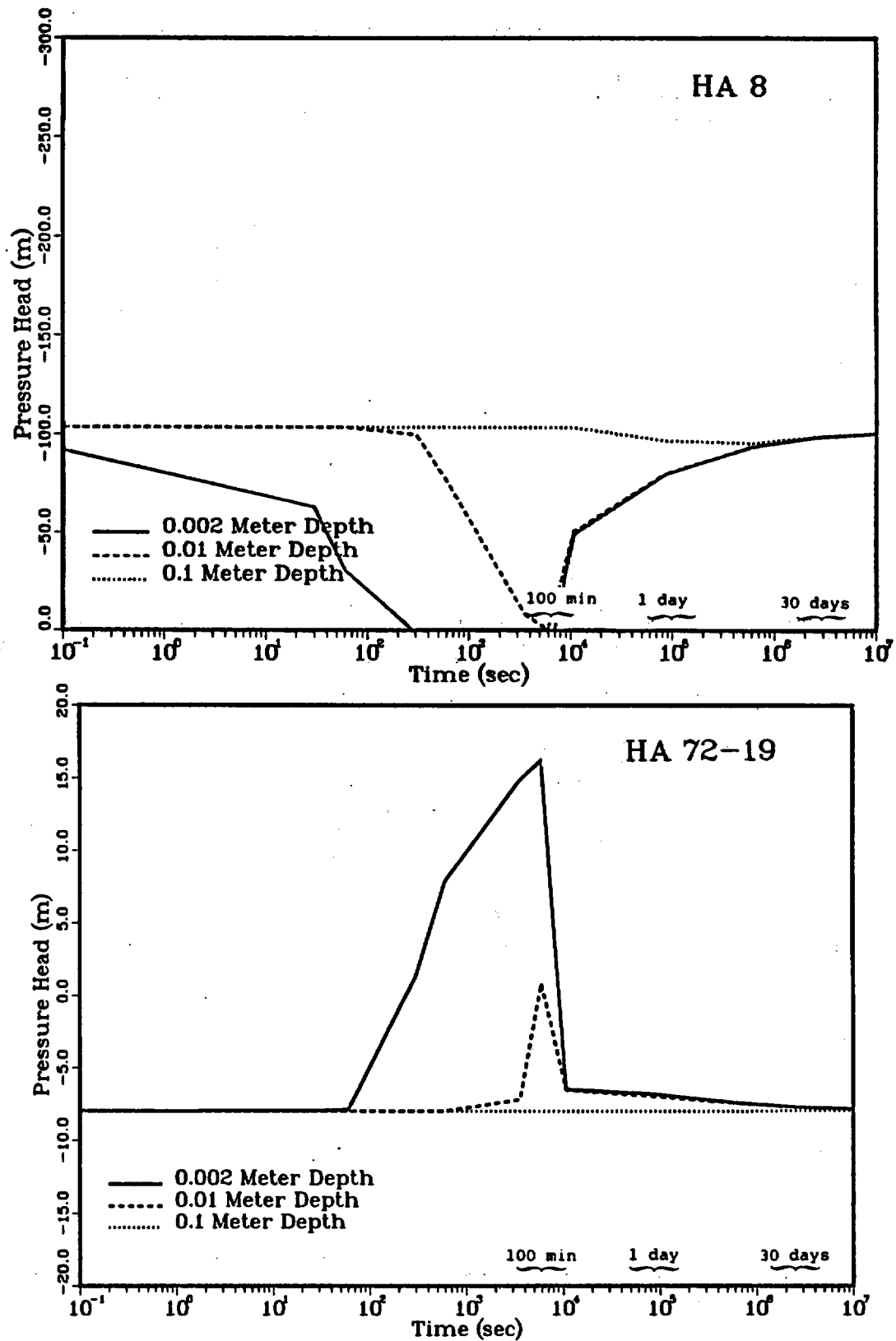


Fig. 7. Pressure head versus time at specified locations near the top of the column for the high pressure water application problem: results of Analysis 8 are on the top; results of Analysis 72-19 are on the bottom.

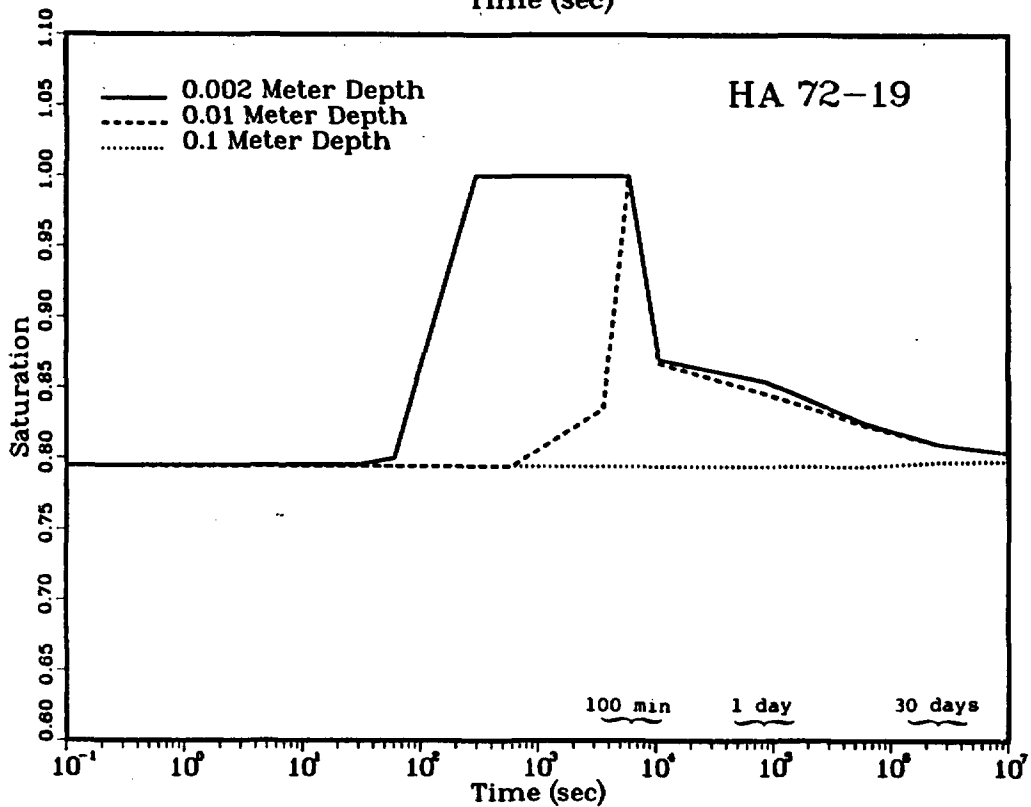
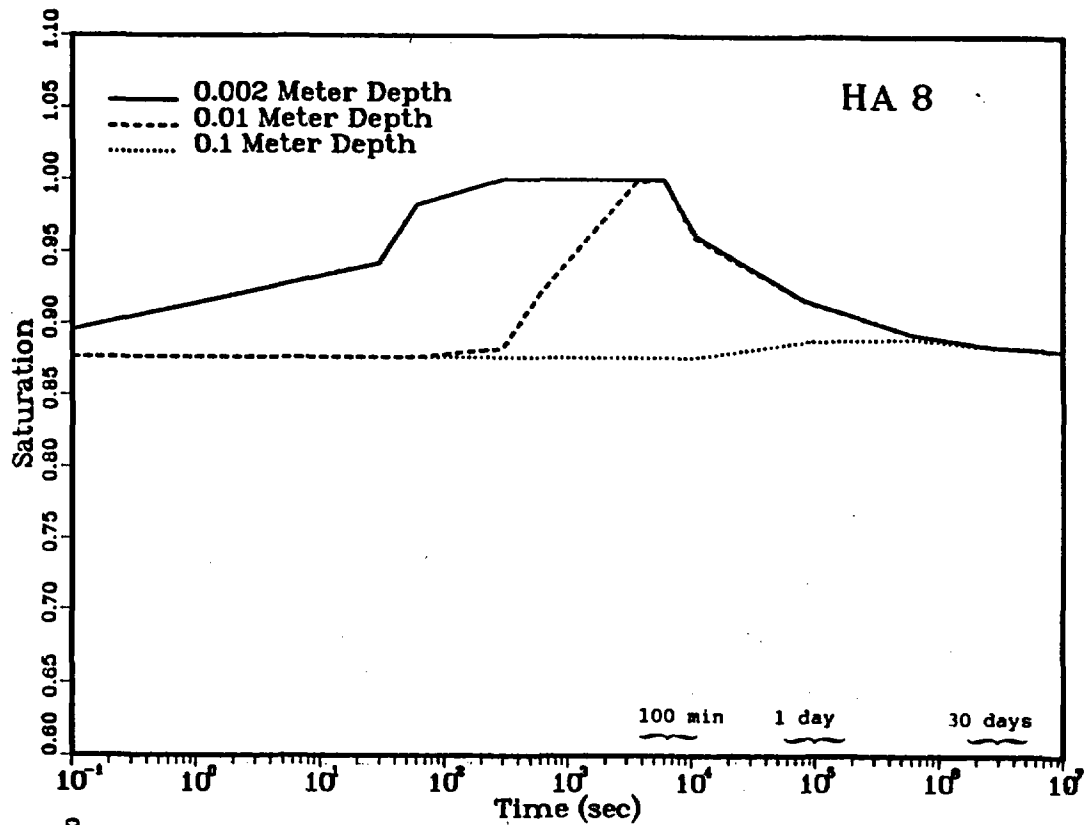


Fig. 8. Saturation versus time at specified locations near the top of the column for the high pressure water application problem: results of Analysis 8 are on the top; results of Analysis 72-19 are on the bottom.

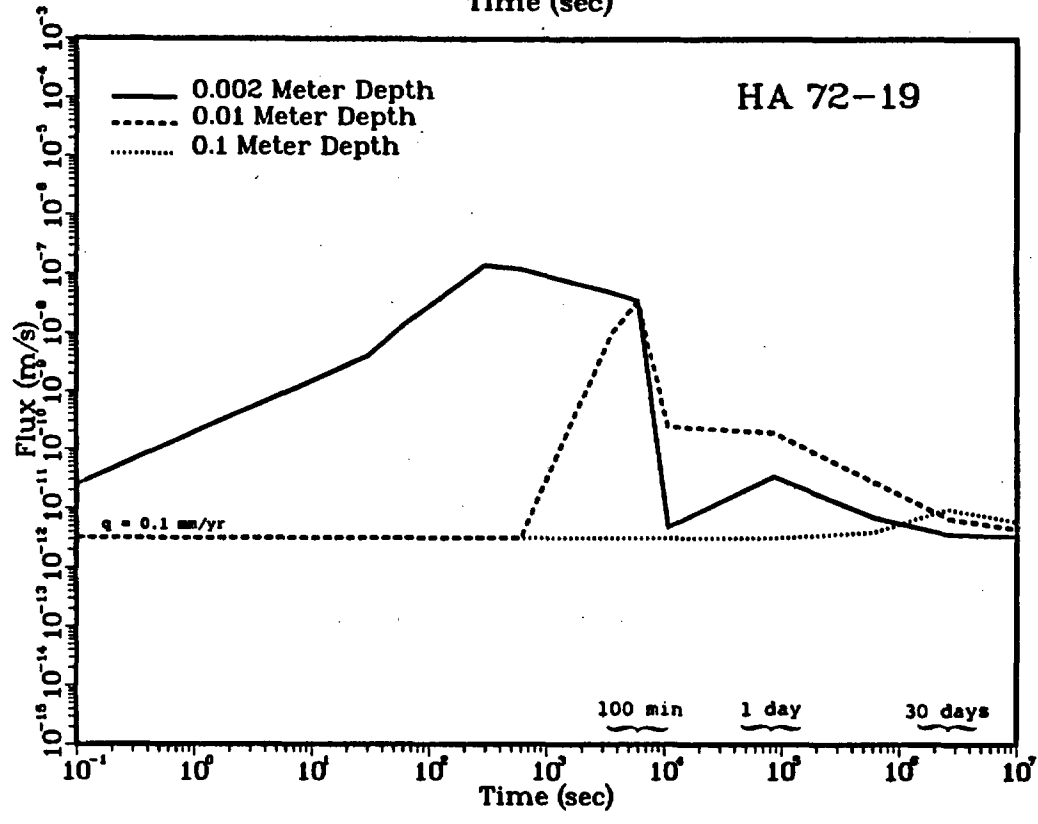
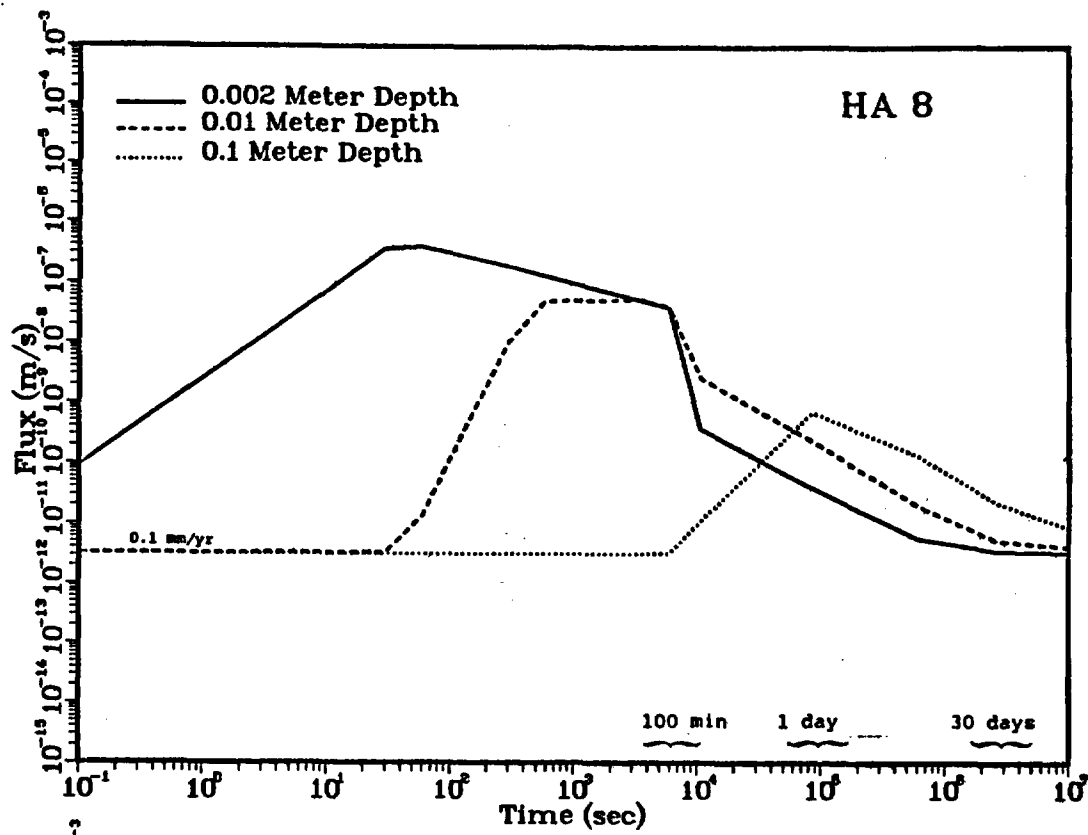


Fig. 9. Water flux versus time at specified locations near the top of the column for the high pressure water application problem: results of Analysis 8 are on the top; results of Analysis 72-19 are on the bottom.

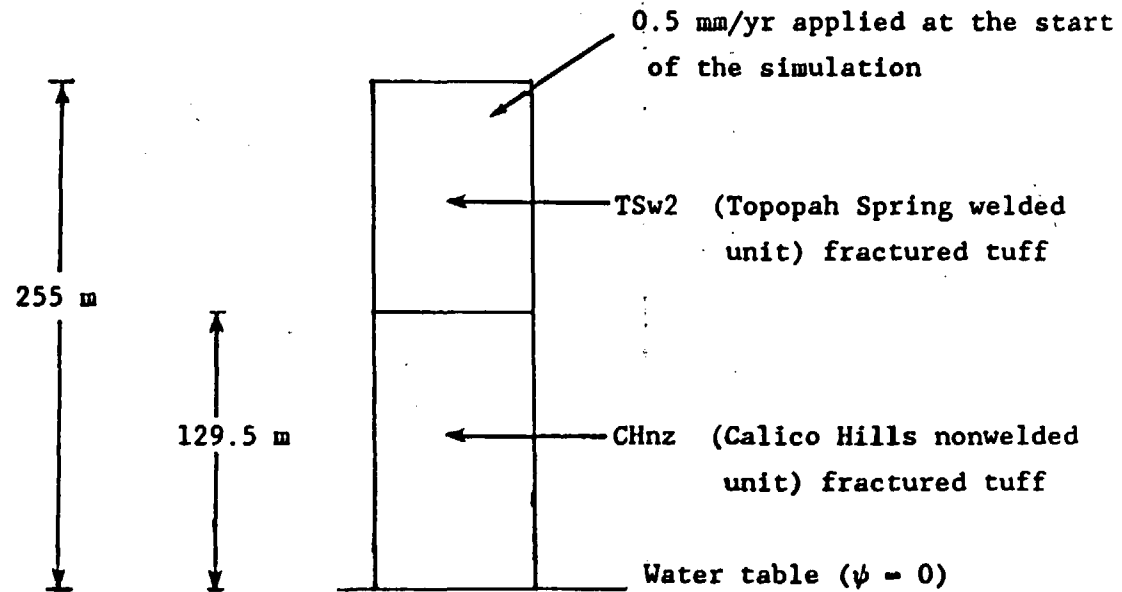


Fig. 10. Matrix column geometry and boundary conditions for the flux-change experiment problem; Analysis 72-19 used material properties for TSw2 throughout the column.

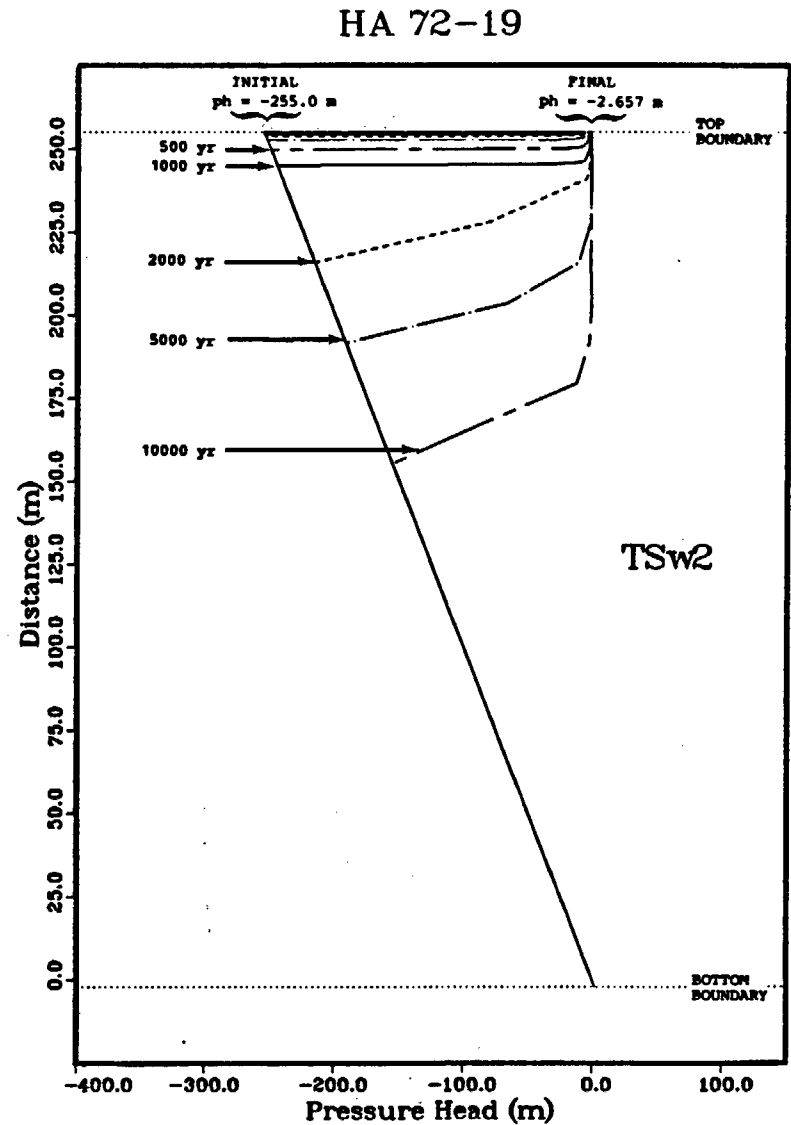
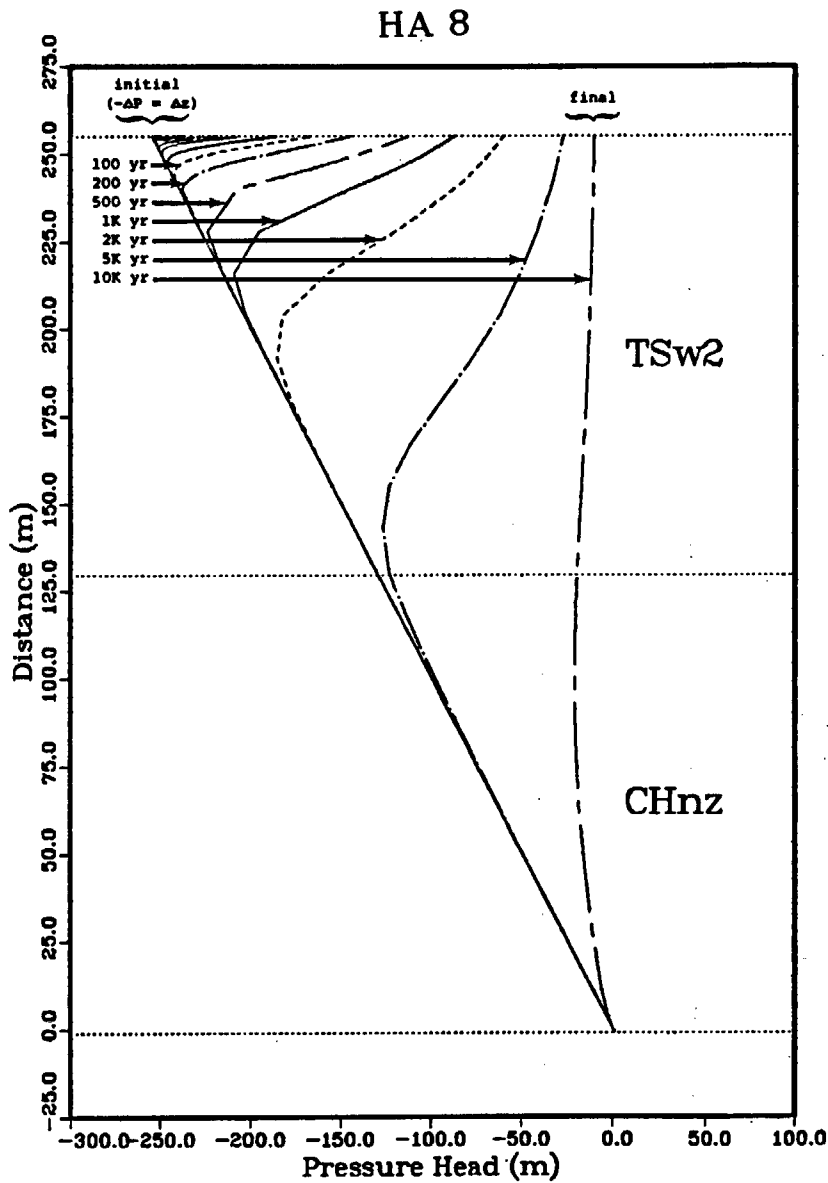
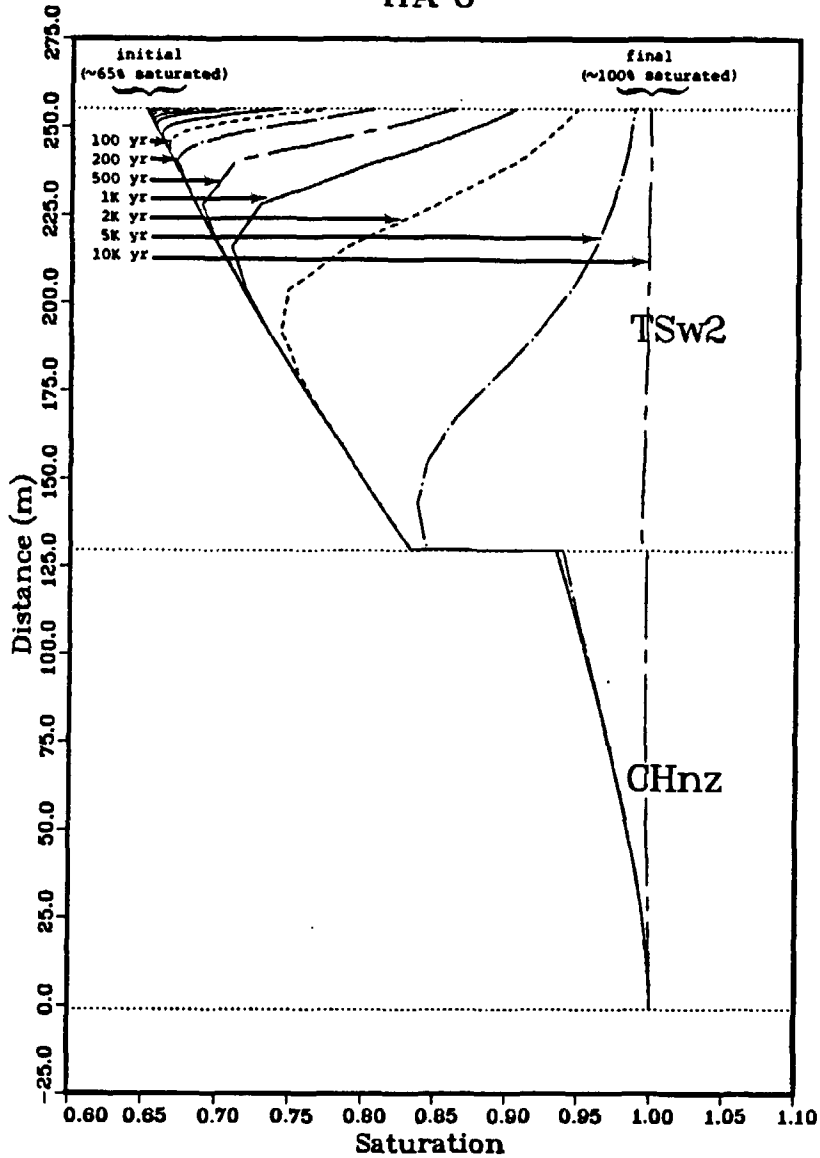


Fig. 11. Pressure head versus distance (entire column) at specific times for the flux-change experiment problem (noflow initial condition): results of Analysis 8 are on the left; results of Analysis 72-19 are on the right.

HA 8



HA 72-19

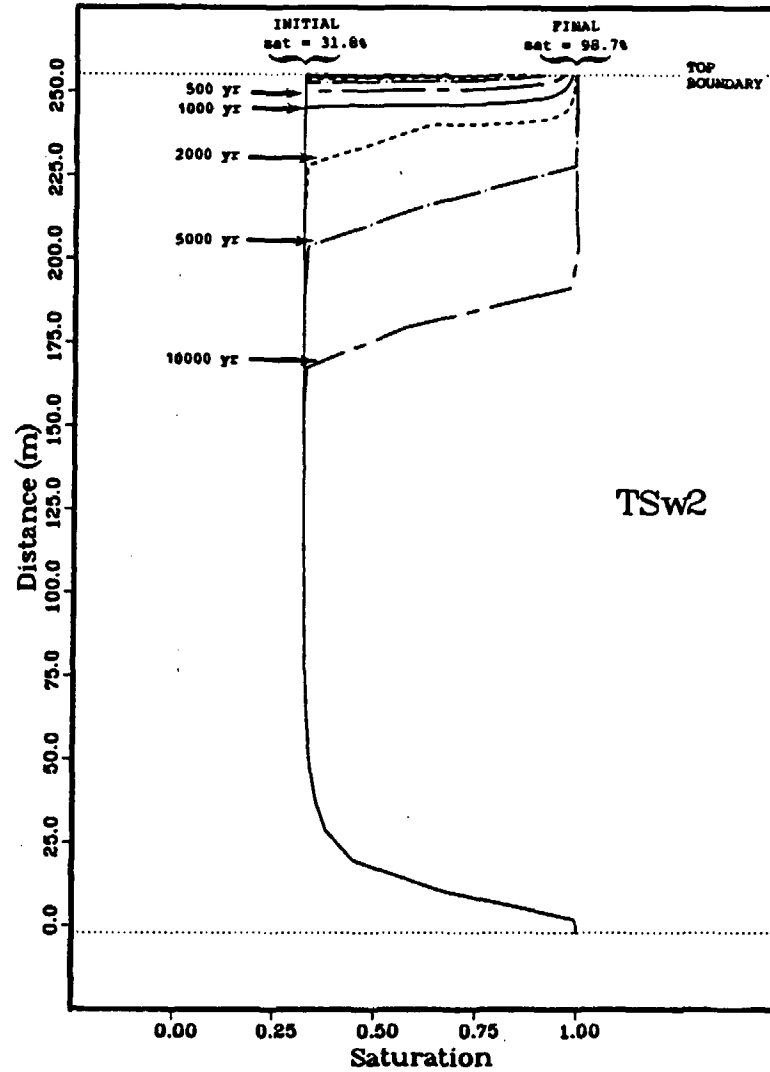


Fig. 12. Saturation versus distance (entire column) at specific times for the flux-change experiment problem (noflow initial condition): results of Analysis 8 are on the left; results of Analysis 72-19 are on the right.

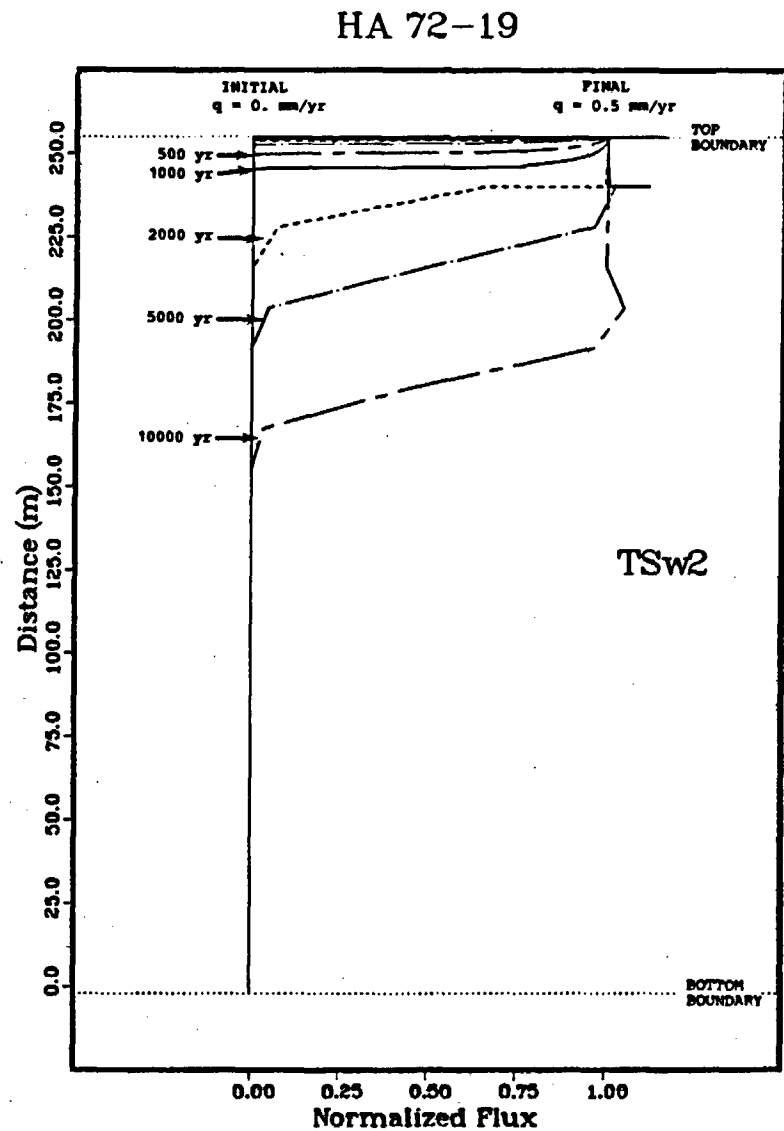
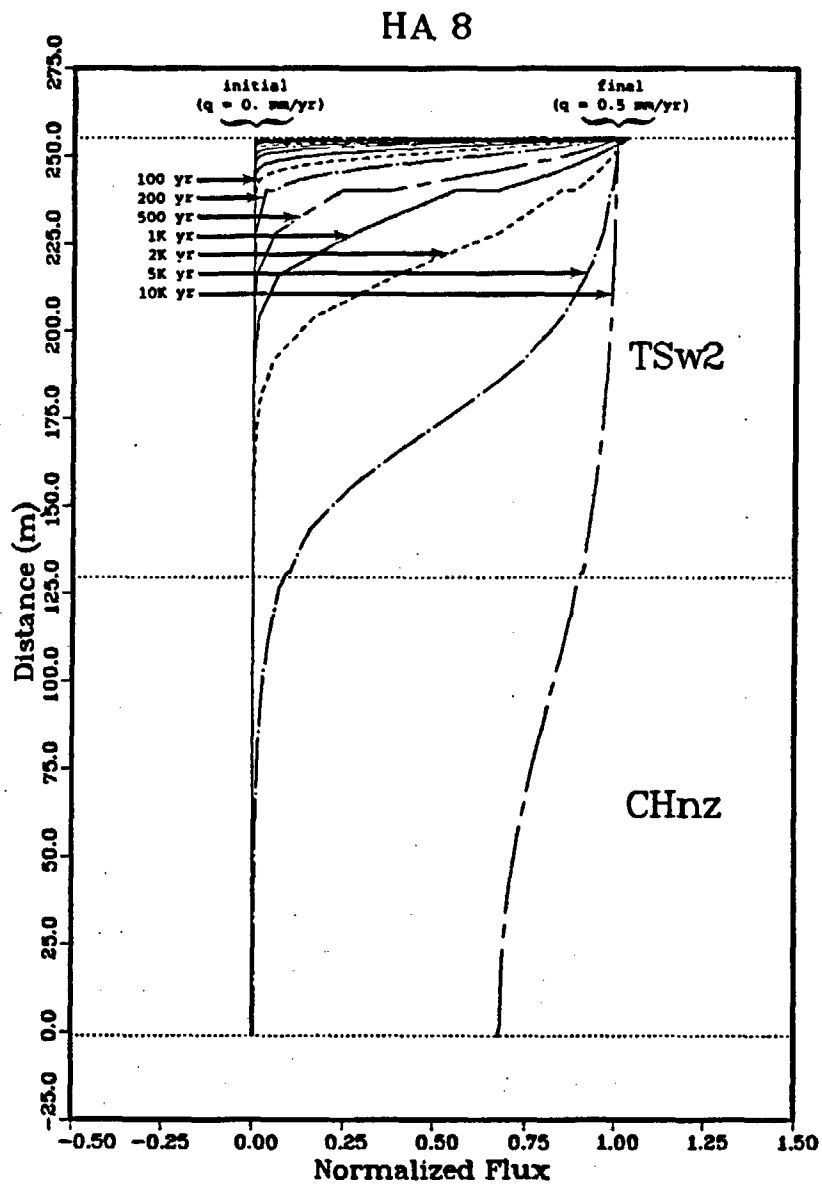


Fig. 13. Water flux (normalized to $q = 0.5$ mm/yr) versus distance (entire column) at specific times for the flux-change experiment problem (noflow initial condition): results of Analysis 8 are on the left; results of Analysis 72-19 are on the right.

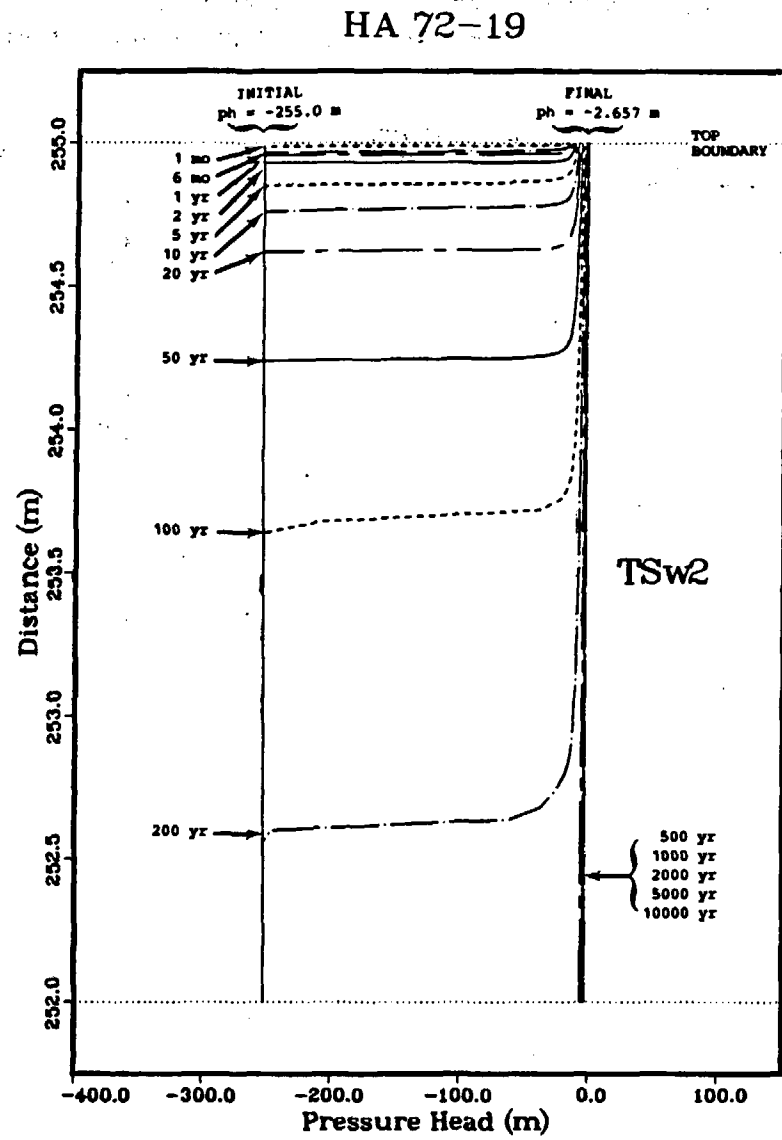
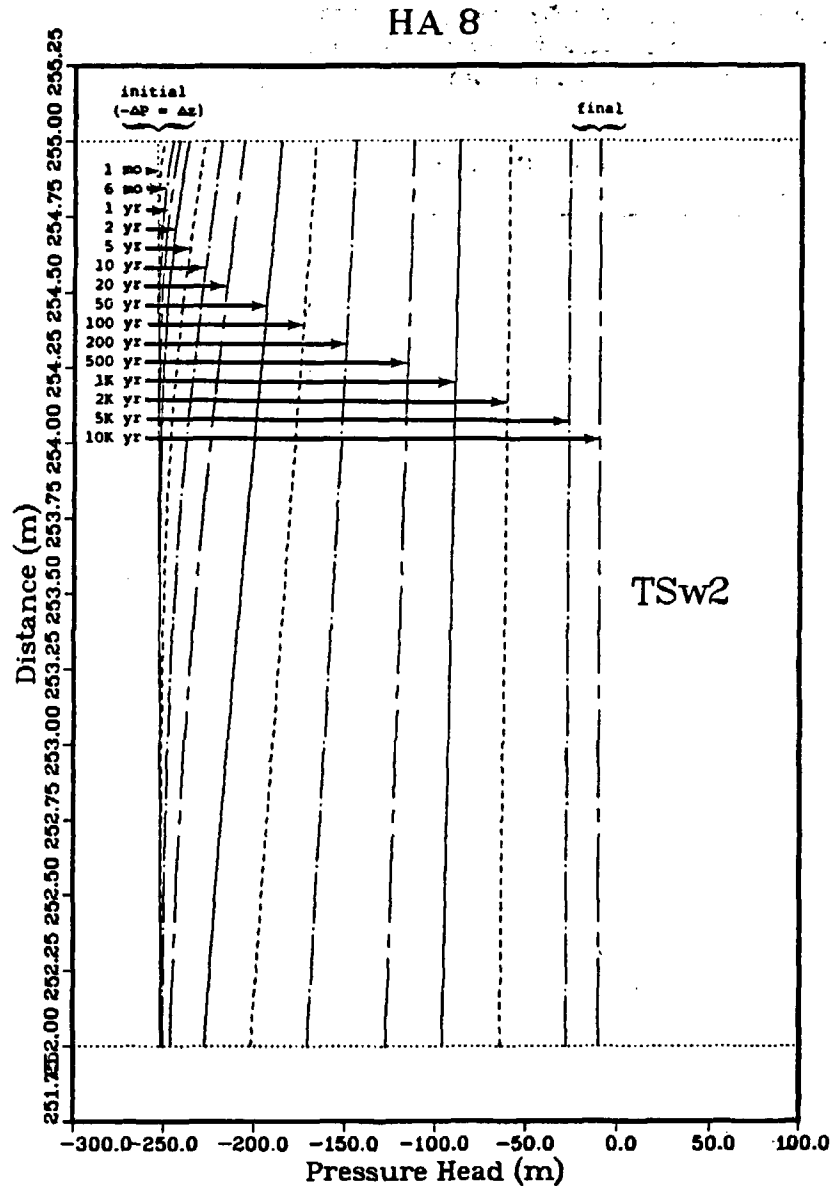


Fig. 14. Pressure head versus distance (top 3 m of the column) at specific times for the flux-change experiment problem (noflow initial condition): results of Analysis 8 are on the left; results of Analysis 72-19 are on the right.

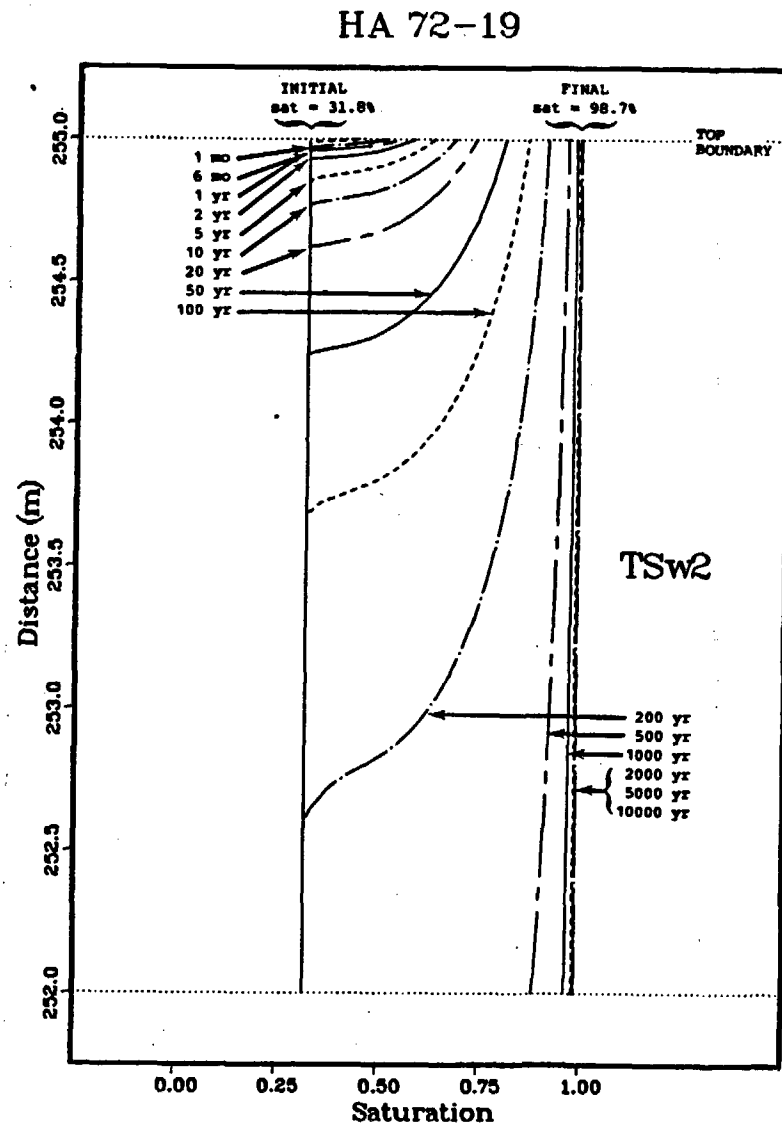
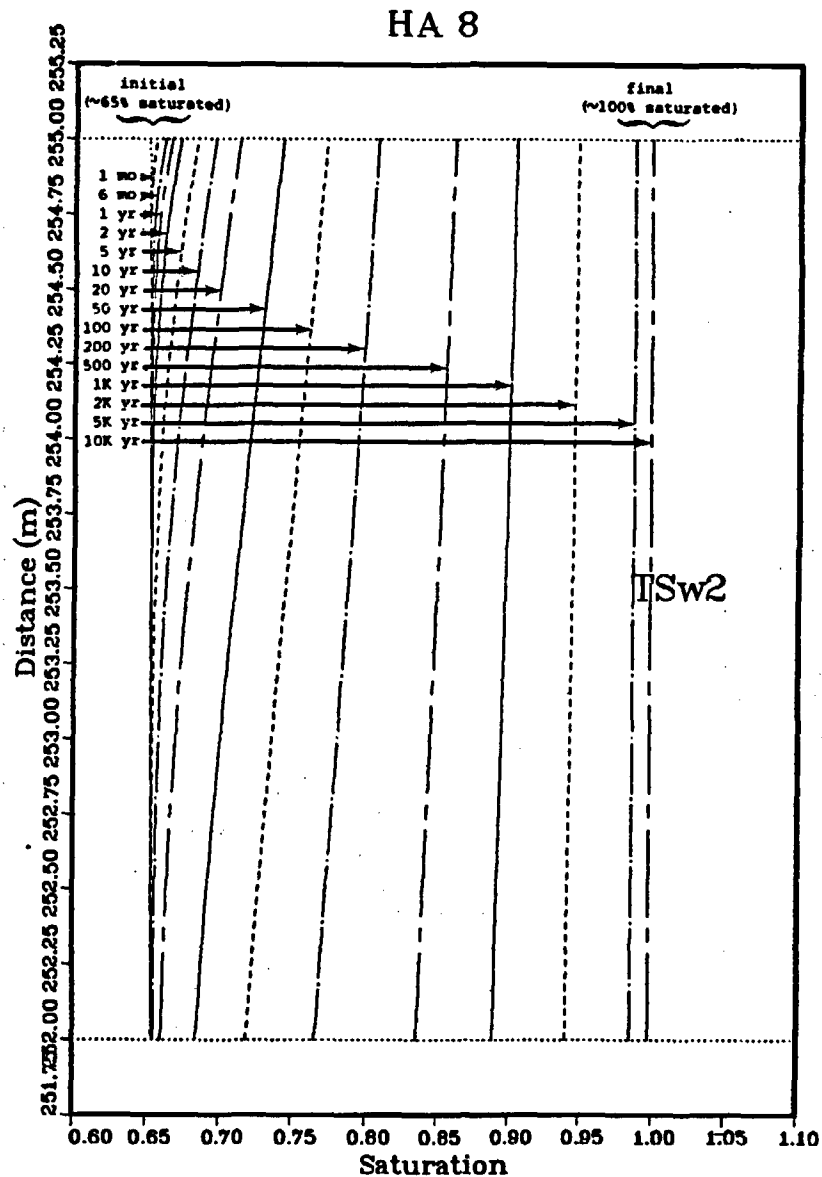


Fig. 15. Saturation versus distance (top 3 m of the column) at specific times for the flux-change experiment problem (noflow initial condition): results of Analysis 8 are on the left; results of Analysis 72-19 are on the right.

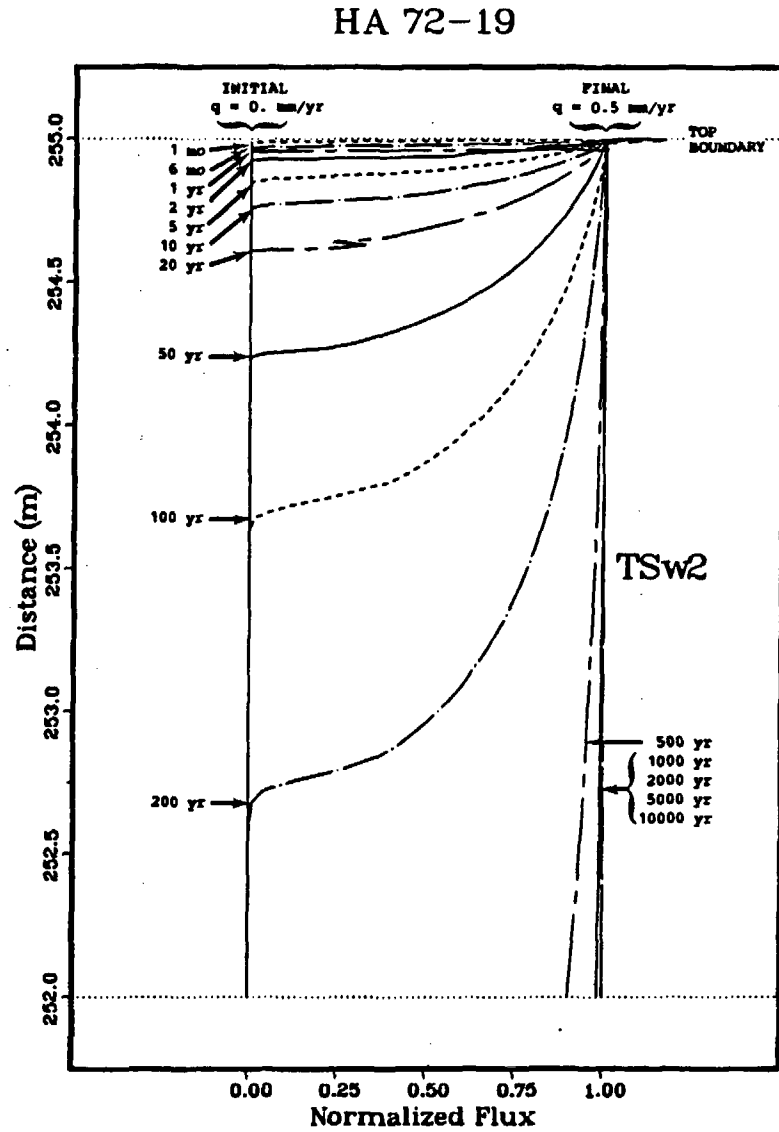
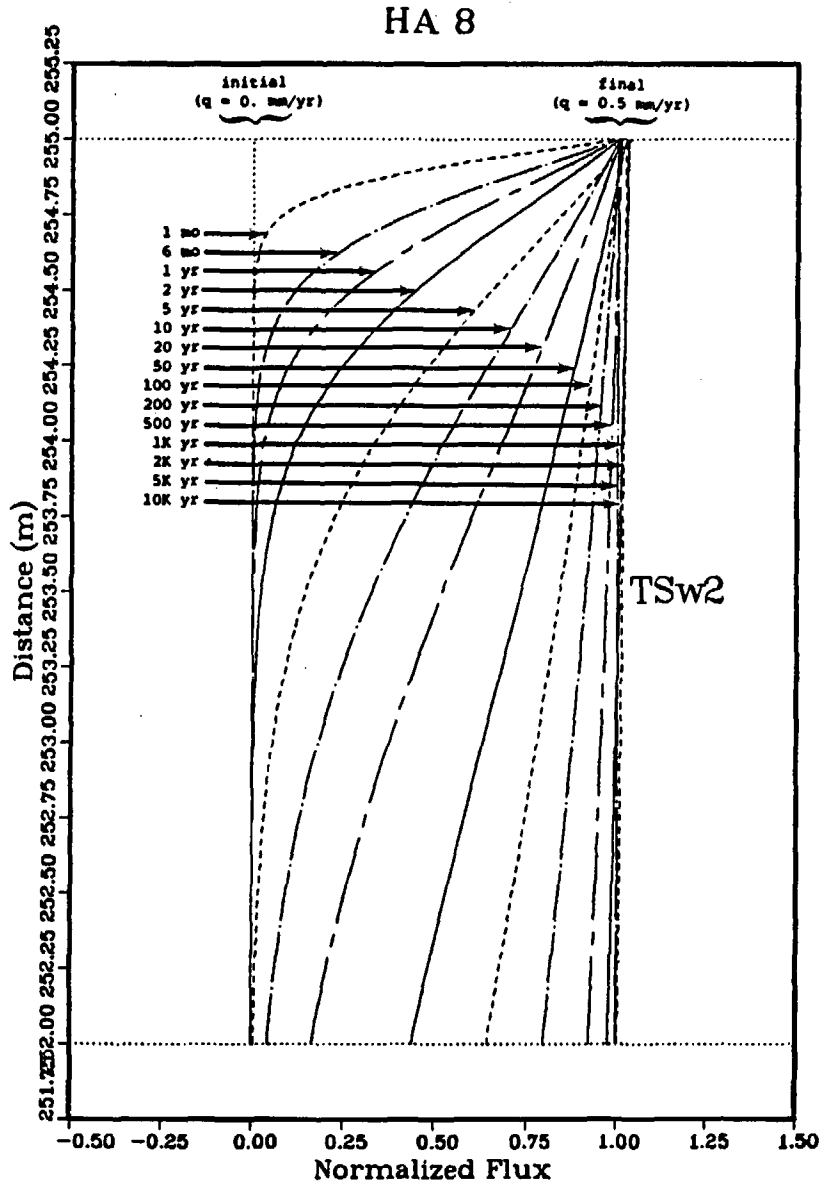


Fig. 16. Water flux (normalized to $q = 0.5 \text{ mm/yr}$) versus distance (top 3 m of the column) at specific times for the flux-change experiment problem (noflow initial condition): results of Analysis 8 are on the left; results of Analysis 72-19 are on the right.

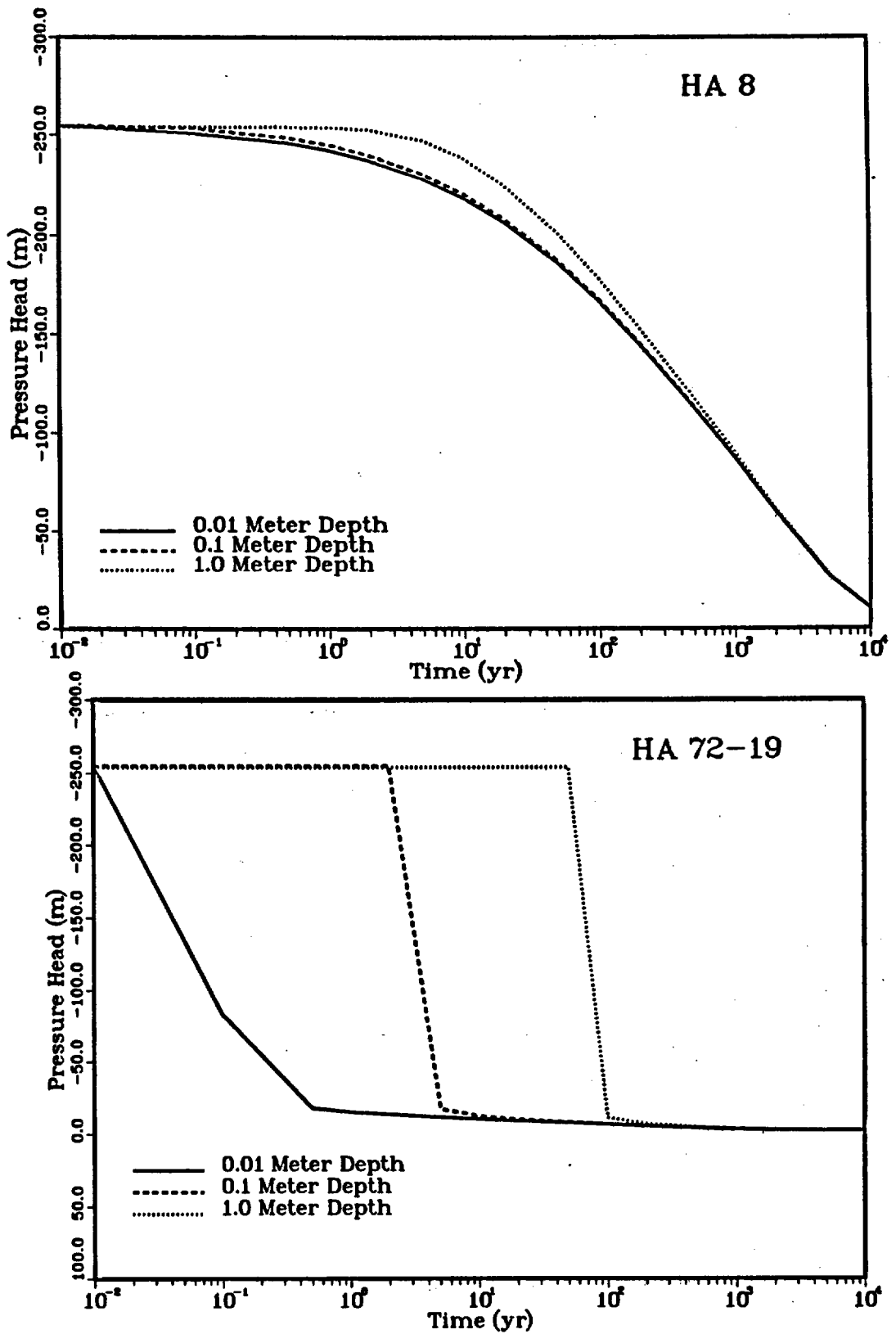


Fig. 17. Pressure head versus time at specified locations near the top of the column for the flux-change experiment problem (noflow initial condition): results of Analysis 8 are on the top; results of Analysis 72-19 are on the bottom.

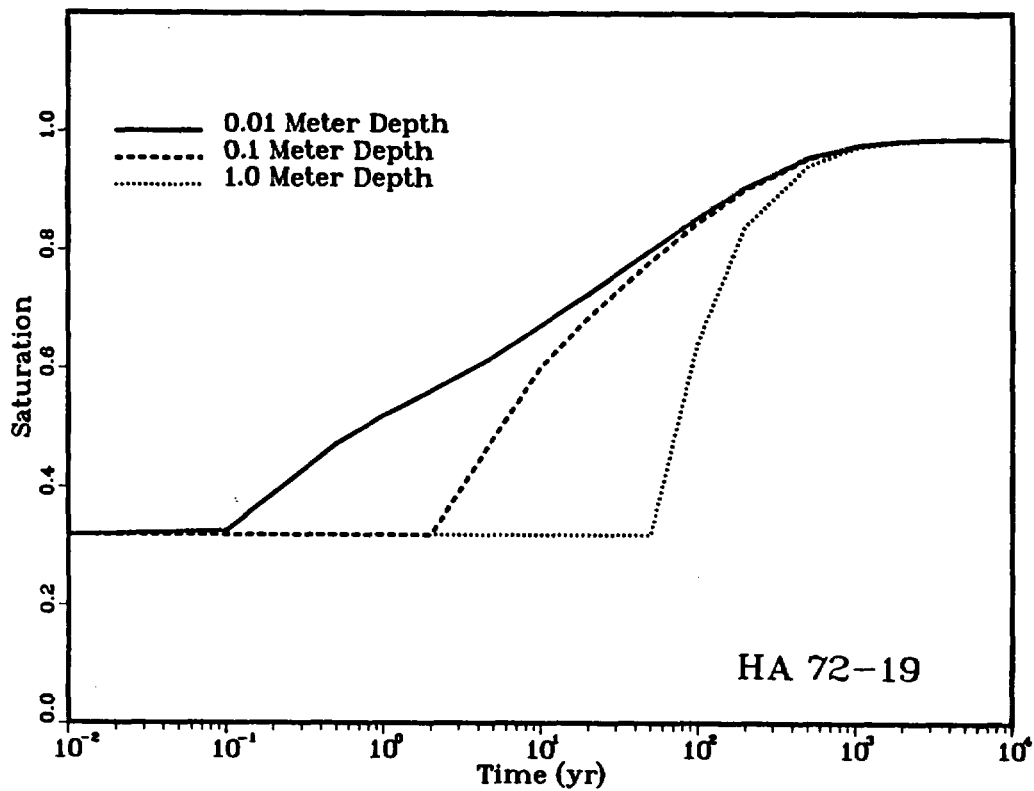
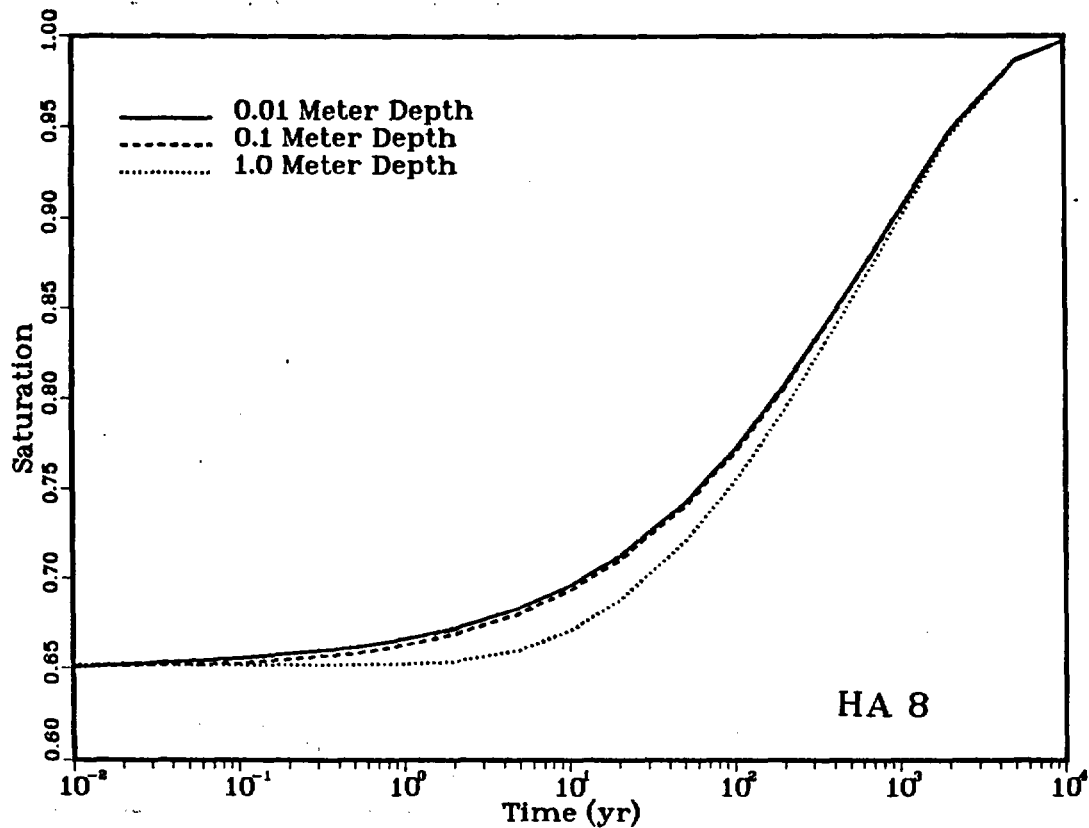


Fig. 18. Saturation versus time at specified locations near the top of the column for the flux-change experiment problem (noflow initial condition): results of Analysis 8 are on the top; results of Analysis 72-19 are on the bottom.

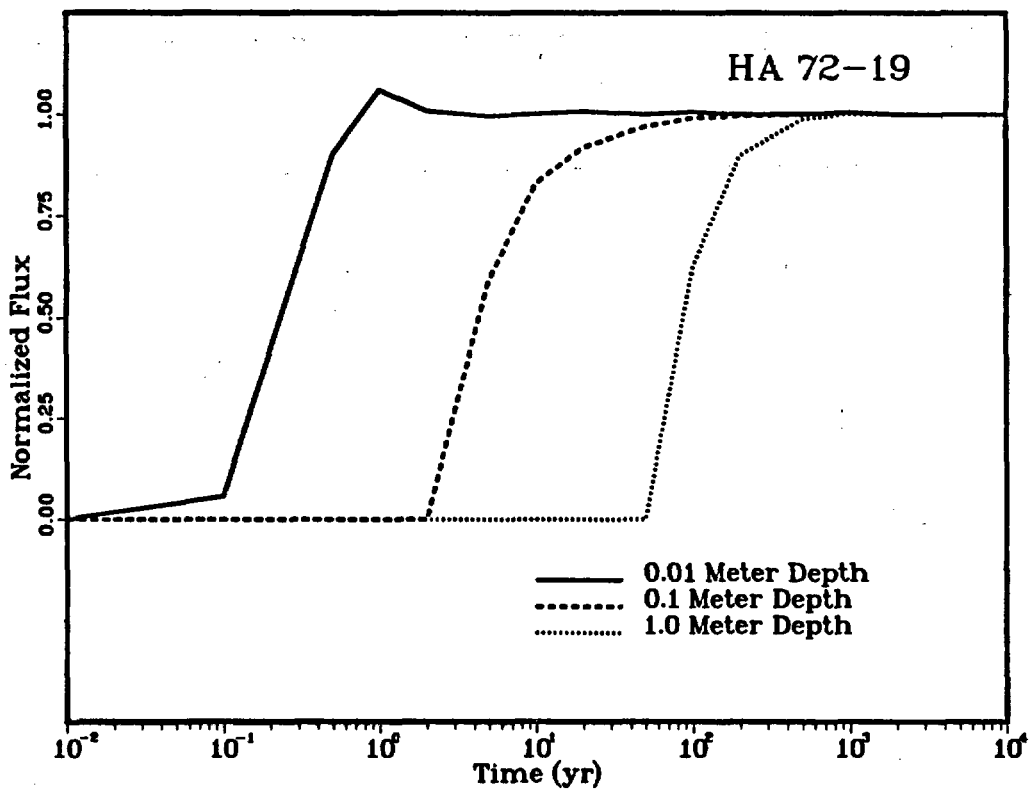
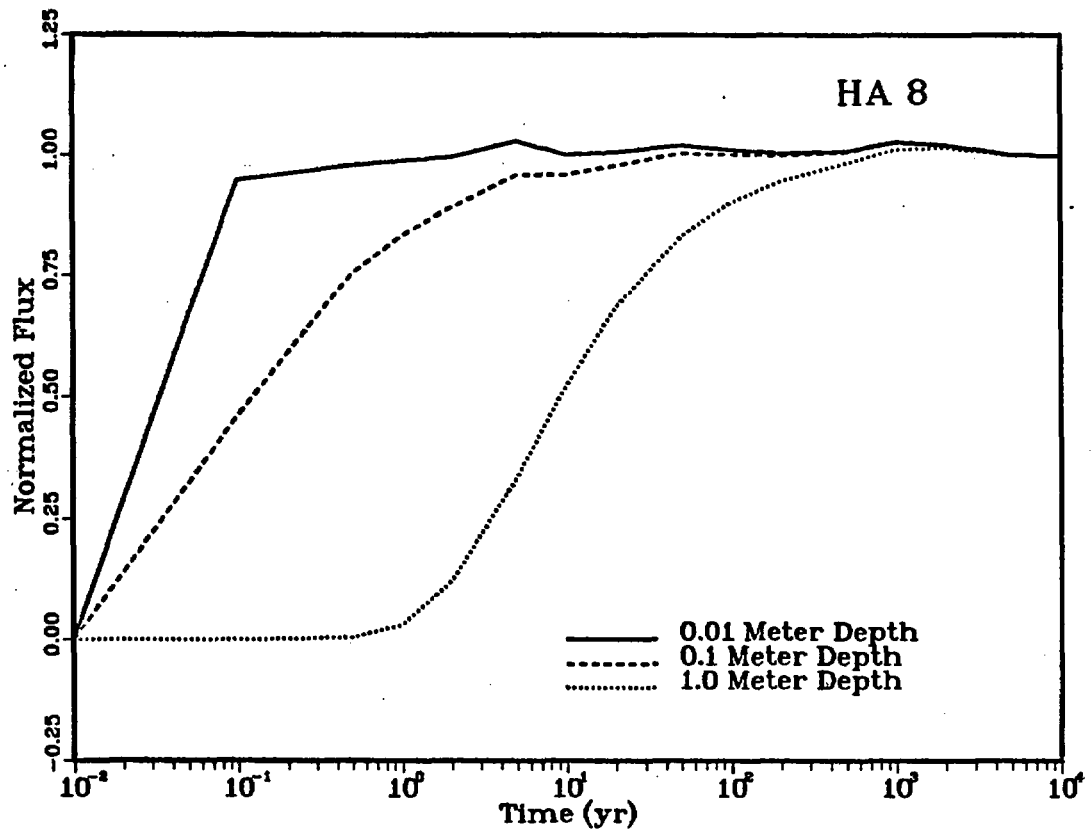


Fig. 19. Water flux versus time at specified locations near the top of the column for the flux-change experiment problem (noflow initial condition): results of Analysis 8 are on the top; results of Analysis 72-19 are on the bottom.

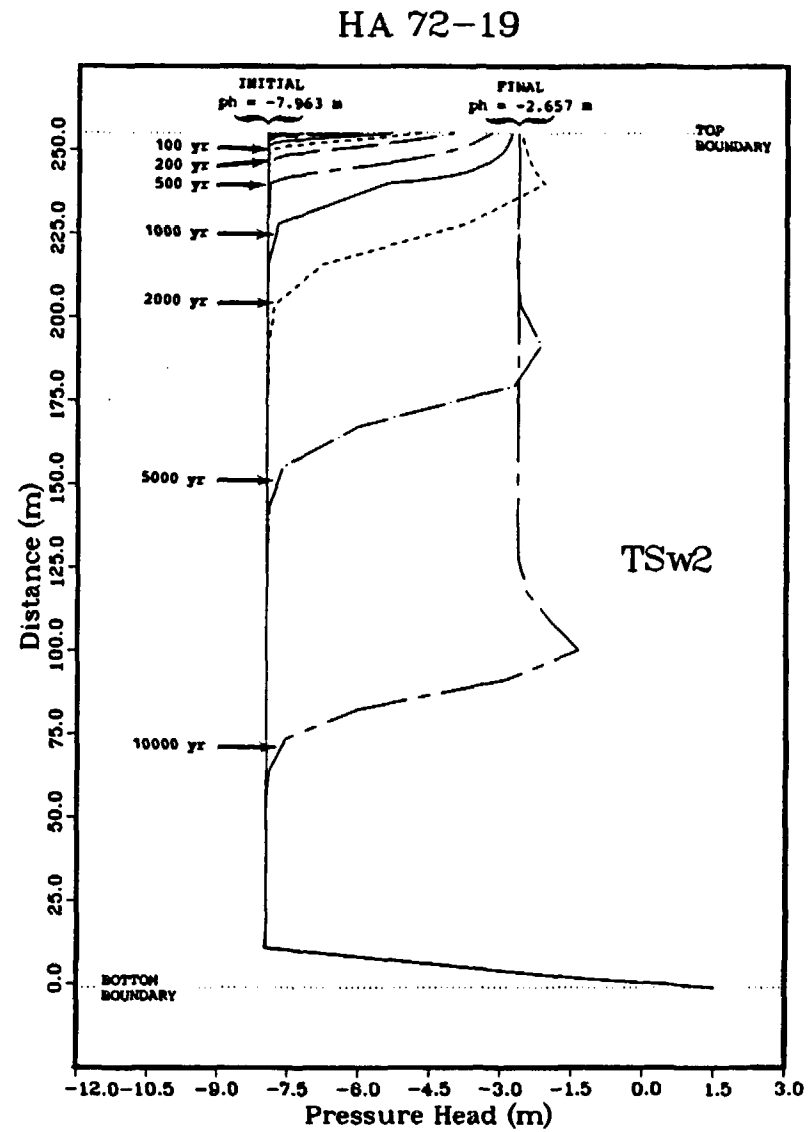
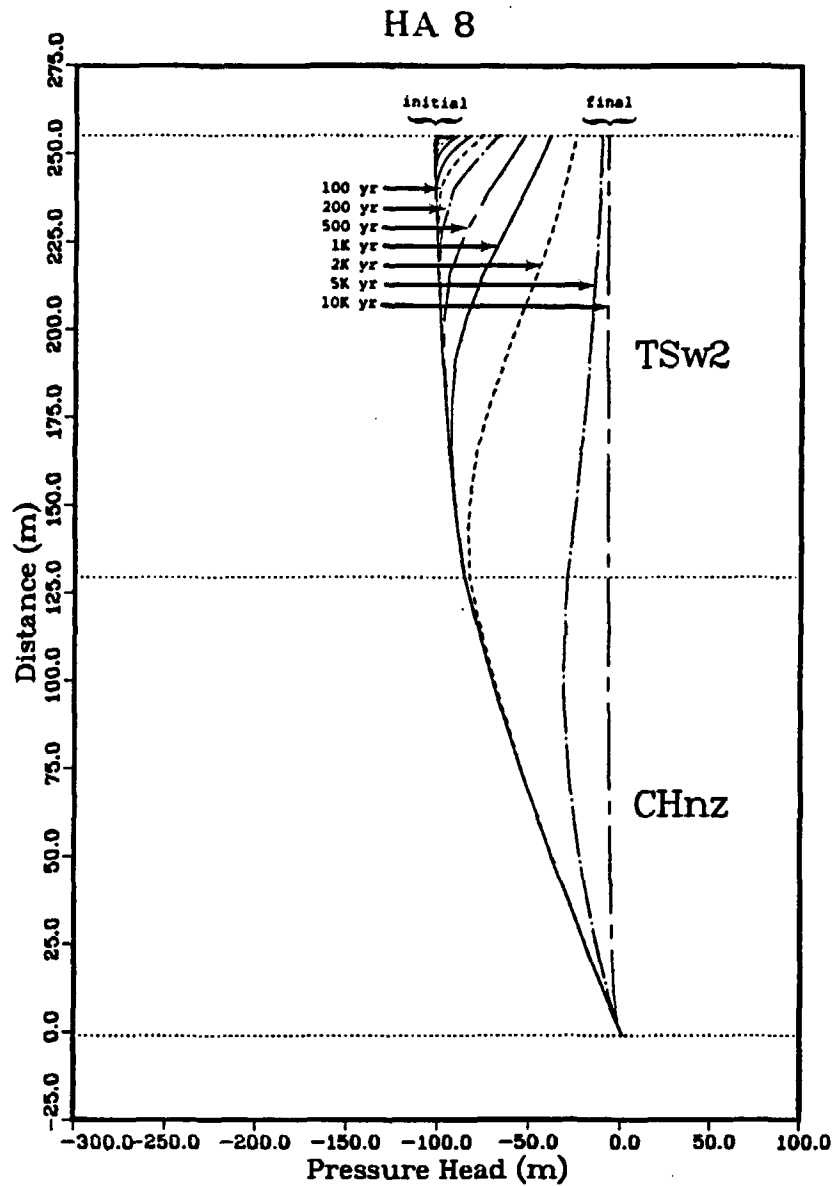


Fig. 20. Pressure head versus distance (entire column) at specific times for the flux-change experiment problem ($q = 0.1$ mm/yr initial condition): results of Analysis 8 are on the left; results of Analysis 72-19 are on the right.

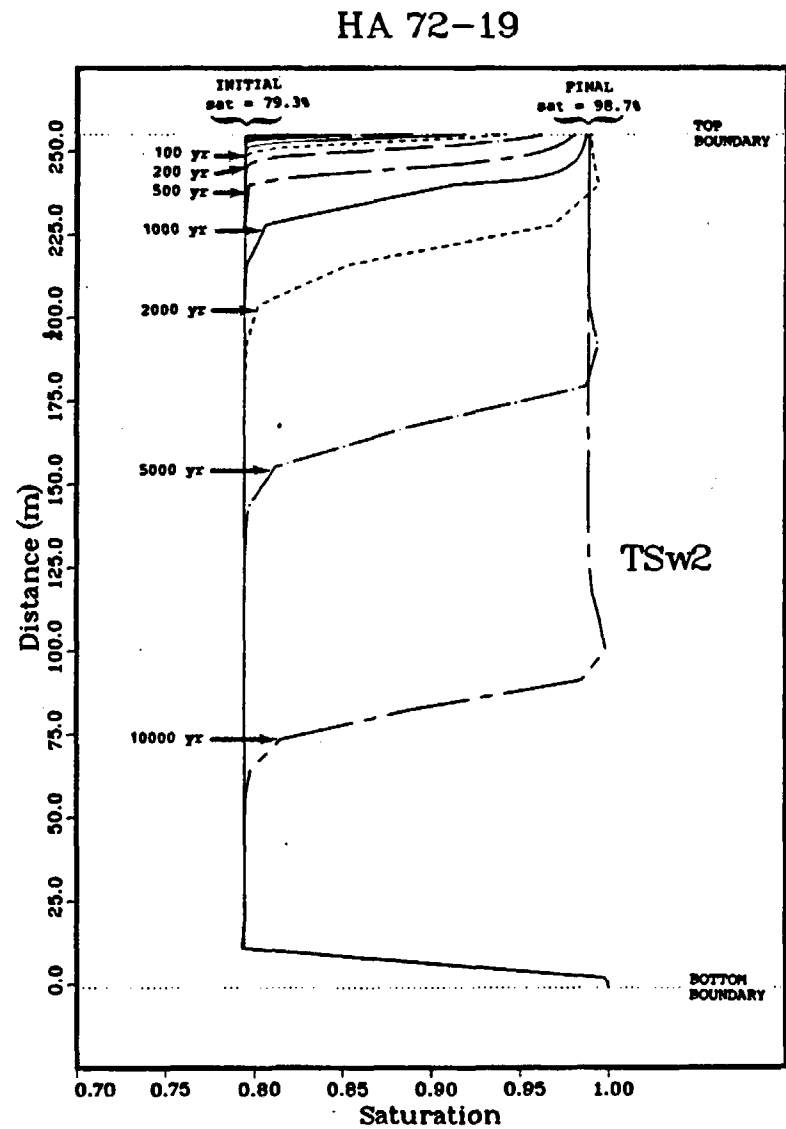
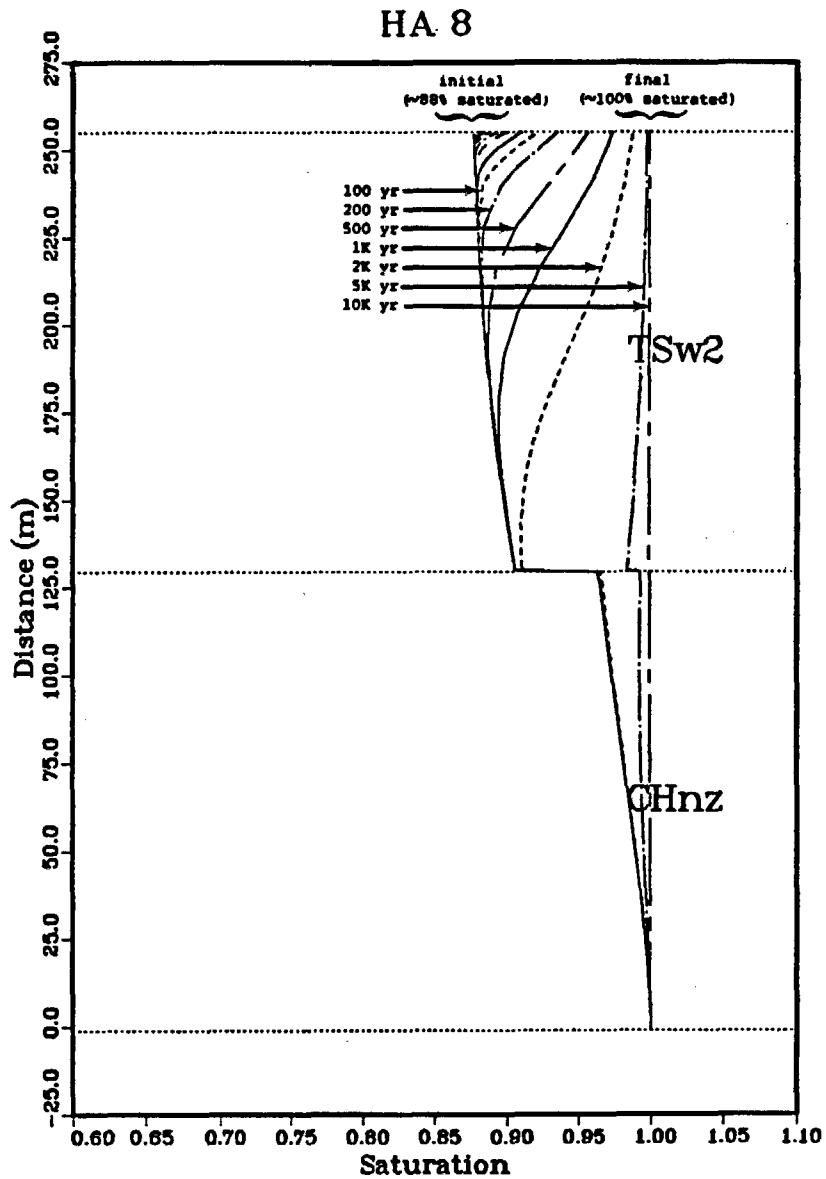


Fig. 21. Saturation versus distance (entire column) at specific times for the flux-change experiment problem ($q = 0.1$ mm/yr initial condition): results of Analysis 8 are on the left; results of Analysis 72-19 are on the right.

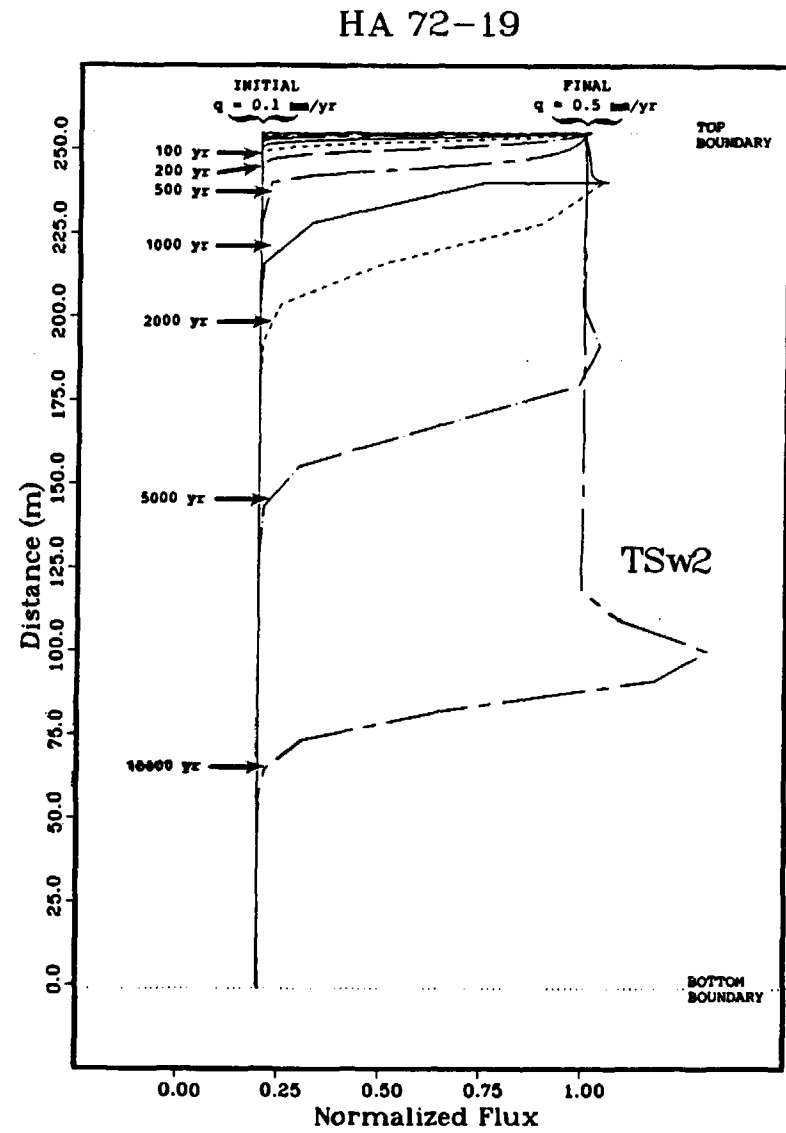
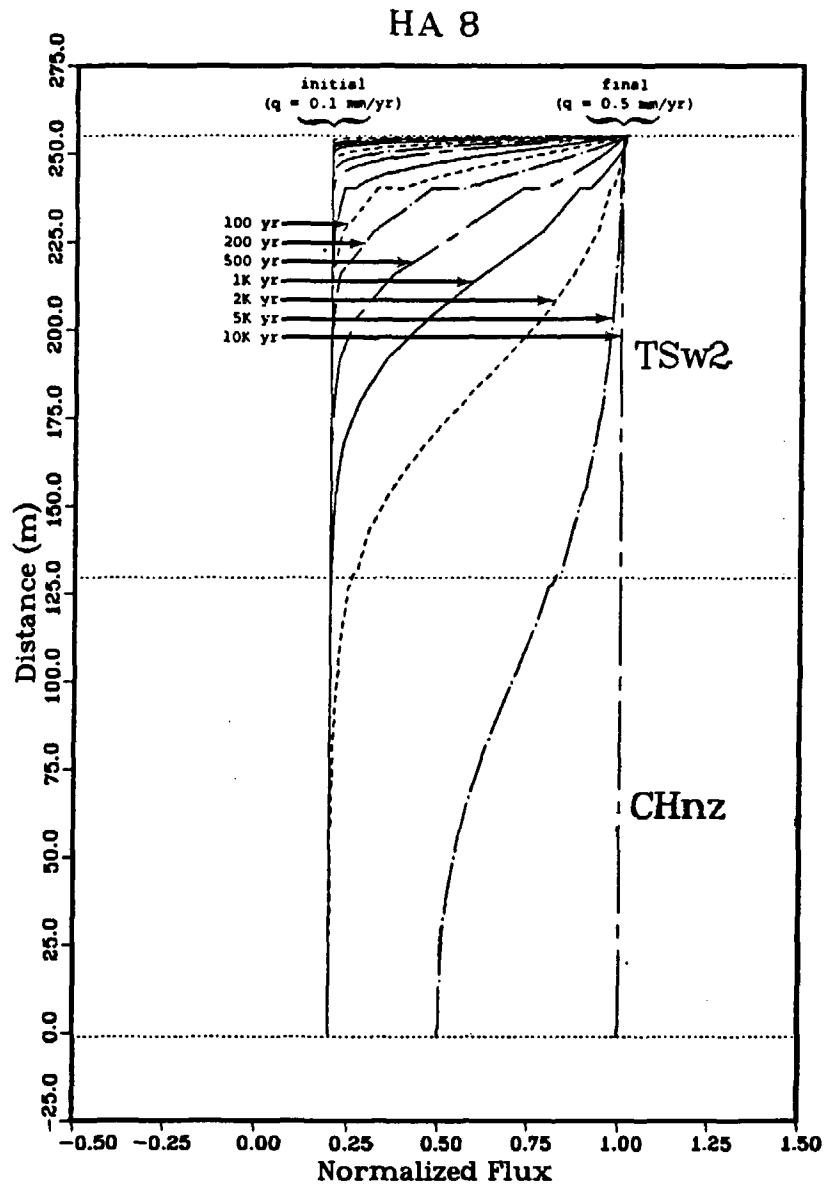


Fig. 22. Water flux (normalized to $q = 0.5 \text{ mm/yr}$) versus distance (entire column) at specific times for the flux-change experiment problem ($q = 0.1 \text{ mm/yr}$ initial condition): results of Analysis 8 are on the left; results of Analysis 72-19 are on the right.

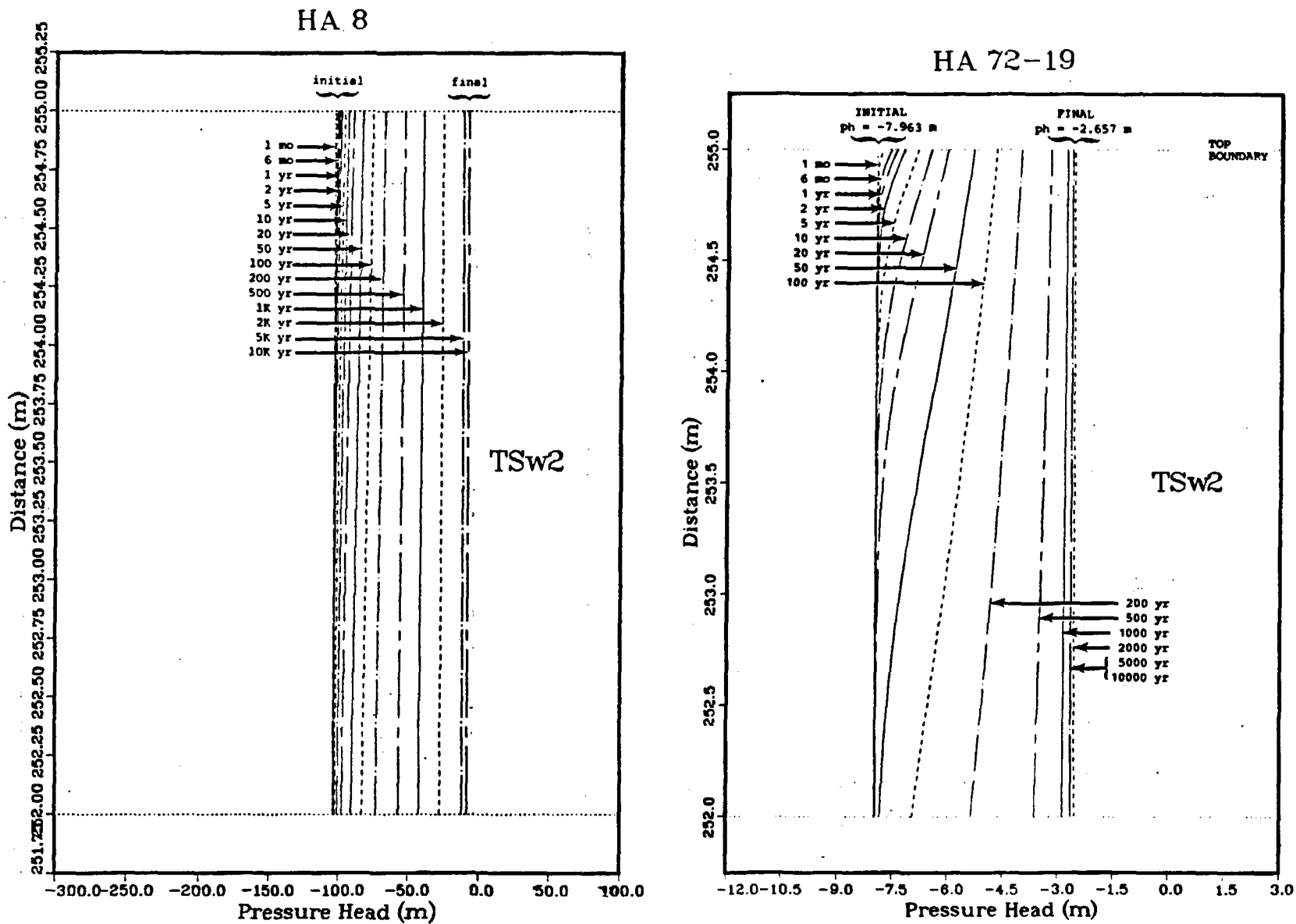


Fig. 23. Pressure head versus distance (top 3 m of the column) at specific times for the flux-change experiment problem ($q = 0.1$ mm/yr initial condition): results of Analysis 8 are on the left; results of Analysis 72-19 are on the right.

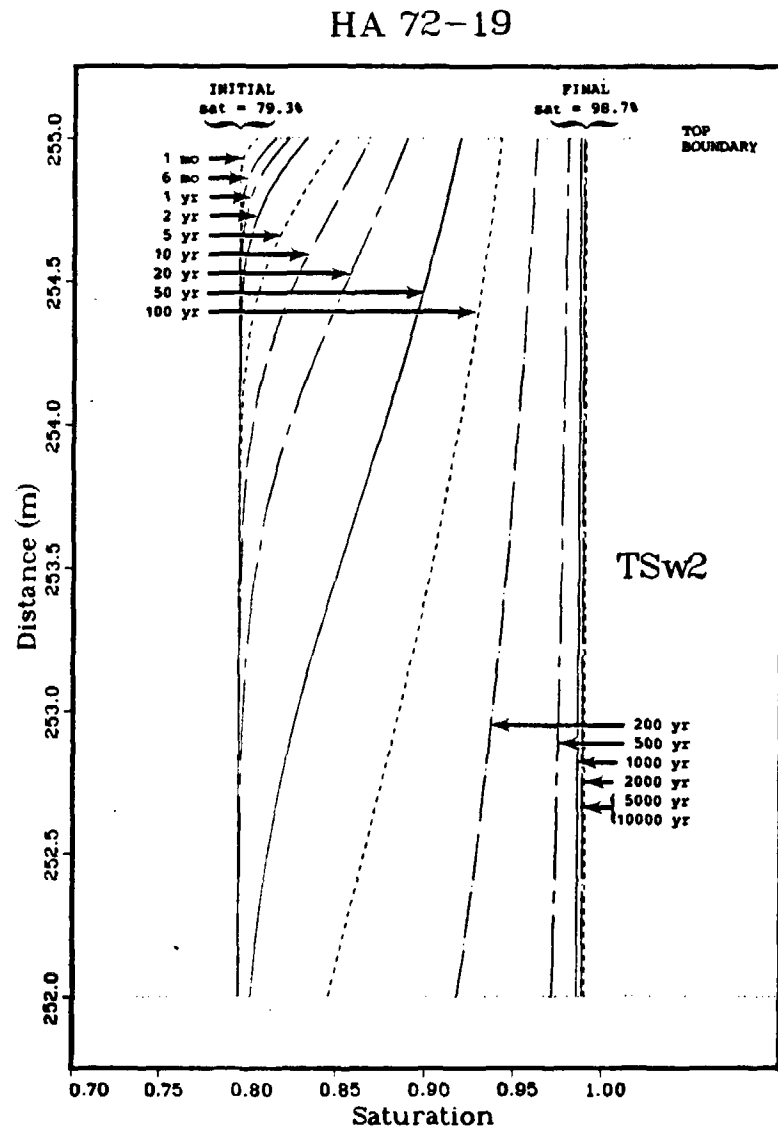
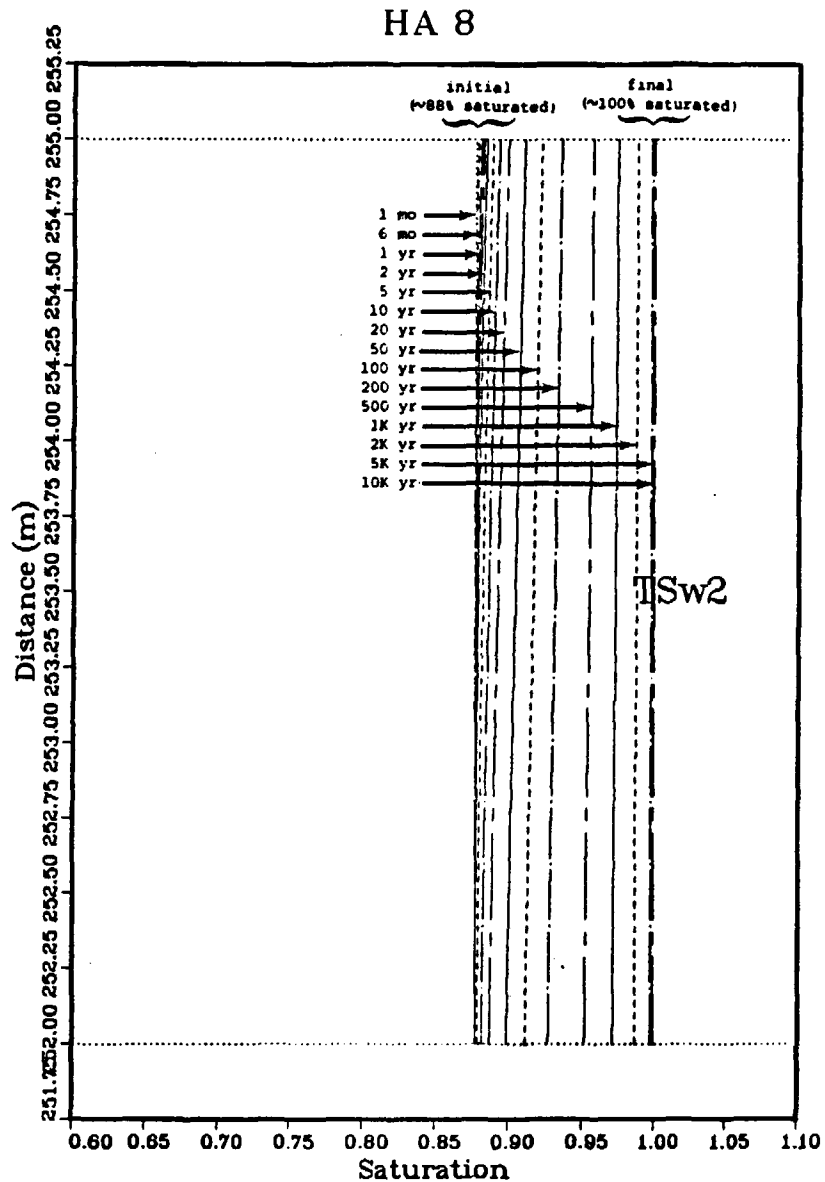


Fig. 24. Saturation versus distance (top 3 m of the column) at specific times for the flux-change experiment problem ($q = 0.1$ mm/yr initial condition): results of Analysis 8 are on the left; results of Analysis 72-19 are on the right.

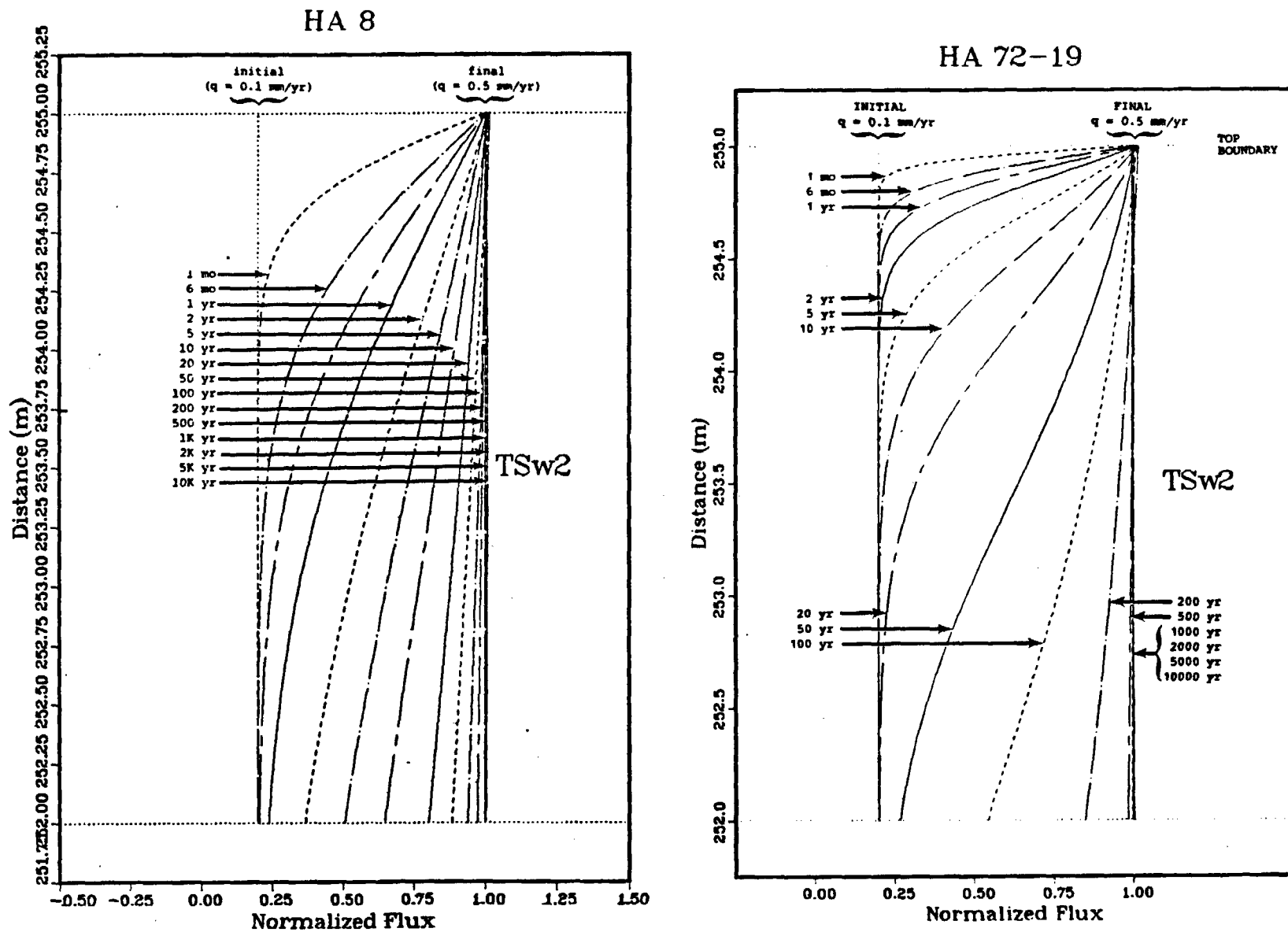


Fig. 25. Water flux (normalized to $q = 0.5 \text{ mm/yr}$) versus distance (top 3 m of the column) at specific times for the flux-change experiment problem ($q = 0.1 \text{ mm/yr}$ initial condition): results of Analysis 8 are on the left; results of Analysis 72-19 are on the right.

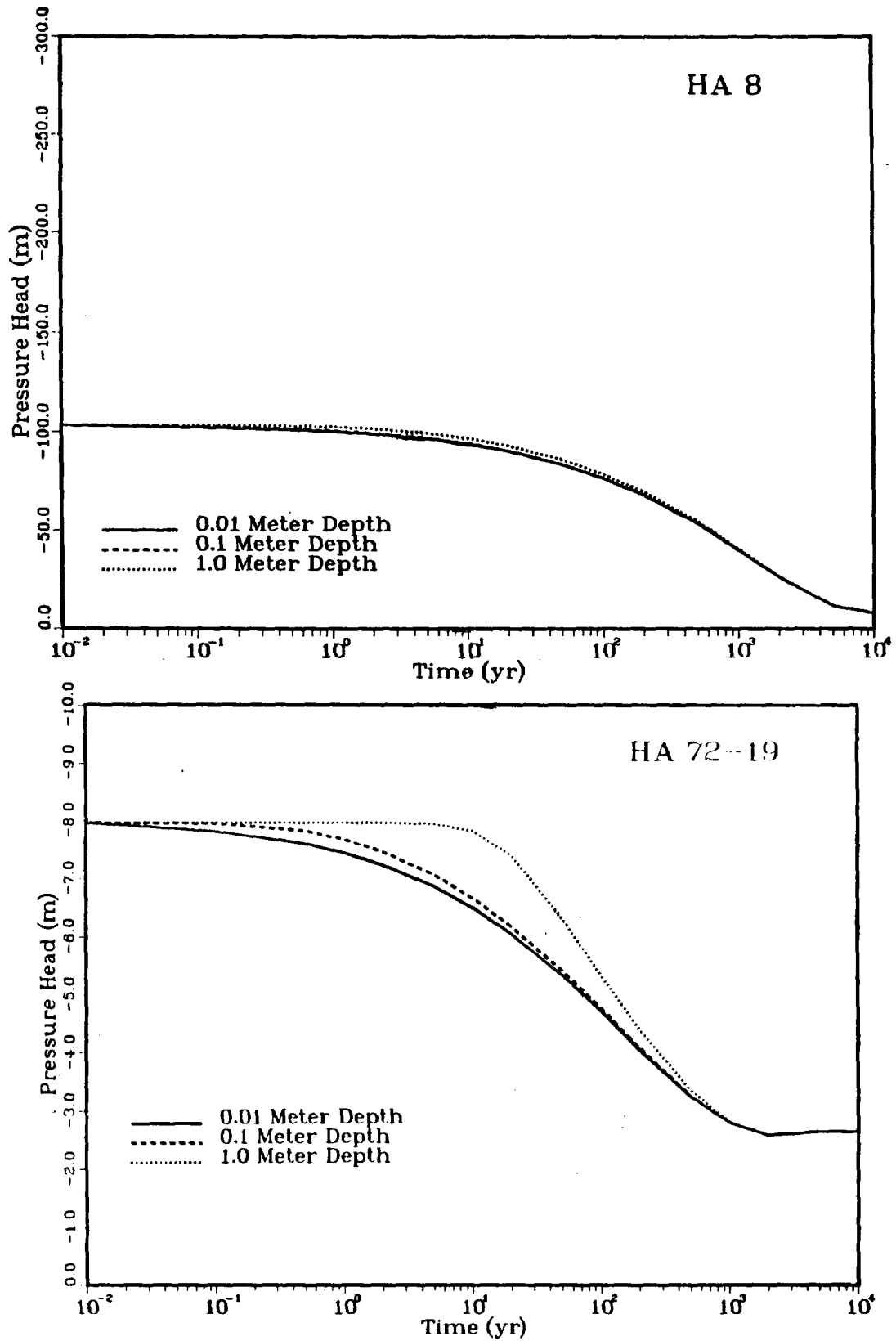


Fig. 26. Pressure head versus time at specified locations near the top of the column for the flux-change experiment problem ($q = 0.1$ mm/yr initial condition): results of Analysis 8 are on the top; results of Analysis 72-19 are on the bottom.

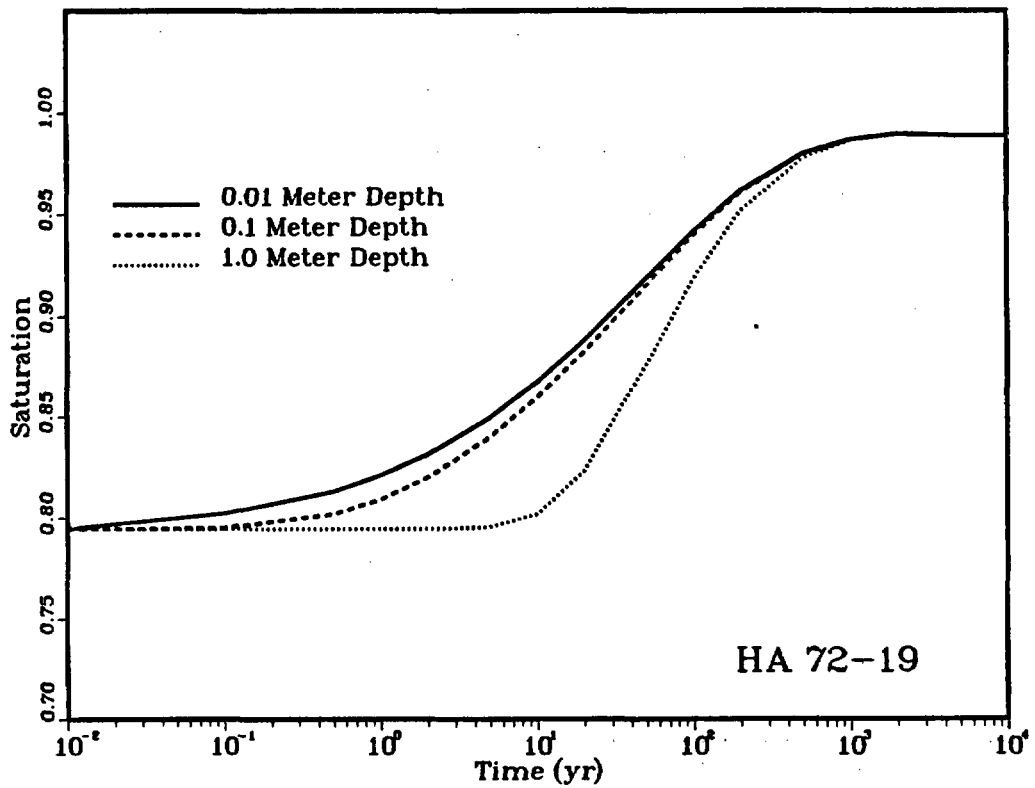
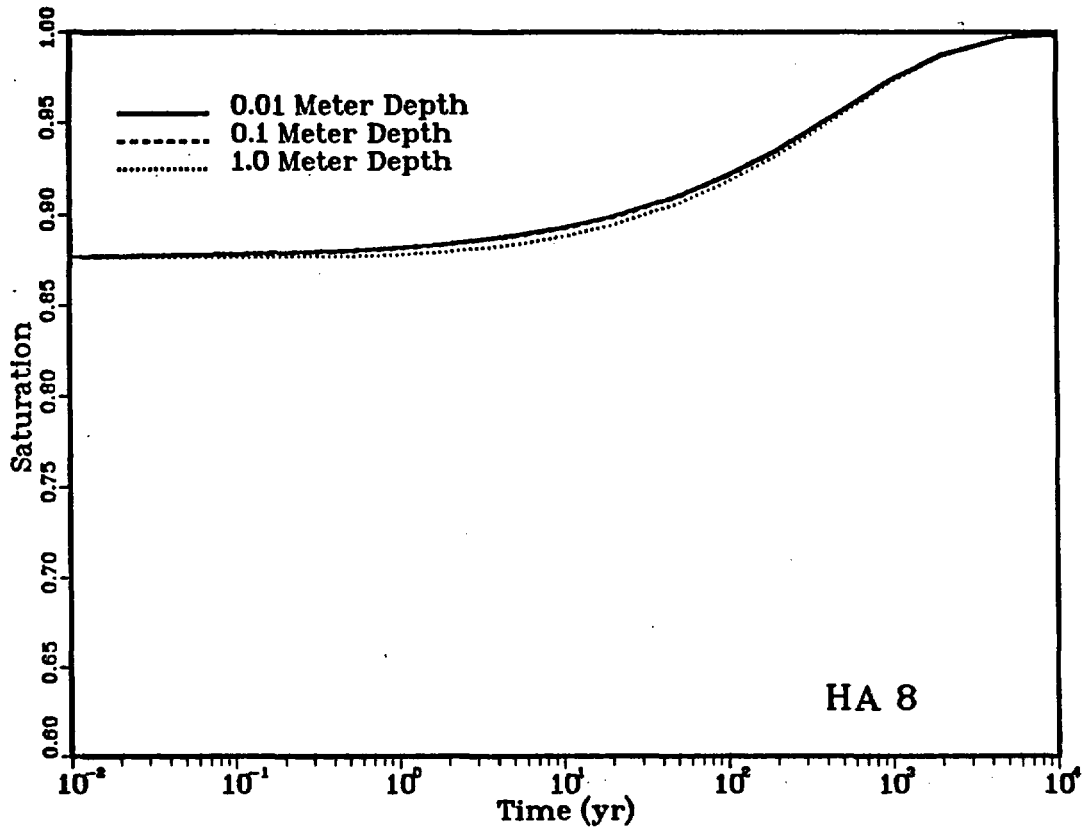


Fig. 27. Saturation versus time at specified locations near the top of the column for the flux-change experiment problem ($q = 0.1$ mm/yr initial condition): results of Analysis 8 are on the top; results of Analysis 72-19 are on the bottom.

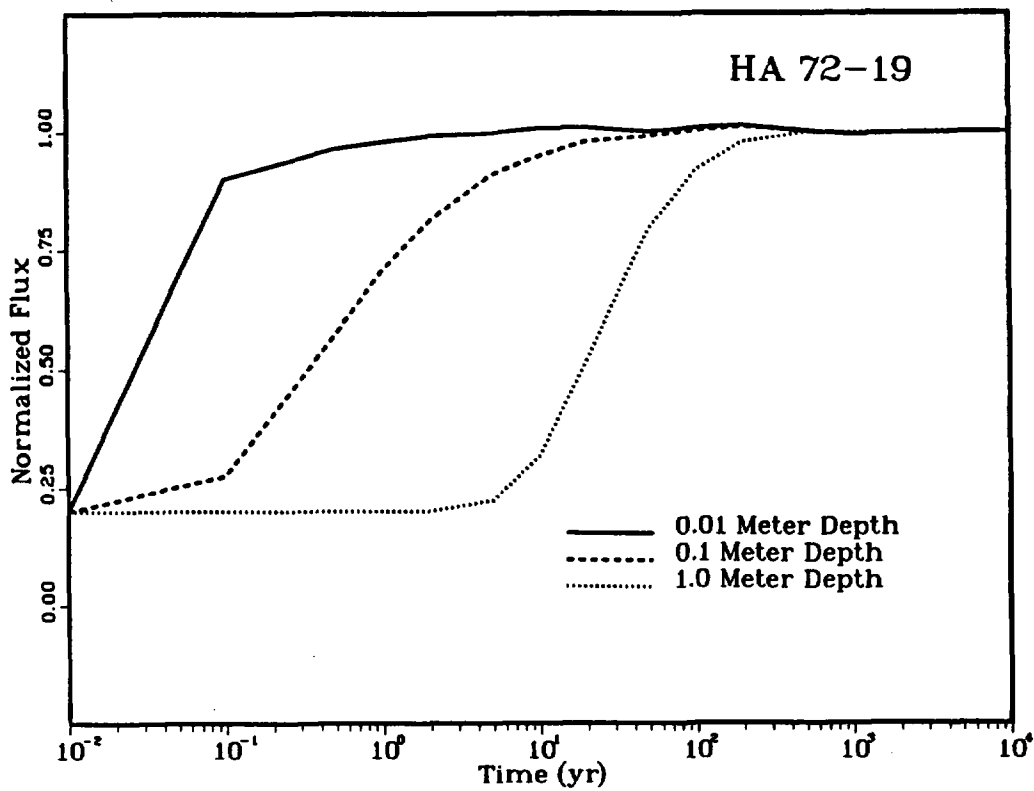
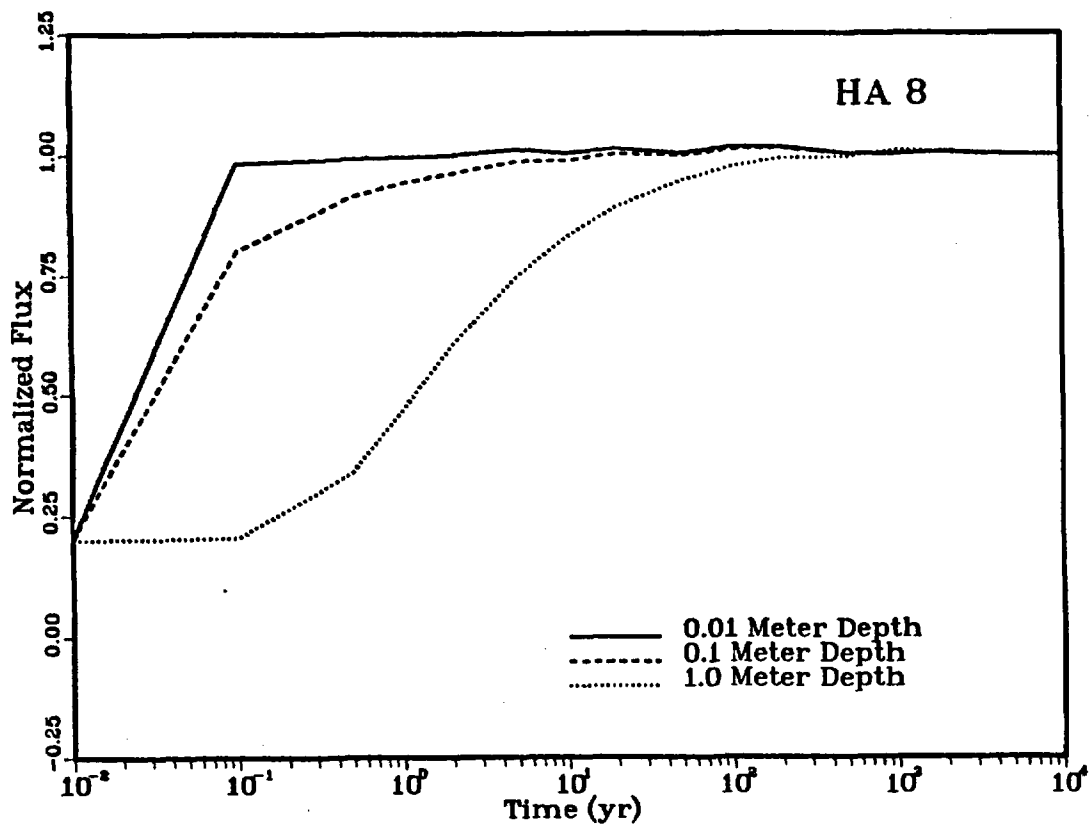


Fig. 28. Water flux versus time at specified locations near the top of the column for the flux-change experiment problem ($q = 0.1$ mm/yr initial condition): results of Analysis 8 are on the top; results of Analysis 72-19 are on the bottom.

MEMORANDUM NO. 3

NNWSI HYDROLOGIC ANALYSIS NO. 9
1-D HYDROLOGIC CALCULATIONS CONCERNING GROUNDWATER
TRAVEL TIME FOR THE REPOSITORY AS A RESULT OF WATER
REDISTRIBUTION CAUSED BY REPOSITORY HEATING

Sandia National Laboratories

Albuquerque, New Mexico 87185

date: June 10, 1986

to: B. S. Langkopf, 6312

from: J. Gauthier, 6312
R. R. Peters, 6312

Jack Gauthier
R. Peters

subject: NNWSI Hydrologic Analysis No. 9 -- 1-D Hydrologic Calculations
Concerning Groundwater Travel Time for the Repository as a Result of
Water Redistribution Caused by Repository Heating

NNWSI Hydrologic Analysis No. 9, as specified in your Problem Definition Memo of March 21, 1986, has been completed. Attached to this memo is a report that defines the calculations performed and discusses the results of the calculations.

JHG:RRP:6312:mjh:1590r
Attachment

Copy to:

6310 T. O. Hunter
6311 L. W. Scully
6312 F. W. Bingham
6312 A. L. Dudley
6312 M. S. Tierney
6313 T. E. Blejwas
6313 E. A. Klavetter
6314 J. R. Tillerson
6315 S. Sinnock
6315 Y. T. Lin
6310 10/12142/SNL/QII
6310 72/12142/9/QII
6310 NNWSI CF

1-D HYDROLOGIC CALCULATIONS
CONCERNING GROUNDWATER TRAVEL TIME FROM THE REPOSITORY
AS A RESULT OF WATER REDISTRIBUTION
CAUSED BY REPOSITORY HEATING

INTRODUCTION

It is postulated that heat from decaying nuclear waste in a repository at Yucca Mountain will vaporize groundwater within a radius of 10 meters over a period of approximately 90 years. This groundwater can be expected to condense outside the heated region, causing increased levels of saturation in the rock, resulting in changes in flux, pressure head, and hydraulic conductivity that could potentially influence groundwater travel times. Thus, there may be an impact on the bounds of the repository disturbed zone as defined in 10 CFR 60: "that portion of the controlled area the physical or chemical properties of which have changed as a result of underground facility construction or as a result of heat generated by the emplaced radioactive wastes such that the resultant change of properties may have a significant effect on the performance of the geologic repository."

PROBLEM DEFINITION

The part of Yucca Mountain of interest extends from the water table up to a point 10 meters below the repository horizon. Drill core measurements taken at drill hole G-4 indicate that there are two significant thermomechanical units in this region (Ortiz, et al., 1985). The Calico Hills nonwelded unit, zeolitized zone (CHnz), extends from the water table to an elevation of 129.5 meters. The Topopah Springs welded unit, nonlithophysal zone (TSw2), extends from 129.5 meters up to an elevation of 335.2 meters, although a point 10 meters below the repository horizon corresponds to an elevation of 219.5 meters. Figure 1 shows a graphic of the one-dimensional column used to model this geometry. Table 1 gives a listing of the rock properties used to model TSw2 and CHnz (Peters, et al., 1984).

The best current estimate of the Darcy velocity (flux) of groundwater through the Yucca Mountain repository zone is 0.1 mm/yr or less; at this flux, rock in the repository zone would be approximately 87 percent saturated (Peters, et al., 1986). The porosity of TSw2 is approximately 11 percent

(Peters, et al., 1984). One can calculate that the 10 meters of TSw2 dried out by the repository heat pulse should hold about 1 meter of groundwater. In a 90 year period, the addition of this 1 meter of water to the normal hydrologic regime would increase the flux, on average, to 11 mm/yr.

Using the above assumptions and resulting numbers, two analyses are defined. Both analyses begin with an initial condition throughout the column of 0.1 mm/yr flux, which is increased to 11 mm/yr at the upper boundary for 90 years. After 90 years, the first analysis examines the case where the influx immediately returns to 0.1 mm/yr; the second analysis looks at the case where there is no flux for 1000 years (i.e., until a problem time of 1090 years), followed by a return to the initial condition influx of 0.1 mm/yr. Table 2 presents an overview of the two analyses.

The second analysis is concerned with the perhaps more realistic case where the dry rock in the repository zone does not allow flow into the region below the repository for an extended period of time. Indeed, the dry rock may actually pull some of the condensed groundwater back up; thus, both analyses may overestimate the actual effect.

Of special interest is the influence of the water pulse on the groundwater travel time. Both analyses include the tracking of various particles of water scattered both spacially and temporally through the problem. Spacially, water particles are released at 10 meter intervals up the column, as well as at elevations of 129.5 and 219.5 meters (the interface between TSw2 and CHnz, and the top of the column, respectively); temporally, these particles are released at the following times: initially (0 years), plus at 30, 60, 90, 100, 200, 400, 600, 800, 1000, 2000, 4000, 6000, 8000, 10,000, 20,000, 40,000, 60,000, 80,000, 100,000, 200,000, and 400,000 years. Because the groundwater travel time from the repository to the water table is expected to be on the order of 400,000 years at a constant flux of 0.1 mm/yr, it is assumed that the groundwater would return to a steady-state condition before that time. Thus, the travel times of the particles released at 400,000 years are used for normalizing the other particle travel times to steady state. In fact, both analyses showed that hydrologic steady state is reached in about 40,000 years. Both analyses are run to a million years in order to assure that all released particles reached the water table by the end of the simulation.

MODELING NOTES

The computer program TOSPAC (Dudley, et al., in preparation), a one-dimensional, finite difference code specifically created to solve problems involving fluid flow and transport with highly nonlinear parameters in multiple media, was used for these calculations.

The DYNAMICS module of TOSPAC was modified in order to track the travel times of water particles. Modifications included the addition of subroutines to perform the travel time calculation based on the integration of the water velocity over a given time step; the addition of new data arrays to keep track of water particle starting and current position as well as its cumulative travel time (i.e., the sum of the time steps ending when the particle reached the water table); and the addition of a method to input and output particle data in a logical manner consistent with existing DYNAMICS parameter input and output.

When tracking a water particle, the particle was assigned the fracture water velocity if the fracture water contributed to more than one percent of the total flux; otherwise, the particle was assigned the matrix water velocity. (This almost-worst-case method of calculating travel time is consistent with the method used in the STATICS module of TOSPAC, where it was found that travel times were fairly insensitive to switching between fracture and matrix velocities at fracture fluxes ranging between 10 percent and 0.01 percent of the total flux.)

The distance a particle traveled in a given iteration was calculated by multiplying the time step by the velocity. The velocity was linearly interpolated when the starting position of the particle did not correspond exactly to a prescribed mesh point position value. If a mesh point was crossed by the particle, the remaining time in the iteration was calculated and the new mesh point velocity was used to continue the trapezoidal-approximation integration.

The time that a particle crossed the water table, i.e., exited the column, was linearly interpolated. To estimate the extent of the error due to linearly interpolating these highly nonlinear functions the Case 1 problem was rerun with mesh cell sizes divided by two; there was no appreciable difference in the results--the graphic output appeared identical.

The DYNAMICS module of TOSPAC allows specifying boundary conditions according to either flux or pressure, and allows them to be changed at arbitrary times. For these problems the upper boundary condition was specified as a flux ($3.17\text{E}-12$ m/s or 0.1 mm/yr, $3.49\text{E}-10$ m/s or 11 mm/yr, and 0 m/s or 0 mm/yr), while the lower boundary was specified as a pressure head (0 meters of pressure corresponding to the water table). Any water reaching the lower boundary was calculationaly allowed to leave the mesh at its current flux.

The one-dimensional mesh was set up so that the mesh points were spaced from 0.5 to 2 meters apart. This rather coarse mesh was chosen because preliminary runs showed that to simulate the first 90 years of the problem took over 50,000 iterations; thus, performing several calculational runs--a necessity just to debug the modifications to the code--could have proven prohibitively expensive with a finer mesh. As mentioned above, however, a trial run with a finer mesh did not show a significant difference in the results. To simulate times from 90 years to one million years took only a few hundred iterations. The predominately fracture flow at earlier times caused DYNAMICS to hunt for a solution on the most nonlinear areas of the hydraulic conductivity and capacitance coefficient curves. (For a more complete discussion of the calculational efficiency of DYNAMICS see Dudley, et al., in preparation.)

RESULTS

The results of both cases showed that groundwater travel times can be significantly influenced by the additional influx of water only when the influx saturates the rock matrix and induces flow in the fractures. Such flow in the fractures only took place in TSw2.

Also, there was very little quantitative difference in the travel time results of Case 1 and Case 2. Case 2 returned to steady state slightly quicker than Case 1, probably due to the fact that less water overall was added to the column, buffering the effect of the 11 mm/yr influx.

Figures 2 and 3 present the change in composite flux over distance at various times. The composite flux is the area-weighted average of the flux in the matrix and the flux in the fractures. Figure 2 shows the flux change for

Case 1 and Figure 3 shows it for Case 2. The initial condition of 0.1 mm/yr corresponds to a flux of $3.17\text{E}-12$ m/s, while the 90 year influx pulse of 11 mm/yr corresponds to $3.49\text{E}-10$ m/s. The saturated hydraulic conductivity of the TSw2 matrix is $1.9\text{E}-11$ m/s; therefore, any values above this figure indicate water flow in the fractures.

In the first 30 years the influx pulse causes a composite flux increase in the upper 30 meters of the column; at 60 years there is a flux increase in the upper 60 meters; and at 90 years the increase extends downward almost 90 meters. Note that at 90 meters the flux has been either reset to 0.1 mm/yr (Case 1) or set to 0 mm/yr (Case 2), and this action is reflected in the 90 year curves at the top of the column. In Case 2, the influx is not reset to 0.1 mm/yr until after 1,000 years, as shown in Figure 3. Also note that the curves at 30, 60, and 90 years show small wiggles at the 11 mm/yr influx, indicating the difficulty DYNAMICS was having in determining exact pressure head values while working in the most nonlinear regions of the hydraulic conductivity and capacitance coefficient curves.

After 90 years the flux change dissipates in magnitude rapidly, but continues to extend down the column. Between 400 and 600 years the flux increase reaches the water table; at 2,000 years this increase has reached its maximum at a value approximately double that of the initial condition flux. These increases in flux have a direct influence on the water velocity and groundwater travel time, as discussed below (Figures 12 through 15).

Figures 4 and 5 show the change in matrix saturation over distance at various times for Case 1 and Case 2, respectively. (These plots effectively show total saturation since the fracture area is on the order of 0.001 percent.) The initial saturation at the top of the column is approximately 88 percent; the initial saturation at the bottom of the column is 100 percent and indicates the presence of the water table. There is a discontinuity in the initial saturation at the TSw2/CHnz interface. This discontinuity is due to different saturation curves used for the different units: the curve used for the CHnz material returns a higher saturation value at these pressure heads than the curve used for the TSw2 material (Peters, et al., 1984). The change from one material to another at the TSw2/CHnz interface is abrupt; thus, the change in saturation is abrupt.

Application of the 11 mm/yr influx causes the saturation to jump to approximately 100 percent at the top of the column. Complete saturation of the matrix implies that water is now flowing in the fractures in this area. At 90 years, when the influx is reduced, the saturation begins a gradual return to the initial condition. Figure 5 shows that the return to the initial condition is quicker during the 1,000 year period when the influx has been set to zero. Note that the saturation in the lower portion of CHnz is nearly 100 percent, allowing the flux pulse to move through this region rapidly (see Figures 2 and 3) compared to the top of CHnz.

Figures 6 and 7 show the change in pressure head--the quantity DYNAMICS solves for--over distance at various times for Case 1 and Case 2, respectively. The initial, steady-state pressure head at the top of the column is approximately -100 meters. The 11 mm/yr influx immediately increases the pressure head to almost 0 meters, indicating saturation of the rock matrix and the probable initiation of water flow in the fractures. At 90 years, this pulse has proceeded over 80 meters into the column. (As discussed below, this downward extent of the pressure head pulse corresponds to the position of the knee in the groundwater travel time curves in Figures 12 through 15.) After 90 years, the shape of the pressure head curve smooths, decreasing in TSw2 and increasing in CHnz for about 2,000 years. The pressure head returns to the initial condition in about 40,000 years. At 2,000 years the pressure head is at its maximum in CHnz; thus the influence of the 11 mm/yr influx extends throughout the column in 2,000 years, even though minimum travel times for water particles associated with the 11 mm/yr influx are on the order of 300,000 years (see the discussion of Figures 12 through 15 below).

Figures 8 and 9 show the average linear velocity of water in the matrix at various times over distance for Case 1 and Case 2. The curves at 30, 60, and 90 years track the velocities associated with the 11 mm/yr influx. The velocity spike at the influx front is due to the large pressure head gradient (approximately 100 meters in pressure head change over 10 meters distance--see Figures 6 and 7 above). At the initial condition, the pressure head is roughly -100 meters in unit TSw2. Water cannot move into the fractures until the pressure head increases to about -1 meter. Therefore, the pressure head

gradient causes the water velocity to increase tremendously in the matrix until the pressure head reaches -1 meter. At this point, water flows in the fractures, the pressure head pulse passes, and the water velocity in the matrix subsides. For a more complete discussion of this effect, see Dudley, et al., in preparation.

At the bottom of the column, note the approximately twofold increase in velocity at 2,000 years. At the initial condition flux of 0.1 mm/yr, a water particle released at 10 meters above the water table has a travel time of approximately 8,000 years (see Figures 14 and 15 below); therefore, the increased velocity at 2,000 years is responsible for the 50 percent decrease in travel time for the water particles released at the 10 meter elevation.

Figures 10 (Case 1) and 11 (Case 2) present the average linear velocity of water in the fractures at various times over distance. At the top of the column, flow in the fractures was significant only for the first 90 years of the simulation--i.e., while the 11 mm/yr influx persisted. From 90 years to 100 years fracture velocities decreased over four orders of magnitude; after 100 years they were negligible. At the bottom of the column, there was always a measureable velocity of water in the fractures due to the high saturation levels near the water table. Therefore, all of the many line types are plotted upon one another, giving the apparent dark line at the bottom.

Figures 12 and 13 present the groundwater travel times as a function of starting elevation of water particles released at various times. During the computer simulation, water particles were placed in the column at 10 meter intervals, plus at the top and at the unit interface, and tracked until they reached the water table (see the discussion in the Modeling Notes section, above). The different curves in the Figures show the travel times calculated for the set of water particles that were all inserted in the column at the specified time. Figure 12 presents the results for Case 1; Figure 13 for Case 2.

The Figures show a decrease in groundwater travel time for water particles released at the top of the column in the first 90 years. This decrease is expected due to the fracture flow and resulting high water velocities caused by the 11 mm/yr influx. Note that the flat portion of the 0, 30, 60 year curve indicates that particles released at these elevations all reach the

water table at approximately the same time--300,000 years. Thus, fracture flow induced by the 11 mm/yr influx moves these particles in a very short time down to an elevation of roughly 130 meters; at this point fracture flow ceases, and the particles continue down to the water table through matrix flow at a much slower rate. Travel times of particles released at the top of the column return to within a few percent of the steady-state travel times immediately after the 11 mm/yr influx is halted, as shown by the 90 year and the 100 year curves.

Figures 14 (Case 1) and 15 (Case 2) present groundwater travel times normalized to steady-state travel times as a function of starting elevation of water particles at various release times. In these figures the expected decrease in travel times due to fracture flow is seen in the upper 90 meters of the column, above the "knee" at 130 meters elevation.

Figures 14 and 15 also show that the normalized travel times drop even more near the bottom of the column where there is no fracture flow (except for the fracture flow near the water table that is always present). The reason for this somewhat unexpected result is that the pressure head change, and thus the flux change, associated with the 11 mm/yr influx influences the entire column within 2,000 years. Water particles in the lower part of the column can essentially "ride" this flux pulse out of the column during the time period of 2,000 to about 10,000 years. Water particles in the upper part are only affected by the flux pulse for a tiny portion of their overall travel time, then they must proceed at velocities more closely resembling the initial steady-state condition.

This situation is reflected in the normalized travel time curves, but it is not reflected in the absolute travel time curves (Figures 12 and 13). At a steady-state flux of 0.1 mm/yr, the absolute travel time is about 400,000 years for a particle released at the top of the column, and about 8,000 years for a particle released 10 meters above the water table. A 25 percent drop in the absolute groundwater travel time corresponds to a decrease of 100,000 years at the top of the column; a 50 percent drop in absolute groundwater travel time corresponds to a decrease of 4,000 years at the bottom of the column. A change of 100,000 years is clearly visible in Figures 12 and 13, while a change of 4,000 years is barely noticeable.

REFERENCES

- Dudley, A. L., R. R. Peters, M. S. Tierney, E. A. Klavetter, J. H. Gauthier, and M. Wilson. In preparation. "Total Systems Performance Assessment Code (TOSPAC) Volume 1: Physical and Mathematical Bases," SAND85-0002, Sandia National Laboratories, Albuquerque, NM.
- Ortiz, T. S., R. L. Williams, F. B. Nimick, B. C. Whittet, and D. L. South. 1985. "A Three-Dimensional Model of Reference Thermal/Mechanical and Hydrological Stratigraphy at Yucca Mountain, Southern Nevada," SAND84-1076, Sandia National Laboratories, Albuquerque, NM.
- Peters, R. R., E. A. Klavetter, I. J. Hall, S. C. Blair, P. R. Heller, and G. W. Gee. 1984. "Fracture and Matrix Hydrologic Characteristics of Tuffaceous Materials from Yucca Mountain, Nye County, Nevada," SAND84-1471, Sandia National Laboratories, Albuquerque, NM.
- Peters, R. R., J. H. Gauthier, and A. L. Dudley. 1986. "The Effect of Percolation Rate on Water-Travel Time in Deep, Partially Saturated Zones," SAND85-0854, Sandia National Laboratories, Albuquerque, NM.

TABLE 1. Material Hydrologic Properties.

	Unit TSw2-3	Unit CHnz
MATRIX PROPERTIES		
Porosity (n_m)	0.11	0.28
Hydraulic Conductivity (K), (m/s)	1.9×10^{-11}	2.0×10^{-11}
Residual Saturation (S_r)	0.080	0.110
Alpha (α) - 1/m	0.00567	0.00308
Beta (β)	1.798	1.602
FRACTURE PROPERTIES		
Porosity (n_f)	$18. \times 10^{-5}$	4.6×10^{-5}
Compressibility ($\partial n_f / \partial \sigma'$), 1/m	12.0×10^{-8}	2.8×10^{-8}
Hydraulic Conductivity (K), m/s	3.1×10^{-9}	9.2×10^{-9}
Fracture Saturation Coefficients are $S_r = 0.0395$, $\alpha = 1.285/m$, $\beta = 4.23$		
Rock Mass Coefficient of Consolidation (α'_{bulk} - 1/m)	5.8×10^{-7}	$26. \times 10^{-7}$
Compressibility of Water (β') is $9.8 \times 10^{-7}/m$		

TABLE 2. Overview of the Two Analysis Cases.

	<u>INITIAL STEADY-STATE CONDITION</u>	<u>0 TO 90 YEAR INFLUX</u>	<u>90 TO 1090 YEAR INFLUX</u>	<u>1090 TO 1 MILLION YEAR INFLUX</u>
CASE 1	0.1 mm/yr	11 mm/yr	0.1 mm/yr	0.1 mm/yr
CASE 2	0.1 mm/yr	11 mm/yr	0. mm/yr	0.1 mm/yr

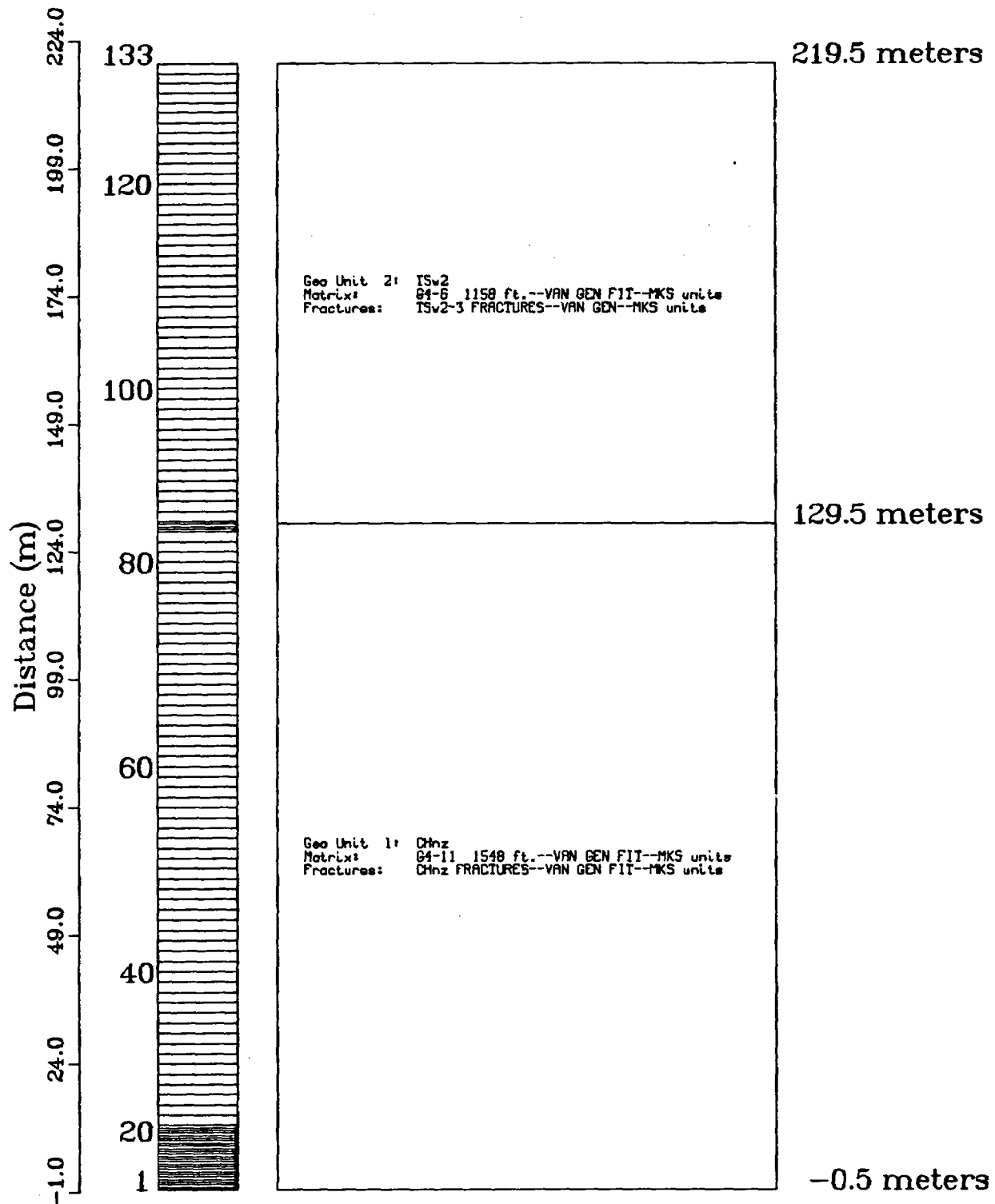


Figure 1. Mesh setup and geologic parameters used in TOSPAC for the two analysis cases

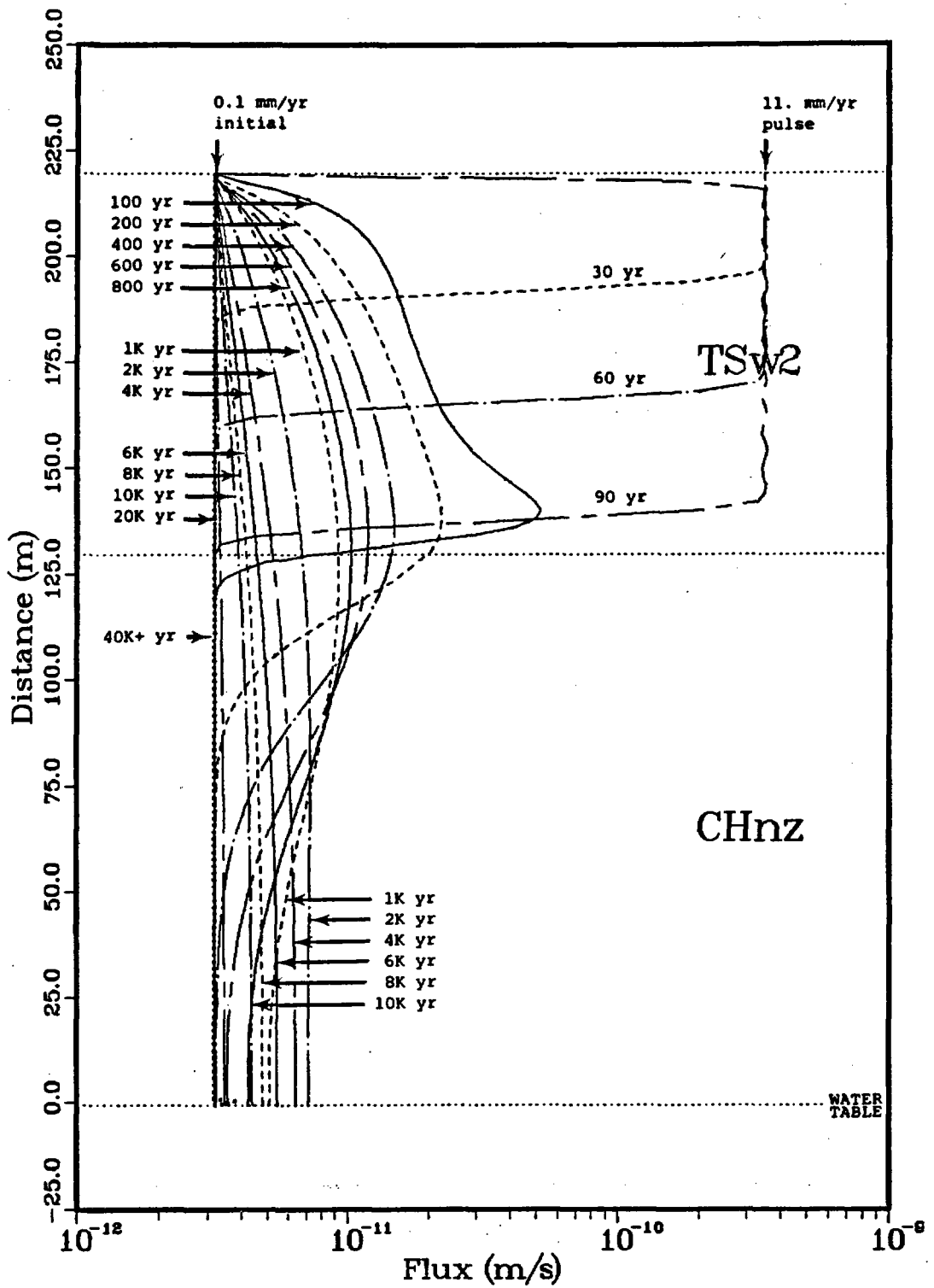


Figure 2. Composite flux vs distance at various times for Analysis Case 1

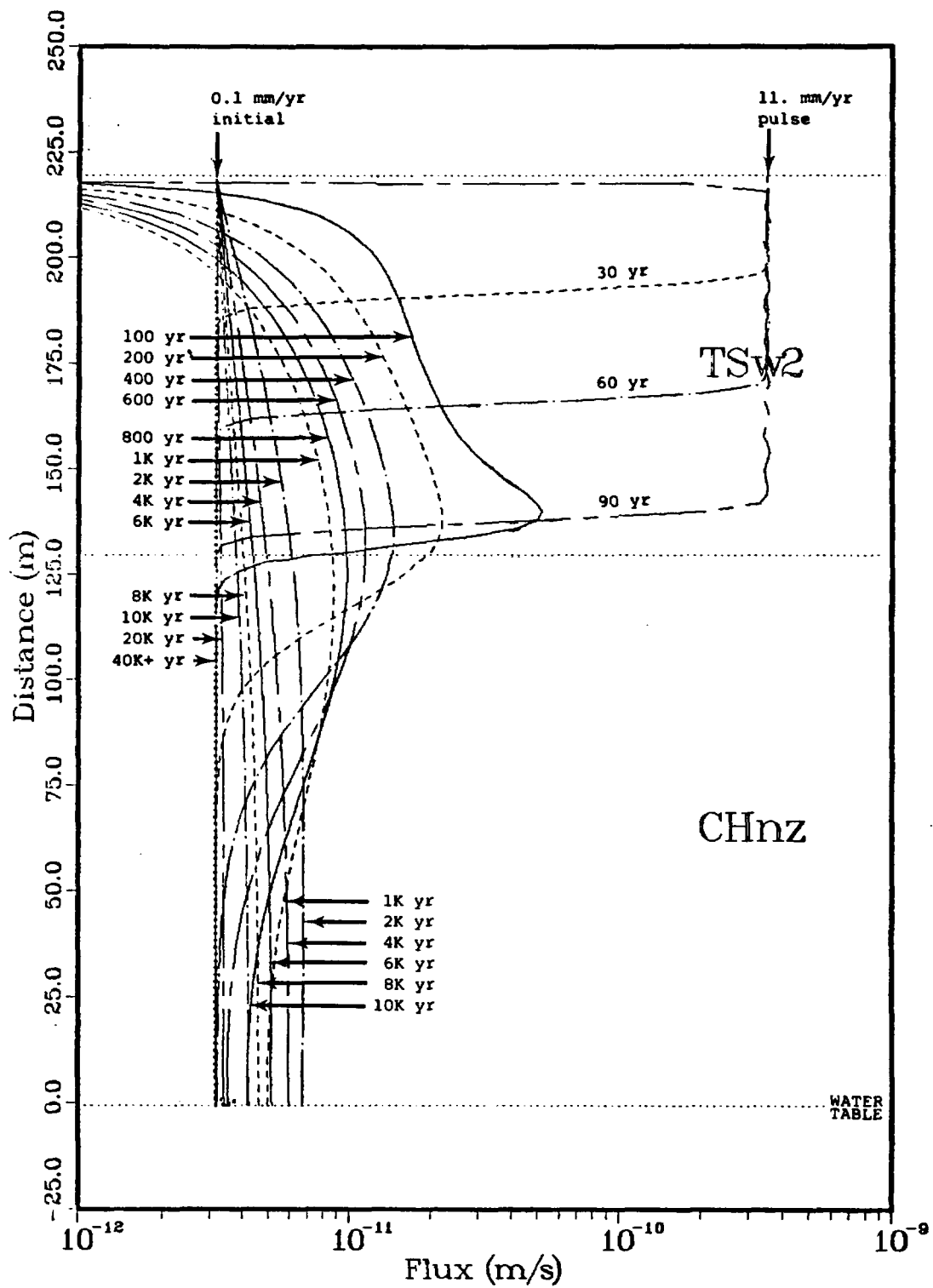


Figure 3. Composite flux vs distance at various times for Analysis Case 2

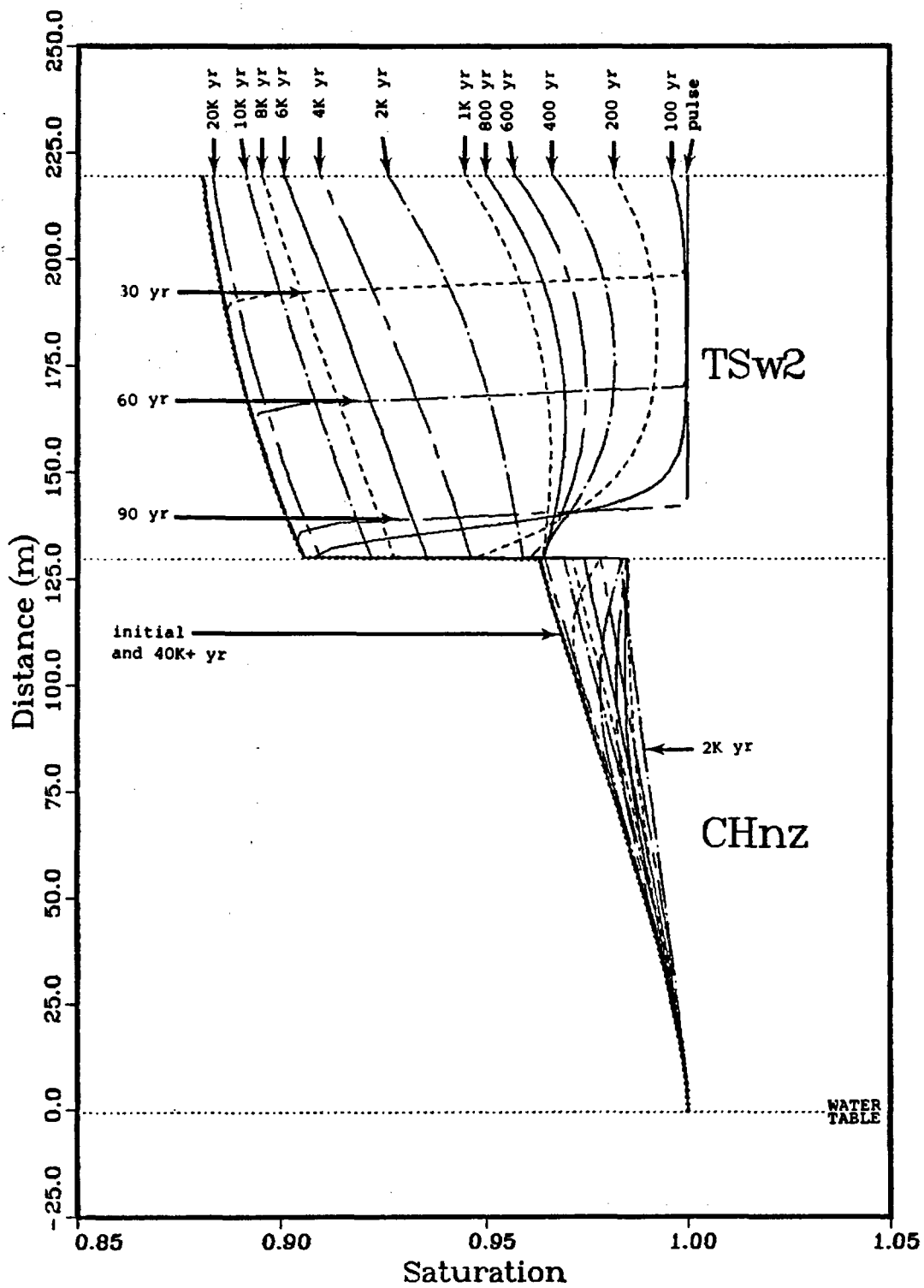


Figure 4. Saturation vs distance at various times for Analysis Case 1

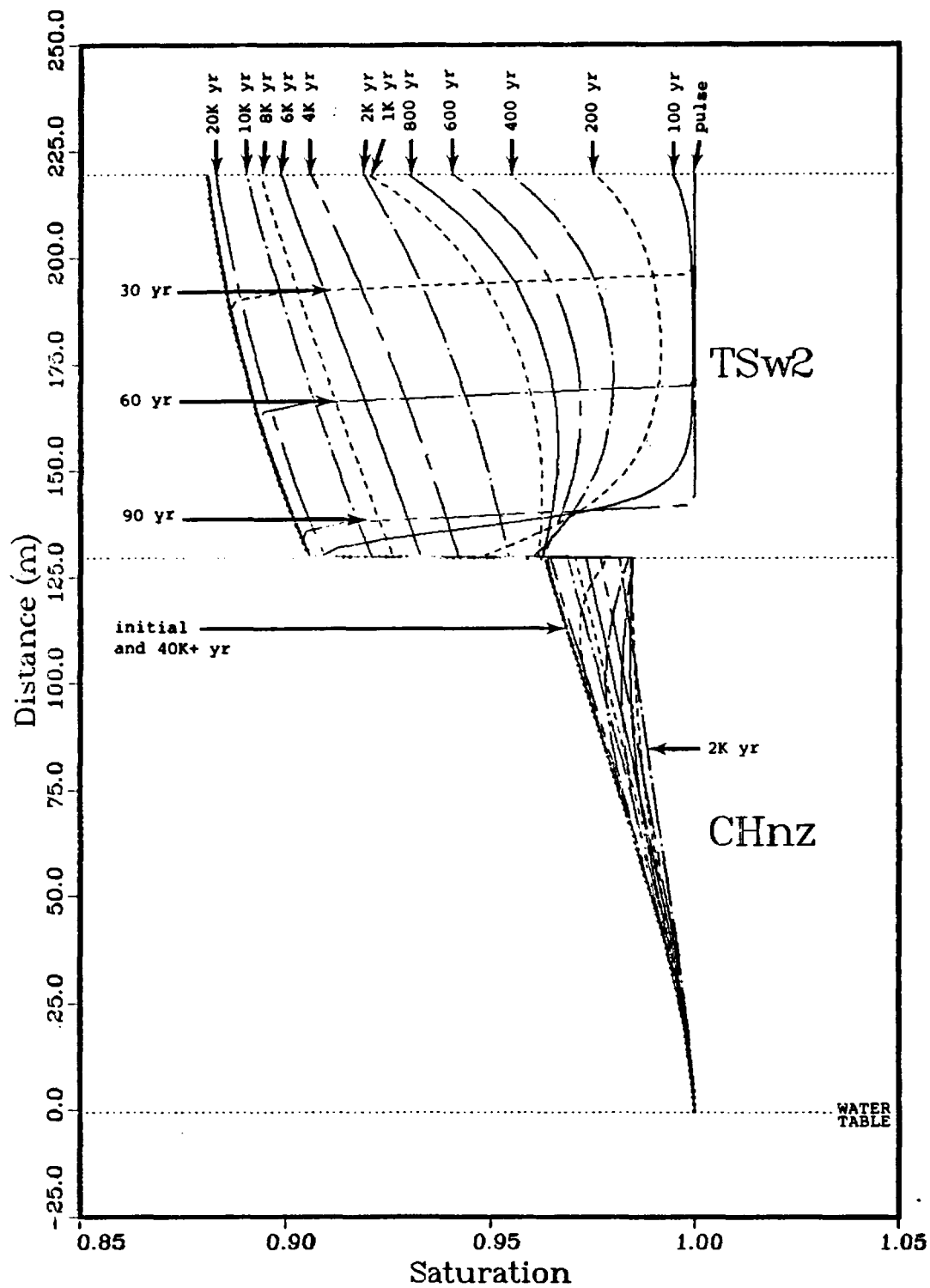


Figure 5. Saturation vs distance at various times for Analysis Case 2

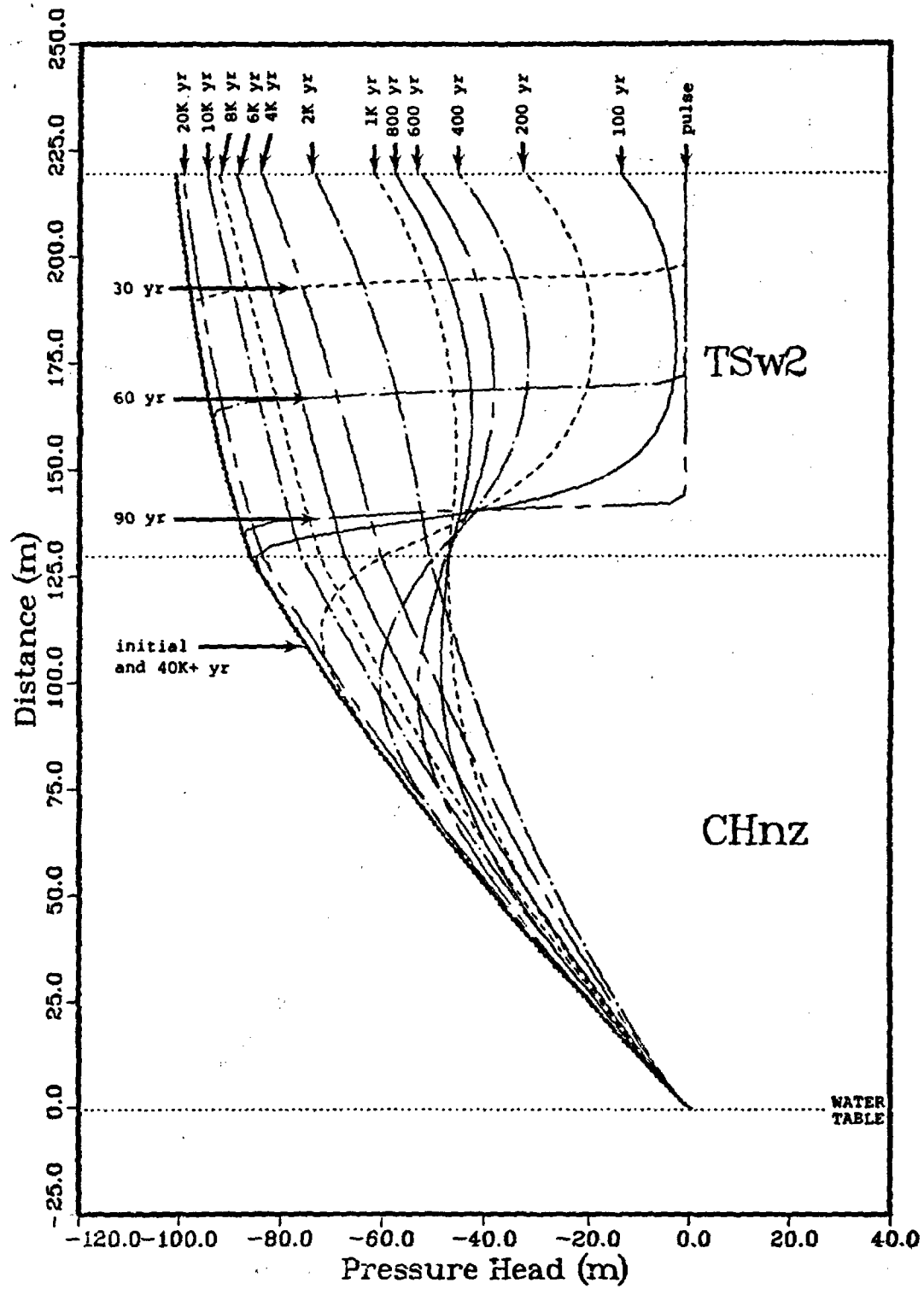


Figure 6. Pressure head vs distance at various times for Analysis Case 1

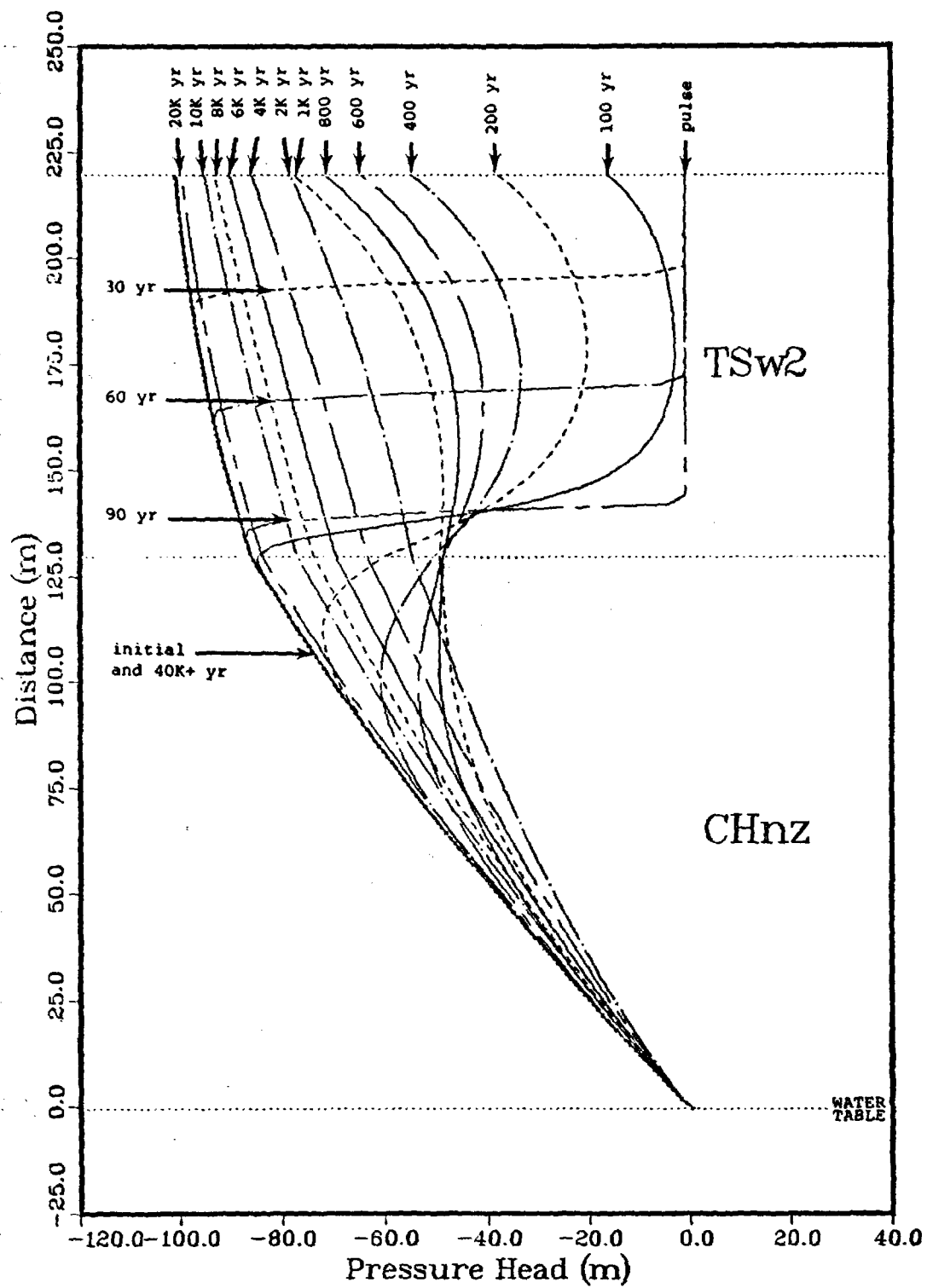


Figure 7. Pressure head vs distance at various times for Analysis Case 2

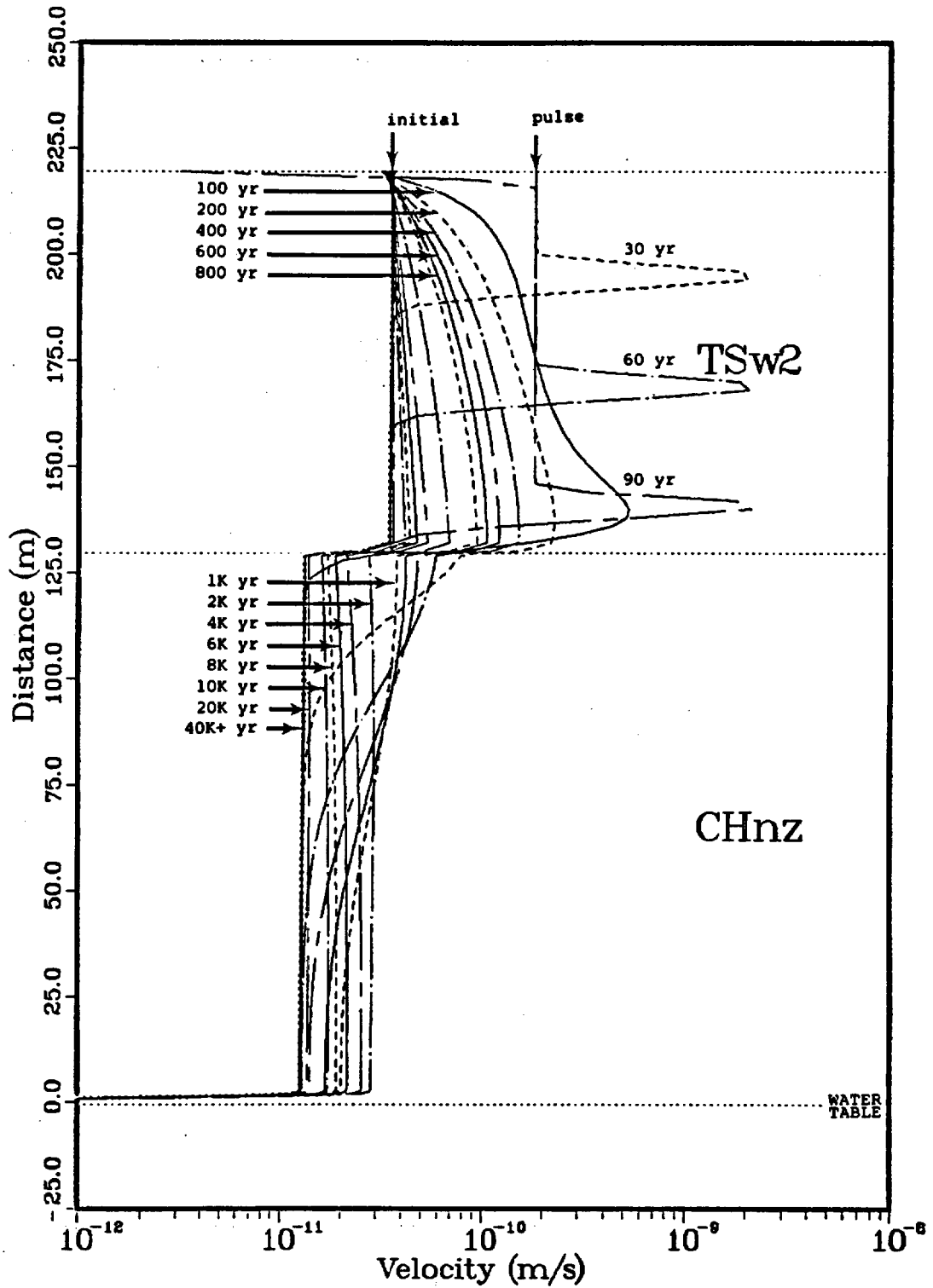


Figure 8. Average linear velocity of groundwater in the matrix vs distance at various times for Analysis Case 1

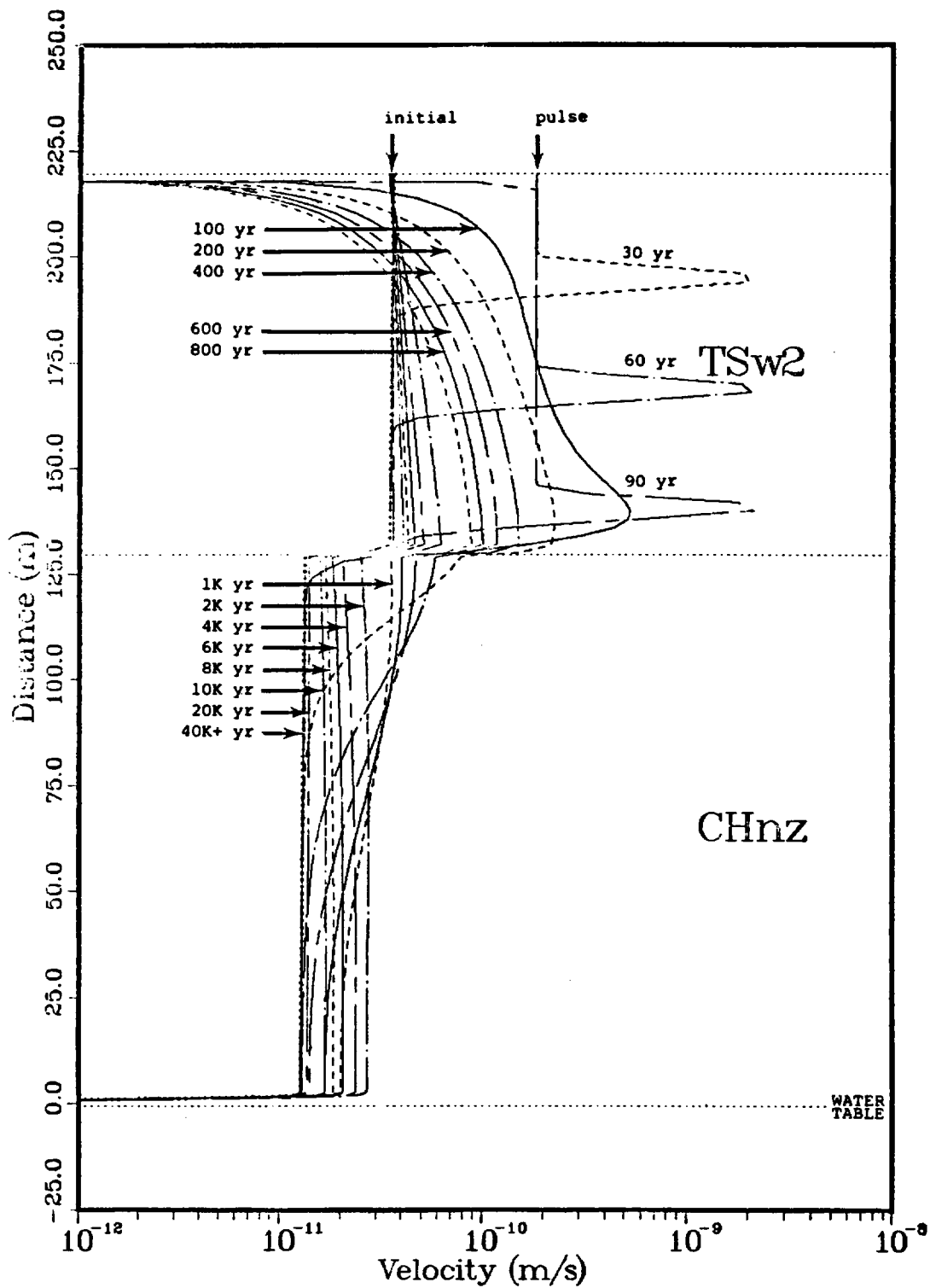


Figure 9. Average linear velocity of groundwater in the matrix vs distance at various times for Analysis Case 2

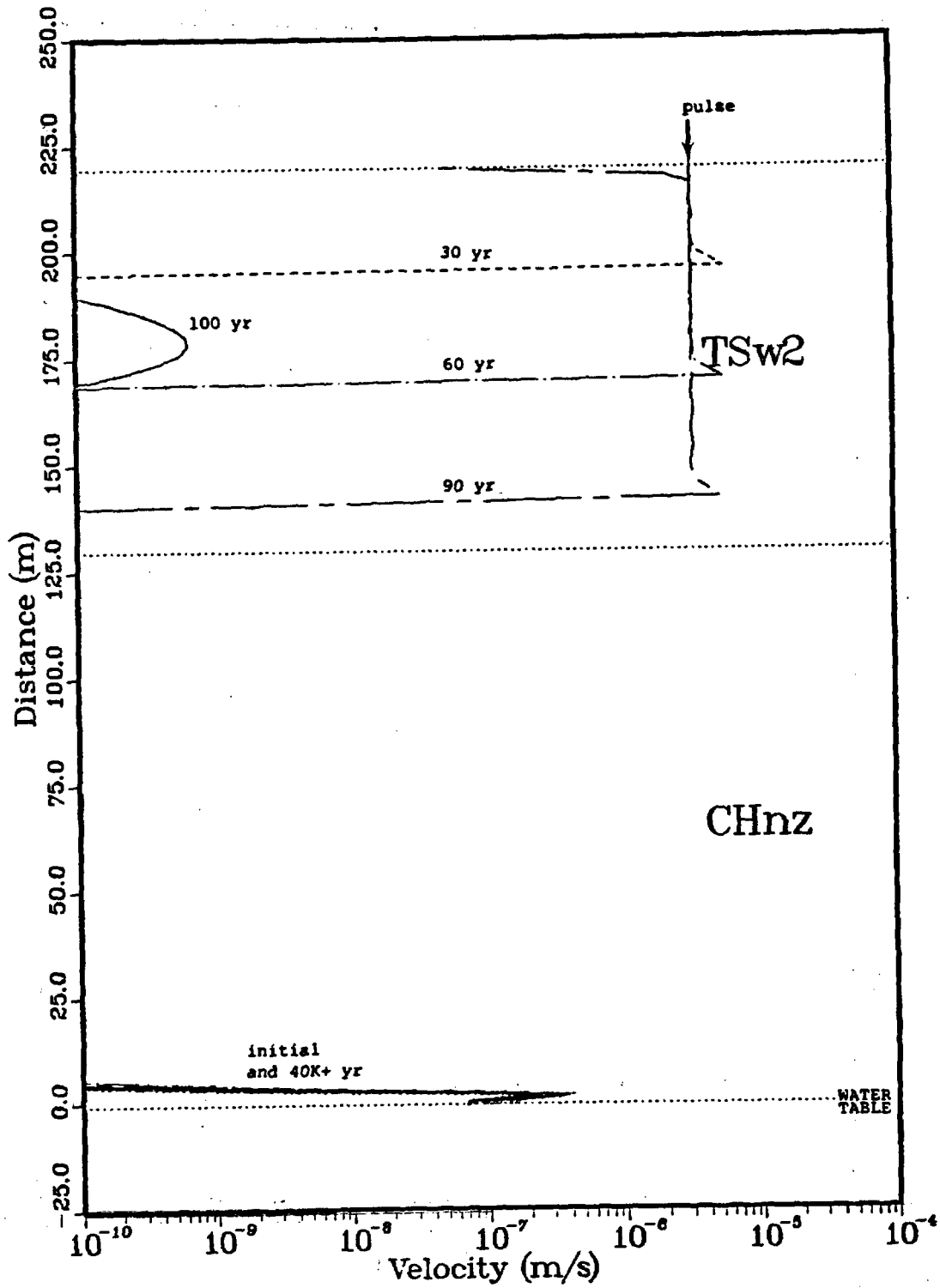


Figure 10. Average linear velocity of groundwater in the fractures vs distance at various times for Analysis Case 1

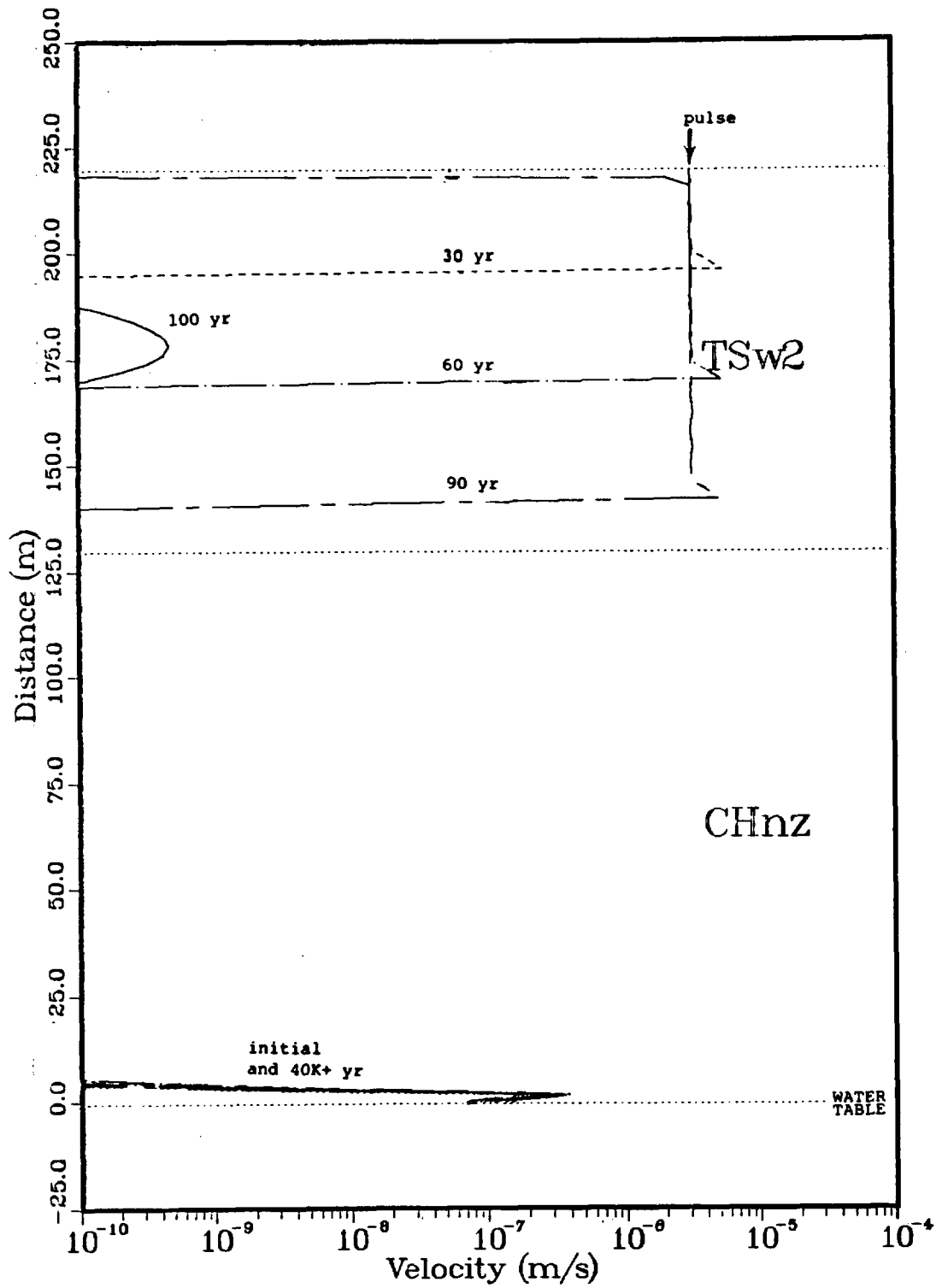


Figure 11. Average linear velocity of Groundwater in the fractures vs distance at various times for Analysis Case 2

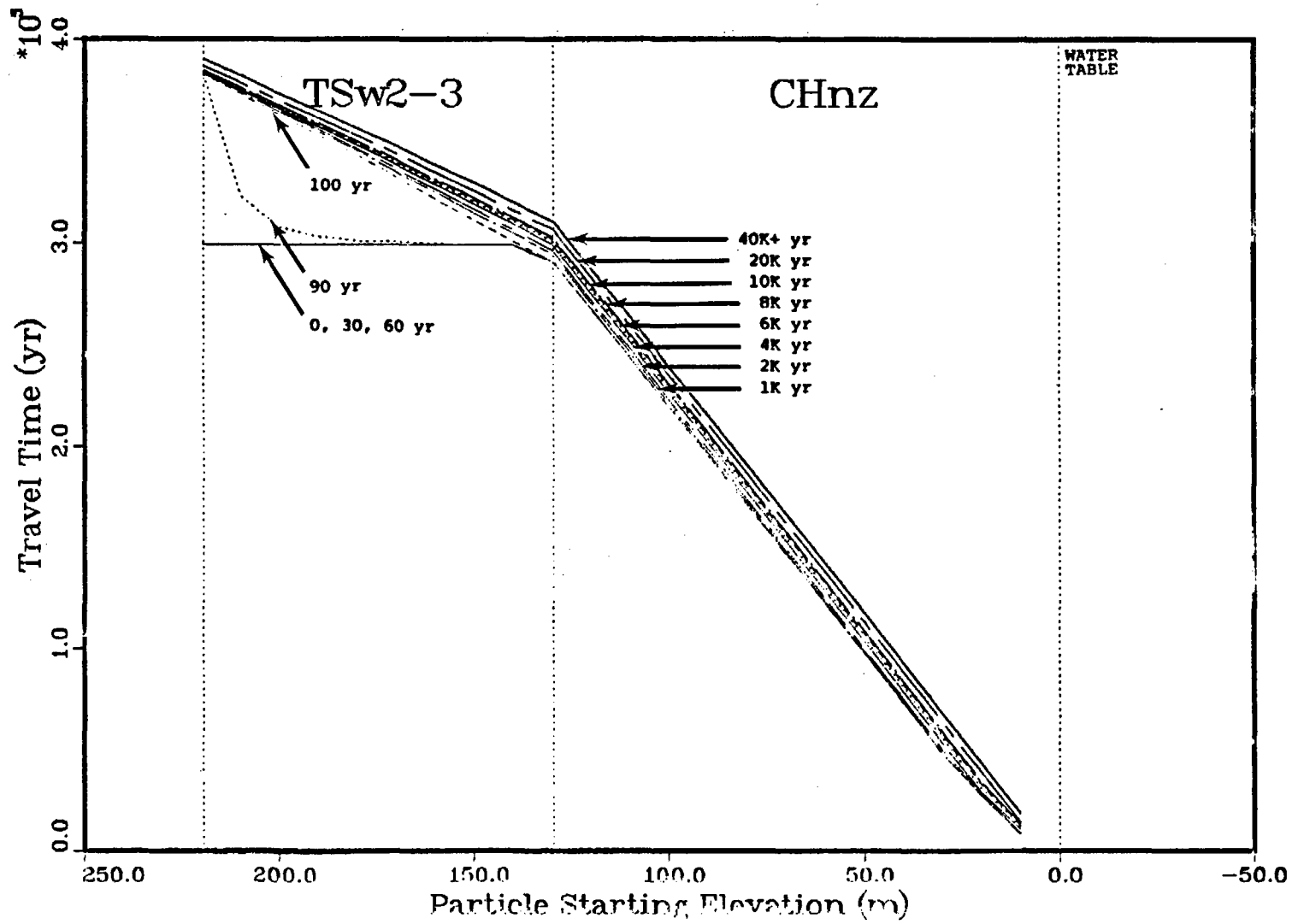


Figure 12. Absolute travel times for Analysis Case 1

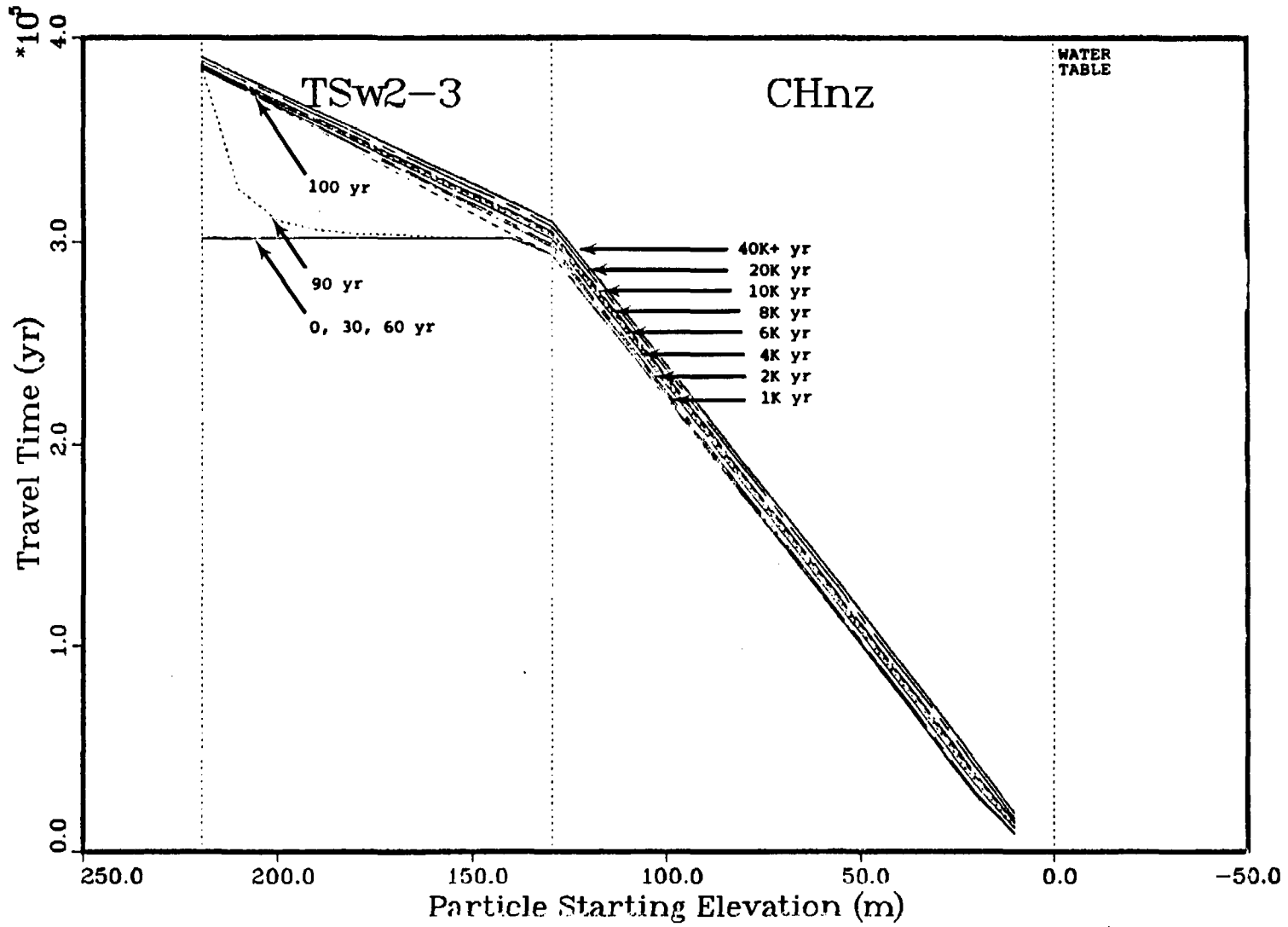


Figure 13. Absolute travel times for Analysis Case 2

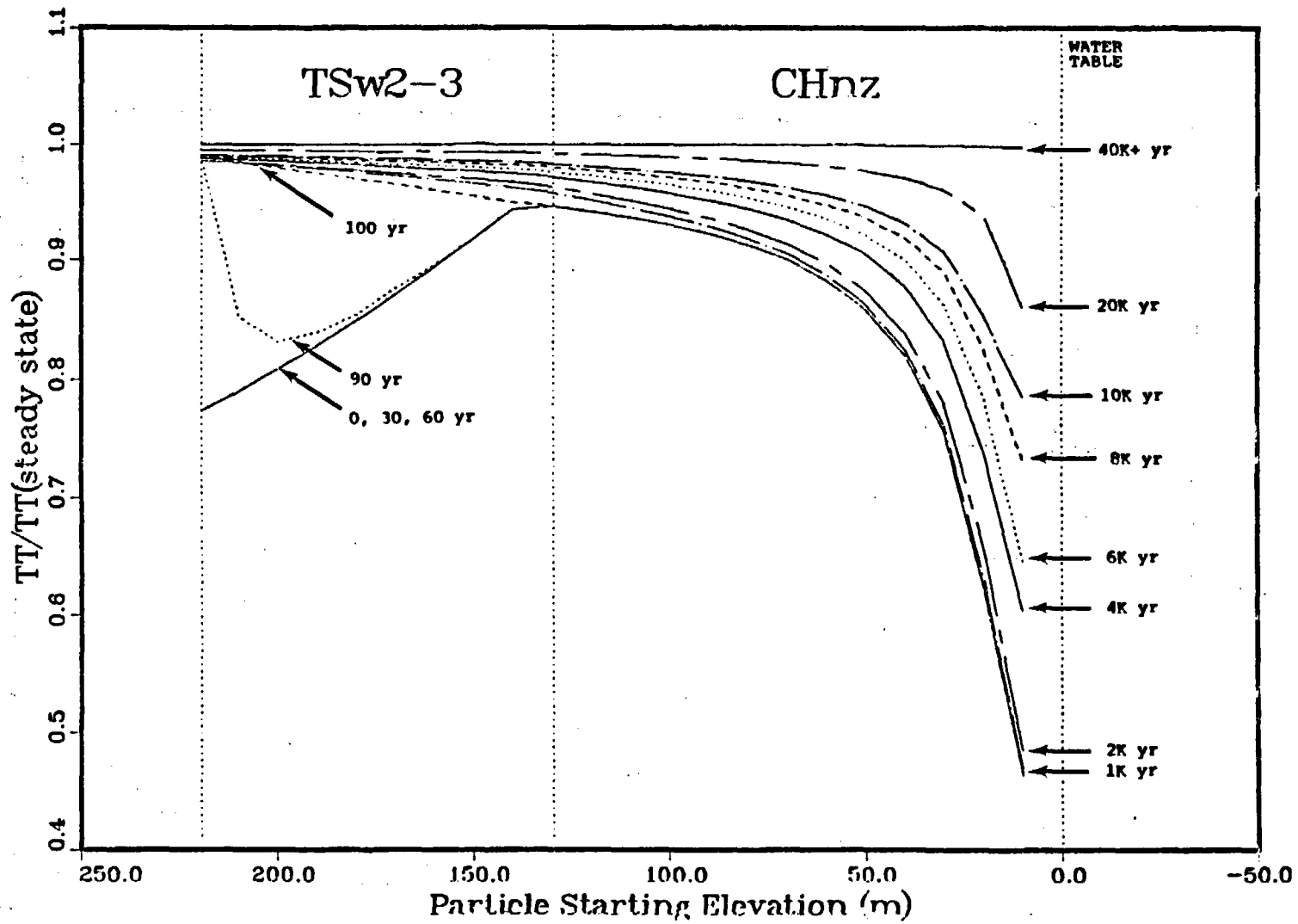


Figure 14. Normalized travel times for Analysis Case 1

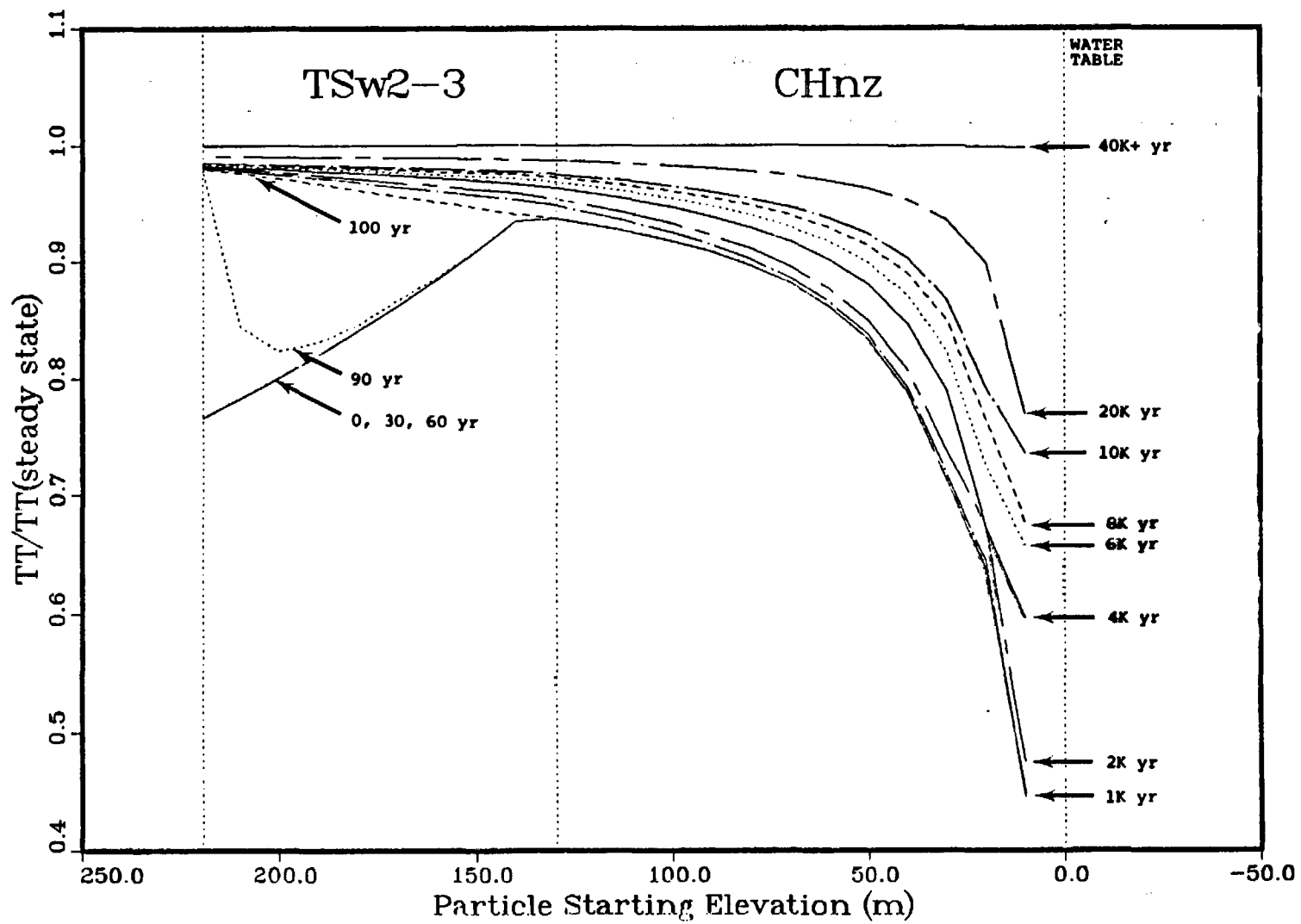


Figure 15. Normalized travel times for Analysis Case 2

MEMORANDUM NO. 4

THE EFFECT OF SEISMIC AND TECTONIC ACTIVITY ON
RADIONUCLIDE CONTAINMENT AT YUCCA MOUNTAIN, NEVADA

Sandia National Laboratories

Albuquerque, New Mexico 87185

date: January 17, 1986

to: F. W. Bingham, 6312

from: R. R. Peters, 6312
J. H. Gauthier, 6312

Ralph F. Peters
Jack Gauthier

subject: The Effect of Seismic and Tectonic Activity on Radionuclide
Containment at Yucca Mountain, Nevada

The short article that follows discusses the probable affect of seismic and tectonic activity on the repository's postclosure containment of radionuclides. It was written in response to a request for input to the Seismic and Tectonic Position paper currently being worked on by DOE/HQ and the projects.

RRP:JHG:6312:mjh

Copy to:

DOE/NVO J. S. Szymanski
6310 T. O. Hunter
6311 L. W. Scully
6311 J. T. Neal
6312 F. W. Bingham
6312 J. H. Gauthier
6312 R. R. Peters
6312 M. S. Tierney
6313 T. E. Blejwas
6313 E. A. Klavetter
6313 B. M. Schwartz (DRMS all FO8)
6314 C. Subramanian
6315 S. Sinnock
6310 10-WBS12144-SNL/NQ

The Effect of Seismic and Tectonic Activity
on Radionuclide Containment at Yucca Mountain, Nevada

I Introduction

The containment of radionuclides at a repository located at the proposed Yucca Mountain site may be affected by seismic and tectonic activity. The NNWSI project is now contributing to a position paper concerned with the affect of seismic and tectonic activity on both the pre-closure and post-closure operation of a repository. In support of this effort, this article will address the effect of seismic and tectonic activity on the transport of radionuclides to the accessible environment. Analyses of radionuclide transport in deep unsaturated zones (DOE, 1984) indicate that radionuclide transport will be primarily by water. Thus, this memo will discuss the transport of radionuclides by water through the unsaturated zone to the water table. It is possible that the water table position may be affected by seismic and tectonic activity but the Draft Environmental Assessment for the Yucca Mountain Site specifically states "...large-scale structures control the ground-water system, and tectonic deformations of a magnitude or scale to affect the regional flow system are not expected" (DOE, 1984, Table 6-31). The focus of this memo will be on the ways seismic and tectonic activity may affect the movement of water in the unsaturated zone.

There appear to be two general regions where seismic and tectonic activity could affect the proposed site and its ability to contain radionuclides.

- 1) The first region is the rock mass adjacent to the fault zone. In this region the primary affect would be on the fracture density and aperture. The changes in these parameters would depend on the rock type (e.g. densely welded tuff would fracture more than the bedded, zeolitized tuffs) and the proximity to the fault zone. The consequence could be that the general flow pattern throughout the block is altered in a manner that increases the velocity of downward water movement and thus the rate at which radionuclides are transported to the water table.

2) The second region is the localized area where fault motion would occur. The primary affects of fault motion on the fault region would be additional displacement of the rock mass on one side of the fault relative to that on the other side of the fault, and changes in the fracture density and aperture. Waste package breakage, changes in fracture hydrologic properties, and surface affects such as landslides could occur in this region. The consequences of waste package breakage would be that the radionuclides would be available for transport sooner than expected. The consequence of changes in fracture properties could be that the velocity of water movement in some localized area is significantly increased to increase the rate at which radionuclides are transported to the water table. The consequence of changes in the local surface topography could be that the local infiltration rate is increased due to ponding of arroyos and so the amount of water moving downward and the velocity of water movement downward is increased.

It has been stated on a number of occasions by USGS personnel (e.g., Robert E. Wallace on 7/23/85 at the Seismic/Tectonic meeting in Las Vegas, NV) that significant fault movement (1 m or so) most likely will occur on pre-existing faults that are readily identifiable both above and below ground. Thus, it would seem reasonable that the problem of waste package breakage as a result of fault movement could be reduced or possibly eliminated by not placing any waste packages in those areas which appear to be in or immediately adjacent to a large fault zone. The remaining affects of seismic and tectonic activity on radionuclide transport then could result from (1) changes in the flow field resulting from changes in the fracture properties, and (2) changes in the local infiltration resulting from changes in surface topography. In order to estimate the affect of seismic and tectonic activity on the flow field a model of flow in a fractured, porous medium must be adopted.

The following sections contain a discussion of the model used to estimate that affect of seismic and tectonic activity on the flow field and a discussion of the estimates made by the model.

II Hydrologic Model

The modeling of water flow in unsaturated, fractured porous media has recently received attention (e.g., Montazer and Wilson, 1984; Klavetter and Peters, In prep.). The model developed by Klavetter and Peters will be used to investigate the affect of seismic and tectonic activity on both the general and local flow field. This model is a continuum model which lumps the fractures and the porous medium into a "composite medium" for the purpose of calculating the pressure field in the medium. Two major assumptions that allow this lumping are:

- 1) The fracture aperture is less than several millimeters. This assumption allows capillary bundle theory to be applied. Reports by a variety of authors (Sinnock et al., 1984; Peters et al., 1984) suggest that the fracture aperture at Yucca Mountain is 0.1 millimeters or less.
- 2) The flow field is changing relatively slowly allowing the pressure head in the fractures and the matrix to be equal in a direction perpendicular to the flow lines in the composite medium. A discussion of this assumption may be found in the paper by Klavetter and Peters (In prep.).

The paper by Klavetter and Peters (In prep.) contains a complete discussion of the derivation of the equations listed below. The governing equation for steady-state flow in the composite medium follows.

$$-[\bar{K}_{m,b} + \bar{K}_{f,b}] \cdot \nabla(\psi + z) = \bar{q}_m + \bar{q}_f = \bar{q}_{total} \quad \text{Eq. 1}$$

This equation allows the pressure-head field (ψ) in the composite medium to be calculated with the boundary conditions and material properties specified.

The average linear velocity of water in the matrix (V_m) and the fractures (V_f) may be calculated using the following equations along with the pressure-head field solution and material properties.

$$\bar{V}_m = \bar{q}_m / [n_m(S_m - S_{m,r})] = -\bar{K}_{m,b} \cdot \nabla(\psi + z) / [n_m(S_m - S_{m,r})] \quad \text{Eq. 2}$$

$$\bar{V}_f = \bar{q}_f / [n_f(S_f - S_{f,r})] = -\bar{K}_{f,b} \cdot \nabla(\psi + z) / [n_f(S_f - S_{f,r})] \quad \text{Eq. 3}$$

The variables used in the above equations are defined below.

ψ - the pressure head

\bar{K} - the conductivity. The conductivity is usually expressed as the saturated conductivity (K_{sat}) times the relative conductivity (K_{rel}) which is a function of the pressure head and the material. It ranges from unity at a pressure head of zero or greater to zero at large negative pressure heads.

n - the porosity

\bar{q} - water flow per unit area or specific discharge

S - saturation, a function of ψ

z - vertical position

The subscripts "m" and "f" refer to the matrix and fractures respectively. The subscripts "m,b" and "f,b" refer to bulk properties of the matrix and the fractures. The subscripts "m,r" and "f,r" refer to the residual saturation of the matrix and fractures.

III Conceptual Hydrologic System at Yucca Mountain

The conceptual hydrologic system at Yucca Mountain is discussed in a variety of documents (DOE, 1984; Klavetter and Peters, In prep.; Montazer and Wilson, 1984) and will not be repeated here. The major point of these discussions is that the matrix is partially saturated and thus the percolation rate downward through Yucca Mountain is less than the saturated conductivity of the matrix. A value quoted as an upper bound for the repository horizon and below is 0.5 mm/year (DOE, 1984). Bill Wilson of the USGS has recently proposed that the maximum flux below the repository horizon is 0.2 mm/yr (Wilson, 1985).

IV Effect of Seismic and Tectonic Activity on the Flow Field within the Repository Block

In order for seismic and tectonic activity to affect the velocity of water movement in Yucca Mountain it must affect the hydrologic properties in the flow equation (either Eq. 1 or 2) or the boundary conditions. It is thought that neither the average infiltration rate of water at the surface of Yucca Mountain nor the position of the water table will be affected by seismic or tectonic activity. (The affect of seismic and tectonic activity on the local infiltration rate and the local flow field will be discussed in a later section.) Therefore, seismic and tectonic activity can only affect the flow field by affecting the values of hydrologic properties in the flow equation. The only parameters that may be affected are those associated with the fractures (e.g., S_f and $K_{f,b}$) which would change as a result of changes in the fracture density and aperture. Eq. 1 can be used to examine the long-term response of the flow field to changes caused by seismic and tectonic activity. The only independent parameter in this equation that will change is the bulk fracture conductivity ($\bar{K}_{f,b}$) which may change the pressure-head field (ψ) and thus the amount of water in the fracture system and the matrix (\bar{q}_f and \bar{q}_m) and the velocity of water in the matrix and fracture system (\bar{V}_m and \bar{V}_f).

There is currently a fairly large body of information available on the saturated conductivity of fractures, however, there is little data concerning the unsaturated behavior of fractures. There are a number of articles speculating on the behavior of flow in unsaturated fractures (Wang and Narasimhan, 1985; Klavetter and Peters, In prep.; and Montazer and Wilson, 1984). These articles model the fracture conductivity as a function of the fracture aperture distribution and the fracture saturation. The fracture saturation is itself a function of the pressure head and the fracture aperture distribution. The major point in these articles is that a continuous path in the fracture must be saturated in order for the fracture to have a non-zero conductivity along the plane of the fracture. If the surrounding matrix is only partially saturated, then in order to obtain this saturated path the fracture aperture along the path must be the same size as the maximum size of the nearby saturated pores. The average pore size in the tuffs that have low matrix conductivities is very small (of the order of 0.00003 millimeters or less according to Peters et al. (1984)) compared to that of the fracture aperture (of the order of 0.1 to 0.01 millimeters according to Peters et al. (1984)). Therefore, it is reasonable to assume that the fractures are currently "dry" and seismic activity which opens the fractures will further decrease the ability of the fractures to carry water at the conditions observed at Yucca Mountain. Data concerning average fracture aperture as a function of confining stress (Peters et al., 1984) indicate that it is not reasonable to suppose that the fracture aperture can be closed sufficiently by seismic and tectonic forces so that saturated pathways can occur in the fractures under conditions that are now present at Yucca Mountain (i.e., fracture apertures that are now of the order of 0.1 millimeters cannot be closed to 0.00003 millimeters if the stress increases by a factor of ten from the current values). Finally, if the the aperture could be decreased so that the fracture system could carry water then the flow in the fracture system would be very small; in fact the characteristics of flow in the fracture system would be very similar to that in the matrix. Thus, it appears that seismic and tectonic activity cannot affect the fractures in a manner that will allow them to carry water in regions where the matrix is only partially saturated. Therefore, it is reasonable to assume that seismic and tectonic activity cannot affect the movement radionuclides downward to the water table.

VI Effect of Seismic and Tectonic Activity on Infiltration

There appears a possibility that seismic and tectonic activity could affect the surface causing landslides. These landslides could, in turn, dam an arroyo allowing ponding to occur as a result of severe storms. This scenario is one that has caused some discussion and thus a bounding calculation has been performed. The Draft Environmental Assessment states that there is no evidence of ponding occurring at Yucca Mountain (DOE, 1984).

The situation modeled was that of injecting a 10 m slug of water into a fault zone. A reasonable depth for a pond was thought to be 10 m. If ponds of this depth (and consequently size) have existed at Yucca Mountain in the recent past then there should be evidence of them. The Draft Environmental Assessment (DOE, 1984) states that there is no evidence for damming of arroyos. Therefore, a 10 m deep pond represents a reasonable upper limit and this was assumed to be the height of the slug injected into the fault zone.

The calculation was performed by TOSPAC (Dudley et al., In prep.), which is a one-dimensional systems performance assessment code. The values of flux, velocity, and penetration distance of the slug of water in the fault zone calculated by TOSPAC are upper bounds because the one-dimensional code does not allow for seepage of water out of the fault zone into the surrounding rock (e.g., out of the fault zone into the highly conductive Paintbrush Tuff nonwelded unit which is above the repository horizon). The one-dimensional column used in the calculations is shown in Figure 1. It is based on the stratigraphy found at well USW G-4 (Ortiz et al., 1985). The units in order of decreasing depth are: (1) the Tiva Canyon welded unit (TCw), (2) the Paintbrush Tuff nonwelded unit (PTn), (3) the upper lithophysal rich zone of the Topopah Spring welded unit (TSw1), (4) the lower lithophysal poor zone of the Topopah Spring welded unit (TSw2-3) - the proposed repository unit, and (5) the zeolitized Calico Hills nonwelded unit (CHnz). Unit PTn has a high matrix conductivity (about 10,000 mm/yr) while the rest of the units have matrix conductivities of about 1 mm/yr. The hydrologic data for the calculations are very similar to those used in the paper by Peters, Gauthier, and Dudley (In prep.). The only change made to the hydrologic data was to increase the saturated conductivity of each unit's fracture system by a factor of ten-thousand to represent the increase in fracture conductivity due to

changes in fracture density, etc. found in a fault zone. The saturated conductivity of the uppermost unit is such that a slug of water 10 m tall will infiltrate the surface in a little over 2 days. The hydrologic data used for these calculations are listed in Table 1. The initial pressure-head distribution was specified by a constant flux through the mountain of 0.1 mm/yr and the position of the water table at the bottom of the column. The percolation rate of 0.1 mm/yr lies within the range thought applicable for Yucca Mountain (DOE, 1984).

The results of the calculation are shown in Figures 2-5. Figure 2 shows the water flux versus distance above the water table for times ranging from 1 day after initiating injection to 200,000 years after initiating injection. Figure 3 shows the matrix saturation profiles for the same times as in Figure 2. Figures 4 and 5 show the velocity of water in the matrix and fracture system versus distance. The injection of the 10 m slug occurred over a period of 2.2 days. At that point in time the slug of water had traveled through unit TCw and about two-thirds of the way through unit PTn. According to Figure 3 the upper two-thirds of PTn is saturated and, according to Figures 4 and 5, there are high velocities throughout the region containing the slug of water.

After the injection of water at the surface is cut off (2.2 days) the water starts to redistribute itself in response to gravity and pressure-head gradients. The water flows fairly quickly to the bottom of PTn (see the 1 month and 1 year profiles in Figure 3). Because there is not enough water to saturate the bottom of unit PTn the water movement in the next unit (TSw1) is limited to the matrix (see Figures 4 and 5). The 100 yr through 200,000 profiles in Figure 3 indicate unit PTn is slowly drained by the lower units. Figure 2 shows the flux profile approaches the initial condition after approximately 200,000 years. The flux pulse resulting from the injection of the 10 m slug of water does not reach the water table until almost 10,000 years have passed.

Figure 4 indicates the water velocity in the matrix in the units below PTn is within a factor of 5 of the initial water velocity. For most of the simulation the water velocity is within a factor of 2. Thus, a particle of water injected into the surface at the start of a simulation has a travel time from the ground surface to the water table that is approximately the same as that of a water particle traveling the same distance with a steady flux of 0.1 mm/yr. The total travel time for the latter case is about 600,000 years with most of the time spent in the two lowermost units (Peters, Gauthier, and Dudley, In prep.) which are least affected by the water slug. We may conclude that radionuclide transport and travel times are not significantly influenced by the injection of a 10 m slug of water into a fault zone. It would require a slug of water approximately 15 m tall to initiate water movement in the fractures of unit TSw. Water movement in the fractures would quickly stop as soon as the bottom of PTn became unsaturated. Additional water would be required to maintain saturation in all units above the water pulse. This model indicates that in order for water movement to occur in the fractures throughout the fault zone, the fault zone would have to be saturated from the surface to the water table. The height of a slug of water require to saturate the entire fault zone can be estimated using the porosity of each unit and its initial saturation. The calculation estimates that the slug of water would have to be about 20 m tall.

This analysis assumes that there is no leakage out of the fault zone into the surrounding rock while, in fact, there may be significant leakage all along the fault zone. The results should only be used to indicate that ponding of water above a fault zone may not have significant affect on water travel times and radionuclide transport times locally. The affect of ponding on the flow field throughout the block would appear to be insignificant.

VII Summary

It appears that seismic and tectonic activity cannot affect the fractures in a manner that will allow them to carry water in regions where the matrix is only partially saturated. Therefore, it is reasonable to assume that seismic and tectonic activity alone cannot affect the movement radionuclides downward to the water table.

A scenario that has been discussed is that of damming an arroyo and then filling the reservoir with a large flood. A bounding calculation indicates that reasonable assumptions concerning the amount of water injected into the fault zone result in no significant consequence.

These topics will continue to be addressed as a part of the ongoing performance assessment effort. The positions taken in this memo are based on information and models currently available. They are subject to change as new data and the results of future calculations become available.

References:

DOE. 1984. "Draft Environmental Assessment - Yucca Mountain Site, Nevada Research and Development Area, Nevada," U.S. Department of Energy, Washington, D.C.

Dudley, A. L., R. R. Peters, M. S. Tierney, E. A. Klavetter, J. H. Gauthier, and M. Wilson. In preparation. "Total Systems Performance Assessment Code (TOSPAC) Volume 1: Physical and Mathematical Bases," SAND85-0002, Sandia National Laboratories, Albuquerque, NM.

Klavetter, E. A., and R. R. Peters. In prep.. "Estimation of Hydrologic Properties for an Unsaturated, Fractured Rock Mass," SAND84-2642, Sandia National Laboratories, Albuquerque, NM.

Montazer, P., and W. E. Wilson. 1984. "Conceptual Hydrologic Model of Flow in the Unsaturated Zone, Yucca Mountain, Nevada," Water-Resources Investigations Report 84-4345, U.S. Geological Survey, Denver, CO.

Ortiz, T. S., R. L. Williams, F. B. Nimick, B. C. Whittet, and D. L. South. 1985. "A three-dimensional model of the thermal-mechanical units at Yucca Mountain, Southern Nevada," SAND84-1076, Sandia National Laboratories, Albuquerque, NM.

Peters, R. R., J. H. Gauthier and A. L. Dudley. In preparation. "The Effect of Percolation Rate on Water Travel Time in Deep Partially Saturated Zones," Proceedings of Symposium on Groundwater Flow and Transport Modeling, May 20-21, 1985, Albuquerque, NM.

Peters, R. R., E. A. Klavetter, I. J. Hall, S. C. Blair, P. R. Heller, and G. W. Gee. 1984. "Fracture and Matrix Hydrologic Characteristics of Tuffaceous Materials from Yucca Mountain, Nye County, Nevada," SAND84-1471, Sandia National Laboratories, Albuquerque, NM.

Sinnock, S., Y. T. Lin, and J. P. Brannen. 1984. "Preliminary Bounds on the Expected Postclosure Performance of the Yucca Mountain Repository Site, Southern Nevada," SAND84-1492, Sandia National Laboratories, Albuquerque, NM.

Wang, J. S. Y., and T. N. Narasimhan. 1985. "Hydrologic Mechanisms Governing Fluid Flow in Partially Saturated, Fractured, Porous Tuff at Yucca Mountain," SAND84-7202, Sandia National Laboratories, Albuquerque, NM.

Wilson, W. E. 1985. "Rationale for Flux Estimates and Flow Pathways Used in Travel Time Calculations," Personal Communication.

Table 1 Unsaturated zone, hydrologic unit properties

Matrix Properties [a]

Unit	Sample Code	Grain Density (g/cm ³)	Porosity (n)	Hydraulic Conductivity (m/s) [b]	S _r	Alpha (1/m)	Beta
TCw	G4-1	2.49	0.08	9.7E-12	0.002	0.821E-02	1.558
PTn	GU3-7	2.35	0.40	3.9E-07	0.100	1.50 E-02	6.872
TSw1	G4-6	2.58	0.11	1.9E-11	0.080	0.567E-02	1.798
TSw2-3	G4-6	2.58	0.11	1.9E-11	0.080	0.567E-02	1.798
CHnz	G4-11	2.23	0.28	2.0E-11	0.110	0.308E-02	1.602

Fracture Properties [c]

Unit	Sample Code	Horizontal Stress [d] (bars)	Fracture Aperture (microns)	Fracture Conductivity (m/s)	Fracture Density ₃ [e] (No./m ³)	Fracture Porosity [f]	Fracture Compressibility (1/m)	Bulk Frac. Conductivity (m/s) [g]
TCw	G4-2F	1.1	67.4	3.8E-3	200	14. E-3	132. E-8	5.3 E-5
PTn	G4-3F	3.3	270.	61. E-3	10	2.7E-3	19. E-8	16. E-5
TSw1	G4-2F	9.5	51.3	2.2E-3	80	4.1E-3	5.6E-8	0.90E-5
TSw2-3	G4-2F	21.9	45.5	1.7E-3	400	18. E-3	12. E-8	3.1 E-5
CHnz	G4-4F	34.3	15.5	20. E-3	30	4.6E-3	2.8E-8	9.2 E-5

Fracture saturation coefficients are S_r = 0.0395, Alpha = 1.2851/m, Beta = 4.23

Unit	TCw	PTn	TSw1	TSw2-3	CHnz
Coefficient of consolidation (1.E-7/m) [h] (α' _{BULK})	6.2	82.	12.	5.8	26.

The compressibility of water (β'_w) is 9.8E-7/m

This table is based on information in the report by Peters, Gauthier and Dudley (In prep.).
The full references for the following footnotes may be found in that document.

- Notes: a) All matrix data in this section are from Peters et al. (1984).
 b) The matrix saturated conductivity and the bulk matrix saturated conductivity (K_{fb}) are essentially the same because the factor that converts the matrix value to the bulk matrix value (1-n_f) is nearly equal to 1.0
 c) Unless noted otherwise, this fracture information is from Peters et al.(1984).
 d) Horizontal stress assumed to be one-third the overburden weight, evaluated at average unit depth in USW G-4.
 e) Based on the report by Scott et al.(1983).
 f) Calculated as fracture volume (aperture times 1 square meter) times number of fractures per cubic meter.
 g) This value of "K_{fb}" was obtained by multiplying the fracture conductivity by the fracture porosity.
 h) Based on the report by Nimick et al.(1984).

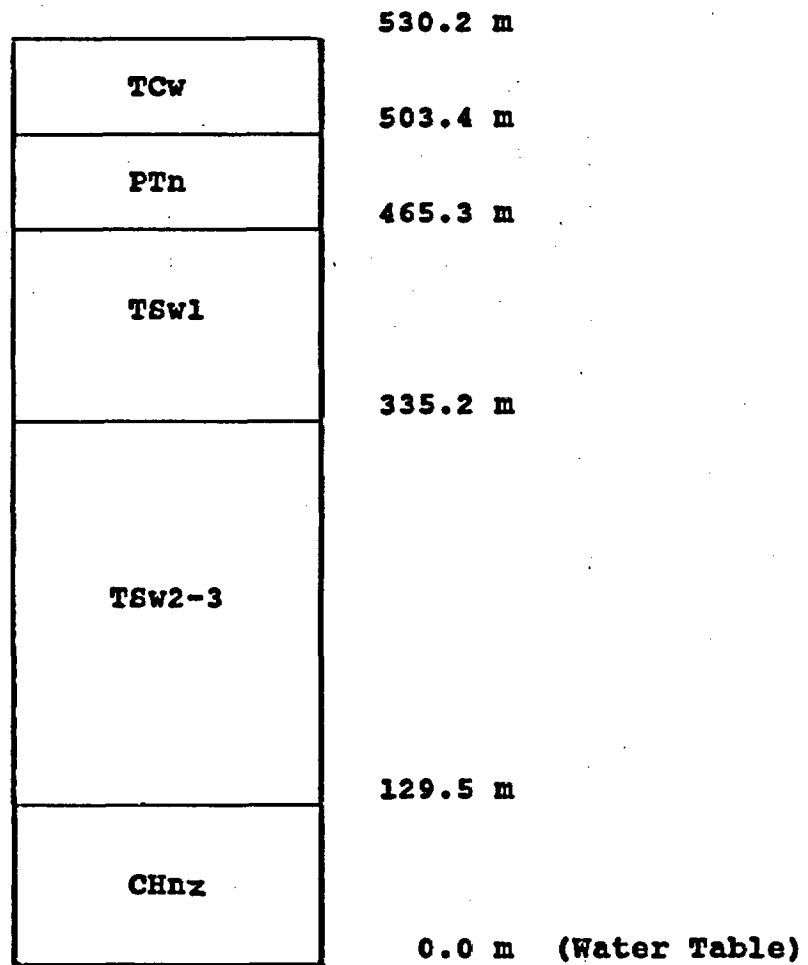


Figure 1 One-dimensional column used in calculations

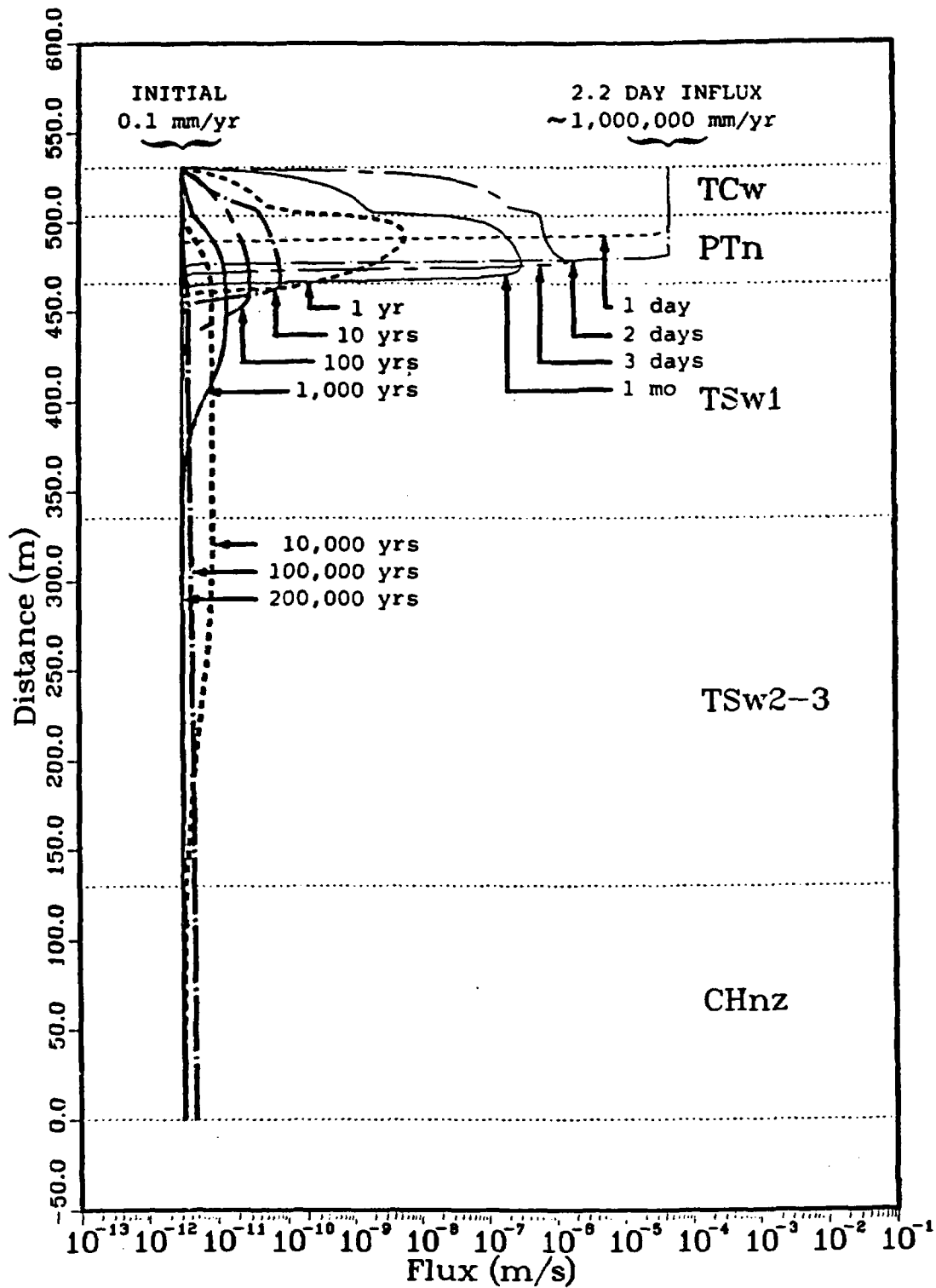


Figure 2. Water Flux Profiles

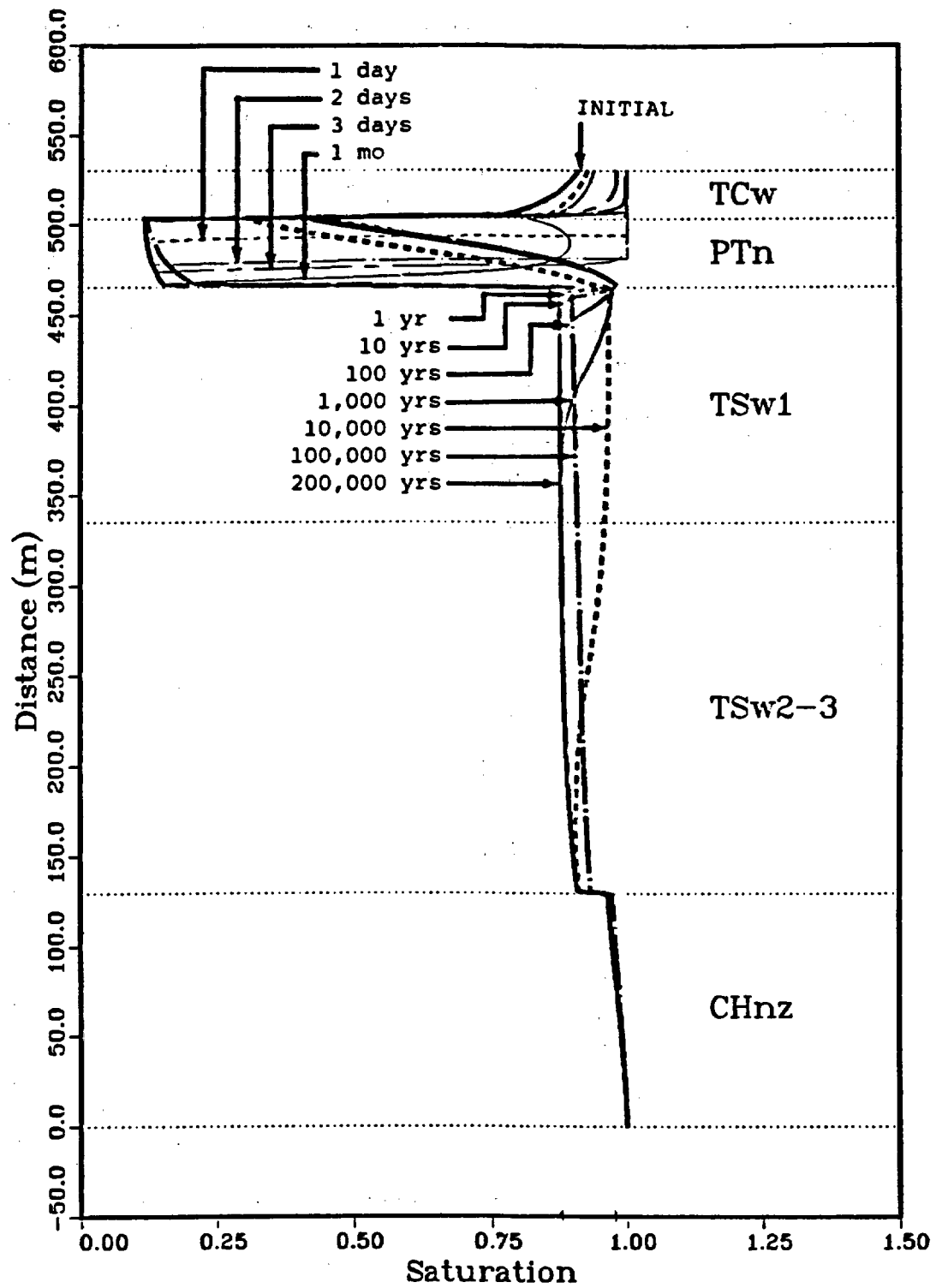


Figure 3. Saturation Profiles

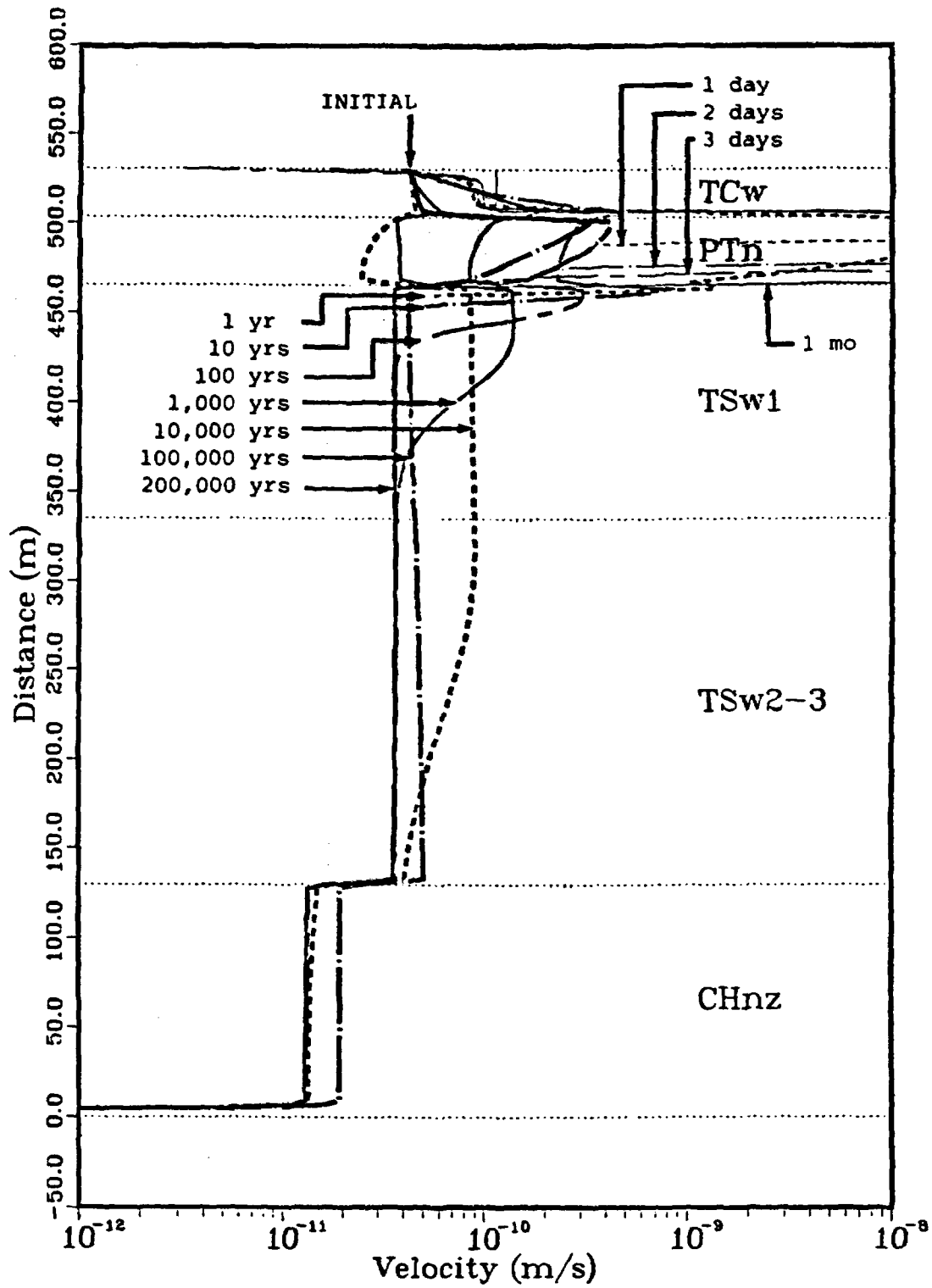


Figure 4. Profiles of Water Velocity in the Matrix

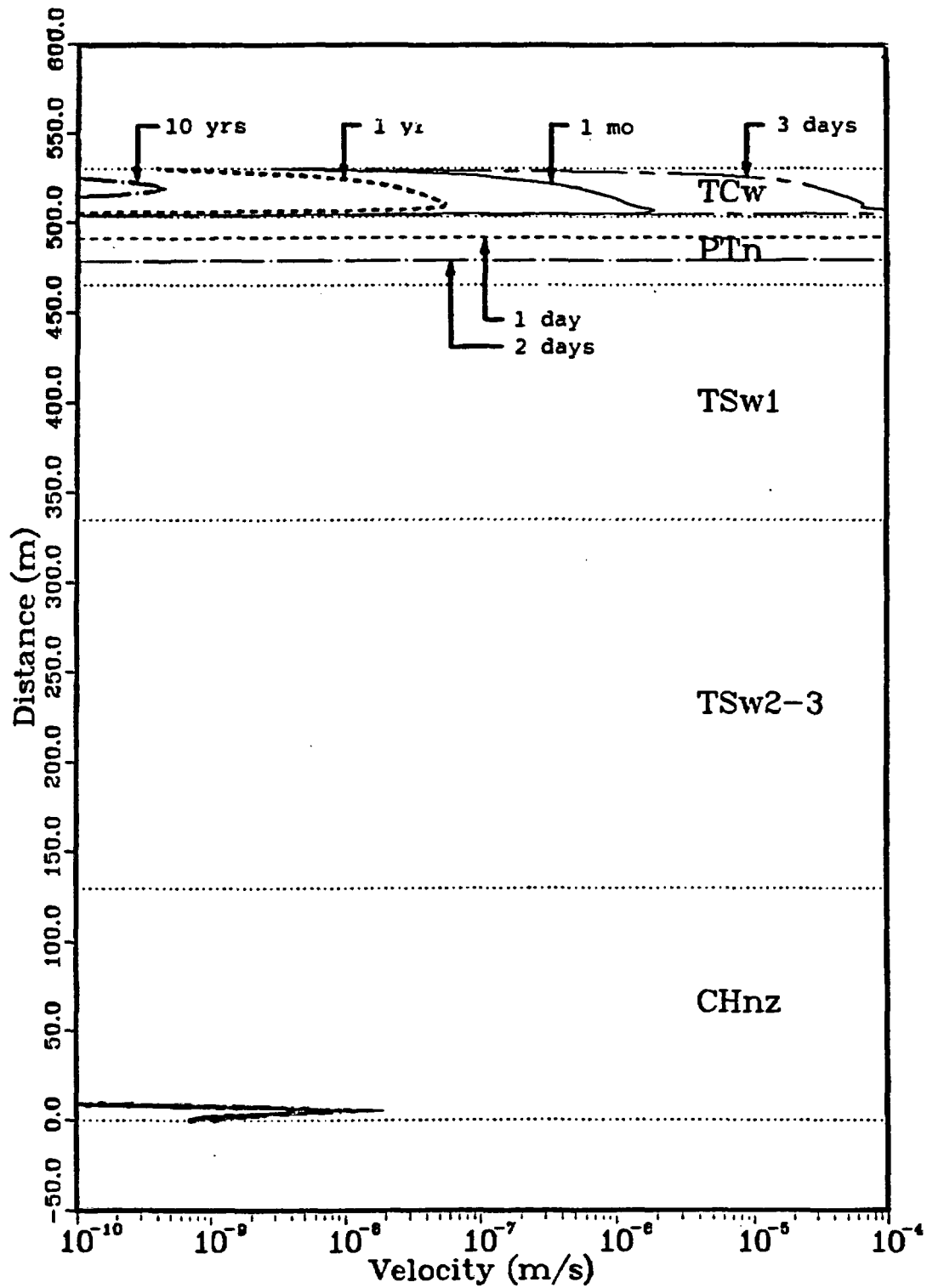


Figure 5. Profiles of Water Velocity in the Fracture System

MEMORANDUM NO. 5

NNWSI HYDROLOGIC ANALYSIS NO. 72-26
A 1-DIMENSIONAL CALCULATION INVESTIGATING
WATER-TABLE FLUCTUATION AT YUCCA MOUNTAIN

Date: 31 October 1988

To: George Barr, 6312
Ralph Peters, 6312

From: Jack Gauthier, 6312

Subject: NNWSI Hydrologic Analysis 72-26,
"A 1-Dimensional Calculation Investigating
Water-Table Fluctuation at Yucca Mountain"

NNWSI Hydrologic Analysis 72-26, as defined by the Problem Definition Memo (PDM) dated 13 October 1988, from George Barr and Ralph Peters to Jack Gauthier, has been completed and the final report is attached to this memo.

The problem examines the time necessary for the Yucca-Mountain-hydrologic system to return to its presently assumed state after a major fluctuation in the water-table level. The results of the simulation show noticeable deviation from a steady-state flow of 0.1 mm/yr for approximately 50,000 years after the water table subsides.

Copy with Attachment to:

6310 T. O. Hunter
6312 F. W. Bingham
6312 M. S. Tierney
6312 A. C. Peterson
6312 A. L. Dudley
6312 J. H. Gauthier
6313 E. A. Klavetter
6310 10/12144/SNL/QIII
6310 72/12144/26/QIII

Copy without Attachment to:

6311 A. L. Stevens
6313 T. E. Blejwas
6314 J. R. Tillerson
6315 L. E. Shephard
6316 R. P. Sandoval
6310 NNWSI CF

Yucca Mountain Project
Hydrologic Analysis 72-26
31 October 1988
Quality Assurance Level 3
Work Breakdown Structure (WBS) No. 1.2.1.4.4
Case Number 1561.240

Principal Investigators: George Barr (6312)
Ralph Peters (6312)
Analyst: Jack Gauthier (6312)

**A 1-Dimensional Calculation Investigating
Water-Table Fluctuation at Yucca Mountain**

Introduction

Yucca Mountain, Nevada is being considered for the site of a high-level-radioactive-waste repository. It is located in the Great Basin of the United States, where in the past tectonic forces have caused fault movement and concomitant volcanic activity.

Szymanski (1987) has postulated that tectonic forces have caused, and continue to cause, fluctuations in the water-table level at Yucca Mountain. Because water pathways are considered to be a major avenue for the release radioactive contaminants, a rise in the water table could have significant implications for the performance of the repository.

A simulation problem has been defined to investigate the response of Yucca Mountain to large changes in the water-table level. The object of the simulation is to estimate the drain-back time to the present hydrologic state. This information can aid in deciding if such an event could have happened in the recent past.

Problem Statement

The problem involves the aftermath of a water-table rise at Yucca Mountain. Ground-water is assumed to be in a steady-state flow of 0.1 mm/yr through a 1-dimensional, vertical column of materials representative of Yucca Mountain. A tectonic event causes a significant rise in the water table, i.e., the water table rises to some level above the proposed-repository horizon, for a period of time sufficient to saturate the rock matrix.

The water table then subsides suddenly to its original position. The flow relaxes to another 0.1 mm/yr steady state. We are interested in the time of this relaxation.

The problem is divided into 2 cases:

- 1) the water table has risen to the top of the geologic unit proposed to contain the repository (TSw2), and
- 2) the water table has risen to the surface.

The first case provides a rough lower bound on the relaxation time; the second case provides a rough upper bound. The difference between the 2 drain-back times indicates the sensitivity of the results to the assumption of how high the water-table rises.

Computer Program

The computer program TOSPAC (Dudley et al., 1988) was used to solve this problem. TOSPAC simulates 1-dimensional groundwater flow with the transport of radioactive contaminants in partially-saturated, fractured media. TOSPAC uses the finite difference method to solve both the highly-nonlinear differential equations for groundwater flow (Darcy's law and Richards' equation) and the linear differential equation for contaminant transport (a generalized advective-dispersive equation).

Appendix A contains the input data files for TOSPAC used in the Case 1 and Case 2 calculations, respectively. These files reproduce the information discussed in the Problem Geometry, Material Properties, Initial Condition, and Boundary Condition sections, following. See Gauthier, et al. (in preparation) for more information.

TOSPAC was developed at Sandia National Laboratories (SNL) for the Yucca Mountain Project (YMP).

Problem Geometry

The problem applies to a 1-dimensional, vertical column, with geologic units and geologic-unit thicknesses as found at drill hole USW G-4 at Yucca Mountain (Ortiz et al., 1985). These data are not contained in the SNL Reference Information Base for the YMP.

Figure 1 presents a layout of the problem geometry. The left-hand column is a schematic of the calculational mesh used by TOSPAC. The right-hand column shows the matrix and fracture materials assigned to each geologic unit.

The mesh for the calculation is the same as that used in Dudley, et al. (1988). Based on the formula given in this report for calculating the mesh-point spacing, this mesh is adequate for Case 1 and all but the first year of Case 2. At the beginning of the Case 2 calculation, when the water in unit PTn tries to drain into TSw1, the length scale is on the order of a few millimeters. A spacing this fine would require too many mesh points—approximately 100,000. However an error of a year turns out not to be significant in this problem. Thus the same calculational mesh is used for both cases.

Hydrologic Properties

Hydrologic properties for the unsaturated column are taken from representative properties for each geologic unit as defined in Dudley et al. (1988). These properties define saturation *versus* pressure head and hydraulic conductivity *versus* pressure head characteristic curves in the method given by van Genuchten (1980).

Table 1 contains the hydrologic properties used in the analysis. The hydrologic properties for fractures are included in the SNL Reference Information Base for the YMP with candidate status (Chapter 1, Section 1, Subsection 4, Item 3). The matrix hydrologic properties are not contained in the Reference Information Base.

Initial Condition (Case 1)

The initial hydrologic flow for the first case of the problem is defined in 2 parts:

- 1) The upper geologic units—TCw, PTn, and TSw1—have a steady-state flow of 0.1 mm/yr with the water table placed in its present position, at the bottom of geologic unit CHnz.
- 2) The lower geologic units—TSw2 and CHnz—have an arbitrary pressure head of -1 m assigned to every mesh point.

This initial condition represents Yucca Mountain sustaining a 0.1 mm/yr steady-state flow, when subjected to a rising water table. The water table rises to the top of TSw2—an elevation of 335.2 m, approximately 100 m above the repository horizon—maintains

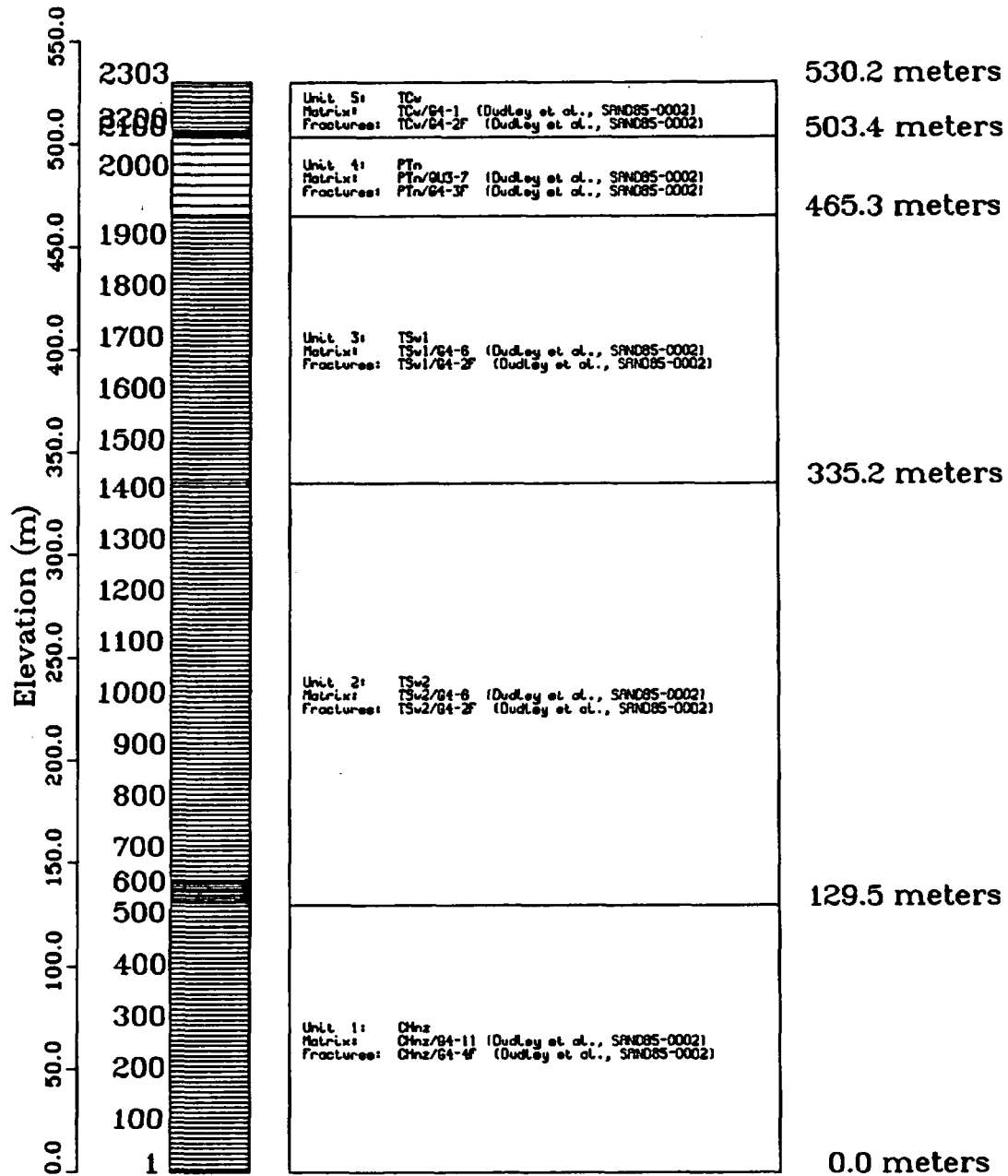


Figure 1. The calculational mesh (left-hand column) and the geohydrologic unit stratigraphy (right-hand column) versus elevation; the bottom of the mesh (0.0 m) corresponds to the present water table at Yucca Mountain and the top (530.2 m) corresponds to the surface.

Table 1. Unsaturated-zone hydrologic properties of the matrix and fractures for Cases 1 and 2; only data for units TCw, PTn, TSw1, TSw2, and CHnz are used in the calculations (taken from Dudley et al., 1988).

Matrix properties							
Unit	Sample code	Grain density (g/cm ³)	Porosity n _m	Hydraulic conductivity K _{m,b} (m/s)	Residual sat. S _r	van Gen. params.	
						α (10 ⁻² /m)	β
TCw	G4-1	2.49	0.08	9.7 × 10 ⁻¹²	0.002	0.821	1.558
PTn	GU3-7	2.35	0.40	3.9 × 10 ⁻⁰⁷	0.100	1.50	6.872
TSw1	G4-6	2.58	0.11	1.9 × 10 ⁻¹¹	0.080	0.567	1.798
TSw2	G4-6	2.58	0.11	1.9 × 10 ⁻¹¹	0.080	0.567	1.798
TSw3	GU3-11	2.38	0.07	1.5 × 10 ⁻¹²	0.080	0.441	2.058
CHnv	GU3-14	2.37	0.46	2.7 × 10 ⁻⁰⁷	0.041	1.60	3.872
CHnz	G4-11	2.23	0.28	2.0 × 10 ⁻¹¹	0.110	0.308	1.602
PPw	G4-18	2.59	0.24	4.5 × 10 ⁻⁰⁹	0.066	1.41	2.639

Fracture properties								
Unit	Sample code	Horizontal stress (bars)	Fracture aperture (μm)	Fracture conductivity (10 ⁻⁶ m/s)	Fracture density (No./m ³)	Fracture porosity n _f (10 ⁻⁵)	Fracture compressibility ∂n _f /∂σ' (10 ⁻⁸ /m)	Bulk frac. conductivity K _{f,b} (10 ⁻⁹ m/s)
TCw	G4-2F	1.1	6.74	3.8	20	14.	132.	5.3
PTn	G4-3F	3.3	27.0	61.	1	2.7	19.	16.
TSw1	G4-2F	9.5	5.13	2.2	8	4.1	5.6	0.90
TSw2	G4-2F	21.9	4.55	1.7	40	18.	12.	3.1
TSw3	G4-2F	29.9	4.34	1.6	10	4.3	2.1	0.69
CHnv	G4-4F	34.3	15.5	20.	3	4.6	2.8	9.2
CHnz	G4-4F	34.3	15.5	20.	3	4.6	2.8	9.2
PPw	G4-2F	39.2	4.16	1.4	3	1.3	0.5	0.18

Fracture-saturation coefficients are S_r = 0.0395, α = 1.2851/m, and β = 4.23.

Unit	TCw	PTn	TSw1	TSw2	TSw3	CHnv	CHnz	PPw
Coefficient of consolidation α' _{bulk} (10 ⁻⁷ /m)	6.2	82.	12.	5.8	5.8	39.	26.	17.

The compressibility of water (β'_w) is 4.3 × 10⁻⁶/m.

that position for a period of time sufficient to saturate the rock matrix, then rapidly falls back to its present position. (It is estimated that it would take approximately 1 year to saturate the matrix completely when water is introduced through the fractures.)

The problem begins after the water table has returned to its normal position (an elevation of 0 m).

The Case 1 initial condition is potentially inaccurate in 2 aspects. First, flow has not come to equilibrium at the interface between geologic units TSw1 and TSw2. There exists a large pressure head gradient that will force water upwards for approximately 1,000 years (see the Late-Time Results section below) after the start of the simulation. Thus if the water table stays elevated for a long period of time, this initial condition is inaccurate; however, it may be reasonably accurate when the water table stays elevated for only a short period of time.

Second, the constant pressure head in the lower 2 geologic units is arbitrary. It was selected because it is approximately the point at which the fractures are desaturated and the matrix saturated for both lower units. Perhaps a better initial condition would be to set a pressure head of 0 m at the TSw1/TSw2 interface with a hydrostatic-head in the lower 2 units, and let the water drain of its own weight. However, we do not know if this is the process by which the water table subsides. And if it is the process, we do not know the appropriate lower boundary condition. In any event, the hydrostatic-head initial condition would probably add time to the drainage—because there is more water to drain—and thus the prescribed initial condition will probably underestimate the time required to relax to steady-state flow (providing a conservative answer).

Initial Condition (Case 2)

The initial condition for Case 2 of the problem is an arbitrary pressure head of -1 m assigned to the entire column (every mesh point in every geologic unit).

This initial condition represents Yucca Mountain being completely immersed by the rising water table. The water table rises to the ground surface—an elevation of 503.2 m above the present water table, approximately 270 m above the repository horizon—maintains that position for a period of time sufficient to saturate the rock matrix, then rapidly falls back to its present position.

The problem begins after the water table has returned to its normal position (an elevation of 0 m).

This initial condition suffers the same inaccuracy discussed for Case 1.

Boundary Conditions

The top of the column has a flux boundary condition of 0.1 mm/yr (3.17×10^{-12} m/s) imposed for the entire simulation. The bottom of the column has a pressure head boundary condition of 0 m imposed for the entire simulation. The bottom boundary condition corresponds to the water table. The top boundary condition corresponds to an estimate of the present rate of infiltration into Yucca Mountain (DOE, 1986).

Results Times

Preliminary calculations indicated that suitable problem times to specify results for both Cases 1 and 2 are as follows:

- 1) 1 hour,
- 2) 1 day,
- 3) 1 week,
- 4) 1 month,
- 5) 1 year,
- 6) 10 years,
- 7) 100 years,
- 8) 1,000 years,
- 9) 10,000 years,
- 10) 20,000 years,
- 11) 50,000 years,
- 12) 100,000 years,
- 13) 200,000 years.

The result times are closely spaced at the beginning of the simulation and coarsely spaced at the end, to distinguish periods of greatest variation in flow.

Calculation Note

The Case 1 calculation took approximately 10 minutes of VAX 8700 computer time; the Case 2 calculation took almost 11 hours. Both calculations were executed in the batch mode. Both calculations were executed twice, using different time step factors and implicitness factors. For both cases the different runs produced essentially identical results. In order to reduce computation time, the final calculations were executed using the table-interpolation method of determining the saturations and hydraulic conductivi-

ties for the various mesh points (rather than computing them from the pressure head at each iteration). See Gauthier et al. (in preparation) for more information.

Early-Time Results

The problem results can be separated into 2 categories: early time and late time. The first 10 years are an adjustment period, very dependent on the specified initial condition, especially for Case 2. These early-time results are not especially important to answering the basic questions surrounding drain-back times (10 years is insignificant in a 100,000-year process). However early-time behavior offers a glimpse at the processes involved in a water-table fluctuation.

Figure 2 presents the change in pressure head with elevation and time as calculated for Cases 1 and 2. TOSPAC solves for pressure head; the other hydrologic variables are calculated from pressure head.

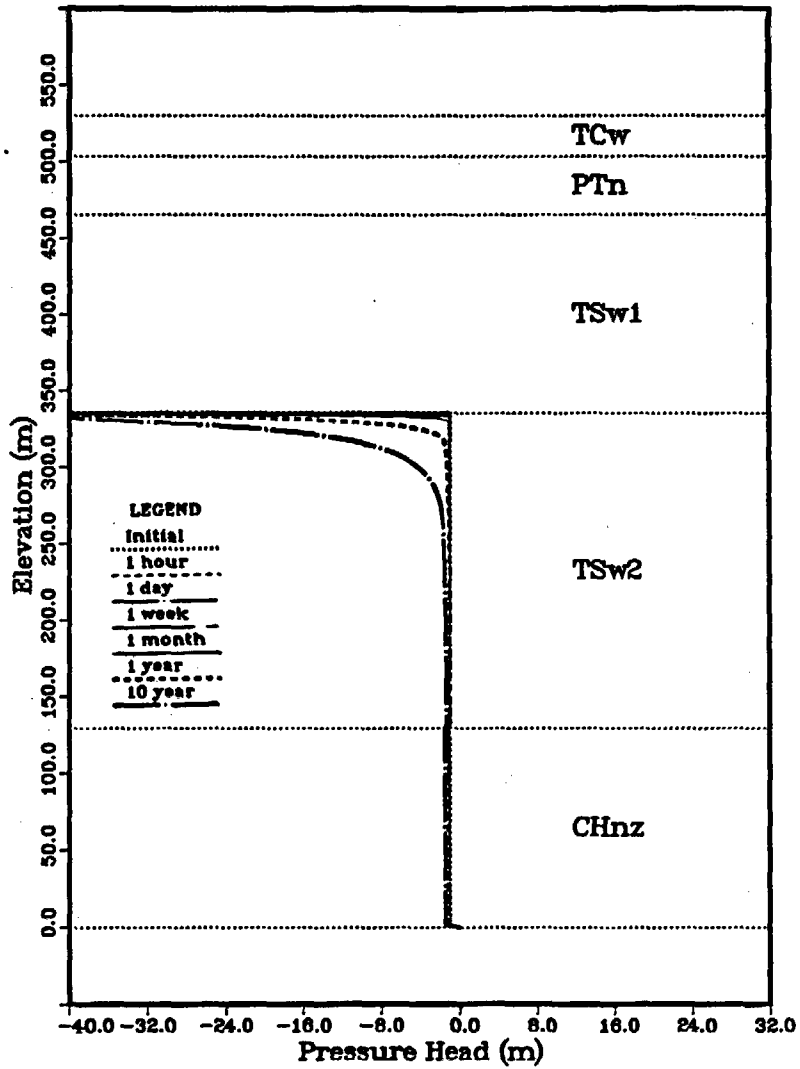
Figure 2a shows that for Case 1, the pressure head drops, and correspondingly the drain-back proceeds, in a regular manner at early time.

Figure 2b shows that the behavior for Case 2 is much more animated. TOSPAC's attempts to track this early-time behavior caused the long computer times for Case 2. Figure 2b indicates that after only 1 hour a large perturbation forms in the pressure head in unit PTn. The pressure head has deviated from the initial condition of -1 m to approximately -10 m at the top of PTn, and over 10 m at the bottom of PTn. (Positive pressures imply fully saturated conditions.) This perturbation increases for approximately 1 week, at which time the pressure head reaches 20 m at the top of PTn and the positive-pressure region extends 100 m down into TSw1. At 1 year the pressure head is decreasing although all of TSw1 is still at positive pressure.

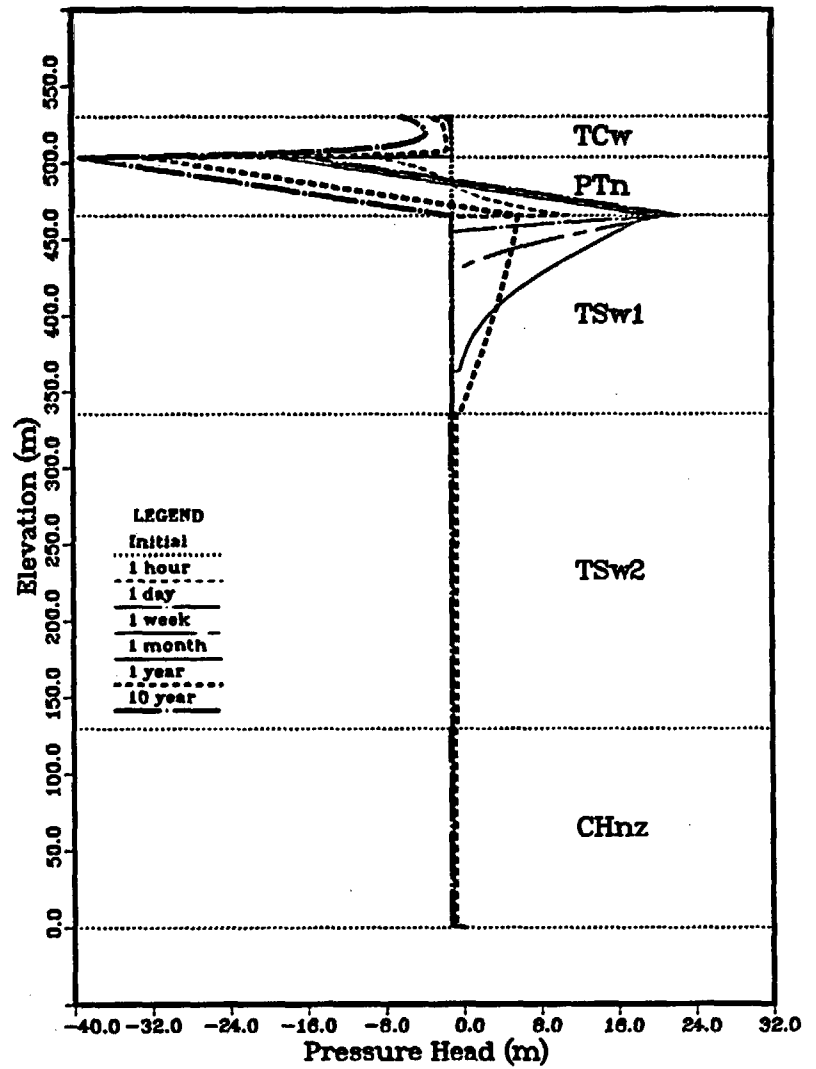
To explain this behavior, consider that PTn is composed of highly-conductive, highly-porous, nonwelded tuff. At the -1 m initial condition, almost one-half of the volume of PTn is water. When the simulation starts, gravity attempts to drain this water. However, immediately below PTn is unit TSw1, which is composed of fractured tuffs of generally low permeability. The water ponds at the interface, causing the positive pressure heads, then drains into the TSw1 fractures.

The saturation of the matrix and the fractures at early times for Cases 1 and 2 are shown in Figures 3 and 4, respectively.

The saturation of the matrix changes little in the first 10 years of the simulation. Figure 3a indicates that an equilibration is taking place at the TSw1-TSw2 interface (the

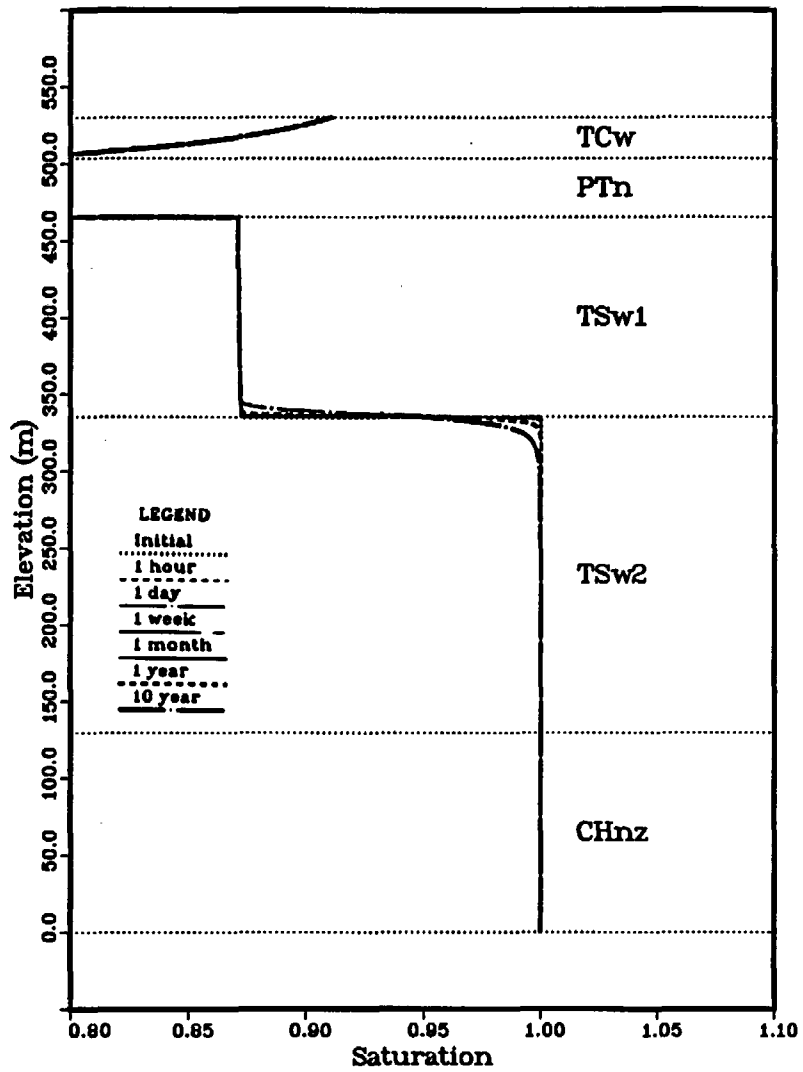


(a)

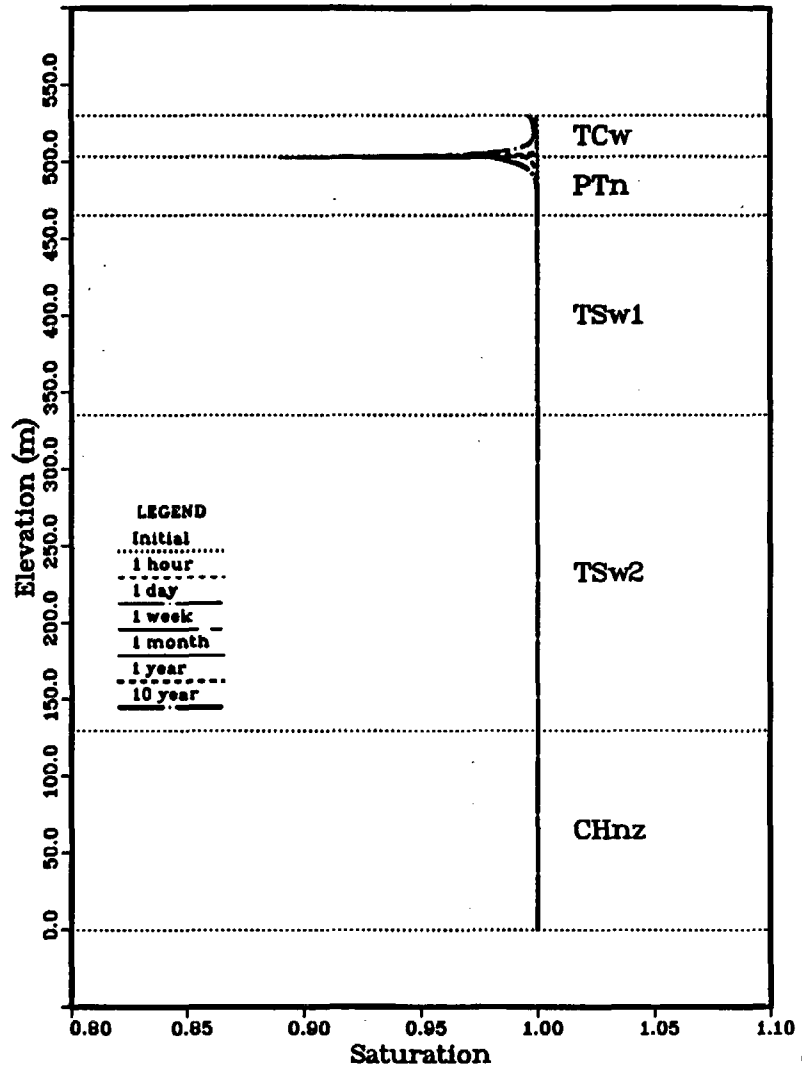


(b)

Figure 2. Pressure head versus elevation at early times. (a) Case 1, (b) Case 2.



(a)



(b)

Figure 3. Saturation of the matrix versus elevation at early times. (a) Case 1, (b) Case 2.

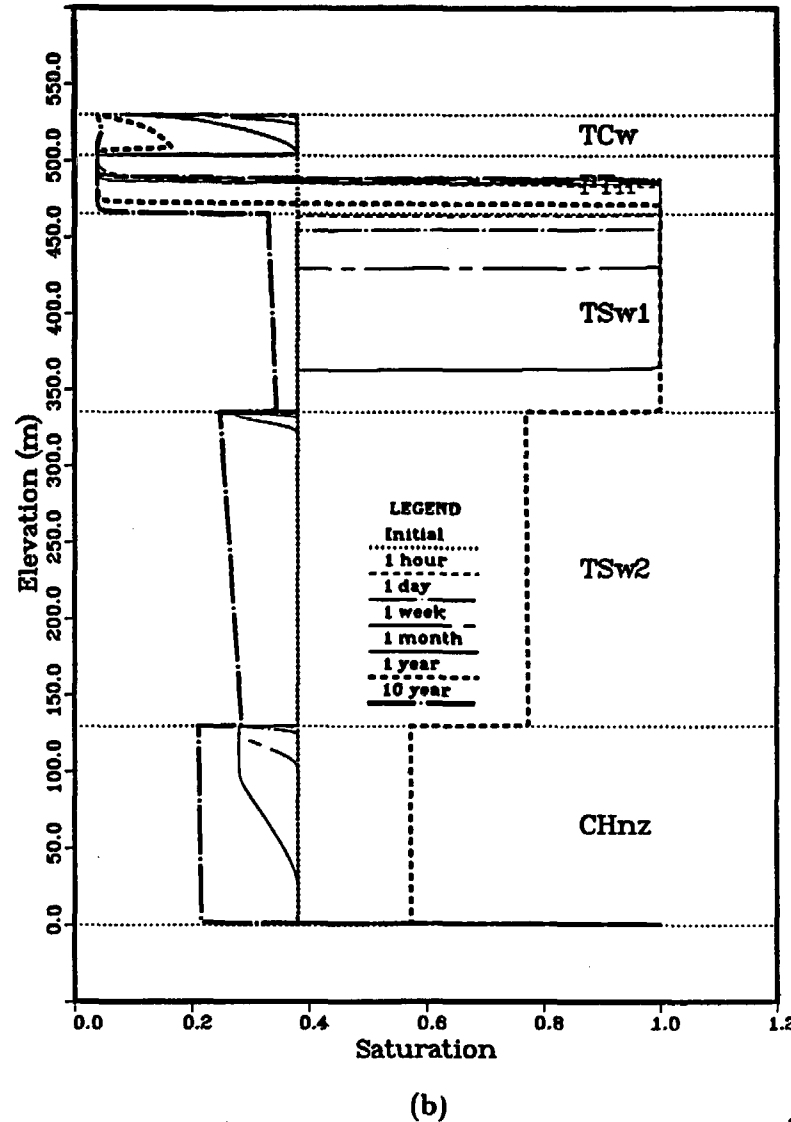
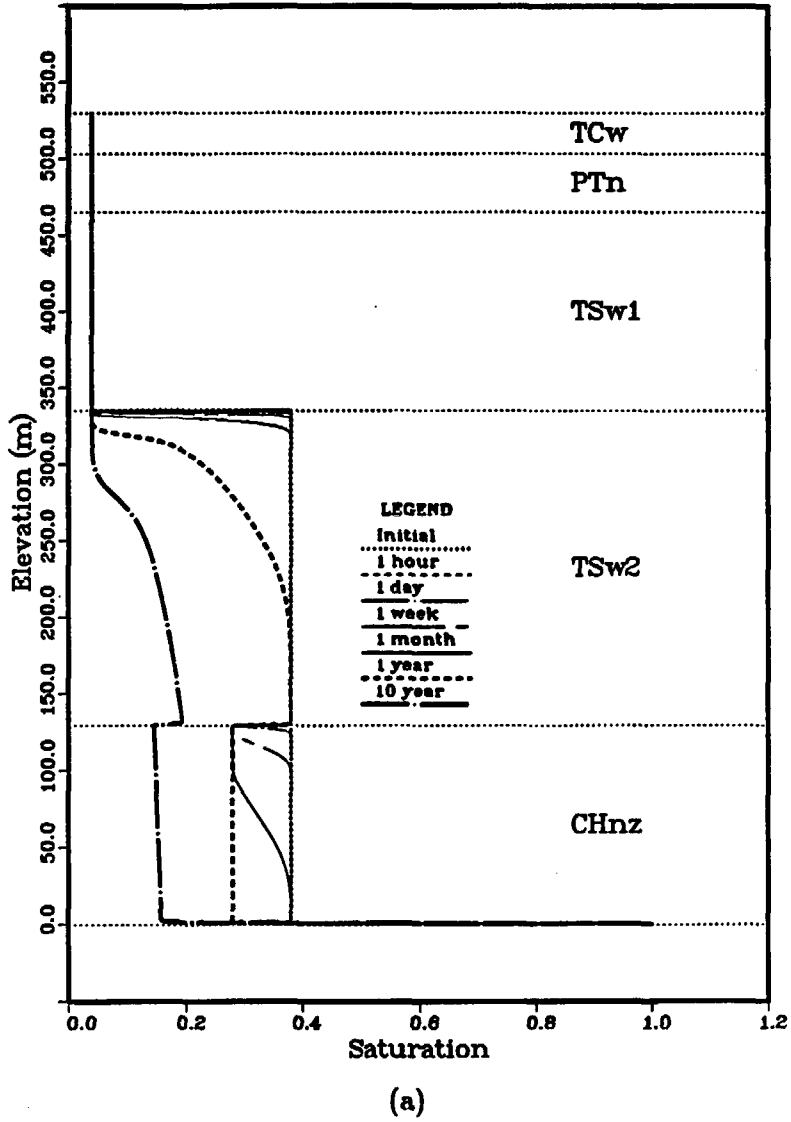


Figure 4. Saturation of the fractures *versus* elevation at early times. (a) Case 1, (b) Case 2.

assumed maximum rise of the water table). This equilibration is discussed further below. Figure 3b shows a drop in saturation at the TCw-PTn interface caused by the abrupt draining of PTn. The ponding implied by the positive pressures seen in Figure 2b is not obvious because most of the column is within 0.1 percent of complete saturation.

Figure 4 shows the saturation of the fractures at early times for both cases. Because the specified fracture materials all used the same characteristic curves, the initial condition of -1 m of pressure head causes a saturation of approximately 40 percent in all units where it is imposed. As the columns relax to a steady-state flow of 0.1 mm/yr, the fractures in both Case 1 and Case 2 should desaturate (except near the water table where the imposed 0 pressure head forces the fractures to be saturated).

For Case 1, Figure 4a shows a regular decrease in fracture saturation over time. The fractures in unit CHnz drain somewhat faster than the fractures in TSw2 because the conductivity of the CHnz fractures is approximately an order of magnitude greater than the TSw2 fractures. (Hydraulic conductivity in the unsaturated zone is computed as the saturated hydraulic conductivity times the relative hydraulic conductivity— $K = K_{sat} * K_{rel}$. Although the characteristic curves for the relative hydraulic conductivity of the fractures for both units are the same, the saturated conductivity value for the CHnz fractures is 20×10^{-5} m/s, while it is only 1.7×10^{-5} m/s for the TSw2 fractures.)

For Case 2, as shown in Figure 4b, the fractures in TSw2 and CHnz begin to desaturate as in Case 1. Above them, however, the fractures are completely saturated by the pulse of water building in PTn. This pulse proceeds as a square wave (because of the nonlinearity of the fracture material) down through TSw1. At 1 month the pulse is near the TSw1-TSw2 interface; at 1 year it has flowed through the column, increasing the saturation of the fractures in CHnz and TSw2. At 1 year the fractures are still saturated in TSw1 and in the lower portion of PTn.

It should be pointed out that it is not the water from PTn that is increasing the saturation in the lower units at 1 year. The saturation pulse is in response to a pressure-head pulse. Based on the average linear velocity of the fracture water (shown in Figure 9b below), it can be estimated that water from PTn would take approximately 5 years to first reach the water table through the fractures. Much of the increased saturation in TSw2 and CHnz at 1 year is caused by the redistribution of water that was originally below PTn.

The total flux of water in the column is presented in Figure 5. Total flux is the sum of the flux of water in the matrix and the flux of water in the fractures. A steady-state flow of 0.1 mm/yr would be indicated by a vertical line at 3.17×10^{-12} m/s, i.e., very close to 0 on the scale of the plots. In 1-dimensional flow, flux is the same quantity as Darcy velocity.

In these calculations, downward water flux and velocity have been arbitrarily defined as positive quantities, and upward flux and velocity as negative quantities. These assignments are arbitrary.

Figure 5a shows the total flux profiles at early times for Case 1. The upper 3 units of the column are already at 0.1 mm/yr steady-state flux. The initial condition of -1 m of pressure head produces a flux of approximately 3 mm/yr in unit TSw2 and a flux of approximately 8 mm/yr in unit CHnz. (Units TSw1 and CHnz have different hydraulic conductivity curves and thus -1 m of pressure head produces different conductivities and different fluxes.) As the problem begins, the flux decreases in the lower 2 units.

The most noticeable feature of Figure 5a is the negative fluxes at the TSw1-TSw2 interface. As stated above, negative fluxes imply that water is flowing up the column. This behavior is part of the equilibration process mentioned in the description of Figure 3a. Initially, above this interface the pressure head is less than -100 m; below this interface the pressure head is -1 m. Flux is calculated in TOSPAC using Darcy's law as follows:

$$q = K(\psi) \left(\frac{\Delta\psi}{\Delta z} - 1 \right),$$

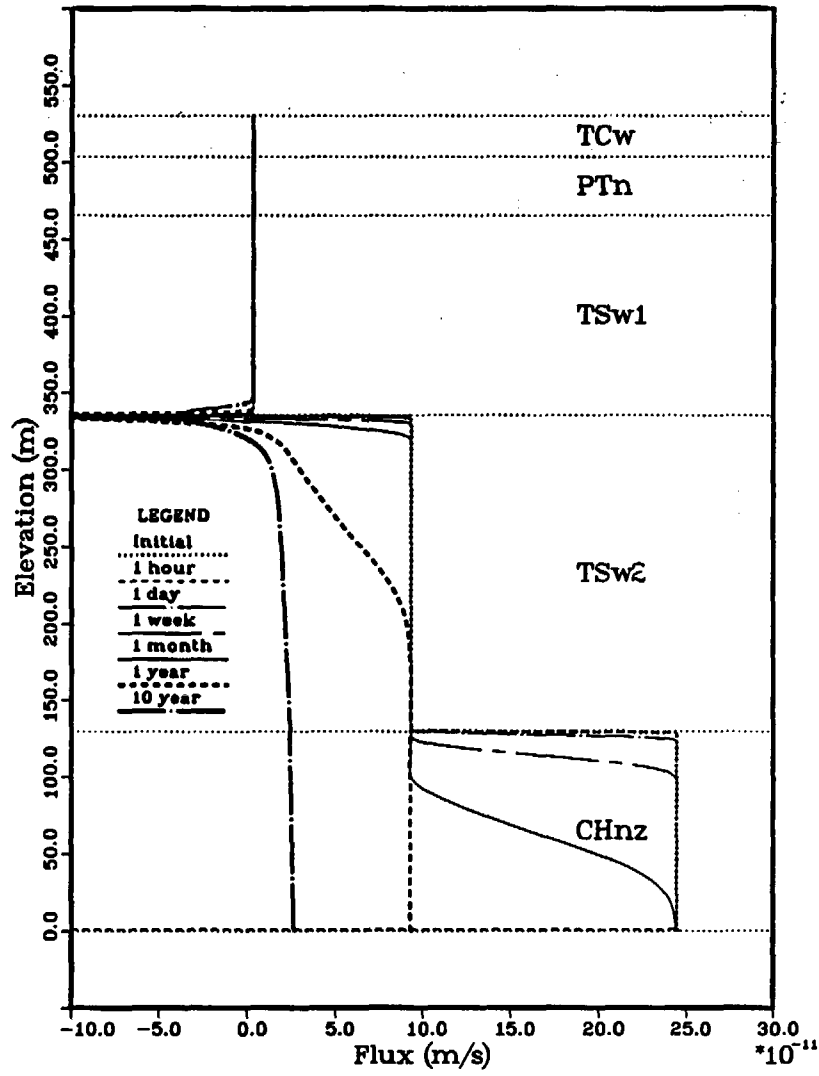
where q is the flux, K is the hydraulic conductivity (as a function of pressure head), ψ is the pressure head, and z is the elevation. Thus, the extremely large $\Delta\psi$ produces a large flux as water is drawn upwards into TSw1 by capillary suction.

Figure 5b shows the total flux profiles at early times for Case 2. The major flux pulse coming from PTn runs off the plot at this scale. The entire 1-year time line in the lower 4 units is also missing from the plot because it is greater than 30×10^{-11} m/s (approximately 3 times as large). These large fluxes are due primarily to fracture-water flux, as shown in Figure 7 below.

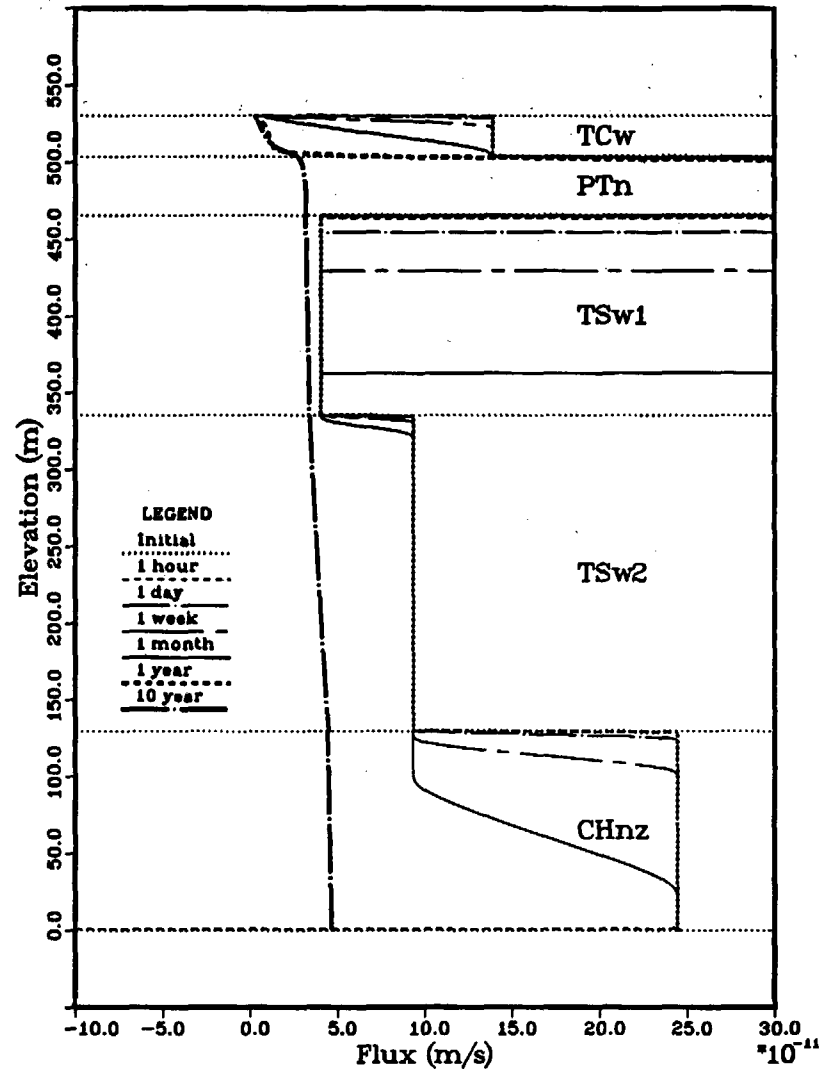
Figure 6 presents the flux of water in the matrix at early times for Cases 1 and 2. The plots show a sharp decrease in flow in the matrix at the water table. This decrease is caused by water being transferred into the fractures at the imposed boundary pressure head of 0.

Figure 6a shows that the major activity in the first 10 years is the upward flux of water at the TSw1-TSw2 interface. Figure 6b is of interest because the logarithmic scale allows presentation of the large fluxes in PTn. The fluxes in TSw1 are not nearly as large because much of the flow is being carried in the fractures in this unit. The flux profiles in unit TSw1 show a spike on the leading edge of the fronts: this spike is caused by water in the matrix being accelerated by a large pressure head gradient before the pressure head has reached a level that allows significant fracture flow. See Dudley et al. (1988) for a discussion of this effect.

Figure 7 presents the flux of water in the fractures at early times for Cases 1 and 2.



(a)



(b)

Figure 5. Total flux versus elevation at early times. (a) Case 1, (b) Case 2.

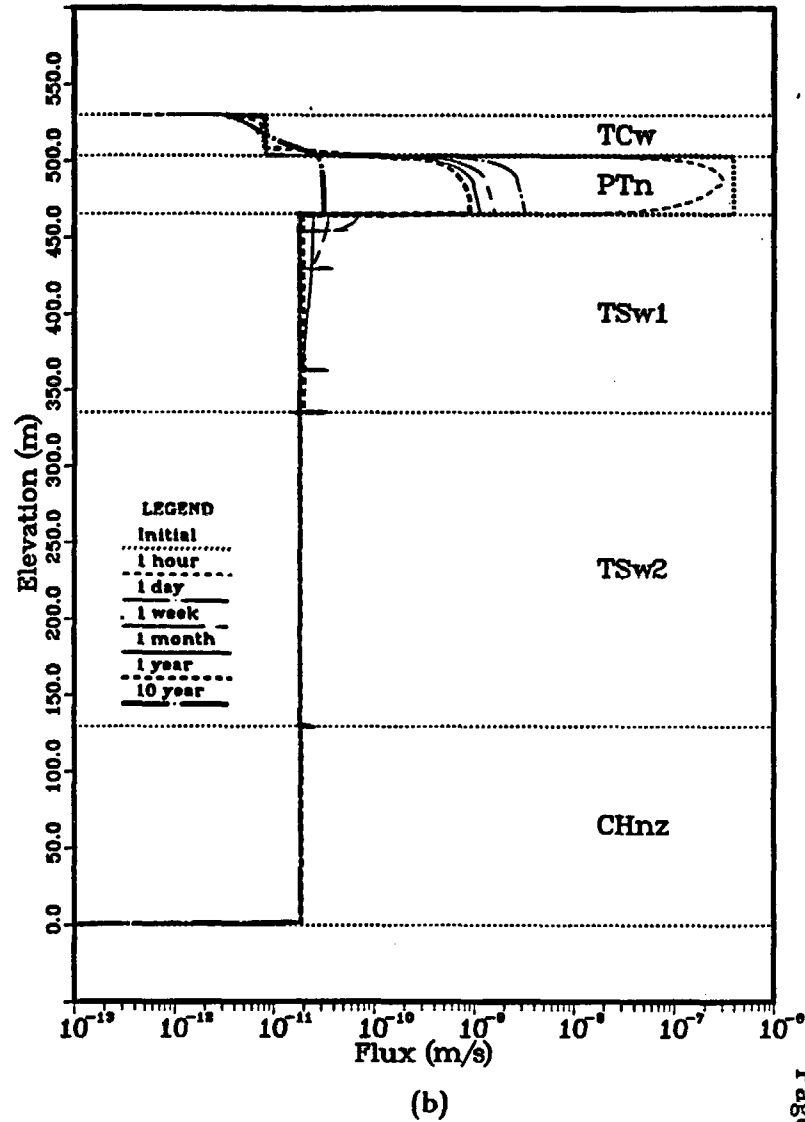
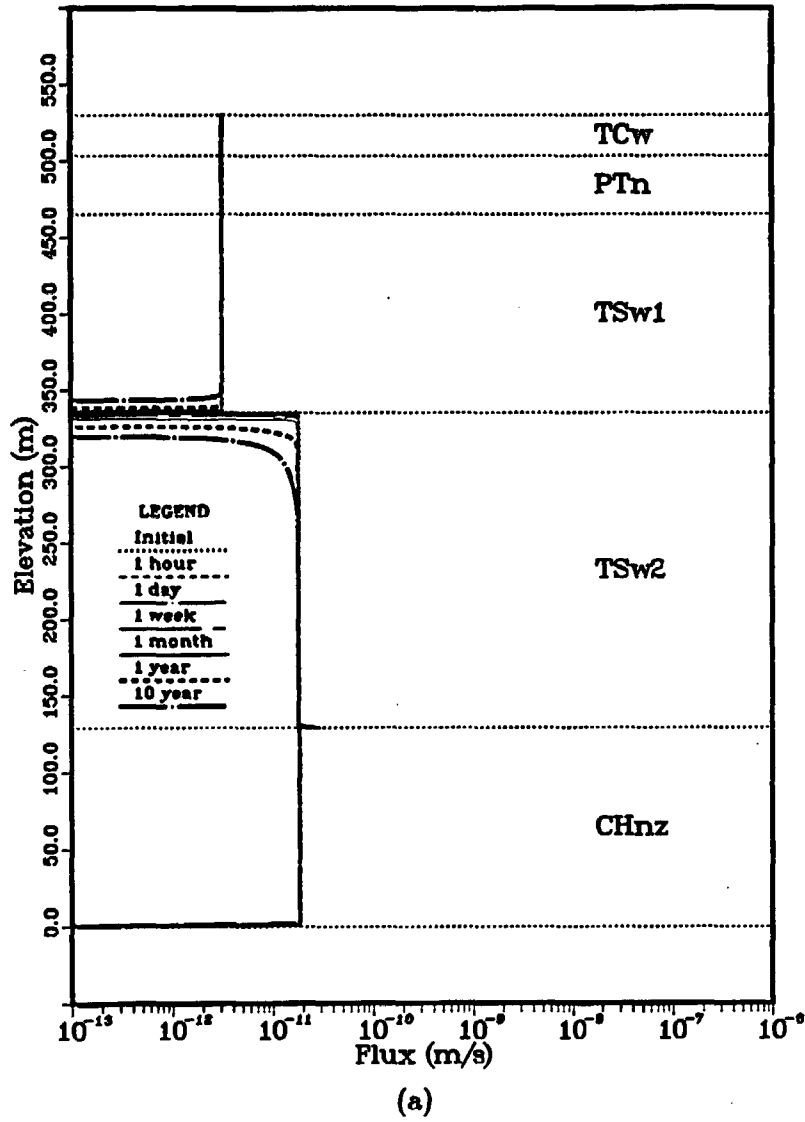
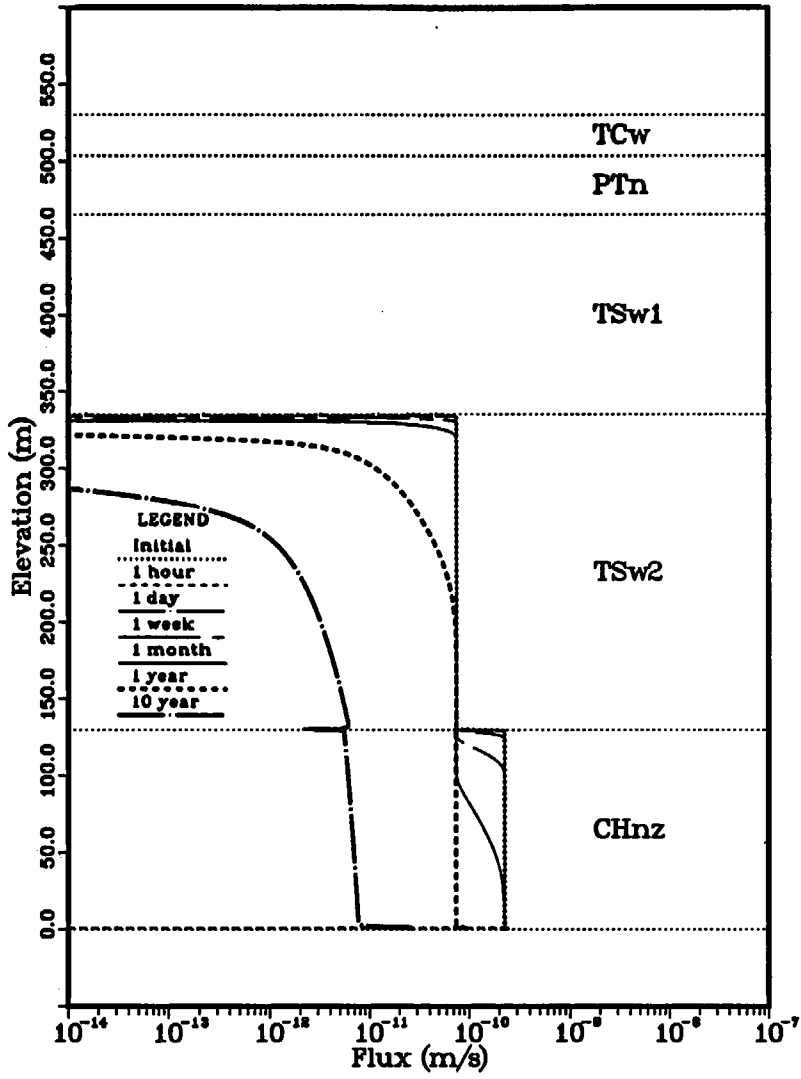
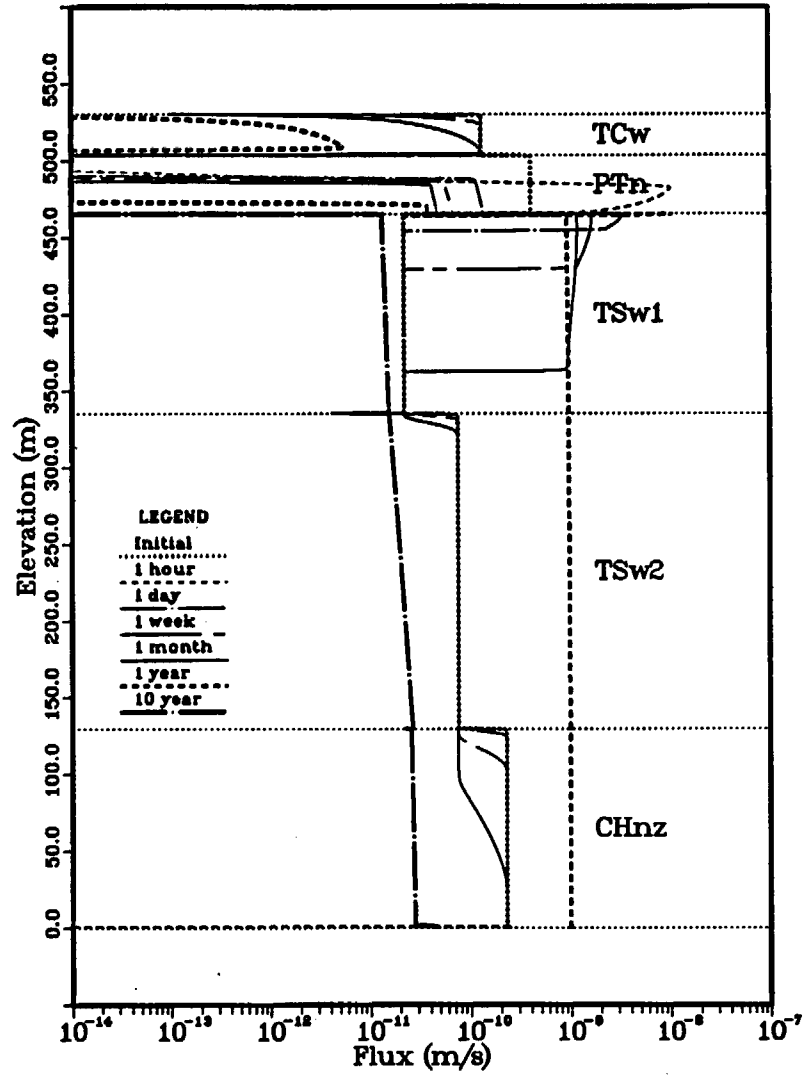


Figure 6. Flux of water in the matrix *versus* elevation at early times. (a) Case 1, (b) Case 2.



(a)



(b)

Figure 7. Flux of water in the fractures *versus* elevation at early times. (a) Case 1, (b) Case 2.

In Figure 7a the flux of water in the fractures is virtually 0 in the upper 3 units and decreases regularly in the lower 2 units. There is no upwards flux of water in the fractures at the TSw1-TSw2 interface: firstly, because the fractures do not afford a large capillary suction, and secondly, any water that is in the fractures near the interface would move immediately into the matrix as the pressure head plunged with the upward flow.

For Case 2, Figure 7b shows a complicated pattern for the change in fracture-water flux. In TCw the flux decreases in a regular manner as the water drains from the fractures, primarily downwards into PTn. In PTn the flux decreases abruptly (within 1 hour) in the upper-half of the unit and increases abruptly in the lower-half of the unit. The flux in the lower-half then decreases dependent upon flow in TSw1, until at 10 years the flux of water in the fractures is virtually 0 for the entire PTn unit. In TSw1 the flux increases by over 2 orders of magnitude as the water from PTn floods the unit. Below TSw1 the flux begins to decrease somewhat, but at 1 year the water from PTn has boosted the flux throughout the lower 3 units. The average linear velocity of this fracture water is approximately 100 m/yr (see Figure 9b below), however the flux pulse has travelled over 400 m in the first year. Thus most of the water involved in the flux increase in TSw2 and CHnz was in these units at the beginning of the problem (placed there by the initial condition).

Fracture-water flux is an important quantity in this problem because it is one of the few fracture-related variables that can be measured.

Figures 8 and 9 show the average linear velocity of water in the matrix and the fractures, respectively, for Cases 1 and 2. The average linear velocity is defined as the flux divided by the effective area for flow (the effective porosity). The average linear velocity of matrix water is computed as follows:

$$v_m = \frac{q_m}{(S_m - S_{r,m})n_m},$$

where v_m is the average linear velocity of the matrix water, q_m is the flux of the matrix water, S_m is the saturation of the matrix, $S_{r,m}$ is the residual saturation of the matrix material, and n_m is the porosity of the matrix. The average linear velocity of the water in the fractures is computed similarly. These plots show fundamentally the same information as Figures 6 and 7, and are included here to supplement the discussion of the other figures.

Late-Time Results

Late-time results involve the drain-back process after 10 years. Late-time results directly address the problem posed in the problem definition. The early-time results can be viewed as setting up a more realistic initial condition for the late-time results.

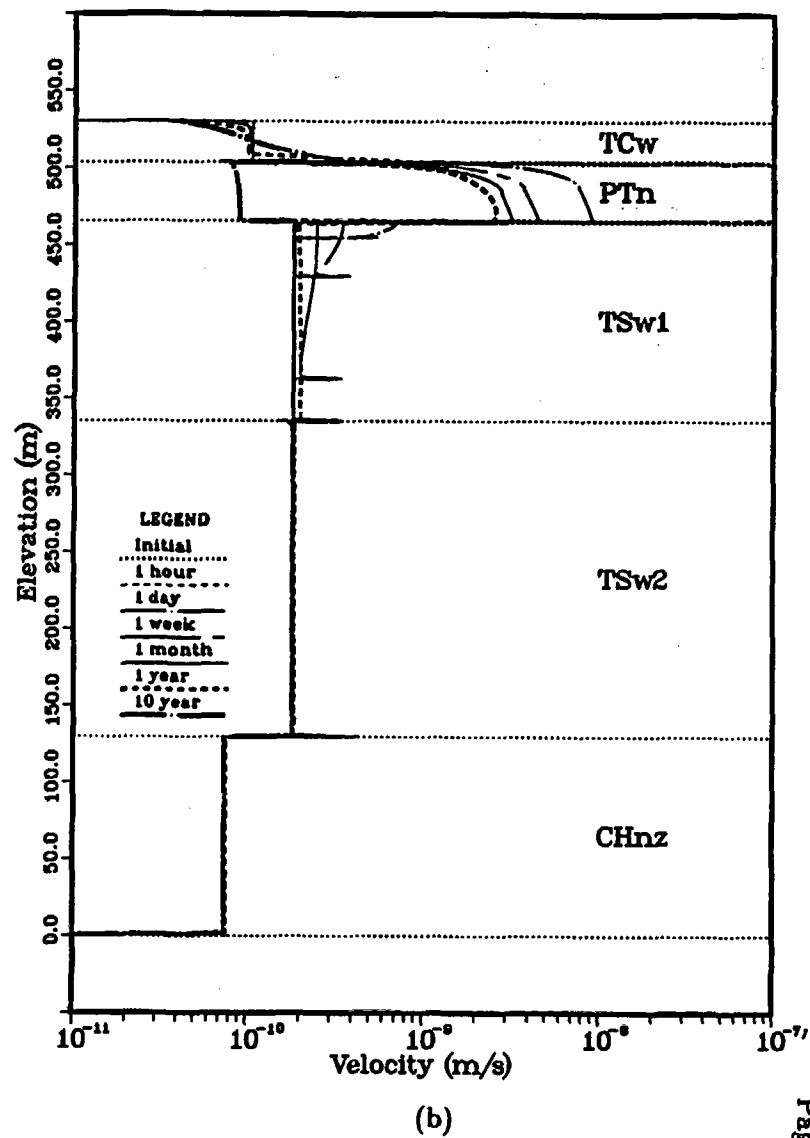
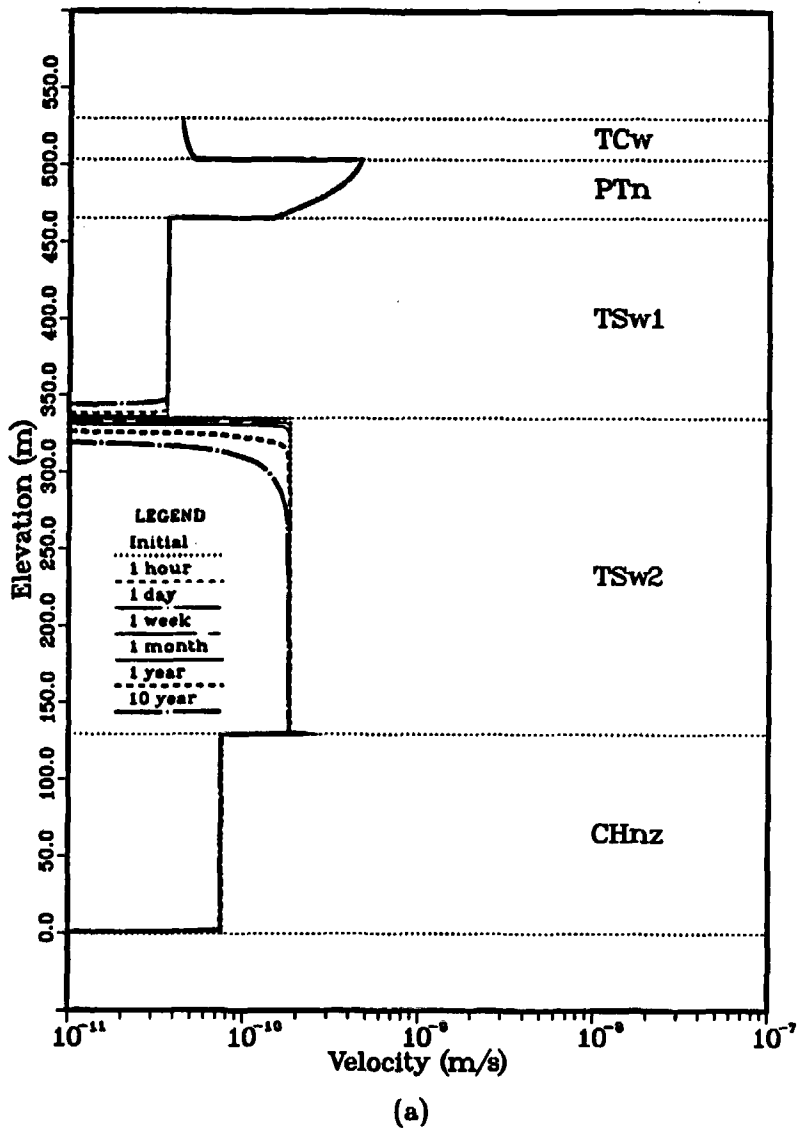


Figure 8. Average linear velocity of water in the matrix *versus* elevation at early times. (a) Case 1, (b) Case 2.

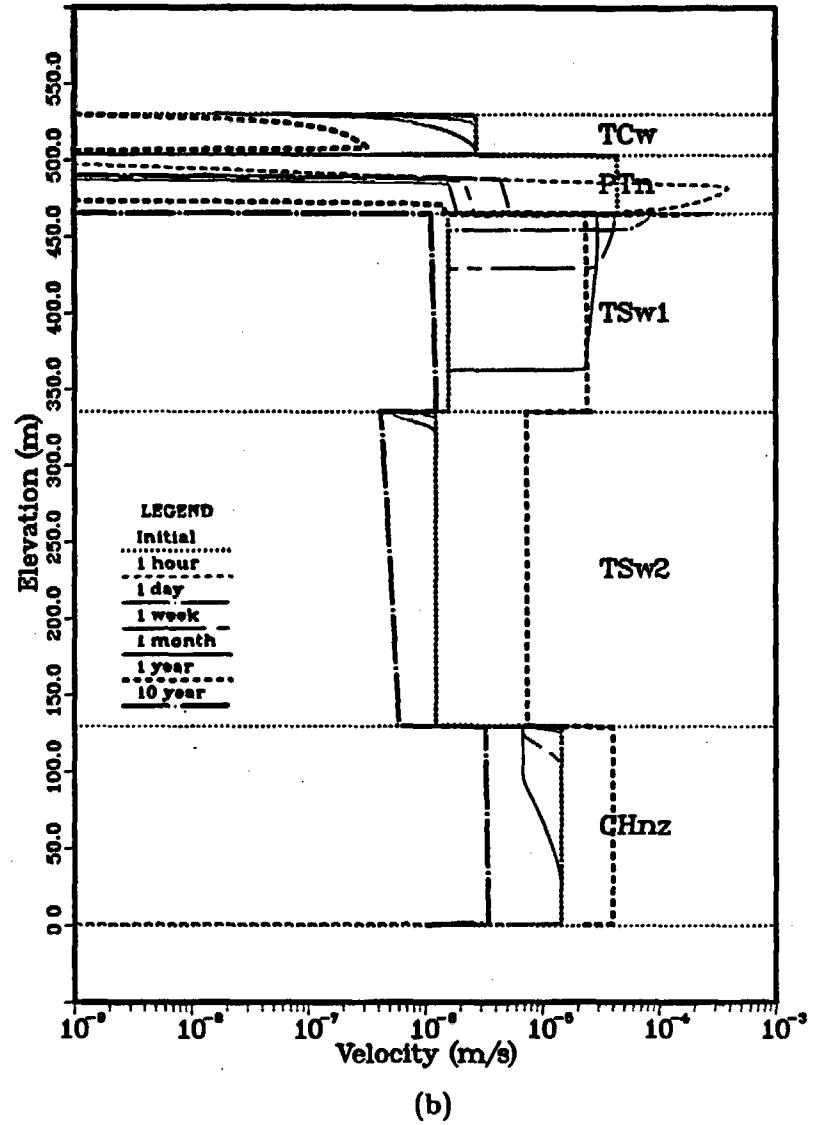
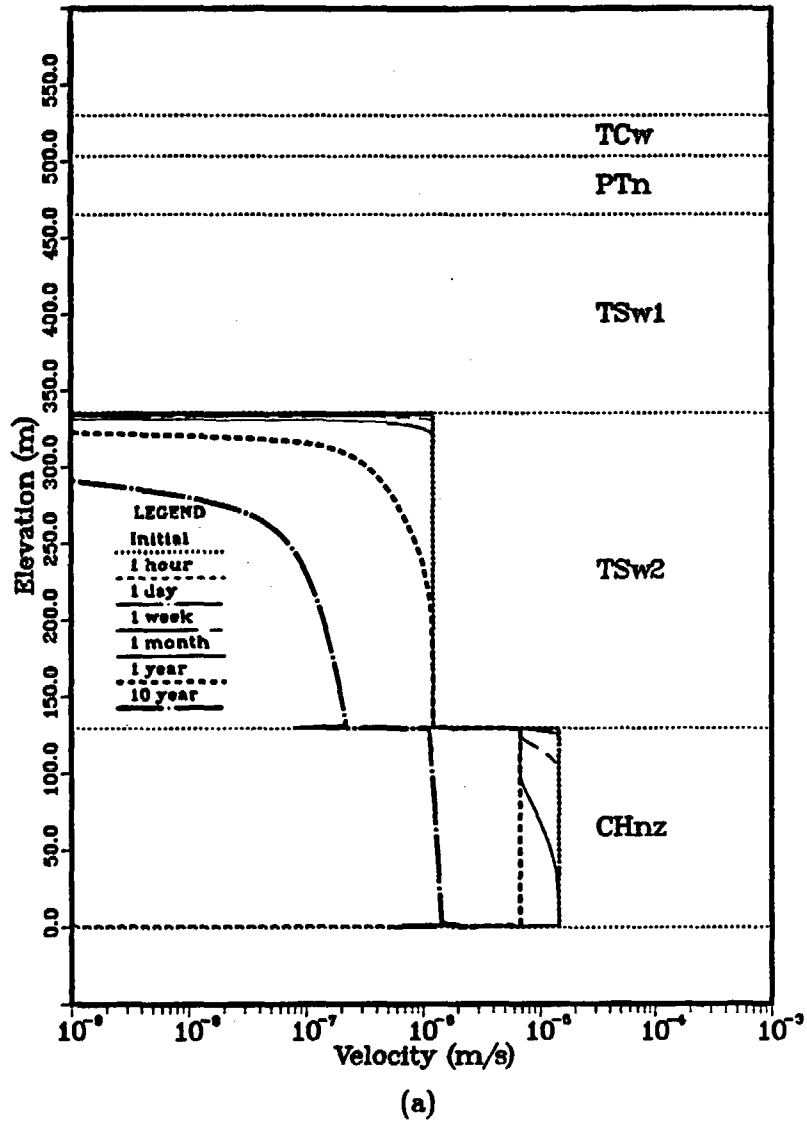


Figure 9. Average linear velocity of water in the fractures *versus* elevation at early times. (a) Case 1, (b) Case 2.

Figure 10 presents the change in pressure head with elevation and time as calculated for Cases 1 and 2 at late time. The plots show that drain-back begins rapidly, but slows with time.

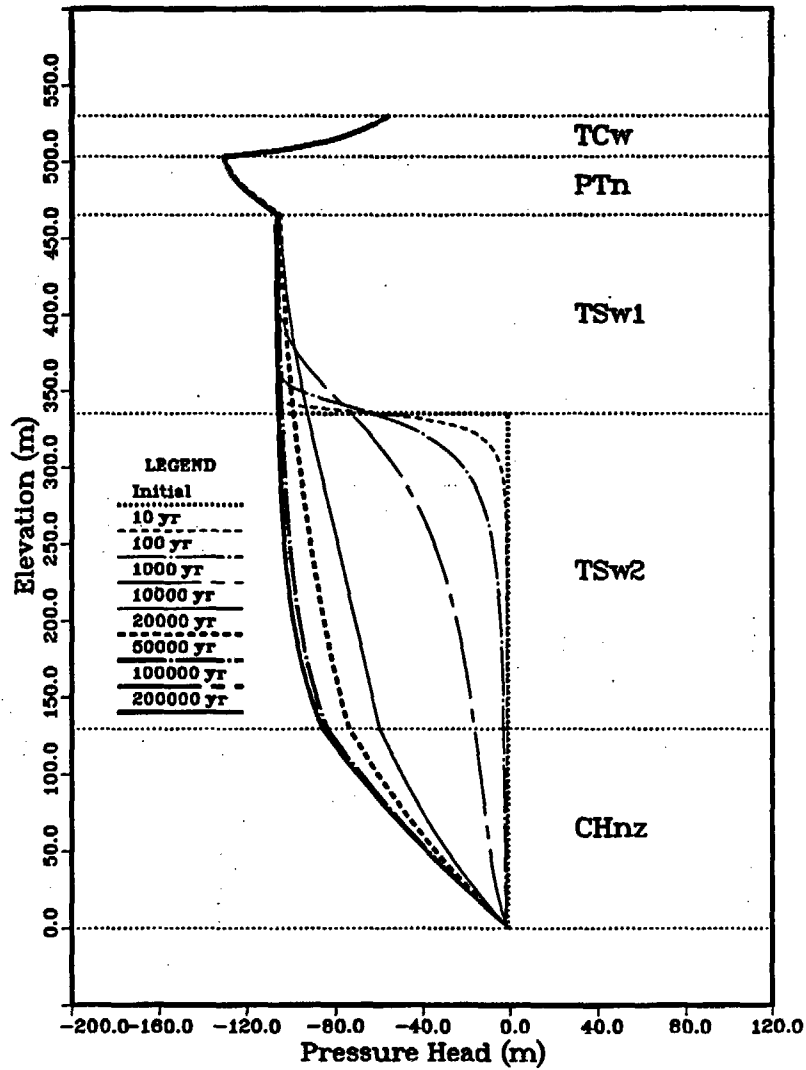
For Case 1, Figure 10a shows that the equilibration at the TSw1-TSw2 interface continues for over 1,000 years. Thus the initial condition for this case, which contains a sharp discontinuity at the TSw1-TSw2 interface, is appropriate for the simulation of an event where the water table is elevated for a short period of time, i.e., less than 1,000 years. In TSw1, the pressure head does not return to steady state until the whole column returns to steady state. At the repository horizon in unit TSw2, the pressure head at 20,000 years is approximately -90 m—about 20 m greater than the steady-state pressure head. Pressure head reaches steady state in the entire column somewhat after 50,000 years.

For Case 2, Figure 10b indicates a more uniform relaxation to steady state. The pressure head at 20,000 years is approximately -40 m at the repository horizon—about 70 m greater than the steady-state pressure head. At 200,000 years the problem is very close to steady state (compare the 200,000 year line in Figure 10a and 10b and see the discussion of Figure 18 below).

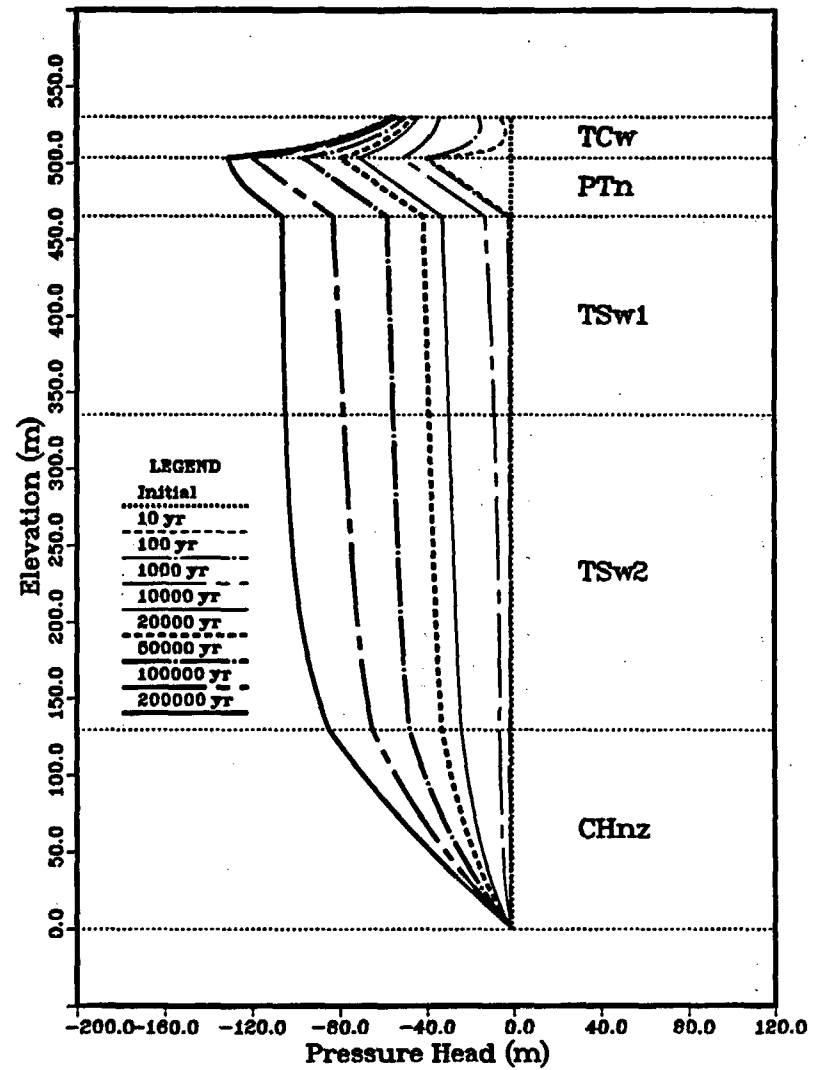
Figure 11 shows the change in the saturation of the matrix over elevation and time. For Case 1, Figure 11a shows a distinct increase in saturation above the TSw1-TSw2 interface. Between 1,000 and 10,000 years the saturation equilibrates across this interface; after 10,000 years the lower 3 units relax to steady-state uniformly. For Case 2, Figure 11b shows a uniform drain-back to steady state.

In both cases, at -1 m of pressure head, the matrix is saturated. At a 0.1 mm/yr steady-state flow, at the repository horizon, the matrix is approximately 87 percent saturated. This difference is only a 13 percent difference in saturation, or approximately a 1.3 percent difference in moisture content. In Case 1, at 20,000 years, the matrix is approximately 90 percent saturated—3 percent above the steady-state saturation and approximately 0.3 percent above the steady-state moisture content. In Case 2, at 20,000 years, the matrix is approximately 97 percent saturated—10 percent above the steady-state saturation and approximately 1 percent above the steady-state moisture content. The implication is that moisture content would not be the best hydrologic variable to measure in order to determine if a significant fluctuation in the water table had occurred in the recent past.

Figure 12 shows the change in the saturation of the fractures for both cases. Initially, a pressure head of -1 m causes a fracture saturation of approximately 40 percent. The rapid change in saturation at unit interfaces is due to the different matrix saturation *versus* pressure head functions, which cause different amounts of water to transfer to the matrix at different pressure heads.

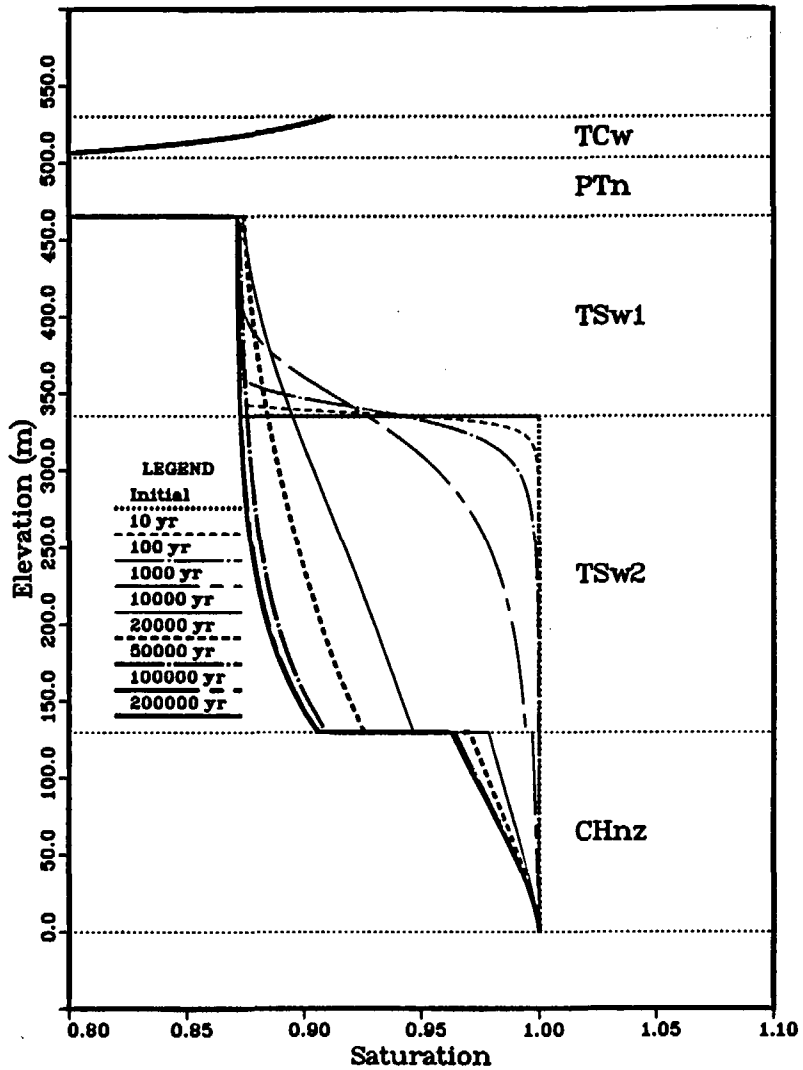


(a)

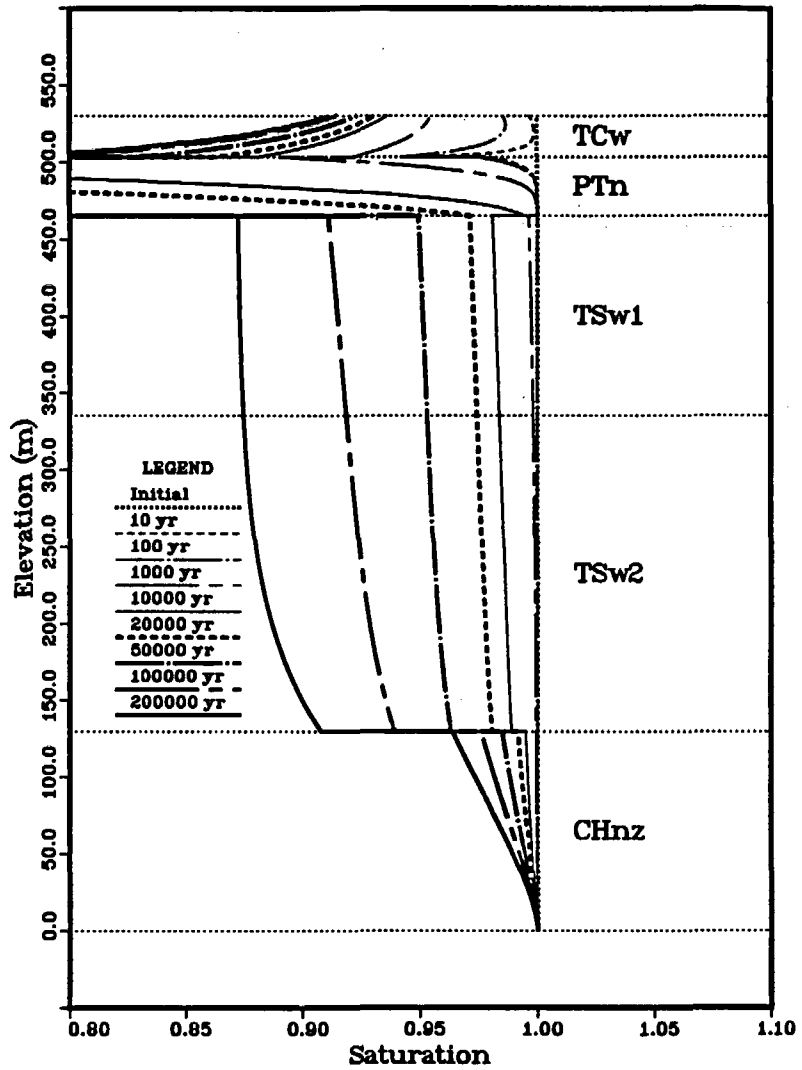


(b)

Figure 10. Pressure head *versus* elevation at late times. (a) Case 1, (b) Case 2.



(a)



(b)

Figure 11. Saturation of the matrix *versus* elevation at late times. (a) Case 1, (b) Case 2.

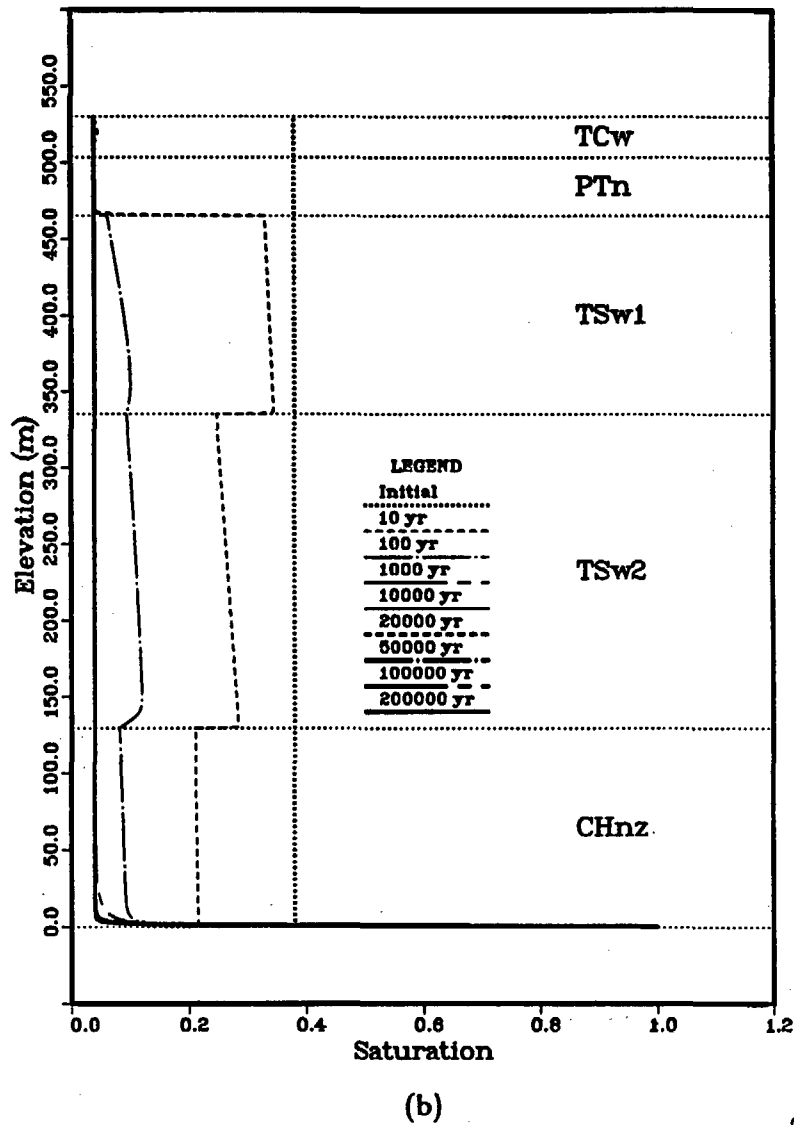
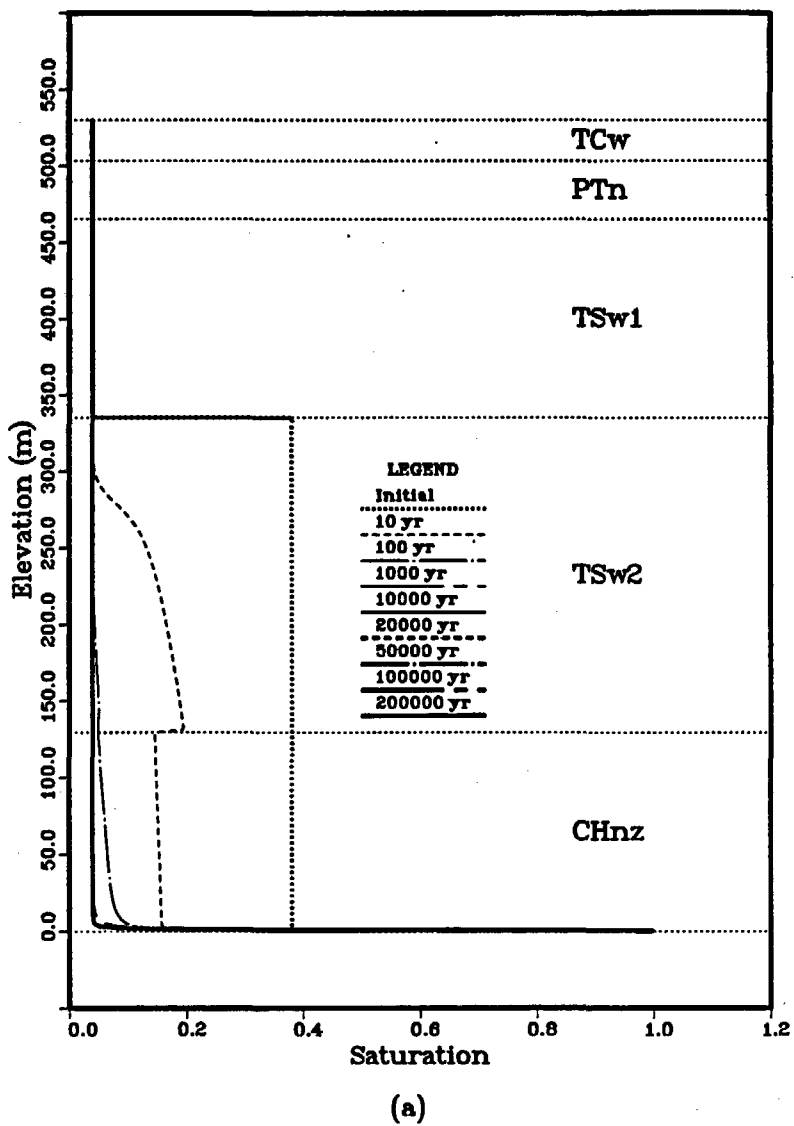


Figure 12. Saturation of the fractures *versus* elevation at late times. (a) Case 1, (b) Case 2.

In Figure 12a, it is interesting to note that, for Case 1, no increase in the saturation of the fractures is seen above the TSw1-TSw2 interface, even at early time. The upflow visible in Figure 5a occurs completely in the matrix. Because of the width of the fractures, there is not enough capillary pressure to generate appreciable suction.

Also of interest is that fracture saturation in Case 1 decreases regularly. There is no evidence of downward flow in the matrix causing overflow into the fractures (see also Figure 4 above).

Both Figures 12a and 12b indicate soon that after 100 years the fractures are desaturated.

The change in total flux with elevation at late times is presented in Figure 13. (A discussion of total flux, Darcy velocity, flux as a positive quantity, etc. is given in the description of Figure 5, above.)

For Case 1, Figure 13a shows the tremendous upward (negative) flux at the initial time line, followed by strong upward (negative) fluxes at 10 and 100 years. The lower half of the column shows a rapid relaxation of the flux to near steady state—at the repository horizon at 20,000 years the total flux is approximately 50 percent above steady state.

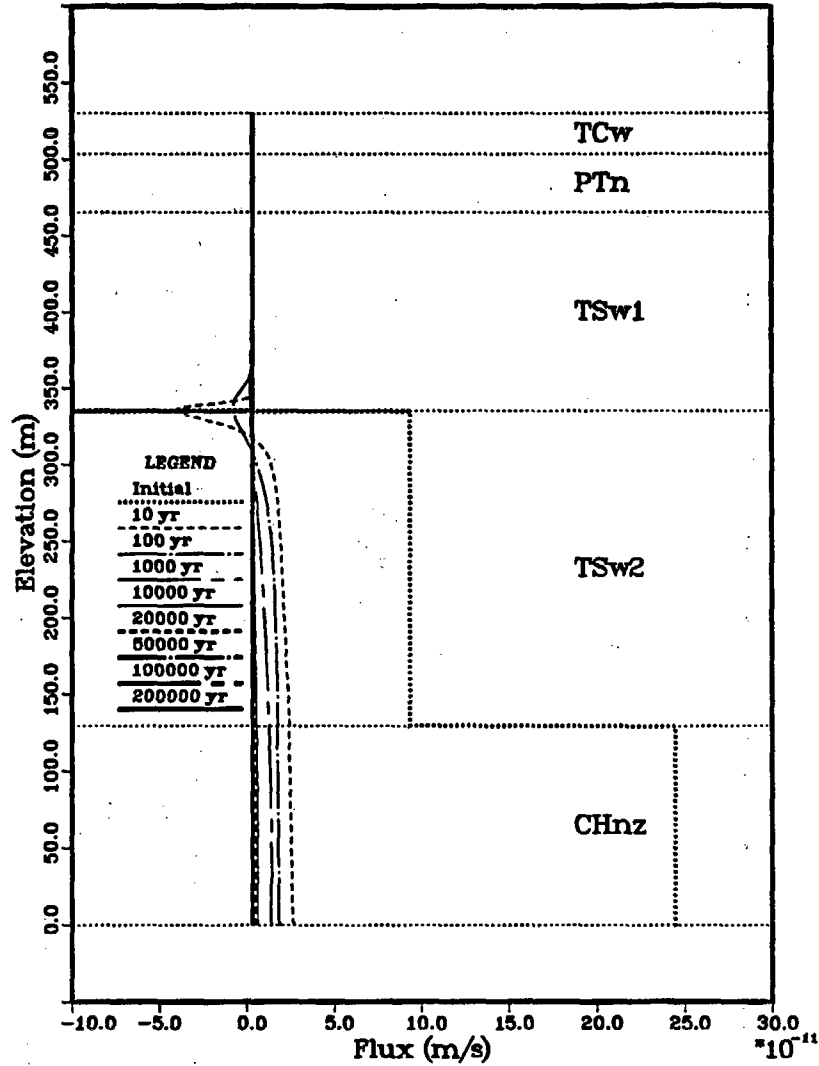
For Case 2, Figure 13b indicates a regular and rapid relaxation to steady state. At the repository horizon at 20,000 years, the flux is approximately 3 times greater than steady state.

Figures 14 and 15 present the flux of water in the matrix and the fractures, respectively, for Cases 1 and 2.

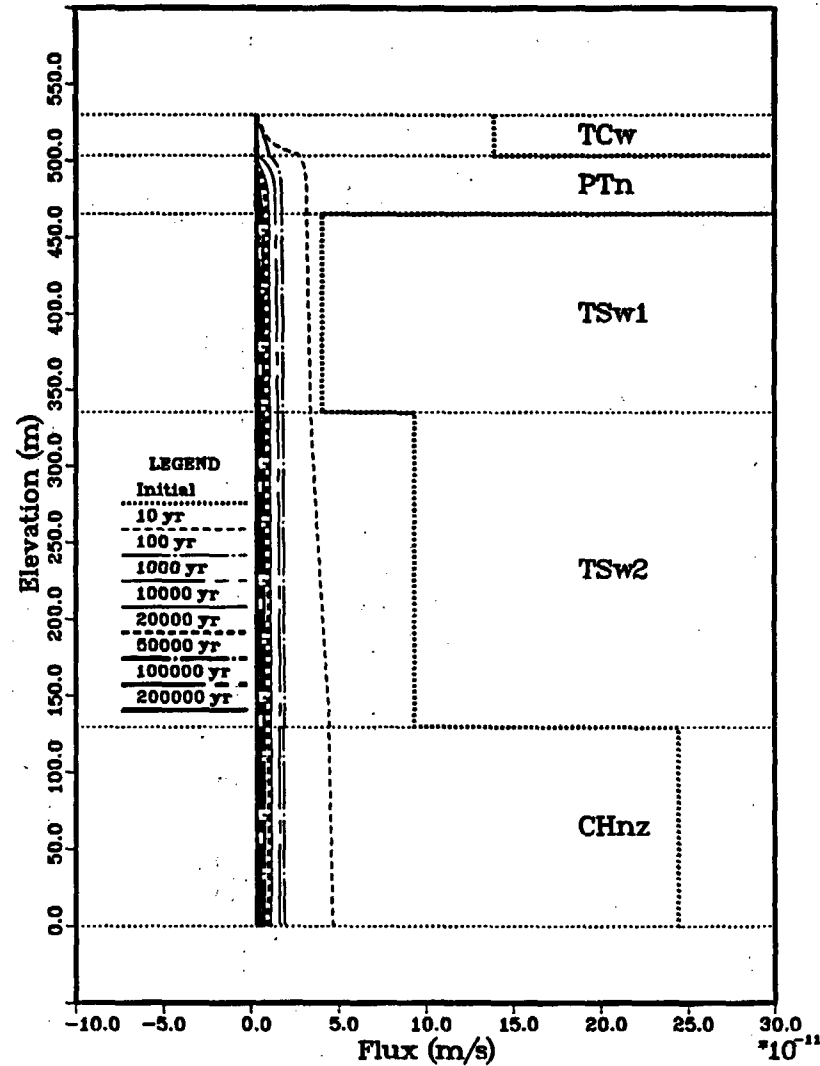
Figure 14 indicates that, on the average, matrix-water flux decreases an order of magnitude over the course of the problem. Except for the equilibration in Case 1 during the first 1,000 years, shown in Figure 14a, the decrease in matrix-water flux is regular and slowing with time.

Figure 15 shows that the fracture-water flux decreases relatively quickly in both cases. By 100 years the flux of water in the fractures is less than the flux of water in the matrix in much of the column; by 1,000 years the fracture-water flux is orders of magnitude less than the matrix-water flux everywhere except at the water table (which is an affect of the boundary condition).

Figure 16 shows the average linear velocity change for water the matrix; Figure 17 shows the average linear velocity change for water the fractures. (See the discussion of Figures 8 and 9 for a definition of the average linear velocity.) For the most part, the information contained in Figures 16 and 17 reproduce the information in Figures 14 and 15.



(a)



(b)

Figure 13. Total flux versus elevation at late times. (a) Case 1, (b) Case 2.

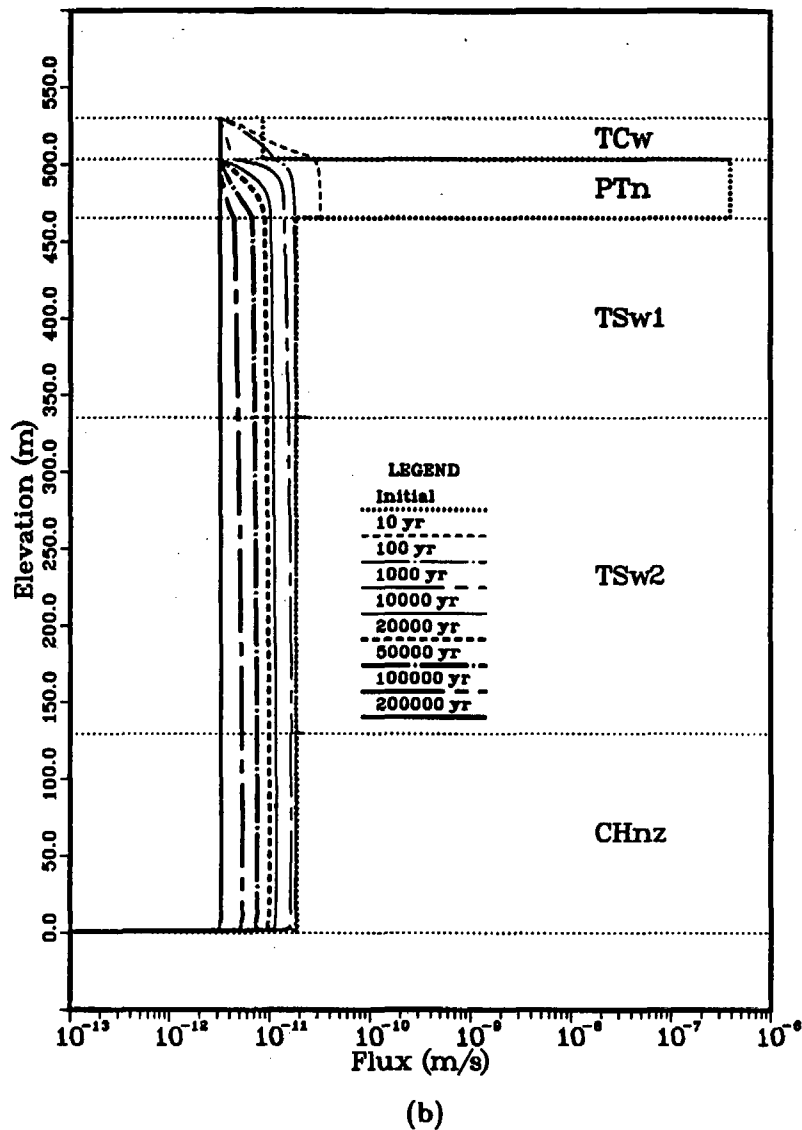
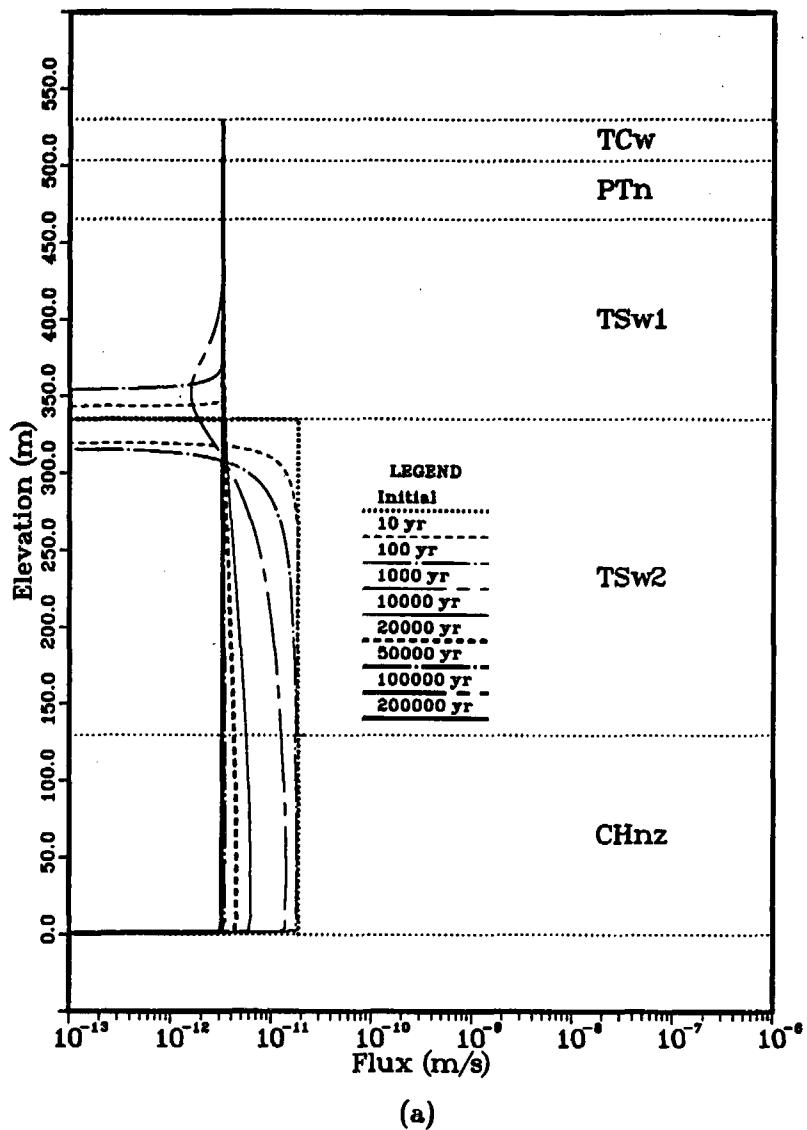
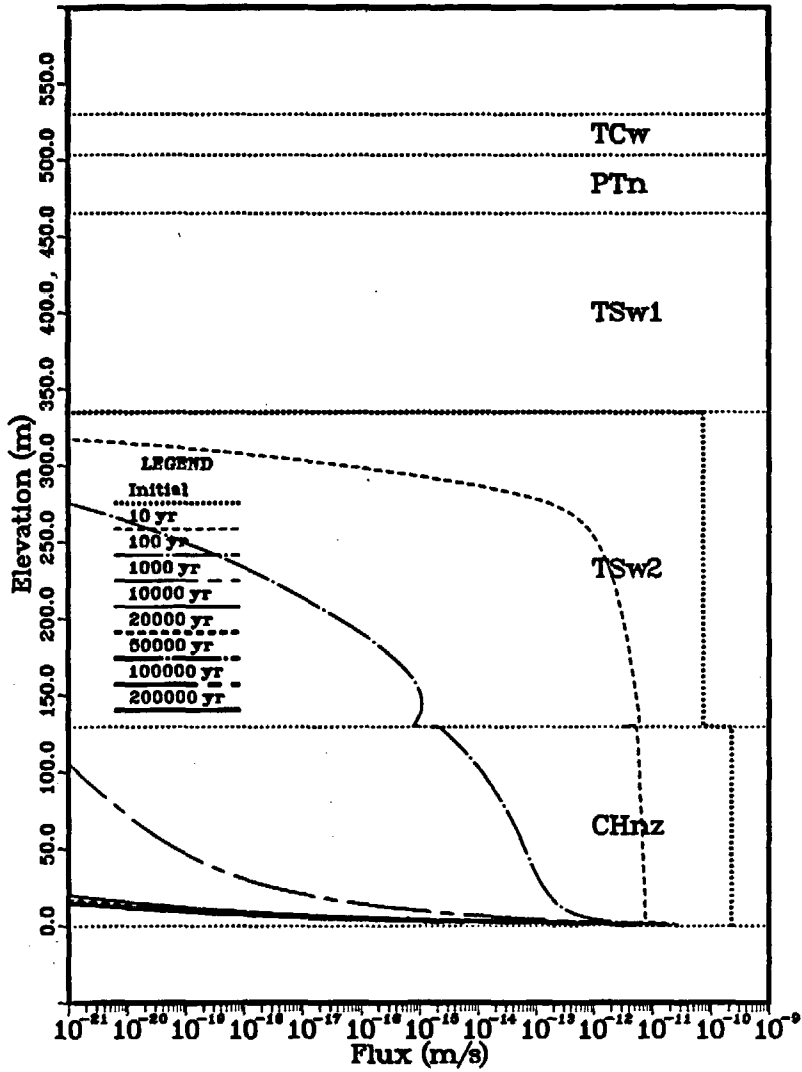
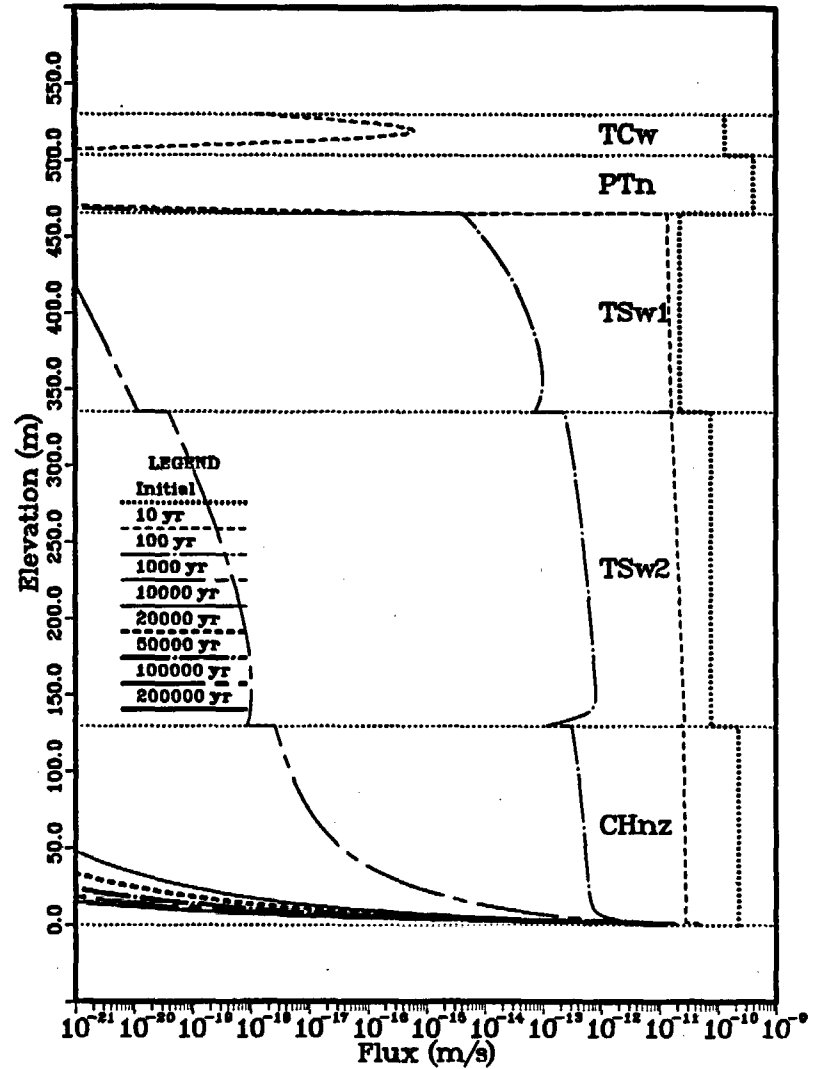


Figure 14. Flux of water in the matrix *versus* elevation at early times. (a) Case 1, (b) Case 2.



(a)



(b)

Figure 15. Flux of water in the fractures *versus* elevation at early times. (a) Case 1, (b) Case 2.

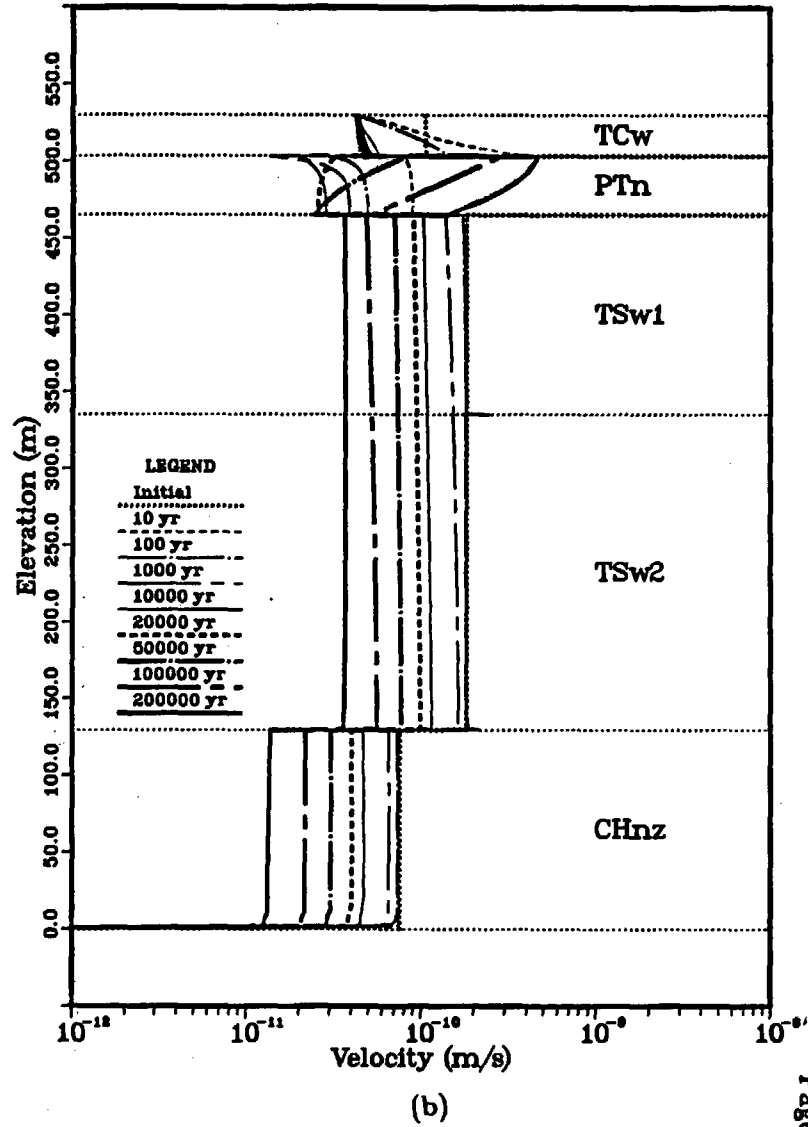
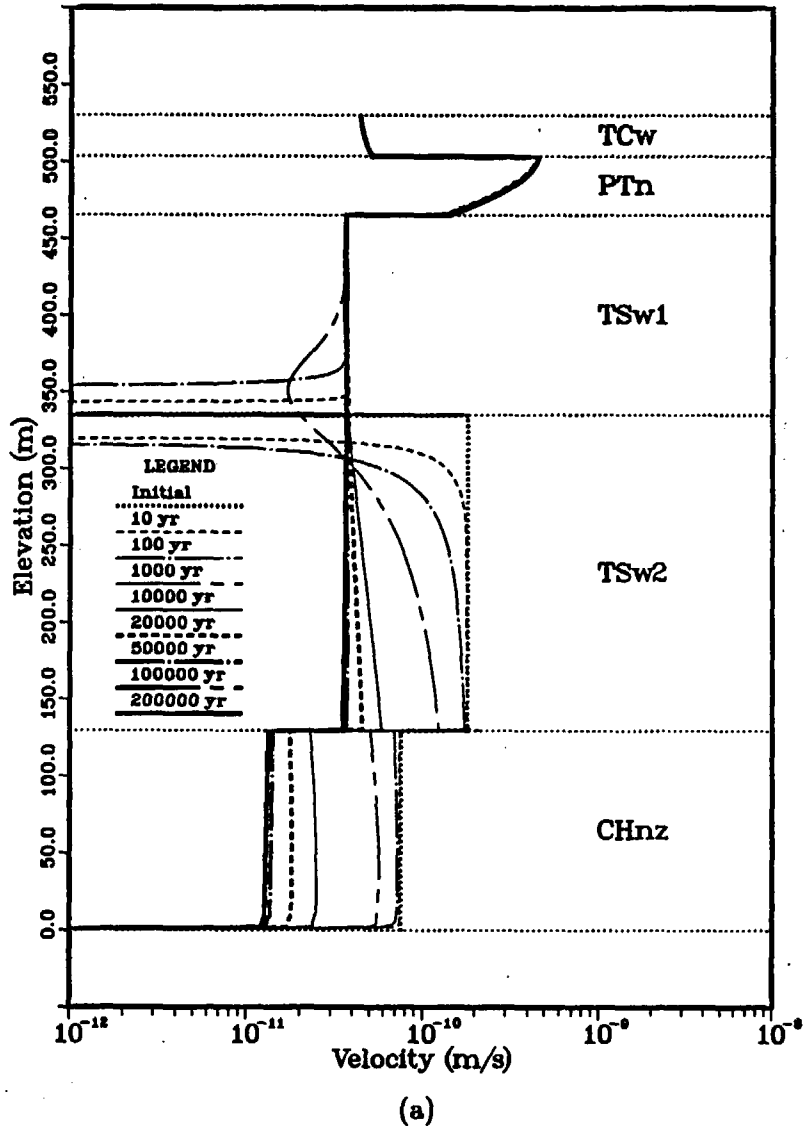
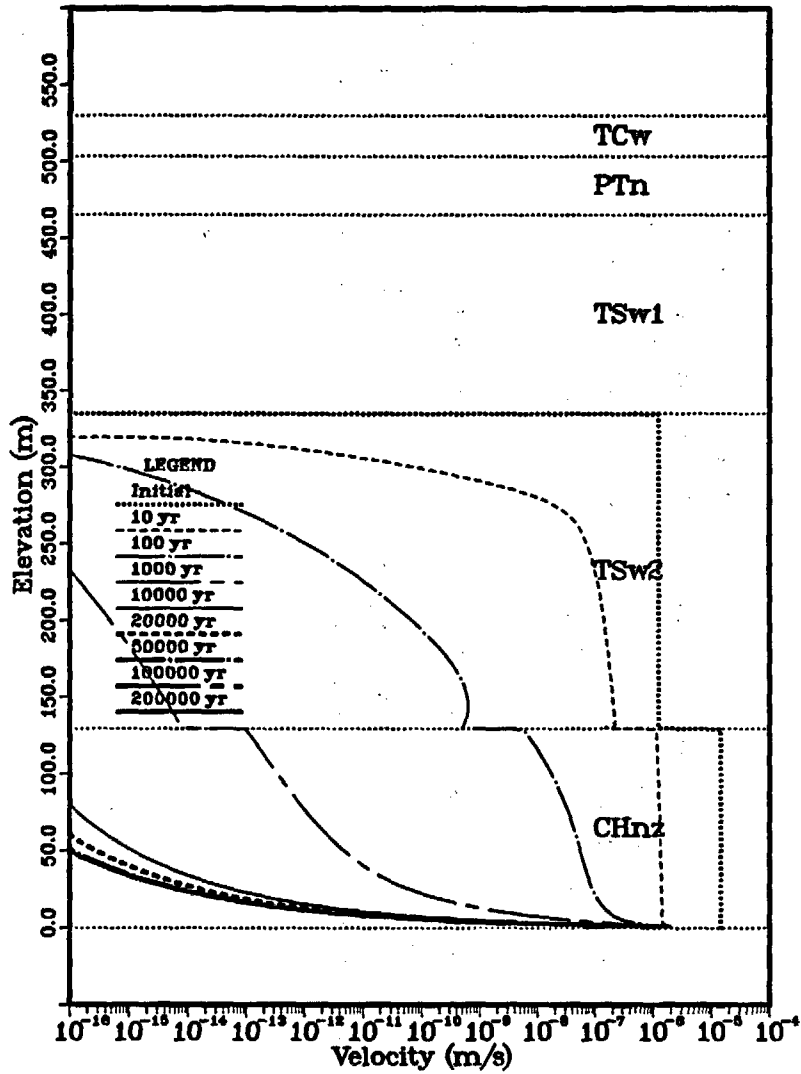
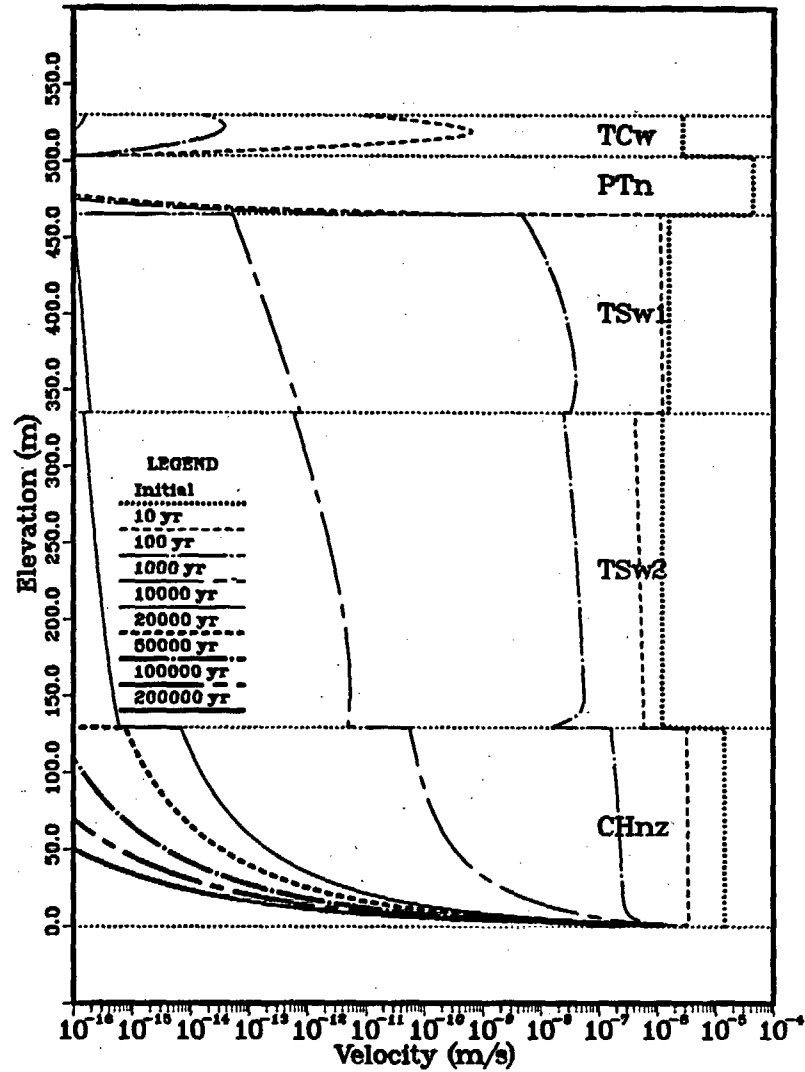


Figure 16. Average linear velocity of water in the matrix versus elevation at late times. (a) Case 1, (b) Case 2.



(a)



(b)

Figure 17. Average linear velocity of water in the fractures versus elevation at late times. (a) Case 1, (b) Case 2.

They are included for completeness.

The temporary increase in water velocity in the matrix of unit PTn, shown in Figure 16b, occurs because the saturation decreases faster than the flux decreases, thus increasing the flux over effective porosity ratio (i.e., the average linear velocity). See Dudley, et al. (1988) for a more complete discussion of this effect. A similar situation in the PTn fractures is not seen, however, because the drop in the saturation of the fractures does not outpace the drop in the fracture-water flux.

Figure 18 shows how the average saturation of the entire column changes with time for Cases 1 and 2. The average saturation is defined as the sum of the saturations at every mesh point (weighted by the half the distances to the next upper and next lower mesh points), as follows:

$$S_{ave} = \sum_j \frac{1}{2}(z_{j+1} - z_{j-1})S_j,$$

where S_{ave} is the average column saturation, j is the mesh point indice, z_{j+1} is the elevation at mesh point $j+1$, and S_j is the saturation at mesh point j .

As Figure 18a shows, Case 1 perturbs the average saturation for the column by approximately 5 percent—from 90 percent down to 85 percent. Figure 18b shows that Case 2 perturbs the average saturation for the column by approximately 15 percent—from 100 percent down to 85 percent.

The leveling of the tail of the Case 1 curve at late time indicates that steady state has been reached, and that the steady-state baseline average saturation is approximately 85 percent. Although it is not obvious because of the downward slant of the curve, examination of the output listing file for the Case 2 calculation shows that at 200,000 years Case 2 is virtually at steady state—within 0.1 percent of the steady-state average saturation.

At 20,000 years (6.32×10^{11} seconds), the Case 1 drain-back is 80 percent complete; the average saturation of the entire column is 1 percent above the steady-state baseline. At 20,000 years the Case 2 drain-back is 30 percent complete. It takes approximately 100,000 years before the Case 2 average entire-column saturation is within 1 percent of the baseline.

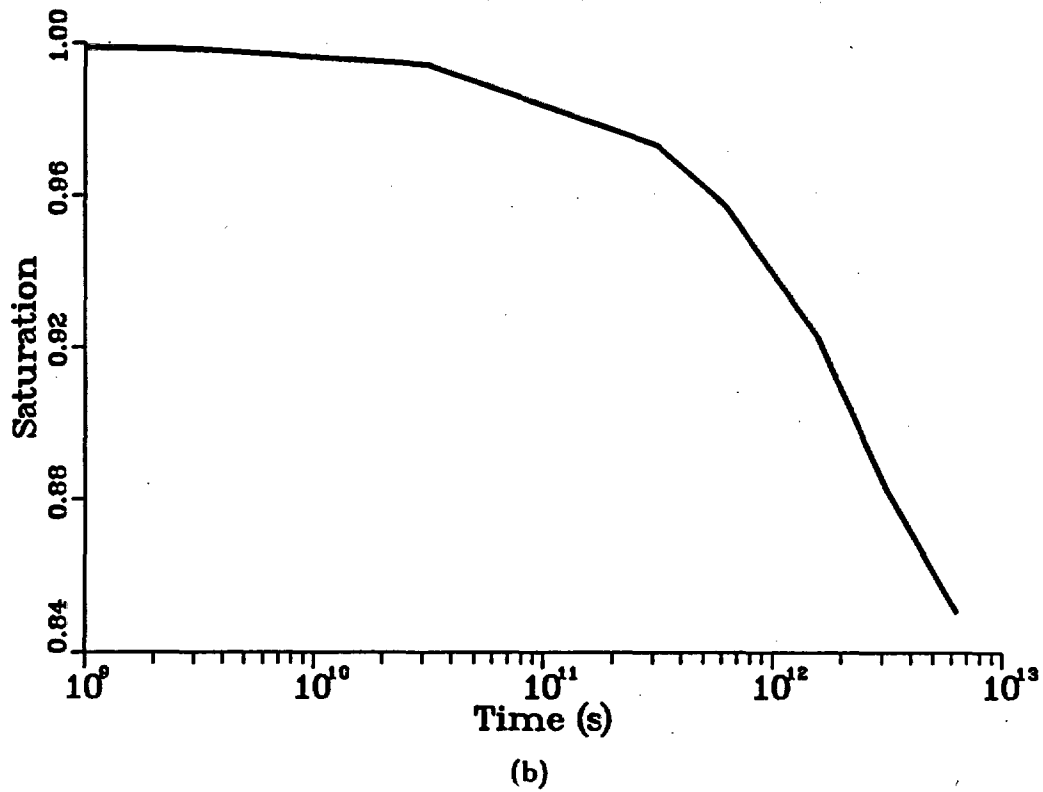
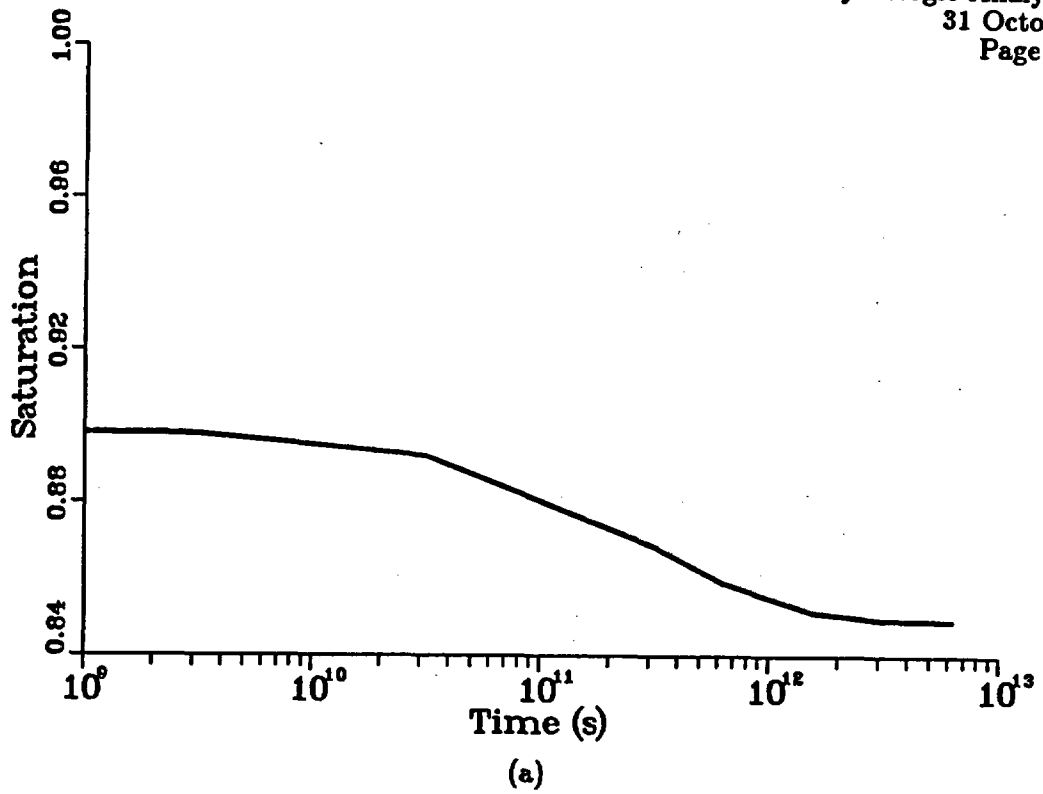


Figure 18. Average saturation of the entire column *versus* time. (a) Case 1, (b) Case 2.

Conclusion

The simulation indicates that the drain-back time of the Case 1 fluctuation is between 50,000 and 100,000 years. However it might prove difficult to identify the fluctuation after 20,000 years.

The drain-back time for Case 2 is sometime over 200,000 years. In this case, after 100,000 years it would probably be difficult to identify the fluctuation.

To contrast the 2 cases, notice that raising the water table an extra 200 meters (approximately 40 percent of the column) causes drain-back time to increase by a factor of 4. This effect is likely caused by the large amount of water stored in the PTn unit in Case 2. There is an 80 percent change in saturation in this highly-porous unit, as partially shown in Figure 11b. The contrast in the drain-back times of the 2 cases implies that these results cannot be used to estimate the drain-back times for cases where the water-table rises are lower than specified in Case 1.

Based on the simulation, the pressure head could be the best hydrologic variable to measure in Yucca Mountain if a significant water-table fluctuation is suspected. If an event happened within the last 20,000 years, significant pressure-head increases would be expected. In contrast, the moisture-content variation might be imperceptible.

These results probably underestimate the drain-back time. With an actual fluctuation in the water table, more water would be pumped up into the mountain than was accounted for in the initial conditions of the simulation (see the Initial Condition sections above).

These results are dependent on the accuracy of the input data. The results are also subject to the assumptions on which the analysis is based:

- 1) the assumption that the hydrologic properties are appropriate for the geologic units (the geologic units have highly variable properties and assigning a single set for each entire unit might be an over-simplification),
- 2) the assumption that the water-table fluctuation lasts long enough to saturate the matrix (approximately 1 year),
- 3) the assumption that present flow in the mountain is 0.1 mm/yr,
- 4) the assumption that flow is vertical, and
- 5) the assumptions built in the hydrologic model used in TOSPAC (see Dudley et al., 1988).

References

Dudley, A. L., R. R. Peters, M. S. Tierney, E. A. Klavetter, J. H. Gauthier, and M. L. Wilson, *Total System Performance Assessment Code (TOSPAC) Volume 1: Physical and Mathematical Bases*, SAND85-0002, Sandia National Laboratories, Albuquerque, New Mexico, 1988.

DOE, *Environmental Assessment—Yucca Mountain Site, Nevada Research and Development Area, Nevada*, DOE/RW-0073, U. S. Department of Energy, Washington DC, 1986.

Gauthier, J. H., M. L. Wilson, and R. R. Peters, *Total System Performance Assessment Code (TOSPAC) Volume 2: User's Guide*, SAND85-0004, Sandia National Laboratories, Albuquerque, New Mexico, in preparation.

Ortiz, T. S., R. L. Williams, F. B. Nimick, B. C. Whittet, and D. L. South, *A Three-Dimensional Model of Reference Thermal/Mechanical and Hydrological Stratigraphy at Yucca Mountain, Southern Nevada*, SAND84-1076, Sandia National Laboratories, Albuquerque, New Mexico, 1985.

Szymanski, J., *Conceptual Considerations of the Death Valley Groundwater System with Special Emphasis on the Adequacy of this System to Accomodate the High-Level Nuclear Waste Repository*, U.S. Department of Energy, Nevada Operations Office, Waste Management Project Office, 1987 (unpublished but unofficially released).

van Genuchten, M., A closed-form equation for predicting the hydraulic conductivity of unsaturated soils, *Soil Sci. Soc. Am. J.*, 44, 892-898, 1980.

Appendix A: Input Data Files

Figures A-1 and A-2 show the input data files for TOSPAC used in the Case 1 and Case 2 calculations, respectively. These files reproduce the information discussed in the Problem Geometry, Material Properties, Initial Condition, and Boundary Condition sections, following. See Gauthier, et al. (in preparation) for more information.

The only differences between the two input files are the titles and the initial condition blocks. The initial condition block for Case 1 specifies reading the initial pressure-head values from a file. The initial condition block for Case 2 specifies assigning a constant pressure-head value of -1 to each mesh point.

*** TOSPAC hydro input text file ***

***** problem title block *****

George Barr Drainage Problem: TSw2 & CHnz saturated --> q = 0.1 mm/yr

***** constants block *****

9.8 acceleration due to gravity
4.3E-6 compressibility of water
1. area of column
.2 timestep factor
.6 implicitness factor

***** geologic unit block *****

5 # geologic units
geologic unit 1 ...name:
CHnz
0. min elevation
129.5 max elevation
1 matrix material index
2 fracture material index
4.6E-5 fracture porosity
26.E-7 bulk compressibility
2.8E-8 fracture compressibility
geologic unit 2 ...name:
TSw2
129.5 min elevation
335.2 max elevation
3 matrix material index
4 fracture material index
18.E-5 fracture porosity
5.8E-7 bulk compressibility
12.E-8 fracture compressibility
geologic unit 3 ...name:
TSw1
335.2 min elevation
465.3 max elevation
5 matrix material index
6 fracture material index
4.1E-5 fracture porosity
12.E-7 bulk compressibility
5.6E-8 fracture compressibility
geologic unit 4 ...name:
PIn
465.3 min elevation
503.4 max elevation
7 matrix material index
8 fracture material index
2.7E-5 fracture porosity
82.E-7 bulk compressibility
19.E-8 fracture compressibility
geologic unit 5 ...name:
TCw
503.4 min elevation
530.2 max elevation
9 matrix material index
10 fracture material index
14.E-5 fracture porosity
6.2E-7 bulk compressibility
132.E-8 fracture compressibility

***** material property block *****

10 # materials
material # 1 ...name:
CHnz/G4-11 (Dudley et al., SAND85-0002)
0.28 material effective porosity
2 characteristic curve fit
1. saturation value
0.11 residual saturation
0.00308 ALPHA coefficient
1.602 BETA coefficient
2.0E-11 saturated hydraulic conductivity
material # 2 ...name:
CHnz/G4-4F (Dudley et al., SAND85-0002)
1. material effective porosity
2 characteristic curve fit
1. saturation value
0.0395 residual saturation
1.2851 ALPHA coefficient
4.23 BETA coefficient
20.E-5 saturated hydraulic conductivity
material # 3 ...name:
TSw2/G4-6 (Dudley et al., SAND85-0002)
0.11 material effective porosity
2 characteristic curve fit
1. saturation value
0.080 residual saturation
0.00567 ALPHA coefficient
1.798 BETA coefficient
1.9E-11 saturated hydraulic conductivity
material # 4 ...name:
TSw2/G4-2F (Dudley et al., SAND85-0002)
1. material effective porosity
2 characteristic curve fit
1. saturation value
0.0395 residual saturation
1.2851 ALPHA coefficient
4.23 BETA coefficient
1.7E-5 saturated hydraulic conductivity
material # 5 ...name:
TSw1/G4-6 (Dudley et al., SAND85-0002)
0.11 material effective porosity
2 characteristic curve fit
1. saturation value
0.080 residual saturation
0.00567 ALPHA coefficient
1.798 BETA coefficient
1.9E-11 saturated hydraulic conductivity
material # 6 ...name:
TSw1/G4-2F (Dudley et al., SAND85-0002)
1. material effective porosity
2 characteristic curve fit
1. saturation value
0.0395 residual saturation
1.2851 ALPHA coefficient
4.23 BETA coefficient
2.2E-5 saturated hydraulic conductivity
material # 7 ...name:
PIn/GU3-7 (Dudley et al., SAND85-0002)
0.40 material effective porosity
2 characteristic curve fit
1. saturation value
0.1 residual saturation

Figure A-1. The TOSPAC input data file for the Case 1 simulation (Part 1 of 2).

```

0.015      ALPHA coefficient
6.872      BETA coefficient
3.9E-7     saturated hydraulic conductivity
material # 8 ...name:
PIA/G4-3F (Dudley et al., SAND85-0002)
1.         material effective porosity
2         characteristic curve fit
1.         saturation value
0.0395     residual saturation
1.2851     ALPHA coefficient
4.23      BETA coefficient
61.E-5     saturated hydraulic conductivity
material # 9 ...name:
ICW/G4-1 (Dudley et al., SAND85-0002)
0.08      material effective porosity
2         characteristic curve fit
1.         saturation value
0.002     residual saturation
0.00821   ALPHA coefficient
1.558     BETA coefficient
9.7E-12   saturated hydraulic conductivity
material # 10 ...name:
ICW/G4-2F (Dudley et al., SAND85-0002)
1.         material effective porosity
2         characteristic curve fit
1.         saturation value
0.0395     residual saturation
1.2851     ALPHA coefficient
4.23      BETA coefficient
3.8E-5     saturated hydraulic conductivity

```

```

***** mesh block *****
2303      # mesh points
11        # sub-meshes
sub-mesh 1:
0.         min elevation
2.         max elevation
21        # sub-mesh points
sub-mesh 2:
2.         min elevation
130.      max elevation
513       # sub-mesh points
sub-mesh 3:
130.      min elevation
142.      max elevation
121       # sub-mesh points
sub-mesh 4:
142.      min elevation
335.      max elevation
773       # sub-mesh points
sub-mesh 5:
335.      min elevation
336.      max elevation
11        # sub-mesh points
sub-mesh 6:
336.      min elevation
465.      max elevation
517       # sub-mesh points
sub-mesh 7:
465.      min elevation
466.      max elevation
11        # sub-mesh points

```

```

sub-mesh 8:
466.      min elevation
503.      max elevation
75        # sub-mesh points
sub-mesh 9:
503.      min elevation
507.      max elevation
161       # sub-mesh points
sub-mesh 10:
507.      min elevation
530.      max elevation
93        # sub-mesh points
sub-mesh 11:
530.      min elevation
530.2     max elevation
17        # sub-mesh points

```

```

***** boundary condition block *****
8         # time snapshots

```

```

snapshot 1:
3.15576E+8 problem time
1         boundary condition flag
0         lower boundary pressure head
3.17E-12  upper boundary flux
0         max elevation pond
snapshot 2:
3.15576E+9 problem time
0         boundary condition flag
snapshot 3:
3.15576E+10 problem time
0         boundary condition flag
snapshot 4:
3.15576E+11 problem time
0         boundary condition flag
snapshot 5:
6.31152E+11 problem time
0         boundary condition flag
snapshot 6:
1.57788E+12 problem time
0         boundary condition flag
snapshot 7:
3.15576E+12 problem time
0         boundary condition flag
snapshot 8:
6.31152E+12 problem time
0         boundary condition flag

```

```

***** initial condition block *****
1         initial condition flag

```

```

scr:[jhgauth.barr]barr1.11 initial condition filename

```

Figure A-1. The TOSPAC input data file for the Case 1 simulation (Part 2 of 2).

 *** TOSPAC hydro input text file ***

***** problem title block *****
 George Barr Drainage Problem: Saturated Column --> q = 0.1 mm/yr

***** constants block *****
 9.8 acceleration due to gravity
 4.3E-6 compressibility of water
 1. area of column
 .2 timestep factor
 .6 implicitness factor

***** geologic unit block *****
 5 # geologic units
 geologic unit 1 ...name:
 CHnz
 0. min elevation
 129.6 max elevation
 1 matrix material index
 2 fracture material index
 4.6E-5 fracture porosity
 26.E-7 bulk compressibility
 2.8E-8 fracture compressibility
 geologic unit 2 ...name:
 ISw2
 129.6 min elevation
 335.2 max elevation
 3 matrix material index
 4 fracture material index
 18.E-5 fracture porosity
 6.8E-7 bulk compressibility
 12.E-8 fracture compressibility
 geologic unit 3 ...name:
 ISw1
 335.2 min elevation
 465.3 max elevation
 5 matrix material index
 6 fracture material index
 4.1E-5 fracture porosity
 12.E-7 bulk compressibility
 5.6E-8 fracture compressibility
 geologic unit 4 ...name:
 PIn
 465.3 min elevation
 503.4 max elevation
 7 matrix material index
 8 fracture material index
 2.7E-5 fracture porosity
 82.E-7 bulk compressibility
 19.E-8 fracture compressibility
 geologic unit 5 ...name:
 ICw
 503.4 min elevation
 530.2 max elevation
 9 matrix material index
 10 fracture material index
 14.E-5 fracture porosity
 6.2E-7 bulk compressibility
 132.E-8 fracture compressibility

***** material property block *****
 10 # materials
 material # 1 ...name:
 CHnz/G4-11 (Dudley et al., SAND85-0002)
 0.28 material effective porosity
 2 characteristic curve fit
 1. saturation value
 0.11 residual saturation
 0.00308 ALPHA coefficient
 1.602 BETA coefficient
 2.0E-11 saturated hydraulic conductivity
 material # 2 ...name:
 CHnz/G4-4F (Dudley et al., SAND85-0002)
 1. material effective porosity
 2. characteristic curve fit
 1. saturation value
 0.0395 residual saturation
 1.2851 ALPHA coefficient
 4.23 BETA coefficient
 20.E-5 saturated hydraulic conductivity
 material # 3 ...name:
 ISw2/G4-6 (Dudley et al., SAND85-0002)
 0.11 material effective porosity
 2 characteristic curve fit
 1. saturation value
 0.080 residual saturation
 0.00567 ALPHA coefficient
 1.798 BETA coefficient
 1.9E-11 saturated hydraulic conductivity
 material # 4 ...name:
 ISw2/G4-2F (Dudley et al., SAND85-0002)
 1. material effective porosity
 2 characteristic curve fit
 1. saturation value
 0.0395 residual saturation
 1.2851 ALPHA coefficient
 4.23 BETA coefficient
 1.7E-5 saturated hydraulic conductivity
 material # 5 ...name:
 ISw1/G4-6 (Dudley et al., SAND85-0002)
 0.11 material effective porosity
 2 characteristic curve fit
 1. saturation value
 0.080 residual saturation
 0.00567 ALPHA coefficient
 1.798 BETA coefficient
 1.9E-11 saturated hydraulic conductivity
 material # 6 ...name:
 ISw1/G4-2F (Dudley et al., SAND85-0002)
 1. material effective porosity
 2 characteristic curve fit
 1. saturation value
 0.0395 residual saturation
 1.2851 ALPHA coefficient
 4.23 BETA coefficient
 2.2E-5 saturated hydraulic conductivity
 material # 7 ...name:
 PIn/GU3-7 (Dudley et al., SAND85-0002)
 0.40 material effective porosity
 2 characteristic curve fit
 1. saturation value
 0.1 residual saturation

223

Figure A-2. The TOSPAC input data file for the Case 2 simulation (Part 1 of 2).

```

0.016      ALPHA coefficient
8.872      BETA coefficient
3.9E-7     saturated hydraulic conductivity
material # 8 ..name:
PTn/G4-3F (Dudley et al., SAND85-0002)
1.         material effective porosity
2.         characteristic curve fit
1.         saturation value
0.0395     residual saturation
1.2851     ALPHA coefficient
4.23      BETA coefficient
61.E-5     saturated hydraulic conductivity
material # 9 ..name:
TCw/G4-1 (Dudley et al., SAND85-0002)
0.08      material effective porosity
2.         characteristic curve fit
1.         saturation value
0.002     residual saturation
0.00821   ALPHA coefficient
1.558     BETA coefficient
9.7E-12   saturated hydraulic conductivity
material # 10 ..name:
TCw/G4-2F (Dudley et al., SAND85-0002)
1.         material effective porosity
2.         characteristic curve fit
1.         saturation value
0.0395     residual saturation
1.2851     ALPHA coefficient
4.23      BETA coefficient
3.8E-5     saturated hydraulic conductivity

***** mesh block *****
2303      # mesh points
11        # sub-meshes
sub-mesh 1:
0.         min elevation
2.         max elevation
21        # sub-mesh points
sub-mesh 2:
2.         min elevation
130.      max elevation
513       # sub-mesh points
sub-mesh 3:
130.      min elevation
142.      max elevation
121       # sub-mesh points
sub-mesh 4:
142.      min elevation
335.      max elevation
773       # sub-mesh points
sub-mesh 5:
335.      min elevation
336.      max elevation
11        # sub-mesh points
sub-mesh 6:
336.      min elevation
465.      max elevation
517       # sub-mesh points
sub-mesh 7:
465.      min elevation
466.      max elevation
11        # sub-mesh points

sub-mesh 8:
466.      min elevation
503.      max elevation
75        # sub-mesh points
sub-mesh 9:
503.      min elevation
507.      max elevation
161       # sub-mesh points
sub-mesh 10:
507.      min elevation
530.      max elevation
93        # sub-mesh points
sub-mesh 11:
530.      min elevation
530.2     max elevation
17        # sub-mesh points

***** boundary condition block *****
8         # time snapshots
snapshot 1:
3.15576E+8  problem time
1          boundary condition flag
0          lower boundary pressure head
3.17E-12   upper boundary flux
0          max elevation pond
snapshot 2:
3.15576E+9  problem time
0          boundary condition flag
snapshot 3:
3.15576E+10 problem time
0          boundary condition flag
snapshot 4:
3.15576E+11 problem time
0          boundary condition flag
snapshot 5:
6.31152E+11 problem time
0          boundary condition flag
snapshot 6:
1.57788E+12 problem time
0          boundary condition flag
snapshot 7:
3.15576E+12 problem time
0          boundary condition flag
snapshot 8:
6.31152E+12 problem time
0          boundary condition flag

***** initial condition block *****
3         initial condition flag
-1        initial pressure head constant

```

Figure A-2. The TOSPAC input data file for the Case 2 simulation (Part 2 of 2).

APPENDIX A

REFERENCE INFORMATION BASE AND SITE AND ENGINEERING PROPERTIES DATA BASE INFORMATION

The sources of data used in this report are listed below on a memorandum-by-memorandum basis. Complete references for the data sources may be found at the end of each memorandum.

NNWSI Hydrologic Analysis No. 8 Support of Exploratory Shaft Activities

Figure 1 is based on the report by Ortiz et al. (1985). Table 2 on page 6 and Table 4 on page 14 are taken from the report by Klavetter and Peters that was listed as being "in preparation" in the memorandum and was published in July of 1986.

NNWSI Hydrologic Analysis No. 72-19 Support of Exploratory Shaft Activities

Figure 1 is based on the report by Ortiz et al. (1985). Figure 2 uses data from the reports by Peters et al. (1984) and Rulon et al. (1986). Table 1 on pages 6 and 7 contains data from the reports by Klavetter and Peters (1986) and Rulon et al. (1986).

NNWSI Hydrologic Analysis No. 9 1-D Hydrologic Calculations Concerning Groundwater Travel Time for the Repository as a Result of Water Redistribution Caused by Repository Heating

Figure 1 is based on the report by Ortiz et al. (1985). Table 1 contains data from the report by Peters et al. (1984).

The Effect of Seismic and Tectonic Activity on Radionuclide Containment at Yucca Mountain

Figure 1 is based on the report by Ortiz et al. (1985). Table 1 contains data from the report by Peters, Gauthier, and Dudley that was listed as being "in preparation" in the memorandum. This report was published in August of 1986 as part of conference proceedings (PNL, 1986). It was also published in February of 1986 as a Sandia National Laboratories report (Peters et al., 1986).

NNWSI Hydrologic Analysis No. 72-26
A 1-Dimensional Calculation Investigating
Water-Table Fluctuation at Yucca Mountain

Figure 1 is based on the report by Ortiz et al. (1985). Table 1 contains data from the report by Dudley et al. (1988).

None of the data in this report are recommended for inclusion in the Reference Information Base.

References Cited Only in Appendix A

Peters, R. R., J. H. Gauthier, and A. L. Dudley, "The Effect of Percolation Rate on Water-Travel Time in Deep, Partially Saturated Zones," SAND85-0854, Sandia National Laboratories, Albuquerque, NM, 1986.

PNL (Pacific Northwest Laboratory), Proceedings, the Symposium on Ground-Water Flow and Transport Modeling for Performance Assessment of Deep Geologic Disposal of Radioactive Waste: A Critical Evaluation of the State of the Art, NUREG/CP-0079, Richland, WA, 1986.

DISTRIBUTION LIST

Samuel Rousso, Acting Director (RW-1)
Office of Civilian Radioactive
Waste Management
U.S. Department of Energy
Forrestal Bldg.
Washington, D.C. 20585

Ralph Stein (RW-30)
Office of Civilian Radioactive
Waste Management
U.S. Department of Energy
Forrestal Bldg.
Washington, D.C. 20585

M. W. Frei (RW-22)
Office of Civilian Radioactive
Waste Management
U.S. Department of Energy
Forrestal Bldg.
Washington, D.C. 20585

B. G. Gale (RW-23)
Office of Civilian Radioactive
Waste Management
U.S. Department of Energy
Forrestal Bldg.
Washington, D.C. 20585

Samuel Rousso (RW-10)
Office of Civilian Radioactive
Waste Management
U.S. Department of Energy
Forrestal Bldg.
Washington, D.C. 20585

J. D. Saltzman (RW-20)
Office of Civilian Radioactive
Waste Management
U.S. Department of Energy
Forrestal Bldg.
Washington, D.C. 20585

S. J. Brocoum (RW-221)
Office of Civilian Radioactive
Waste Management
U.S. Department of Energy
Forrestal Bldg.
Washington, D.C. 20585

V. J. Cassella (RW-123)
Office of Civilian Radioactive
Waste Management
U.S. Department of Energy
Forrestal Bldg.
Washington, D.C. 20585

S. H. Kale (RW-20)
Office of Civilian Radioactive
Waste Management
U.S. Department of Energy
Forrestal Bldg.
Washington, D.C. 20585

T. H. Isaacs (RW-40)
Office of Civilian Radioactive
Waste Management
U.S. Department of Energy
Forrestal Bldg.
Washington, D.C. 20585

D. H. Alexander (RW-332)
Office of Civilian Radioactive
Waste Management
U.S. Department of Energy
Forrestal Bldg.
Washington, D.C. 20585

C. Bresee (RW-10)
Office of Civilian Radioactive
Waste Management
U.S. Department of Energy
Forrestal Bldg.
Washington, D.C. 20585

Gerald Parker (RW-333)
Office of Civilian Radioactive
Waste Management
U.S. Department of Energy
Forrestal Bldg.
Washington, D.C. 20585

Chief, Repository Projects Branch
Division of Waste Management
U.S. Nuclear Regulatory Commission
Washington, D.C. 20555

NTS Section Leader
Repository Project Branch
Division of Waste Management
U.S. Nuclear Regulatory Commission
Washington, D.C. 20555

Document Control Center
Division of Waste Management
U.S. Nuclear Regulatory Commission
Washington, D.C. 20555

Carl P. Gertz, Project Manager (5)
Yucca Mountain Project Office
Nevada Operations Office
U.S. Department of Energy
Mail Stop 523
P.O. Box 98518
Las Vegas, NV 89193-8518

J. L. Fogg (12)
Technical Information Office
Nevada Operations Office
U.S. Department of Energy
P.O. Box 98518
Las Vegas, NV 89193-8518

C. L. West, Director
Office of External Affairs
U.S. Department of Energy
Nevada Operations Office
P.O. Box 98518
Las Vegas, NV 89193-8518

W. M. Hewitt, Program Manager
Roy F. Weston, Inc.
955 L'Enfant Plaza, Southwest
Suite 800
Washington, D.C. 20024

Technical Information Center
Roy F. Weston, Inc.
955 L'Enfant Plaza, Southwest
Suite 800
Washington, D.C. 20024

L. D. Ramspott (3)
Technical Project Officer for YMP
Lawrence Livermore National
Laboratory
Mail Stop L-204
P.O. Box 808
Livermore, CA 94550

M. E. Spaeth
Technical Project Officer for YMP
Science Applications International
Corp.
101 Convention Center Dr.
Suite 407
Las Vegas, NV 89109

H. N. Kalia
Exploratory Shaft Test Manager
Los Alamos National Laboratory
Mail Stop 527
101 Convention Center Dr.
Suite P230
Las Vegas, NV 89109

D. T. Oakley (4)
Technical Project Officer for YMP
Los Alamos National Laboratory
N-5, Mail Stop J521
P.O. Box 1663
Los Alamos, NM 87545

L. R. Hayes (6)
Technical Project Officer for YMP
U.S. Geological Survey
P.O. Box 25046
421 Federal Center
Denver, CO 80225

K. W. Causseaux
NHP Reports Chief
U.S. Geological Survey
P.O. Box 25046
421 Federal Center
Denver, CO 80225

R. V. Watkins, Chief
Project Planning and Management
U.S. Geological Survey
P.O. Box 25046
421 Federal Center
Denver, CO 80225

Center for Nuclear Waste
Regulatory Analyses
6220 Culebra Road
Drawer 28510
San Antonio, TX 78284

R. L. Bullock
Technical Project Officer for YMP
Fenix & Scisson, Inc.
Mail Stop 403
101 Convention Center Dr.
Suite 320
Las Vegas, NV 89109-3265

James C. Calovini
Technical Project Officer for YMP
Holmes & Narver, Inc.
101 Convention Center Dr.
Suite 860
Las Vegas, NV 89109

Dr. David W. Harris
YMP Technical Project Officer
Bureau of Reclamation
P.O. Box 25007 Bldg. 67
Denver Federal Center
Denver, CO 80225-0007

M. D. Voegele
Science Applications International
Corp.
101 Convention Center Dr.
Suite 407
Las Vegas, NV 89109

J. A. Cross, Manager
Las Vegas Branch
Fenix & Scisson, Inc.
Mail Stop 514
P.O. Box 93265
Las Vegas, NV 89193-3265

P. T. Prestholt
NRC Site Representative
1050 East Flamingo Road
Suite 319
Las Vegas, NV 89109

A. E. Gurrola, General Manager
Energy Support Division
Holmes & Narver, Inc.
Mail Stop 580
P.O. Box 93838
Las Vegas, NV 89193-3838

A. M. Sastry
Technical Project Officer for YMP
MAC Technical Services
Valley Bank Center
101 Convention Center Drive
Suite P-113
Las Vegas, NV 89109

B. L. Fraser, General Manager
Reynolds Electrical & Engineering Co.
Mail Stop 555
P.O. Box 98521
Las Vegas, NV 89193-8521

P. K. Fitzsimmons, Director
Health Physics & Environmental
Division
Nevada Operations Office
U.S. Department of Energy
P.O. Box 98518
Las Vegas, NV 89193-8518

Robert F. Pritchett
Technical Project Officer for YMP
Reynolds Electrical & Engineering Co.
Mail Stop 615
P.O. Box 98521
Las Vegas, NV 89193-8521

Elaine Ezra
YMP GIS Project Manager
EG&G Energy Measurements, Inc.
Mail Stop H-02
P.O. Box 1912
Las Vegas, NV 89125

SAIC-T&MSS Library (2)
Science Applications International
Corp.
101 Convention Center Dr.
Suite 407
Las Vegas, NV 89109

Dr. Martin Mifflin
Desert Research Center
Water Resource Center
2505 Chandler Avenue
Suite 1
Las Vegas, NV 89120

E. P. Binnall
Field Systems Group Leader
Building 50B/4235
Lawrence Berkeley Laboratory
Berkeley, CA 94720

J. F. Divine
Assistant Director for Engineering
Geology
U.S. Geological Survey
106 National Center
12201 Sunrise Valley Dr.
Reston, VA 22092

V. M. Glanzman
U.S. Geological Survey
P.O. Box 25046
913 Federal Center
Denver, CO 80225

C. H. Johnson
Technical Program Manager
Nuclear Waste Project Office
State of Nevada
Evergreen Center, Suite 252
1802 North Carson Street
Carson City, NV 89710

T. Hay, Executive Assistant
Office of the Governor
State of Nevada
Capitol Complex
Carson City, NV 89710

R. R. Loux, Jr. (3)
Executive Director
Nuclear Waste Project Office
State of Nevada
Evergreen Center, Suite 252
1802 North Carson Street
Carson City, NV 89710

John Fordham
Desert Research Institute
Water Resources Center
P.O. Box 60220
Reno, NV 89506

Prof. S. W. Dickson
Department of Geological Sciences
Mackay School of Mines
University of Nevada
Reno, NV 89557

J. R. Rollo
Deputy Assistant Director for
Engineering Geology
U.S. Geological Survey
106 National Center
12201 Sunrise Valley Dr.
Reston, VA 22092

Eric Anderson
Mountain West Research-Southwest
Inc.
Phoenix Gateway Center
432 North 44 Street
Suite 400
Phoenix, AZ 85008-6572

Judy Foremaster (5)
City of Caliente
P.O. Box 158
Caliente, NV 89008

A. T. Tamura
Science and Technology Division
Office of Scientific and Technical
Information
U.S. Department of Energy
P.O. Box 62
Oak Ridge, TN 37831

L. Jardine
Project Manager
Bechtel National Inc.
P.O. Box 3965
San Francisco, CA 94119

R. Harig
Parsons Brinckerhoff Quade &
Douglas
1625 Van Ness Ave.
San Francisco, CA 94109-3679

Dr. Roger Kasperson
CENTED
Clark University
950 Main Street
Worcester, MA 01610

Robert E. Cummings
Engineers International, Inc.
P.O. Box 43817
Tucson, AZ 85733-3817

Dr. Jaak Daemen
Department of Mining and Geotechnical
Engineering
University of Arizona
Tucson, AZ 85721

Department of Comprehensive Planning
Clark County
225 Bridger Avenue, 7th Floor
Las Vegas, NV 89155

Economic Development Department
City of Las Vegas
400 East Stewart Avenue
Las Vegas, NV 89109

Planning Department
Nye County
P.O. Box 153
Tonopah, NV 89049

Director of Community Planning
City of Boulder City
P.O. Box 367
Boulder City, NV 89005

Commission of the European
Communities
200 Rue de la Loi
B-1049 Brussels
BELGIUM

Lincoln County Commission
Lincoln County
P.O. Box 90
Pioche, NV 89043

Community Planning & Development
City of North Las Vegas
P.O. Box 4086
North Las Vegas, NV 89030

City Manager
City of Henderson
Henderson, NV 89015

ONWI Library
Battelle Columbus Laboratory
Office of Nuclear Waste Isolation
505 King Avenue
Columbus, OH 43201

Librarian
Los Alamos Technical Associates,
Inc.
P.O. Box 410
Los Alamos, NM 87544

6300 R. W. Lynch
6300-1 T. O. Hunter
6310 J. E. Stiegler, Actg.
6310 YMPCF
6310 100/12144/SAND88-2784/Q3
6311 A. L. Stevens
6311 C. Mora
6312 F. W. Bingham
6312 P. G. Kaplan
6312 A. C. Peterson
6312 R. R. Peters (10)
6312 M. S. Tierney
6312 J. H. Gauthier
6312 A. L. Dudley
6313 T. E. Blejwas
6313 E. A. Klavetter
6314 J. R. Tillerson
6314 J. A. Fernandez
6315 L. F. Shephard
6316 R. P. Sandoval
6317 S. Sinnock
6332 WMT Library (20)
6410 N. R. Ortiz
3141 S. A. Landenberger (5)
3151 W. I. Klein (3)
8024 J. A. Wackerly
3154-3 C. L. Ward (8)
for DOE/OSTI

60. 7x.

NNA.881202.0204

